SOUND RADIATION MEASUREMENTS ON GUITARS AND OTHER STRINGED MUSICAL INSTRUMENTS

Ian Perry

A thesis submitted to Cardiff University for the degree of Doctor of Philosophy

September 2014

Declaration

Statement 1

This work has not been submitted in substance for any other degree or award at this or any other university or place of learning, nor is being submitted concurrently in candidature for any degree or other award.

Signed .... (candidate)

Date ....

Statement 2

This thesis is being submitted in partial fulfillment of the requirements for the degree of PhD.

Signed .... (candidate)

Date ....

Statement 3

This thesis is the result of my own independent work/investigation, except where otherwise stated. Other sources are acknowledged by explicit references.

Signed .... (candidate)

Date ....

Statement 4

I hereby give consent for my thesis, if accepted, to be available for photocopying and for inter-library loan, and for the title and summary to be made available to outside organisations after expiry of a bar on access previously approved by the Academic Standards & Quality Committee.

Signed .... (candidate)

Date ....

Acknowledgements

Firstly I would like to thank Dr. Bernard Richardson for his help and support throughout my PhD studies. Your help in answering my questions, designing the experimental guitar and aiding the direction of this thesis has been immeasurable. Thanks as well to the Engineering and Physical Sciences Research Council for financial support. Thank you to Carole Tucker, Jonathan Davies and Clarence Matthai for providing me with part-time work in the department during my time in Cardiff.

Thanks to Matt Pearson for help with setting up and explaining the workings of the 3D scanning laser vibrometer system. Thanks to Wil Roberts for assistance with the vibrometry, and other, experiments and for many useful discussions on the subject of musical acoustics. Several of the instruments were provided by those outside of the Cardiff musical acoustics group. I would like to thank to Jimmy O'Donnell for lending the carbon-fibre steel-string guitar to the group and Malcolm Graham for the donation of MAL.

Thanks to all of my fellow members of Wonderbrass, Inc.A and the Occasional Brass Ensemble for the musical entertainment and moral support throughout my thesis, in particular during the final writing up period. Many thanks to Mum and Dad for helping proofread this thesis, many meals out, lifts and encouragement. Social thanks are also in order to the Edinburgh Perrys, the Bishopstoke Berrys, Huw, Dom, Charlie, Paul, Nadia, Chris, Tom and Laura.

Finally, thank you very much to Yuko Perry for your love and support through my studies.

Summary

This thesis focuses on physical measurements of the sound radiated by stringed musical instruments. The radiation efficiency, defined as the ratio of acoustical power output to mechanical power input, was measured to study the acoustical behaviour of the instruments between 80 Hz and 2000 Hz. The research used spherical-harmonic decomposition to determine the power output from monopole and dipole sources. On classical guitars, monopole power produced by the low-frequency resonance triplet provided the greatest contribution to the power output below 300 Hz. At higher frequencies, where the body modes have more complex shapes, dipole sources dominated the total power output. As the dipole contribution to the power output increases, the radiation efficiency of the instrument decreases.

The research demonstrated that the resonance frequencies of the body modes of the instruments do not correspond with either a large or small value of radiation efficiency. Instead it is the mode shape that determines the radiation efficiency. Modes with similar-sized anti-nodal areas, of opposite phase, were found to be less efficient than modes which had unequal-sized anti-nodal areas. Measurements of the in-plane velocity of these modes, made with a 3D scanning laser vibrometer, showed that the less-efficient modes had greater values of in-plane velocity.

The largest values of radiation efficiency for classical guitars occurred between 200 Hz and 600 Hz. The upper frequency limit of this range was determined by the resonance frequency of a particular mode. This was confirmed by experiments on a purpose-built guitar in which the cross-grain stiffness could be adjusted. Experiments on classical guitars, steel-string guitars and violins produced characteristically different radiation efficiencies.

Contents

1 Introduction **1**

1.1 Motivation and aims of the research 1

1.2 A brief introduction to the classical guitar 2

1.2.1 Guitar construction 2

1.2.2 Guitar designs 5

1.3 Sound Production from guitars 6

1.3.1 Strings 7

1.3.2 Coupling strings to the body 8

1.4 Modes of vibration of the classical guitar 9

1.4.1 Classical guitar mode naming convention 10

1.4.2 Low-frequency resonance triplet 11

1.4.3 Body Modes 14

1.5 Thesis structure 16

2 Summary of previous research **17**

2.1 Admittance of guitars 18

2.2 Simple harmonic oscillator model for velocity and pressure responses . . 23

2.3 Sound pressure measurements from body modes 25

2.3.1 Monopole and simple sources 25

2.3.2 Dipole sources 27

2.3.3 Quadrupoles and higher order sources 28

2.4 Sound pressure from several sources 29

2.5 Radiation efficiency 31

2.5.1 R_{eff} 31

2.5.2 Radiation efficiency, η 34

2.6 Input Power 37

2.7 Output Power 38

2.7.1 Sound intensity 38

2.7.2 Spherical-harmonic decomposition 40
2.8 Visualising guitar mode shapes 42
2.9 Psychoacoustics 44

3 Experimental techniques 46
3.1 Instrument excitation 46
3.1.1 Electromagnetic driving 47
3.1.2 Loudspeaker excitation 48
3.1.3 Impulse excitation using an impact hammer 49
3.1.4 Comparison 51
3.2 Velocity response measurement 51
3.2.1 Comparison of admittance measurement methods 52
3.3 The physics of transducers 54
3.3.1 Accelerometer 55
3.3.2 Force transducer (load cell) 58
3.3.3 Impulse hammer force measurement 60
3.4 Reading signals from transducers 61
3.5 Attachment of transducers 61
3.6 Suspension of the instruments 63
3.7 Excitation locations 66
3.8 The coherence function 67
3.8.1 Calculating the CPSD and APSD using Welch's method 68
3.8.2 Coherence between real input and output signals 70
3.9 Calculating power output using spherical-harmonic decomposition . . . 73
3.9.1 Sound Pressure 73
3.9.2 Source strength 76
3.9.3 The half-wavelength problem 77

4 Experimental Methods 80
4.1 Measuring radiation efficiency, η 80
4.2 Calibration 85
4.2.1 Calibration of transducers 85
4.2.2 Calibration of the sound card 88
4.2.3 Microphone calibration 88
4.2.4 Consistency of the automated hammer strikes 89
4.3 Experimental method for measuring velocity with a 3D scanning laser vibrometer 89

4.3.1 3D input admittance method 94
4.3.2 Background noise 94

5 Measurements on four classical guitars 96
5.1 Classical guitar, BR2 100
5.1.1 BR2 excited at position 1 101
5.1.2 BR2 excited at position 2 116
5.1.3 BR2 excited at position 3 119
5.1.4 BR2 excited at position 4 121
5.2 BR1, DLC and MAL classical guitars 123
5.2.1 Comparison with BR2 129
5.2.2 Individual mode behaviour 133

6 η measurements on an experimental guitar 138
6.1 The experimental guitar 138
6.2 η of an isolated top plate 140
6.3 η of the experimental guitar with an 11.5 mm high bridge bar 142
6.4 η of the experimental guitar with a 7 mm high bridge bar 144
6.5 η of the experimental guitar with no bridge bar 145

7 A case study on blocking the sound hole of two classical guitars 147
7.1 The effect of blocking the sound hole on BR2 147
7.1.1 Vibrational behaviour of BR2 147
7.1.2 ODS of the $T(1,1)$ modes 149
7.1.3 Band data measurements 152
7.1.4 η for BR2 excited at position 1 with the sound hole blocked . . 154
7.2 The effect of blocking the sound hole on BR1 158

8 Measurements on other stringed instruments 161
8.1 Steel-string guitars 161
8.1.1 Studied instruments 161
8.1.2 3D input admittance measured on X10 and S&P 162
8.1.3 Top plate band data 166
8.1.4 Back plate band data 166
8.1.5 X10 η 167
8.2 Violin 170
8.2.1 Violin η 172

8.3 The banjo and oud 175
8.3.1 Banjo and oud top plate band data 175
8.3.2 Operating Deflection Shapes of the oud 178

9 Conclusions **181**
9.1 Further work 183

A η data from all instruments **184**

References **200**

Chapter 1

Introduction

1.1 Motivation and aims of the research

The vibrational behaviour of classical guitars is well understood. Many studies have been made of the guitar's vibrational behaviour within its low-frequency range. The sound radiated by the guitar results from a vibrational and an acoustic component. The vibrational behaviour describes the transfer of energy from the strings to the body and the acoustical behaviour describes the sound radiated by the motion of the body. The acoustical behaviour of classical guitars has not been studied to the same extent as the vibrational behaviour. This is also true of violins and pianos, on which there is a much greater body of work. Nevertheless there has been very little work on sound radiation.

In this thesis the radiated sound fields produced by guitars were measured between 80 Hz and 2000 Hz. The sound-field data was used to determine the radiation efficiency, defined as the ratio of acoustical power output to mechanical power input, across this frequency range. This measurement links both the vibrational and the acoustical behaviour of the instruments. Spherical-harmonic decomposition was used to determine the contributions from component sources (monopole, dipole and higher order sources) to the radiated sound. These source strengths were used to determine the total power output and the power output from monopole and dipole components. Several classical guitars of different designs were studied to investigate the effects of their construction on the radiation efficiency. An experimental guitar, with an altered top plate, was also studied to investigate the effect of the body modes on the instrument's radiation efficiency. Radiation efficiency was also measured on a carbon-fibre steel-string guitar and a violin to investigate the effect of their different designs on the radiation efficiency.

The focus of the studies in this thesis was on physical measurements of the sound radiated by instruments rather than making subjective judgements of their 'quality'. Wegst (2006) states that the 'quality' of the instrument can often be decided by "soft factors" such as its appearance. The Cardiff musical acoustics group has focused on relating the designs of instruments to their mechanical and acoustical behaviour. The effect of these changes on the perceived sound have been studied using psychoacoustical techniques but these are not the focus of this work.

1.2 A brief introduction to the classical guitar

The classical, or Spanish, guitar is part of a family of musical instruments known as chordophones. This classification covers any instrument that produces sound from the vibration of a string and includes many instruments such as violins, lutes and pianos. The development of what is now known as the nylon string (classical) guitar has taken place over the last several centuries. The older instruments used gut strings and these are still available for purchase, but nylon has now replaced gut as the typical string construction material. The guitar first appeared during a similar time period to the lute but has developed along separate lines. One of the major developments in classical guitar construction was made by Antonio de Torres Jurado during the nineteenth century when he enlarged the guitar's body to increase the sound output of the guitar. He also attached wooden braces to the plates so they would not be damaged by the tension produced by the strings on the larger plates. The larger instruments radiated a greater amount of sound which allowed them to be used for performances in larger halls rather than just for chamber performances.

1.2.1 Guitar construction

Figure 1.1 shows the construction design of the elements of a typical classical guitar. Typically spruce or cedar is favoured for top plates and rosewood or other hardwoods are used for the back plates and ribs of classical guitars (Haines, 1981). As wood is an inhomogeneous material the top and back plates are constructed so that the grain of the wood runs parallel with the direction of the neck. Typically a thinner plate will be able to vibrate more easily and therefore produce a louder sound than a thicker plate. However, plates which are too thin can produce "disturbing overtones and dissonances" unless the struts are "strategically placed" (Sloane, 1976). Also if the top plate is too thin the instrument will buckle under the tension of the strings far more quickly than if a thicker plate were used, resulting in permanent damage to the instrument.

Figure 1.1: The components used in the construction of the classical guitar. Pictures provided by Bernard Richardson.

Additional stiffness is provided to the plates by gluing thin spruce struts to the underside of the top and back plates. For a typical classical guitar top plate there are two horizontal struts located either side of the sound hole, which constrain the main motion of the plate to the lower bout when it is excited at the bridge. There are also several struts which are placed at a small angle to the grain on the lower bout effectively increasing the stiffness along the grain. There are many different patterns of strut placement (Fletcher and Rossing, 1991) but the traditional pattern is fan bracing, which is also known as Torres bracing as shown in figure 1.2. The bracing patterns shown in (a), (b) and (c) are normally used for classical guitars and the bracing in (d) is used for steel-string guitars as it provides a much greater stiffness to the top plate to support the higher tension steel strings. The bracing on the top plate increases the stiffness both along and across the grain. The back plate is typically more simply strengthened than the top plate with three horizontal cross struts as shown in figure 1.1. These struts increase the stiffness of the back plate across the grain without adding a considerable amount of mass.

The neck of the guitar is glued to the upper bout of the top plate. The fingerboard is glued to the neck and extends to the top edge of the sound hole. At the far end of the neck is the nut which acts as a termination for the string. The strings pass over the nut to the headstock where they are wound around the tuning posts. The tension (and therefore the tuning) of the strings is altered by turning the tuning pegs which are connected to the tuning machines. There are a number (usually 19 for classical guitars) of metal strips known as frets inserted into the neck. By applying pressure between two frets using their fingers the player can reduce the length of the vibrating string and change the note. The frets are located increasingly close to one another so that each fret corresponds with an increase in frequency of one semitone.

An investigation has previously been made into the effect of the coupling of the neck's vibrations to the body's vibrations and how the overall behaviour changes depending on the method of attaching the neck to the body (Garcia-Mayen and Santillan, 2011). In their study the fingerboard was either glued along its full length, glued at 4 points or not attached to the instrument. No significant change was found in the sound production from the guitar below frequencies of 1 kHz with the different attachment techniques used and studies have not yet been undertaken at frequencies above 1 kHz. A study has been made on the contribution of the string termination at the nut to the radiated sound (White, 1981), in this case the instrument was struck at both the bridge and neck with a small piece of metal to excite it. The sound pressure was measured 3 inches from the sound hole and many similarities were found between the two pressure signals. The sound pressure values were not calibrated in the study by White making it difficult to compare the two measurements with those made in the wider literature.

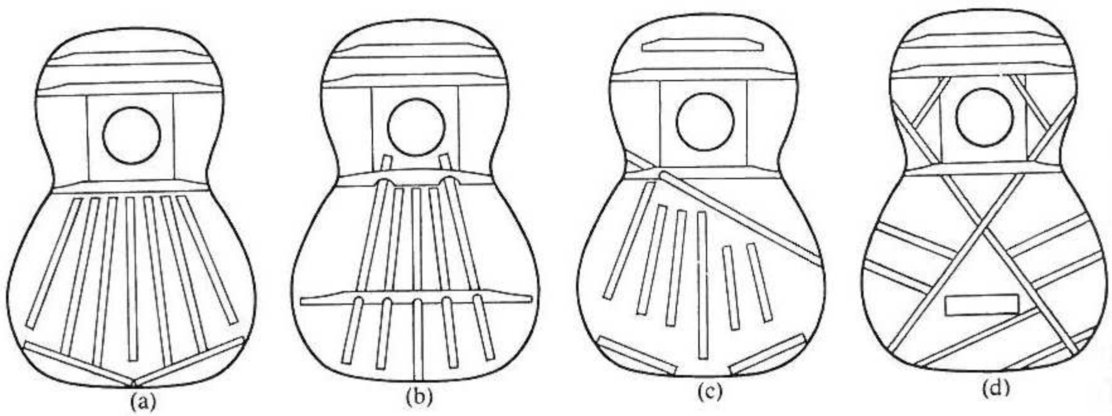

Figure 1.2: Four examples of top plate bracing, (a) Torres fan bracing, (b) Bouchet, (c) Ramirez, (d) crossed bracing. From Rossing et al. (2002). Reprinted with permission from Pearson.

Due to diminishing supplies of rosewood and other woods it has become necessary to investigate possible replacement woods for plates which have similar properties to traditional woods. Parameters have been calculated involving the speed of sound in the wood, c, its density, ρ, and Q values of various woods. Yoshikawa (2007) found that two different linear relationships exist between cQ and ρ/c for woods used for top and back plates. A plot of cQ against ρ/c showed that there are two separate lines of regression for top plate and back plate woods which were found to be orthogonal, showing the different materials required in the construction of guitar plates. Other avenues of investigation for replacement materials have included using carbon-fibre composites for top plates. A study of carbon-fibre composite top plates on guitars found that a plate with unidirectional carbon-fibre reinforcement produced a sound most similar to a wooden top plate (Ono and Okuda, 2007).

1.2.2 Guitar designs

The classical guitar is part of a family of instruments within which there are three main types of instrument, but many variations within these classifications. The three main designs are the classical guitar, steel-string guitar and electric guitar. These instruments normally have six strings but steel-string and electric guitars can be built to accommodate twelve strings as well (six pairs of closely spaced strings with each pair of strings having equal or octave tuning). The classical and steel-string guitars both generate sound using the same principle. Their strings are plucked which causes an excitation of the bridge which in turn excites the top plate, air cavity and back plate. It is the vibration of the body which produces the sounds heard by the listener from the guitar. While steel-string guitars typically have a similar shape to classical guitars there are a few differences in their constructions. Steel strings have a greater tension than nylon strings so the top plate of a steel-string guitar is required to be much stiffer than for a classical guitar. A steel rod (truss rod) is also often inserted into the neck of the instrument to prevent the added string tension bending the guitar's neck. The electric guitar differs from classical and folk guitars in that it typically has a solid rather than a hollow body to reduce the effects of feedback when the sound is amplified. The solid body of the electric guitar reduces the level of string-body coupling so the sound radiated by the body is very small. In order to produce a sound that can be heard by an audience, electromagnetic pick-ups are used which transform the vibrations of the steel strings into an electrical signal which is then sent to an amplifier and loudspeaker.

In this thesis, classical and steel strung guitars were investigated as the body, and the interaction of the strings with it, has a far greater physical contribution to the produced sound than that of the electric guitar where the body is of less importance.

1.3 Sound Production from guitars

The initial source of the sound radiated by a classical guitar is produced by plucking a string that is under tension. The vibrating strings create only a small displacement of the surrounding air and therefore produce only a low level of radiated sound. The strings of a classical guitar are coupled to its body via a wooden bridge to generate a level of sound output that can be heard more easily by the listener. The bridge of a classical guitar is glued to the top of a hollow, usually wooden, body which vibrates when it is driven by the motion of the strings and bridge. It is the vibration of the guitar's body and the air both within and surrounding the body which produces the majority of the radiated sound perceived by the listener. Classical guitar bodies are constructed with a separate top plate and back plate joined by a thin set of wooden ribs which are glued to the edges of the two plates. The top plate has a circular sound hole which increases the level of output, especially at low frequencies (Christensen and Vistisen, 1980).

Violins are constructed using a similar principle but have curved plates and a sound post, which is held in place between the top and back plate by the pressure exerted on the bridge by the strings. The equivalent of the sound hole on a violin takes the form of two 'f-holes' on the top plate. The bridge of a classical guitar is glued onto the top plate but the bridge of a violin in held in place by the tension of the strings.

As the plates are constructed from two pieces of wood joined together, the wood should be symmetrical so that the grain runs in the same direction on both pieces. The plates are designed so that the grain is parallel to the strings which results in a higher level of stiffness in one direction compared to the other.

1.3.1 Strings

There are six strings on a classical guitar and in standard tuning the frequencies of the fundamentals of the strings are 82 Hz, 110 Hz, 147 Hz, 196 Hz, 247 Hz and 330 Hz which correspond with the notes E_2, A_2, D_3, G_3, B_3 and E_4 respectively. When a flexible, uniform string with no stiffness, fixed at both ends, is plucked the fundamental frequency, f_1, is excited. f_1 depends on the tension, T, linear density, ρ_L, and length, L, of the string as shown in equation 1.1 (Kinsler et al., 1980).

$$f_1 = \frac{1}{2L}\sqrt{\frac{T}{\rho_L}} \tag{1.1}$$

The $\sqrt{T/\rho_L}$ term is the phase speed, c. When a string is excited not only is the fundamental frequency of the string driven but so are a series of integer multiples of f_1, which are known as harmonics. To calculate the frequency of the n^{th} harmonic of an ideal string equation 1.1 is multiplied by n. For a *real* string, which has stiffness, the higher-order frequency terms are no longer simply integer multiples of the fundamental although for lower values of n they are similar. As the higher-order components are no longer harmonically related to one another in a real string they are referred to as *partials* rather than harmonics. The equation describing the frequency of a partial, f_n, of a stiff string is (Morse, 1948)

$$\begin{gathered} f_n = nf_1[1 + \beta + \beta^2 + \frac{n^2\pi^2}{8}\beta^2] \\ \beta = \frac{a^2}{L}\sqrt{\frac{\pi E}{T}} \end{gathered} \tag{1.2}$$

where a is the string radius and E is the Young's modulus. The three lowest strings (E_2, A_2 and D_3) of a classical guitar are made of a stranded nylon core wrapped round with metal, typically brass. The top three strings (G_3, B_3 and E_4) are made of nylon monofilament with no metal wrapping. Wrapping the lower strings with metal increases the mass of the strings, which results in a lower f_1. The metal wrapping increases the mass with a smaller increase in the string radius than if the equivalent increase in mass was achieved by increasing the amount of nylon used. Metal wrapping also keeps the string flexible. By keeping the thickness of the strings to a minimum the level of inharmonicity of the higher frequency partials is reduced as a result of the a^2 relationship in β shown in equation 1.2. Inharmonicity is also introduced in real strings by a lack of uniformity in the string. This often results from the strings being worn down by the metal frets during playing.

The strings used for steel-string guitars and violins have a different construction from those used for classical guitars. The four lowest-frequency strings of a steel-string guitar have a steel core which has metal windings and the two highest frequency strings are made of steel monofilament (plain wire). The strings on a violin are made of either steel, gut or nylon which are wound with silver, aluminium or steel (Fletcher and Rossing, 1991).

1.3.2 Coupling strings to the body

All stringed instruments have their strings coupled to their bodies. This creates an interaction between the strings and the body and also vice versa. The coupling occurs at the bridge which allows for the vibrations of the strings to drive the top plate and produce a far louder radiated sound than that produced by the strings alone.

A set of thin wooden ribs are glued to the edge of the top plate and a back plate (of the same dimensions as the top plate) is glued to the ribs. The inclusion of the ribs and back plate creates an air cavity within the instrument which increases the level of sound pressure radiated by the body below 200 Hz (Christensen and Vistisen, 1980). However, it is the top plate that is often regarded as the main source of sound production in classical and steel-string guitars. To demonstrate the importance of the top plate in sound radiation, Antonio de Torres designed a guitar with a papier maché back and sides but a traditional top plate (Romanillos, 1990). The papier maché elements of this instrument were still driven by motion of the top plate but this design was used to show that non-traditional materials could be used in guitar construction and a recognisable guitar sound could still be produced from the top plate. In this case the instrument was judged to have “an excellent sound”.

The vibration of the top plate couples with the air cavity and results in a transfer of vibrations from the plate to the air enclosed in the cavity and the external surroundings (Christensen and Vistisen, 1980). The back plate is coupled to the top plate, through the ribs, and also to the air cavity. Fletcher and Rossing (1991) state that the top plate and bridge provide the high frequency response and the air cavity, back plate and top plate provide the lower frequency response. The back plate does not vibrate as much as the top plate because the strings are coupled to the top plate, therefore the back plate does not contribute as much to the radiated sound as the top plate. The sound hole on the top plate allows the air cavity to act in a similar fashion to a Helmholtz resonator which increases the level of sound radiation produced by the body in the low-frequency range of the guitar.

1.4 Modes of vibration of the classical guitar

When a guitar is excited by an external force, whether from the vibration of the strings or a strike on the instrument, many of the instrument's natural modes of vibration are excited. The resonance frequencies and shapes of these modes are determined by the physical properties of the instrument including the shape, thickness and stiffness of the plates and ribs. The lowest-frequency body mode is known as a neck-bending mode, which produces only a very low level of sound. Figure 1.3 shows the motion of a classical guitar at the resonance frequency of the neck-bending mode. The colour scale in the figure uses a 'reverse rainbow' scale where blue represents the areas of greatest velocity and red represents the areas of smallest velocity. The mode shapes were measured using a 3D scanning laser vibrometer as part of the study into the vibrational behaviour of stringed instruments in this thesis. The instrument pivots about the central nodal line to produce this motion. The neck-bending mode is a dipole-like mode and does not displace a considerable volume of the surrounding air. This occurs because the mode displaces air with opposite phase motions. As the mode is at a low frequency these opposite phase sound pressure components cancel one another out and produce acoustical short circuiting.

Figure 1.4 shows the input admittance and normalised sound pressure measured on a classical guitar below 300 Hz. Input admittance, Y, is defined as the velocity response, v, divided by the applied force, F, (v/F) when both are measured at the same point. The sound pressure was measured 0.45 m from the sound hole with the microphone facing the instrument. The sound pressure measurement was normalised with the input force used to produce the response. The first peak in the input admittance at 75 Hz is the neck-bending mode which was shown in figure 1.3. There is no equivalent peak in the sound pressure data, at any angle, which confirms that the mode does not radiate a measurable level of sound. The next three peaks occur at the same frequencies in both the input admittance and sound pressure data so therefore they radiate sound

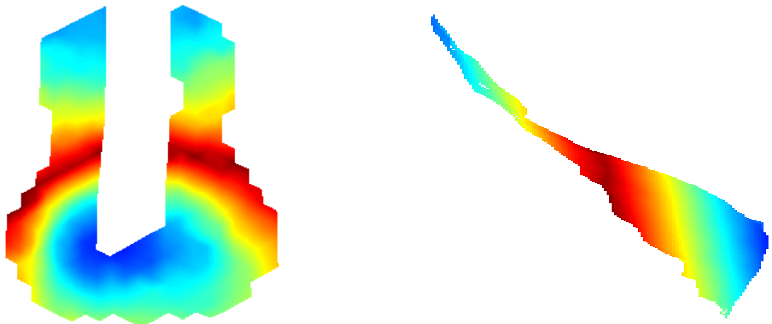

(a) Viewed from above. (b) Viewed from the side.

Figure 1.3: Neck-bending mode of a classical guitar measured using a 3D scanning laser vibrometer.

directly in front of the instrument. In the admittance data there is a peak at 208 Hz but there is a sudden decrease in the radiated sound pressure at this frequency. Unlike the neck-bending mode this body mode does in fact radiate sound but it has a highly directional characteristic with a much greater amount of sound pressure being radiated to the left and right of the instrument than in front of it. The reduction in the sound radiated in front of the instrument therefore results from the directional characteristic of the body mode which has a dipole-like sound field.

The lowest-frequency mode of vibration that radiates an appreciable level of sound pressure from a classical guitar results from the top plate and back plate moving in a single phase movement across a large area of their surfaces. This mode has one large anti-nodal area on the top and back plates which displaces a large volume of air. At higher frequencies it is not possible for a single area of the instrument to vibrate. Instead there are an increasing number of vibrating anti-nodal areas with alternate phases separated by nodal lines. As the frequency increases so do the number of anti-nodal areas of the body modes.

1.4.1 Classical guitar mode naming convention

The convention used in this thesis to describe the shapes of body modes is that generally used by the Cardiff musical acoustics group, where the number of anti-nodal regions both perpendicular and parallel to the grain of the wood are counted[1]. As modes of vibration predominantly occur on either the top plate or back plate, the modes are

[1]Another method used to describe mode shapes within the literature is to count the number of nodal lines perpendicular and parallel to the grain, excluding the nodal lines at the edge of the plate, (Rossing et al., 1985) but this is not used here.

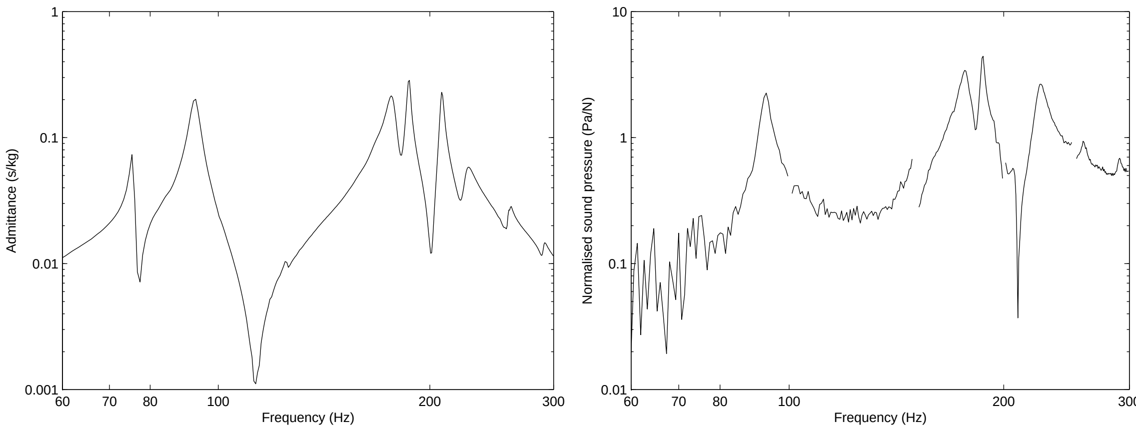

(a) Input Admittance of a classical guitar. (b) Sound pressure measured in front of a classical guitar.

Figure 1.4: Two transfer functions from a classical guitar.

distinguished by using T for top plate modes and B for back plate modes. So a mode on the top plate with two anti-nodal regions perpendicular and one parallel to the grain will be denoted as $T(2,1)$. There are certain body modes which have the same number of anti-nodal areas with the same orientation but at different frequencies. In this case there is a phase difference between the vibrating regions resulting in this frequency difference despite similar mode shapes being present. To distinguish between two modes with the same number of anti-nodal areas, a numbered subscript is used. The lower frequency mode has the lower subscript; i.e. $T(1,2)_1$ has a lower resonance frequency than $T(1,2)_2$. This mode-naming system has limitations at higher frequencies where the anti-nodal areas are less clearly divided horizontally and vertically. This nomenclature is suitable for the body modes within the frequency ranges studied in this thesis.

The guitar's top plate behaves in some ways like a clamped rectangular plate. The similarity results from the ribs acting to clamp the top plate around the edges. The first three modes of a rectangular plate follow the same pattern as for a guitar which are (1,1), (2,1) and (1,2) (Fletcher and Rossing, 1991). This is ignoring any phase changes or additional modes produced by the addition of the air cavity, back plate and ribs to the guitar.

1.4.2 Low-frequency resonance triplet

There are three main resonances which are responsible for much of the radiation of sound below 300 Hz on classical guitars. These resonances are produced by coupling between the lowest frequency modes on the top plate, back plate and the motion of the air

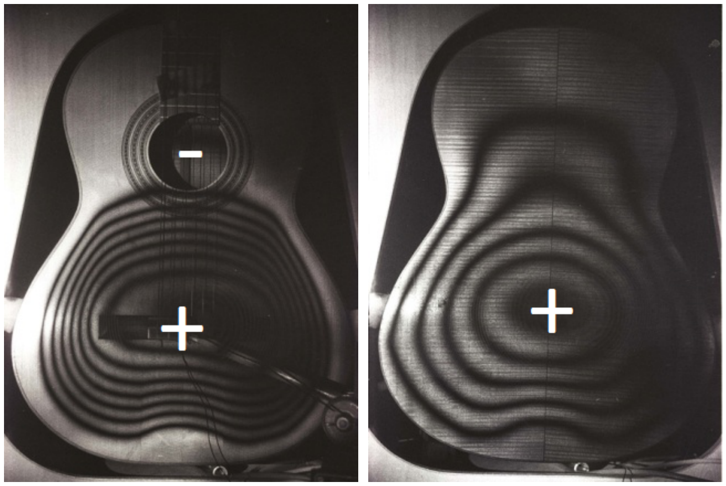

(a) $T(1,1)_1/B(1,1)_1$

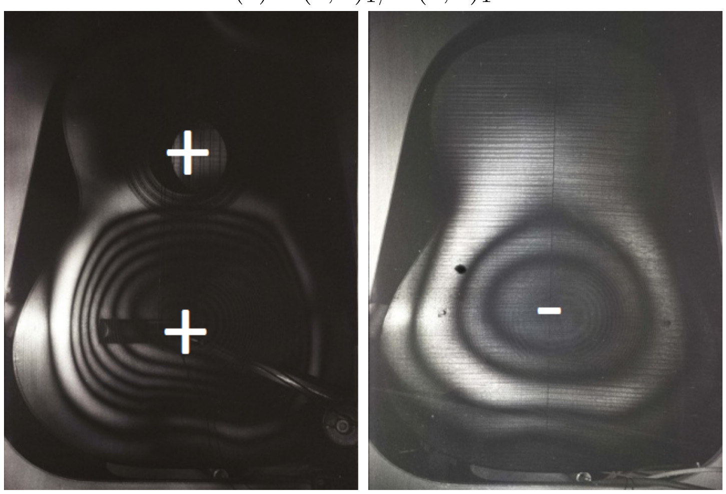

(b) $T(1,1)_2/B(1,1)_2$

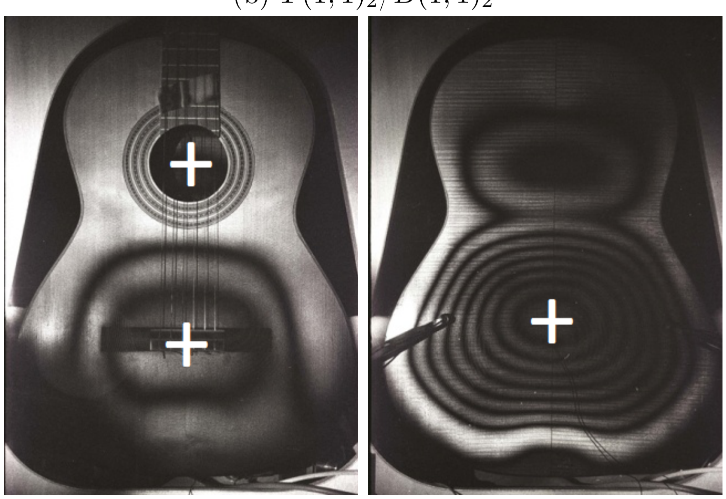

(c) $T(1,1)_3/B(1,1)_3$

Figure 1.5: Low frequency resonance triplet measured on the top plate and back plate of a classical guitar from Richardson et al. (2012). In these figures only one plate is driven and the optical fringes show the relative amount of motion on the top and back plates at each resonance.

through the sound hole. The coupling between the three modes can be described using the three-mass model which was developed by Christensen (1982) and was revisited recently by Richardson et al. (2012). The coupling results in a change of the frequencies of peaks in the response curves in comparison with the resonance frequencies of the isolated modes. The low-frequency sound pressure response in figure 1.4b shows the two lowest frequency peaks produced by coupling between these three modes.

The lowest frequency peak in figure 1.4 at 94 Hz is only present on a completed instrument with a top and back plate (Christensen and Vistisen, 1980). This peak therefore results from an interaction between the plates and the air moving through the sound hole. This peak is therefore often called an 'air' mode despite the fact that the plates will obviously also be in motion at this frequency. This peak is described as being the $T(1,1)_1$ mode in this thesis but there is also motion on the back plate at this frequency resulting in the top and back plates both moving outwards together. The term $T(1,1)_1/B(1,1)_1$ would possibly be a more complete description but is a far more unwieldy term. The top and back plate both move outwards in phase and air moves in through the sound hole. As the plates move inwards the enclosed air moves out through the sound hole. This mode is shown in figure 1.5a where + is a motion outwards from the instrument and - is an inwards motion.

The second peak occurs just below 200 Hz and is described as being the $T(1,1)_2$ mode. The majority of the motion of the instrument occurs on the top plate of the instrument and this can be seen in the holographic interferograms in figure 1.5. This is therefore known as a 'wood' mode although there is motion of the air, in phase with the top plate, and an out of phase motion of the back plate.

The third peak is not visible in the pressure response of the instrument shown in figure 1.4b but there is a $T(1,1)_3/B(1,1)_3$ mode where the majority of the motion of the instrument occurs on the back plate. For this mode the top plate, back plate and air motion all move inwards and outwards with the same phase. When referring to any the $T(1,1)$ modes of any guitar in this thesis, the motion is a result of the coupling of the actual modes of the plates and enclosed air rather than a single mode.

The interaction between these three modes produces a residual response both in velocity and radiated sound pressure at frequencies well above the frequency of the third peak. The residual pressure response is produced by the motion of the top plate and is proportional to A_p/m_p, where A_p is the area of the top plate and m_p is its mass. This residual response is produced by any mode above its resonance frequency. Richardson et al. (2012) showed that changing the frequency of the back plate mode shifted the resonance frequency of $T(1,1)_2$ the most while the resonance frequency of

$T(1,1)_1$ changed by only a few Hz. $T(1,1)_1$ and $T(1,1)_2$ radiate sound fairly evenly in all directions with very little directionality in the sound fields. This results from the single large anti-nodal areas visible on the top and back plate in figure 1.5.

1.4.3 Body Modes

The body modes of a previously studied classical guitar, BR2, are shown in table 1.1. The radiated sound fields were measured as part of the study of radiation efficiency within this thesis, shown in chapter 5.

There are several well-documented body modes at frequencies above the low-frequency resonance triplet which have been studied using holographic interferometry by Richardson (1982). These higher frequency modes are typically 'wood' modes but there is an effect from higher order 'air' modes as well (Elejabarrieta et al., 2002a). The lowest frequency modes involve the movement of larger areas of the lower bouts of the plates. As the frequency of the modes increases, the plates vibrate with increasing numbers of smaller vibrating areas, each with alternate phase. The first of these modes is usually the $T(2,1)$ mode, the third figure in table 1.1 This mode has is a nodal line through the centre of the bridge with two anti-nodal vibrating regions of opposite phase below the sound hole either side of the nodal line. This mode cannot be put into motion by exciting the instrument exactly at the centre of the bridge as the mode undergoes no motion there.

The top-plate modes show increasing numbers of anti-nodal areas at higher resonance frequencies. The increasing number of anti-nodal areas result in more directional sound fields. The $T(1,1)_1$ mode radiates largely equal sound pressure in all directions but there are clear lobes of greater radiated sound pressure for the $T(4,2)$ mode. Modes with higher resonance frequencies show an increase in the number of vibrating regions and nodal lines making it harder to excite the higher frequency modes unless the position of the excitation is chosen carefully.

The resonance frequencies of the body modes of the classical guitar depend upon both the design of the plates and the materials used to construct them. A study made using finite-element-modelling (FEM) showed that the factor that is most influential to the shape of the top plate modes and their resonance frequencies is the Young's modulus of the material (Ezcurra, 1996). The density of the wood changed the resonance frequencies of the body modes but not the relationship between them. The Poisson ratio and shear moduli had only a minimal effect on the modes.

Mode Name	Mode Shape	Sound Field
$T(1,1)_1$ - 93 Hz	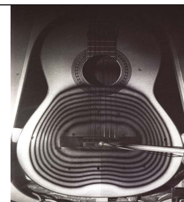	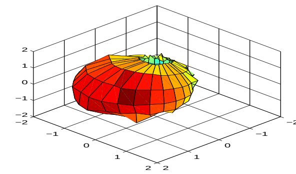
$T(1,1)_2$ - 187 Hz		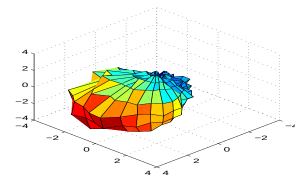
$T(2,1)$ - 208 Hz	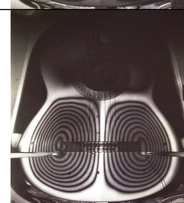	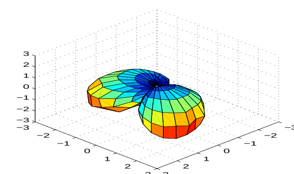
$B(1,2)_1$ - 227 Hz	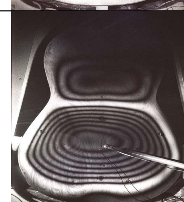	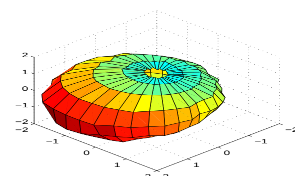
$T(1,2)_1)$ - 371 Hz	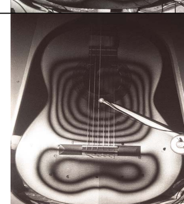	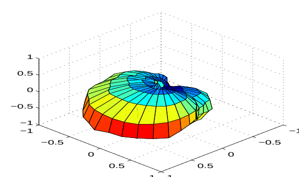
$T(1,2)_2$ - 413 Hz		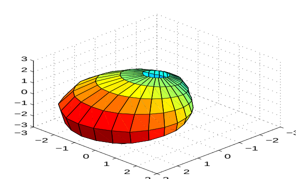
$T(3,1)$ - 446 Hz	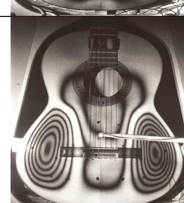	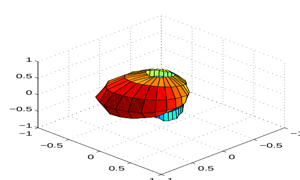
$T(4,2)$ - 537 Hz	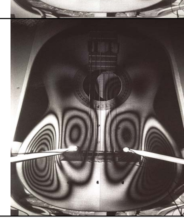	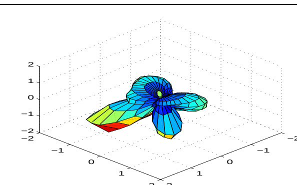

Table 1.1: Body mode shapes and sound fields from a classical guitar (Mode shapes provided by Dr Bernard Richardson).

1.5 Thesis structure

The construction of the guitar and a brief explanation of some of the elements of its design and how it radiates sound have been covered in this chapter. An overview of some of the studies and techniques previously used to investigate the behaviour of stringed instruments is provided in chapter 2. A comparison and explanation of the available experimental techniques and equipment is provided in chapter 3 and the experimental methods used in this thesis are described in chapter 4. Radiation efficiency, power and 3D admittance values are shown in chapter 5. The behaviour of an experimental guitar with an altered top plate is presented in chapter 6 and the effect of the sound hole on the vibrational behaviour and radiated sound of two instruments is studied in chapter 7. Finally, the behaviour of several other stringed instruments including two steel-string guitars, a banjo and an oud is shown in chapter 8.

Chapter 2

Summary of previous research

When making comparisons between musical instruments, 'quality' is a term often used by players and makers to distinguish between them. This is a highly subjective term which varies depending on personal requirements and playing style. While the opinion of an instrument's quality is ultimately important, without making an objective study of the behaviour of a musical instrument it is difficult to create systematically instruments which are deemed to be of a 'good quality'. Within the field of musical acoustics there are two main branches of study, acoustics and psychoacoustics. Acoustics focuses on the physical behaviour of musical instruments whereas psychoacoustics is the study of how changes in the radiated sound are perceived by the listener. The study of the physical behaviour of stringed instruments is the main area of interest for this thesis.

It is not complicated to design an instrument that has a louder initial sound when the strings are plucked or that allows the strings to sustain their vibrations for longer. A louder instrument can be built by using thinner wood for the top plates. If the instrument is designed to have a louder initial amplitude the same amount of energy will typically be supplied from the string to the plate as for an instrument with a lower initial amplitude. The instrument with a louder initial amplitude will have a faster decay of the sound. If the strings are too strongly coupled to the guitar then the issue of wolf notes and over-coupling can occur. Wolf notes occur when there is a strong coupling between a string partial and a body mode which are closely spaced in frequency. The interaction between the two vibrations leads to a "cyclic stuttering response" of the string (Schelleng, 1963) and also beating effects in the radiated sound. A longer sustain from the string vibrations can be achieved by making the bridge and top plate heavier so that less energy is transferred from the strings to the body. This results in a much quieter radiated sound. As such it is not simply a case of making a louder or quieter instrument to appeal more to one style of playing or another.

Any meaningful physical measurement made on a stringed instrument should relate either to the motion of the instrument or its radiated sound. The behaviour of an instrument varies considerably depending on where it is excited and where the response is measured. The measurement locations must therefore be chosen carefully and clearly defined. The difference in the measured response across the surface of the instrument results from the shapes of the body modes (as shown in table 1.1). Each body mode has anti-nodal areas which are easily excited and also nodal lines between them where the mode cannot be driven. Not only must the locations of any measurements made on the surface be carefully defined and recorded but the same applies for sound pressure measurements. It is of importance to know where the sound pressure was recorded in relation to the instrument as musical instruments of all kinds do not radiate sound equally in all directions. Work done by Meyer (1972) showed that stringed instruments radiate sound evenly at low frequencies but at higher frequencies there are clear lobes in the radiated sound pressure.

To make measurements of an instrument's response, such as force, velocity or sound pressure, transducers are used. Transducers convert a physical measurement into an electrical signal. The electrical signal can be sent to a computer or other devices for further analysis. The physics and workings of transducers are described in section 3.3. Transducers and sensors from suppliers are typically factory-calibrated before sale. However, a single measurement of an output response, even if it is correctly calibrated, will not necessarily describe the behaviour of an instrument. Response measurements should be normalised with the excitation to prevent changes in the applied force affecting the value of the response signal.

To describe fully an output response, so that the behaviour of several instruments from different studies can be easily compared, the output should be normalised to a known input, such as force or power. The measurement known as the admittance (or mobility) is the velocity response normalised with the applied force that generated the response.

2.1 Admittance of guitars

The admittance is a measurement known as a frequency response function, or FRF. An FRF shows the frequency dependent output from a system in comparison with its input. Admittance, Y_{ij}, is the ratio between the velocity response, v_i, measured at a position i and the applied force, F_j, at a position j at a frequency ω.

$$Y_{ij}(\omega) = \frac{v_i(\omega)}{F_j(\omega)} \tag{2.1}$$

Two different types of admittance measurements can be made, either an input admittance or a transfer admittance. The input admittance is where the force and velocity are both measured at the same point on the instrument, $i = j$. Input admittance measurements are typically made on the bridge of an instrument as close as possible to where the strings couple with the body. By measuring admittance close to the string termination, the FRF gives an approximation of the velocity generated on the bridge from the force applied by the vibrating strings. As the transfer of vibrations from the strings to the body is of most importance to the production of sound from a classical guitar, the input admittance can be used to give an indication of the level of the transfer of vibrations from the string to the body. The transfer admittance, $i \neq j$, can be used to determine the mode shapes or operating deflection shapes (ODS) of an instrument at a single frequency by measuring the velocity on a grid of points across an instrument. This technique is known as modal analysis. The admittance values at each grid point can then be used to visualise the mode shapes and ODS of the instrument. Mode shapes show the motion of a single mode vibrating at one frequency. This requires the instrument to be driven at the anti-nodal region of the mode of interest whilst avoiding the anti-nodal regions of other body modes. ODS shows the motion of all of the body modes in motion at a single frequency. ODS can inadvertently be produced when studying individual body modes if the driving location of the mode is not chosen carefully.

Admittance measurements have been made on violins and guitars throughout the last few decades. The first measurements of admittance were made with the applied force and velocity both measured in the out-of-plane direction. Jansson et al. (1986) studied several methods for measuring the input admittance on a violin. Moral and Jansson (1982) used the input admittance to show that above 2 kHz on a violin the vibrational properties are determined by the density of body modes rather than individual resonances. Christensen and Vistisen (1980) used the input admittance to study the effect of changes to the top plate and sound hole of a guitar on the lowest frequency body modes. Elejabarrieta et al. (2000) measured the admittance of a guitar top plate as it was constructed to investigate the changes in behaviour of the plate with the adding of struts.

More recently it has become possible to measure the velocity response in the in-plane directions as well as the out-of-plane direction. Lambourg and Chaigne (1993) measured the 2-dimensional admittance at the bridge of a classical guitar. When a string is plucked on a guitar the string is polarised in two directions. The string vibrates into the plate, the x direction, and also perpendicular to the bridge, the y direction. The 2D admittance was measured to investigate the motion that would be produced by an instrument in the out-of-plane and in-plane directions. Boutillon and Weinreich (1999) measured the admittance on a violin bridge in three dimensions by placing three accelerometers on a small block facing in each of the three cardinal directions. While 2D and 3D admittance measurements can be made, the 1D input admittance is the most frequently made measurement as it measures the response from an out-of-plane excitation. This is in the same direction as the motion that produces the greatest displacement of air and the greatest radiation of sound pressure on classical guitars.

Measuring the input admittance across a range of frequencies allows the resonance frequencies of the body modes of the instrument to be determined. Peak fitting techniques can be used to extract the effective mass and Q values of the body modes from the data (Richardson, 2001). These values can be used to compare the behaviours of the body modes of several instruments. The locations of the force excitation and the velocity measurement must be chosen and defined carefully as the location of the two measurements will alter the information in the admittance measurement.

The transfer admittance is obtained when the force and velocity are measured at two separate points on the same instrument, $i \neq j$. It is normally measured with the applied force being measured at the bridge and the velocity measured elsewhere on the body, (Hill et al., 2004) and (Richardson, 2001), but can be made with both measurements made on the bridge at separate locations. (If the velocity is measured at an anti-nodal region of a mode, then the FRF will give an approximation as to how much a mode will be driven by the string vibrations at the bridge.) As guitars are nearly completely linear systems, the location of measurement of force and velocity can be switched and the same FRF characteristics should be present.

If the input admittance is measured with both the force and accelerometer orientated in the same axis, then the measured value of Y can be described as being an element of the admittance matrix, $\boldsymbol{Y}$. $\boldsymbol{Y}$ contains input admittance measurements made in the same directions and also orthogonally. If the direction into the bridge is referred to as x and the two transducers are aligned in this direction then the input admittance can be written as Y_{xx}. Taking the direction across the bridge to be y and parallel to the strings to be the z direction then a 3D admittance matrix can be written as (Boutillon and Weinreich, 1999)

$$\boldsymbol{Y} = \begin{pmatrix} Y_{xx} & Y_{xy} & Y_{xz} \\ Y_{yx} & Y_{yy} & Y_{yz} \\ Y_{zx} & Y_{zy} & Y_{zz} \end{pmatrix} \tag{2.2}$$

To make measurements of an individual component within the admittance matrix in equation 2.2 the force and velocity must both be measured *only* in their respective directions. If either force or velocity is measured in an off-axis direction then the measured input admittance will be a mixture of several components within the 3D admittance matrix. This mixture of admittance measurements cannot be separated and the result will therefore be unusable and will produce a misleading result. Rotational terms should also be included in the admittance matrix, which would result in a 6x6 matrix. These can be ignored if "no torque is exerted on the rigid body when forces are applied to the point" (Boutillon and Weinreich, 1999).

If the guitar is truly a linear system, as it is assumed to be, then the off-diagonal components will be equal as a consequence of the principle of reciprocity (Boutillon and Weinreich, 1999). The excitation and response measurements are usually made at separate points on the instrument rather than at the same point. If the two measurement locations are closely spaced then the measurement can be assumed to be an input rather than a transfer admittance. An example of the reciprocity of a classical guitar is shown in figure 2.1. The locations of the force and acceleration measurements were swapped for the two measurements and the absolute values of admittance and the phase of the admittance are almost exactly equal. This shows that the location of the force and velocity measurements can be switched and the same result will occur.

Classical guitars have a considerable number of modes of vibration and as such they can be classified as Multiple-Degree-Of-Freedom (MDOF) systems (Ewins, 1984). A system with a single mode of vibration would be classified as a Single-Degree-Of-Freedom (SDOF) system. In an SDOF system, the resonance would appear as a single clear peak in a FRF curve but in an MDOF system there are a series of peaks which each relate to a mode of vibration or degree of freedom. The frequency of each clearly separated peak in an admittance curve corresponds to the resonance frequency of a mode of vibration in the guitar. The resonance frequencies can then be used to drive individual body modes of the instrument, providing that the driving location lies in an anti-nodal area. Additionally the driving location should lie at the nodal lines of other body modes if possible so that they are not excited. However, at higher frequencies it is harder to examine individual modes as their peaks have lower amplitudes and they are nearer one another in frequency. The closeness in frequency of the modes results in

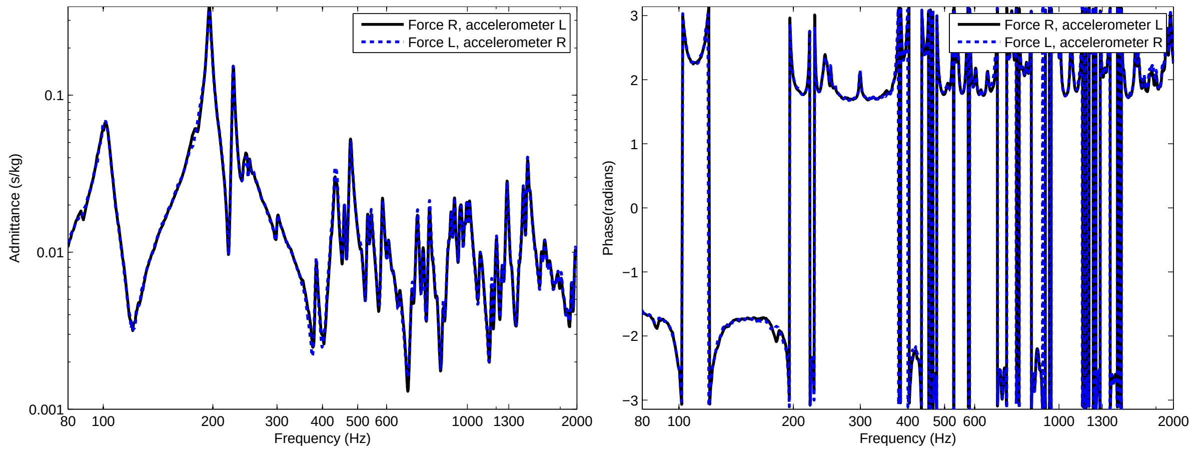

(a) Input admittance. (b) Phase response.

Figure 2.1: Admittance measurements from classical guitar BR1, L denotes a measurement between the B3 and E4 strings and R is a measurement to the right of the E4 string.

modal overlap where individual peaks cannot be separated from neighbouring modes.

A major advantage of measuring the admittance is that it can be measured in any relatively noise-free room. Anechoic conditions are not required as the effect of sound waves reflecting in the room will be negligible on the motion of the instrument. A consideration that must be taken into account is the suspension of the instrument being studied. Any system for supporting a guitar will add some damping, stiffness and mass to the instrument which will change its vibrational behaviour. A discussion of the effects of the damping added to an instrument by a supporting structure is shown in chapter 3. The decision must be made whether the instrument is to be studied under playing conditions or suspended as 'freely' as possible. If the instrument is freely suspended then the effect of a heavier support can be modelled and added to the admittance curve (Ewins, 1984). If there is an effect from damping, additional mass or stiffness on the instrument while the measurement is made then it cannot be removed from the data after the experiment.

An important use of admittance measurements is that they can be used to produce models of the behaviour of a guitar. These models can then be used to see what the effect of changing elements of a guitar's vibrational characteristics has on its output without having to change the construction of a real instrument.

2.2 Simple harmonic oscillator model for velocity and pressure responses

The resonance frequencies of the body modes of a guitar can be easily found by looking at the peaks in an FRF curve. There are also damping factors associated with each mode and it is the combination of the resonance frequencies and decay rates of the modes of the guitar and the strings which produce its characteristic sound. To calculate any damping factors from a mode, curve-fitting techniques must be used. These require a realistic model for the values to have any true meaning.

At low frequencies the radiated sound from body modes is assumed to be monopole in nature and the vibrating modes can be described as damped simple harmonic oscillators with monopole radiation characteristics (Christensen, 1984). Meyer (1972) showed that at low frequencies stringed instruments produce monopole-like sound fields so this is a reasonable assumption. By assuming that a body mode behaves like a piston driven by a force, F, which undergoes a displacement, x, an equation can be developed to describe the velocity, v, (and therefore the admittance) of individual modes of vibration. The piston is described as having a mass, m, a stiffness, k, and a damping coefficient, R. For a mode of a guitar, the value m does not correspond to the actual mass of the system set into motion. Instead it is described as being an effective mass which is the value of m that the distributed mode would have if it were a point mass. The forces acting on a damped harmonic oscillator are

$$m\ddot{x} = F - kx - R\dot{x} \tag{2.3}$$

If the assumption is made that the piston moves sinusoidally then a solution of $x = Xsin(\omega_0 t)$ can be used in equation 2.3, where $\omega_0 = \sqrt{\frac{k}{m}}$ is the resonance frequency of the mode. The velocity of a simple harmonic oscillator at a frequency ω is therefore

$$v(\omega) = \frac{F}{m}\frac{i\omega}{\omega_0^2 - \omega^2 + i\gamma\omega} \tag{2.4}$$

where $\gamma = \frac{R}{m}$ is the damping coefficient. The Q-value is used by the Cardiff musical acoustic group and the relationship between γ and Q is $Q = \omega_0/\gamma$. If v is calculated across a range of frequencies then an FRF of a SDOF system will be calculated. To calculate the admittance, equation 2.4 must be divided by F. Equation 2.4 can be used to describe the low-frequency behaviour of classical guitars as the low-frequency modes behave in a similar way to simple harmonic oscillators. In particular the $T(1,1)$ modes of a classical guitar undergo a single motion in the top plate, which is similar to that of the piston described in equation 2.3.

Using the calculated velocity response of the simple harmonic oscillator, the pressure output can be calculated using the assumption that only monopole radiation is emitted from the source. The sound pressure amplitude, p, at a distance, r, is

$$p = -\frac{i\omega\rho}{4\pi r} vA \tag{2.5}$$

where A is the effective area of the oscillator, ρ is the density of air and c is the speed of sound in air. By combining equations 2.4 and 2.5 the pressure output can be written as

$$p = F\frac{A}{m}\frac{\rho}{4\pi r}\frac{\omega^2}{\omega_0^2 - \omega^2 + i\gamma\omega} \tag{2.6}$$

As with the effective mass in equation 2.4, the effective area is not the literal area of the instrument vibrating at that frequency. Instead A is described as being the effective area of the mode if it was a rigid piston. Christensen (1984) used the effective areas and masses as a combined term, A/m, as only the sound pressure produced by an excitation was recorded and the values of the two separate terms could not be determined. This value of A/m determines the residual pressure response above the resonance frequency of the mode. The residual response radiates sound pressure proportionally to A/m at $\omega > \omega_0$. By measuring the velocity, ideally at the same time as the pressure measurement, the effective mass and Q values can be calculated. These values can then be used to calculate the effective area of the mode. Equations 2.4 and 2.6 can be used for MDOF and SDOF systems as long as the modes can be assumed to radiate monopole sound pressure.

The effective area directly relates to the source strength for a monopole. The source strength is the area velocity, which is the effective area of the mode multiplied by its velocity. The same concept can be applied for dipole oscillators, which have two lobes of high sound pressure, but in this case the source strength is proportional to the effective *volume* of the oscillator. For guitars, the higher frequency modes are not monopole in nature but instead have more complex radiated sound profiles with dipoles, quadrupoles and other higher order sources becoming apparent in the radiated sound fields. Hill et al. (2004) studied the sound fields produced by body modes of a single classical guitar up to 450 Hz and the higher frequency modes showed dipole-like behaviour. For these higher-frequency modes the simple harmonic oscillator model can no longer be used to describe the sound radiated by the instrument. The sound pressure produced by higher order components, which have angular components, must be calculated to build an accurate model.

2.3 Sound pressure measurements from body modes

As discussed in section 1.4, the lowest frequency modes of vibration in the guitar correspond with a movement of the lower bout of the top plate. For the two lowest frequency modes, $T(1,1)_1$ and $T(1,1)_2$, there is a single anti-nodal area covering a considerable area of the lower bout of the top plate. The $T(1,1)_1$ mode sees the top and back plate both moving outward in phase but with an opposite phase to the air motion in the sound hole. $T(1,1)_2$ sees the plates moving out of phase, so as one moves inwards the other moves outwards. The motion through the sound hole is in phase with the top plate but out of phase with the back plate (Richardson et al., 2012). The $T(2,1)$ mode consists of two anti-nodal regions of opposite phase divided by a nodal line down the centre of the top plate. By examining these three modes it is possible to see how the increasing number of vibrating regions changes the sound pressure field measured around the instrument. From previous studies (Hill et al., 2004) it has been shown that the $T(1,1)$ modes produce a monopole-like sound pressure field and the $T(2,1)$ mode generates a dipole-like pressure field.

Figure 2.2 shows a monopole and a dipole sound field in arbitrary units, produced using models of their behaviour. The sound fields produced by musical instruments are neither monopoles nor dipoles. The sound fields instead result from combinations of monopoles, dipoles and some higher order sources. Modes which radiate sound relatively evenly in all directions should be described as being monopole-like rather than as monopoles.

2.3.1 Monopole and simple sources

A monopole generates uniform spherical waves travelling outwards from the source (Morse, 1948). It can be described as a small sphere which is uniformly expanding and contracting so that the generated sound waves have no angular dependence (in θ or ϕ). This is the same sound pressure radiation behaviour produced by the simple harmonic oscillator model in section 2.2. Firstly the case of a point source radiating sound pressure will be considered. As there are no θ or ϕ terms for a monopole, the time-dependent wave equation is given at a distance r and time t is

$$\frac{1}{r^2}\frac{\partial}{\partial r}\left(r^2\frac{\partial p}{\partial r}\right) = \frac{1}{c^2}\left(\frac{\partial^2 p}{\partial t^2}\right) \tag{2.7}$$

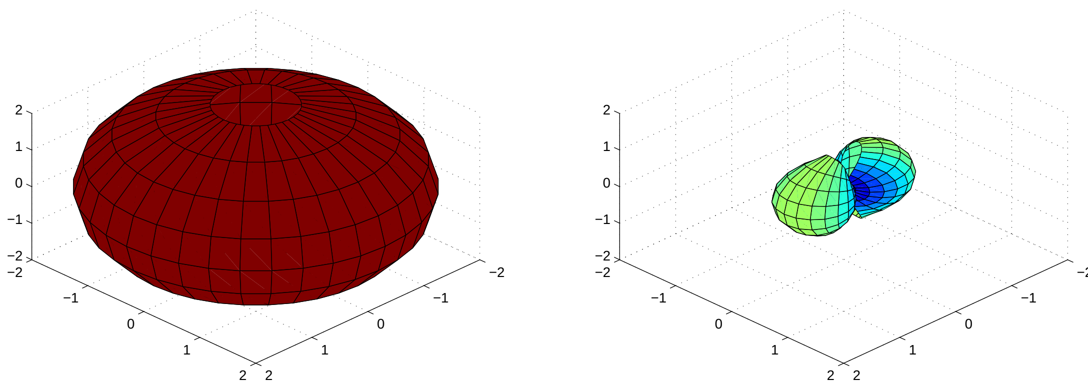

(a) Monopole. (b) Dipole.

Figure 2.2: Monopole and dipole sound fields modelled using MATLAB.

where p is the sound pressure and c is the speed of sound. The general solution used for plane waves can also be applied to equation 2.7 to provide a solution for all cases where $r > 0$ (Fletcher and Rossing, 1991)

$$p = \left(\frac{A}{r}e^{-ikr} + \frac{B}{r}e^{ikr}\right)e^{i\omega t} \tag{2.8}$$

where A is a sound wave moving away from the sound source and B describes a sound wave moving towards the source. To account for the case where $r = 0$ and $p \to \infty$, the sphere must instead be assumed to have a finite size (which is true for all sound sources) of radius a. The radial velocity, v, on the surface of the sphere will still be equal at any point on the surface. The rate of air flow away from the source, S_ω, (which is also the monopole source strength) is then given as

$$S_\omega = 4\pi a^2 v \tag{2.9}$$

To calculate the pressure radiated from this finite sized sphere, a rearrangement of Newton's second law of motion ($F = ma$) is used. This expression is

$$\rho\left(\frac{\partial v}{\partial t}\right) = -\left(\frac{\partial p}{\partial r}\right) \tag{2.10}$$

where ρ is air density. Using equation 2.8 in equation 2.10 for the case where there is only an outgoing wave, $B = 0$, the velocity is given as

$$v = \frac{A}{r\rho c}\left(1 + \frac{1}{ikr}\right)e^{-ikr}e^{i\omega t} \tag{2.11}$$

When $B = 0$ the pressure without a time dependence is simply written as

$$p = \frac{A}{r} e^{-ikr} \tag{2.12}$$

where A is the amplitude of the source. Using equation 2.9 in equation 2.11, at the surface of the sphere where $r = a$, produces a value for A which can then be used in equation 2.12 to show that the pressure, p, is

$$p(r) = -\frac{ik\rho c}{4\pi r} S_\omega e^{-ikr} \tag{2.13}$$

Equation 2.13 is for the case where the vibrating source is small compared to the wavelength of sound. The monopole sound pressure behaves as expected with no directionality term in the equation and the pressure only varies with a dependence on $1/r$.

2.3.2 Dipole sources

A dipole can be described simply as a pair of point sources of equal magnitude and opposite phase separated by a distance, $\boldsymbol{d}$. If the midpoint between the two sources is at point 0 then there is a source of strength S_ω at $\frac{1}{2}\boldsymbol{d}$ and another source of strength $-S_\omega$ at $\frac{1}{2}\boldsymbol{d}$. Unlike monopoles, the sound radiation from dipoles is not spherical. Instead dipoles are characterised by two lobes of higher sound pressure which are orientated in the same axis but facing in opposite directions. Unlike monopoles the orientation of a dipole is important as it will alter the direction of the lobes of higher sound pressure. Due to this directionality the dipole sound pressure is no longer a function of distance alone but also a function of angle. If a measurement of sound pressure is made at a distance r and angle θ from the centre point, 0, then the acoustic pressure, as a function of distance alone (Fletcher and Rossing, 1991), is

$$p = \left(\frac{i\omega\rho}{4\pi}\right)\left(\frac{e^{-ikr_+}}{r_+} - \frac{e^{-ikr_-}}{r_-}\right) S_\omega \tag{2.14}$$

where r_+ is the distance from the centre of the source with positive phase and r_- is the distance from centre of the source with negative phase. As $\boldsymbol{d} \to 0$ then $S_\omega \to \infty$ but the dipole strength, D_ω, remains finite. D_ω can also be written as $S_\omega dz$ where dz is the vanishingly small value of $\boldsymbol{d}$. Equation 2.14 can be rewritten as

$$p = \frac{i\omega\rho}{4\pi}\frac{\partial}{\partial z}\left(-\frac{2e^{-ikr_+}}{r_+}\right) S_\omega dz \tag{2.15}$$

This then gives a final result for the variation of dipole sound pressure as (Fletcher and Rossing, 1991)

$$p = -k^2 D_\omega \frac{\rho c}{4\pi r} \cos(\theta) \left(1 + \frac{1}{ikr}\right) e^{-ikr} \tag{2.16}$$

Equation 2.16 shows that the sound pressure from a dipole source is dependent on both the distance and the angle from the source. This directionality remains even in the far field, so that when $kr \gg 1$ the pressure still varies with $\cos(\theta)$ and $\frac{1}{r}$ in equation 2.16. There is no variation in sound pressure with elevation angle, ϕ, for a dipole source but the dipole can be orientated at any angle of ϕ. As the lobes of the dipole sound pressure output can lie at any angle, either elevation or azimuth, the dipole strength, D_ω, should be written as a vector $\boldsymbol{D_\omega}$ with components D_x, D_y and D_z (Morse and Ingard, 1968). An off-axis dipole can be described in terms of these three different dipole components. The individual dipole components are still functions of frequency but a subscript character should be used to describe the orientation of the dipole. To find the exact contribution of each component to the radiated sound, spherical-harmonic decomposition can be used and this is described in section 3.9. Spherical-harmonic decomposition can be used to determine the source strengths of monopoles, dipoles and other higher order sound sources.

2.3.3 Quadrupoles and higher order sources

As the dipole can be thought of as an arrangement of two simple sources separated by a distance $\boldsymbol{d}$ then a quadrupole source can be thought of as a pair of dipole sources also separated by $\boldsymbol{d}$. As the dipole sources can be described as being orientated on the x, y and z axes, the quadrupole orientations are located across combinations of these three axes. There are five different orientations of the quadrupoles which are xy, yz, z^2, xz and $x^2 - y^2$ (Blanco et al., 1997). The combination of these five quadrupole components form the quadrupole source strength vector $\boldsymbol{Q_\omega}$. The pressure equation for quadrupoles is of a more complicated nature and must be calculated for each orientation of quadrupole; the equation is derived by Morse and Ingard (1968).

The higher order sources (quadrupoles, octopoles etc.) do not generate a considerable amount of pressure in comparison with monopoles and dipoles on classical guitars (Hill et al., 2004). The order of a monopole source can be written as $n = 0$, while $n = 1$ describes a dipole source, a quadrupole has $n = 2$ and so forth. The number of simple sources required to generate a higher order source is therefore 2^n (Morse and Ingard, 1968). It has been found that for sources where $n \geq 2$ (quadrupole or higher), their contribution to a sound pressure field is minimal (Richardson, 2001).

The sound radiated by real instruments does not correspond with a simple monopole or dipole sound field. Instead at any single frequency there will be several body modes vibrating, each with their own radiated sound field characteristics and phase relationships. This results in a sound field which is neither monopole nor dipole in nature but a combination of them both. To describe the sound pressure radiated in a known direction at a particular frequency, an expression for the summed sound pressure from the monopole, dipole and other sources must be used.

2.4 Sound pressure from several sources

At a measurement point there are two different pressure components, sound waves moving towards the source and sound waves moving away from the source. The sound waves moving away from the source are typically of most interest as they show the sound pressure generated by the studied source. The incoming sound waves will either result from reflections within the room where the measurements are made or from any another sound sources present. As such these incoming waves should be kept to a minimum in any experimental set-up, i.e. by making the measurements in an anechoic chamber. At a single measurement point, the total sound pressure from a sound source, $p(r, \theta, \phi)$, as a function of distance and angle is given as (Weinreich and Arnold, 1980)

$$p(r, \theta, \phi) = \sum_{lm} [a_{lm} h_l(kr) + b_{lm} h_l^*(kr)] Y_{lm}(\theta, \phi) \tag{2.17}$$

where $h_l(kr)$ is the spherical Hankel function, a_{lm} is the outgoing wave coefficient, b_{lm} is the incoming wave coefficient and $Y_{lm}(\theta, \phi)$ is a spherical harmonic. The sound pressure is therefore a summation of a series of sources which are based on the spherical harmonic series. If $l = 0$ the source is a monopole, if $l = 1$ the source is a dipole, and $l = 2$ is the equivalent of a quadrupole. The definition used for the spherical harmonic term is

$$Y_{lm}(\theta, \phi) = \left[\frac{2l+1}{4\pi} \frac{(l-|m|)!}{(l+|m|)!} \right]^{\frac{1}{2}} P_l^{|m|}(\cos\theta) e^{im\phi} \tag{2.18}$$

where $P_l^{|m|}(\cos\theta)$ is the associated Legendre function, the square root factor is a normalisation factor, N_{lm}, and l and m are integers used for solutions to the equation. For negative values of m, equation 2.18 is multiplied by 1 and for positive values it is multiplied by $(-1)^m$. The values of l and m describe the order of the spherical harmonics; l can take values from $0 \to \infty$ and m takes values from $-l...0...l$. For $l = 0$ the spherical harmonic corresponds to a monopole shape, $l = 1$ corresponds with a dipole shape with each increase in l resulting in an increase in the order of the source. The equation for spherical harmonics can be used in combination with the other terms in equation 2.17 to describe the pressure field from any sound source which is a combination of polar sources such as monopoles, dipoles and higher order components.

The complex field shapes radiated by stringed instruments can be described as a summation of spherical sources (as shown in equation 2.17). To calculate the incoming and outgoing coefficients for each l and m value, the pressure signal is measured at two different radii at the same θ and ϕ angles. This allows for the incoming and outgoing waves to be distinguished from one another. A technique known as spherical-harmonic decomposition can be used to calculate the a_{lm} and b_{lm} values for each source contained in the summation. By calculating the outgoing coefficient, the source strength can also be calculated. The full details of spherical-harmonic decomposition are discussed in chapter 3.9.

When making measurements of the sound pressure for spherical-harmonic decomposition, it is important to consider the number of measurement locations. To measure the values of a_{lm} and b_{lm} for a monopole only a single measurement position is required, but two separated microphones are still required to distinguish between incoming and outgoing sound waves. The reasoning is that for a *pure* monopole the sound pressure will be the same at any angle providing the radius is constant. For dipoles, $l = 1$, two measurement positions are required if the orientation of the dipole is known. If it is not known then more measurement locations are required to determine it. With increasing values of l, a greater number of measurement positions are required to use spherical-harmonic decomposition accurately. The measurement system used in this thesis involved making sound pressure measurements at 324 points on two measurement spheres. This allowed the use for spherical-harmonic decomposition of components up to and including $l = 3$ (Richardson, 2001). While it is mainly sound sources with $l < 2$ that are of interest, the greater number of pressure measurements allows for the production of higher resolution radiated sound fields.

By plotting the pressure level at each angle of measurement, the radiated sound fields can be depicted. Taking measurements at a greater number of locations results in a higher resolution sound field image which shows the directivity of the sound, even if it does not show the individual source strengths for the components generating the sound.

2.5 Radiation efficiency

Radiation efficiency is a term that has previously been used to describe two different quantities. The first definition, R_{eff}, comes from Fahy (1985), where the radiation efficiency is described as being "the ratio of the average acoustic power radiated per unit area of a vibrating surface to the average acoustic power radiated per unit area of a piston that is vibrating with the same average mean square velocity at a frequency for which $ka \gg 1$". k is the wavenumber and a is the radius of the piston. The other definition of radiation efficiency, η, is used by Lai and Burgess (1990) and Suzuki (1986) and is described as being the ratio between the *acoustic* power output from and the *mechanical* power input to an instrument. The definition of η directly relates the input and the output behaviours. The two definitions of radiation efficiency are presented and compared in this section.

2.5.1 R_{eff}

The equation for the definition of R_{eff} is

$$R_{eff} = \frac{1}{\rho_o^2 c^2} \frac{A}{S} \frac{< p^2 >}{< v^2 >} \tag{2.19}$$

where ρ_o is the density of air, c is the speed of sound in air, A is the surface area of the microphone measurement sphere, $< p^2 >$ is the mean square sound pressure and $< v^2 >$ is the mean square velocity. S is the area of the corpus; that is the total area of the instrument where vibrations can occur and includes the top plate, back plate, ribs and bridge. R_{eff} can be greater than 1, with this result meaning that the instrument would have a greater pressure output than a baffled piston of the same area.

The term R_{eff} has previously been used by Bissinger (2003b, 2004, 2008) to compare the behaviour of a set of violins, with qualities described as varying between 'bad' and 'excellent'. These qualities were determined by a violinist playing scales on the set of instruments (Bissinger, 2003a). The player was then asked to rate the instrument on a scale of 1-10 where 1 was the worst and 10 the best. 'Bad' instruments had a rating of 1-3, 'good' instruments 4-7 and 'excellent' instruments scored 8-10. Bissinger does state that there are issues with only having a single player determining the quality of an instrument but notes that a player is the "only reliable determiner of a 'good' or 'bad' violin".

Values of R_{eff} determined by Bissinger (2003b) are shown in figure 2.3. The black data points are the radiation efficiency measured at the resonance frequency of each of the violin's body modes and the squares show the 250 Hz band average. The band average is the average of R_{eff} measured for the body modes within a 250 Hz range. The figure shows the increase in R_{eff} for both individual modes and the 250 Hz band averages leading to a critical frequency where $R_{eff} = 1$. Above 3000 Hz there are values of $R_{eff} > 1$ where the instruments were able to radiate sound more efficiently than an equivalent baffled piston.

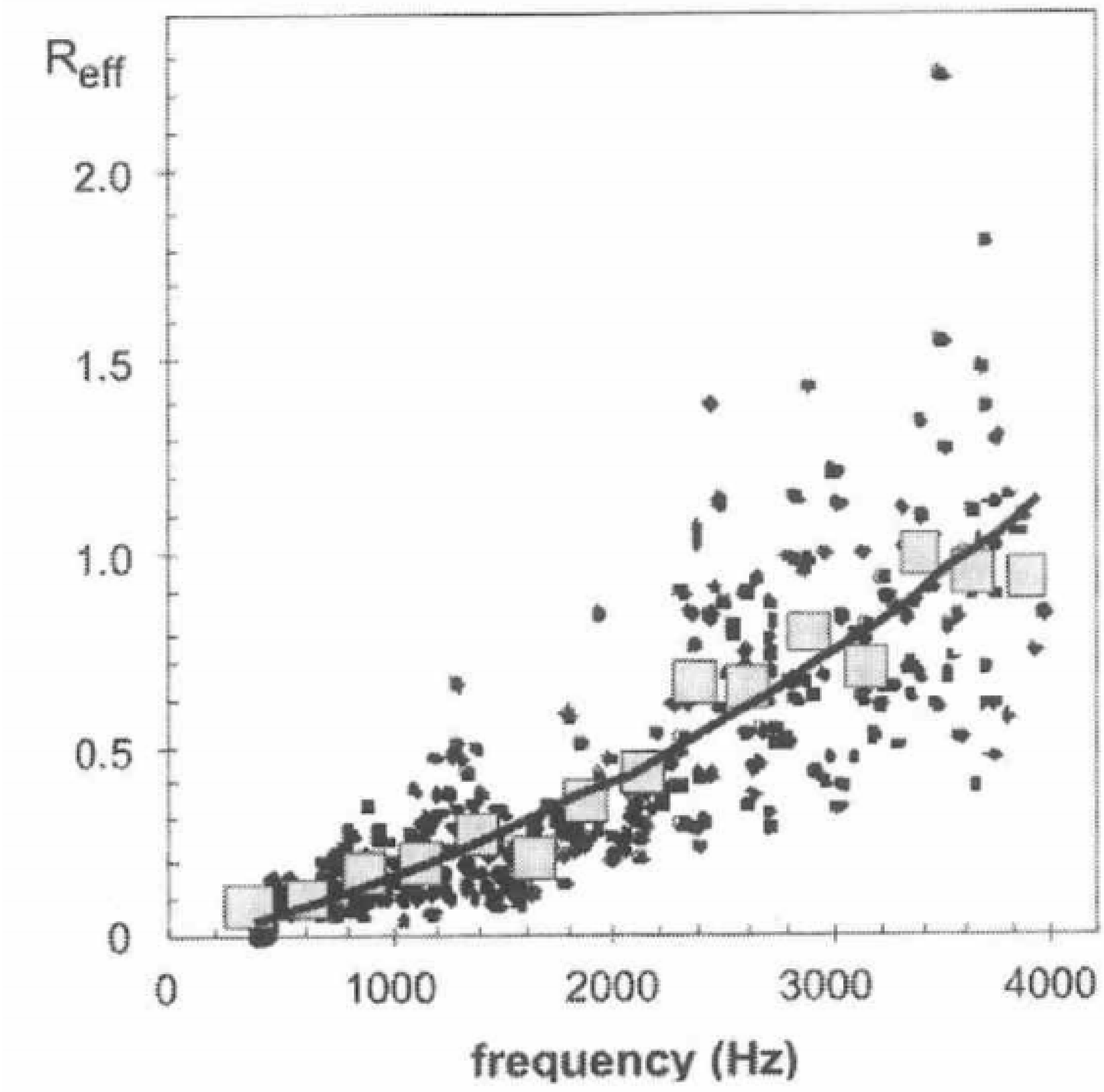

Figure 2.3: R_{eff} determined from 12 violins by Bissinger (2003b). Reprinted by permission of the Catgut Acoustical Society.

In the papers on R_{eff}, an impulse excitation was applied to each violin at the bridge and the resulting sound pressure was measured on a single measurement sphere with a surface area of 18.1m^2, at 266 unique measurement points, in an anechoic chamber.

The mean square pressure was calculated from all 266 pressure measurements. The velocity generated by the impulse excitation was measured separately from the pressure measurements. The velocity was measured using a laser vibrometer at 550 measurement points across the entire corpus. As with the pressure measurements, the mean square velocity was calculated using all 550 locations across the corpus. From measurements made on several violins it was found that the value of R_{eff} increased steadily with frequency (Bissinger, 2003b). R_{eff} was found to increase at a slower rate when the sound post was removed from a violin.

The critical frequency, f_{crit}, of the instrument was determined to occur when $R_{eff} = 1$. The critical frequency is the frequency where the wavelength of the sound waves in air is equal to the wavelength of the natural bending waves in the vibrating plate (Cremer, 1984). Bissinger (2004) states that a lower f_{crit} value is an indicator of a good violin, whereas a higher value of f_{crit} indicates a poorer instrument.

In equation 2.19, A is the only term which relates to a change in the distance of the sound pressure measurement from the instrument. As there is no directionality term in A or elsewhere in equation 2.19, any dipole sound pressure output will not be correctly accounted for. At low frequencies where the sound radiation from musical instruments typically takes the form of monopole radiation (Christensen, 1984) no directional term is required. At higher frequencies the sound radiation fields from musical instruments grow increasingly complex, taking the form of dipoles and other higher order contributions (Hill et al., 2004). At these higher frequencies the instrument can no longer be expected to radiate only spherical sound waves.

As Bissinger's sound pressure measurements were made on a single measurement sphere it is not possible to measure the sound intensity levels of sound waves which are not planar or spherical in shape (Kinsler et al., 1980). It is also not possible to determine whether the sound pressure measured is a result of sound waves moving outwards from the instrument or towards it.

The baffled piston

A baffled piston consists of a vibrating region contained within an otherwise immovable plane and it is often used to describe the sound radiation fields of loudspeakers. The equation used to describe the sound pressure, $p(r, \theta, t)$, in front of a circular baffled piston (Morse, 1948) in the far field ($ka >> 1$) is given as

$$p(r, \theta, t) = -\pi i f \rho_o u_o a^2 \frac{e^{ik(r-ct)}}{r} \left[\frac{2J_1(kasin(\theta))}{kasin(\theta)} \right]^2 \tag{2.20}$$

where f is the frequency, u_o is the velocity of the baffled piston, a is the radius of the piston, k is the wave number, r is the distance from the piston to the measurement location, θ is the angle and t is time. At low values of ka the pressure field has equal levels of sound pressure at all angles, taking the form of a monopole. As the value of ka increases the radiation field becomes increasingly directional with lobes of higher sound pressure levels directly in front and behind the piston but lower levels of sound pressure in other directions. Figure 2.4 shows the change in the directionality of the radiated sound with increasing frequency. These lobes are markedly different from the dipole-like characteristics of some of the higher frequency body modes of the classical guitar, as shown in Hill et al. (2004). The baffled piston therefore does not accurately describe the sound radiated by stringed instruments when they do not radiate a monopole sound pressure field and a different definition of radiation efficiency must be used.

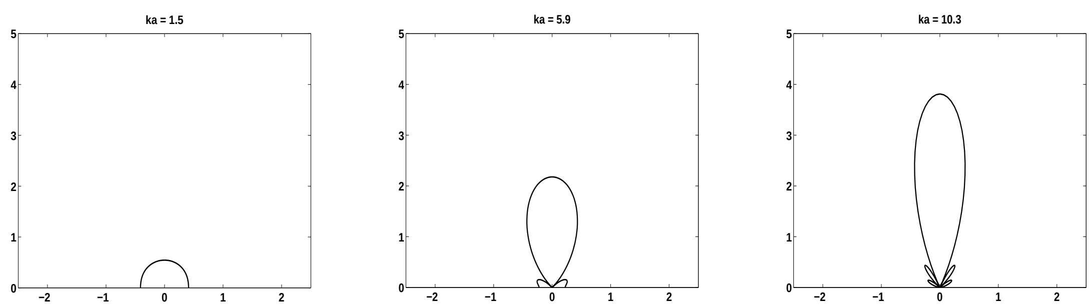

Figure 2.4: Radiated sound pressure (arbitrary units) in front of a baffled piston, with $a = 0.2$m, for increasing values of ka.

2.5.2 Radiation efficiency, η

$$\eta = \frac{\Pi}{P} \tag{2.21}$$

The definition of of radiation efficiency, η, used in this thesis is that it is the ratio of the output *acoustical* power, Π, to input *mechanical* power, P. Unlike R_{eff}, η cannot be greater than 1. η is used to describe radiation efficiency because it directly relates an instrument's output to its input.

η has previously been measured in front of two complete classical guitars (Lai and Burgess, 1990) and from a guitar top plate (Torres and Boullosa, 2011). However, the work on the top plate by Torres only determined values of η at two frequencies as part of study into the differences between "edge and corner modes" on the plate. η was also measured in one-third octave bands on four classical guitars across a frequency range of 100 Hz to 3150 Hz (Boullosa et al., 1999). Both of these works used the same definition for radiation efficiency as shown in equation 2.21 and studied η below 800 Hz. In the work by Lai and Burgess it was not possible to measure η at some frequencies due to the measured power input supplied to the instruments being lower than the power output. This cannot occur in a real instrument and the η data was therefore omitted. As the power input and power output decreased, the measurements may have become affected by noise resulting in the value of $\eta > 1$. The issue of lower input power was not present in the radiation efficiency measurements made on a piano soundboard (Suzuki, 1986). This suggests that some instruments may be susceptible to low power inputs at certain excitation locations resulting in misleading values of η.

Lai and Burgess (1990) and Suzuki (1986) supplied the power input with a vibration exciter and the power output was calculated by measuring the sound intensity. Suzuki determined the power output by measuring the sound intensity at the surface of the piano soundboard. These intensity measurements were also used to study the mode shapes of the soundboard.

Lai and Burgess (1990) also measured η on one of the guitars with an additional 8×15 g masses attached to the lower bout of the instrument, adding a total mass of 120 g. When the guitar was loaded with this additional mass, the radiation efficiency was reduced at frequencies above 200 Hz but remained much the same below 200 Hz. The radiation efficiency was reduced above 200 Hz because the additional mass affected the vibrational behaviour of the body modes which acted predominantly on the top plate. Below 200 Hz the radiated sound is produced mostly by air motion through the sound hole as the instrument undergoes a Helmholtz-like motion. Figure 2.5a shows the values of η calculated on two different guitars and figure 2.5b shows η measured on a single instrument either with or without mass loading of the top plate. These two graphs show that η is low at frequencies less than 80 Hz. This frequency region is below the lowest frequency body mode of most classical guitars and therefore the instrument would not be expected to radiate efficiently. There are no sharply defined peaks in the η data such as one would expect from an input admittance or sound pressure measurement. This suggests that the relationship between the power input and output is not as simple as the relationship between, for example, force and velocity.

Boullosa et al. (1999) calculated the power input by measuring the force and velocity at a single point on each classical guitar. The power output was measured in a "reverberant chamber of 200 m^3 (using the standard method described in ISO-3742 and ANSI-S1.32)". ISO-3742 involves driving the instrument with noise bursts with a one-third octave bandwidth. All four classical guitars had greater values of η below 1000 Hz than above this frequency. The most expensive of the four instruments had

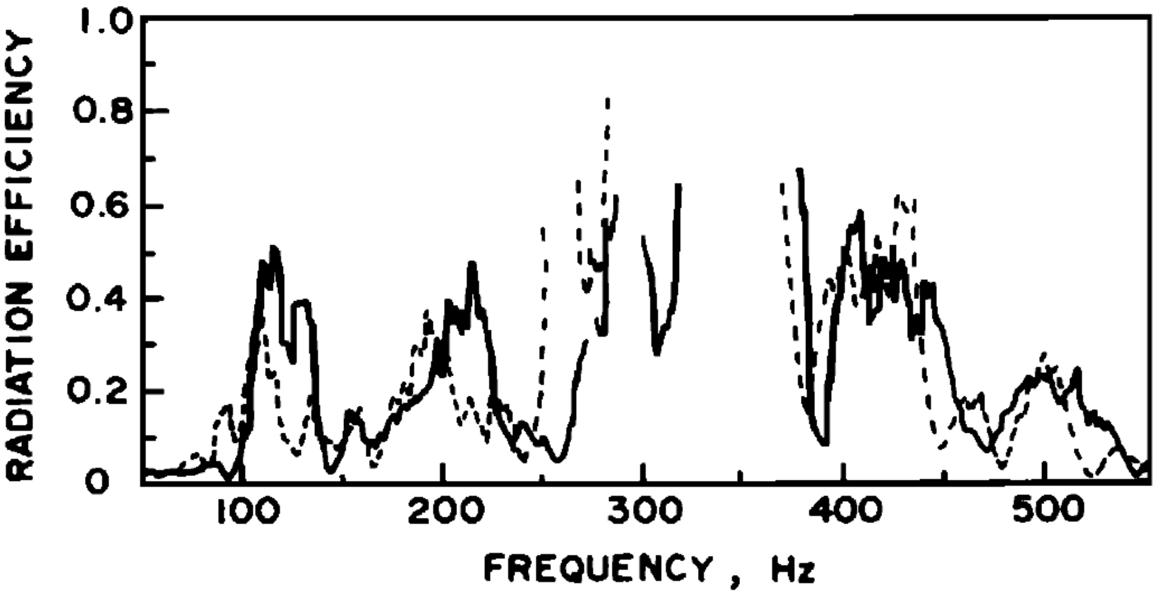

(a) η measured on two guitars

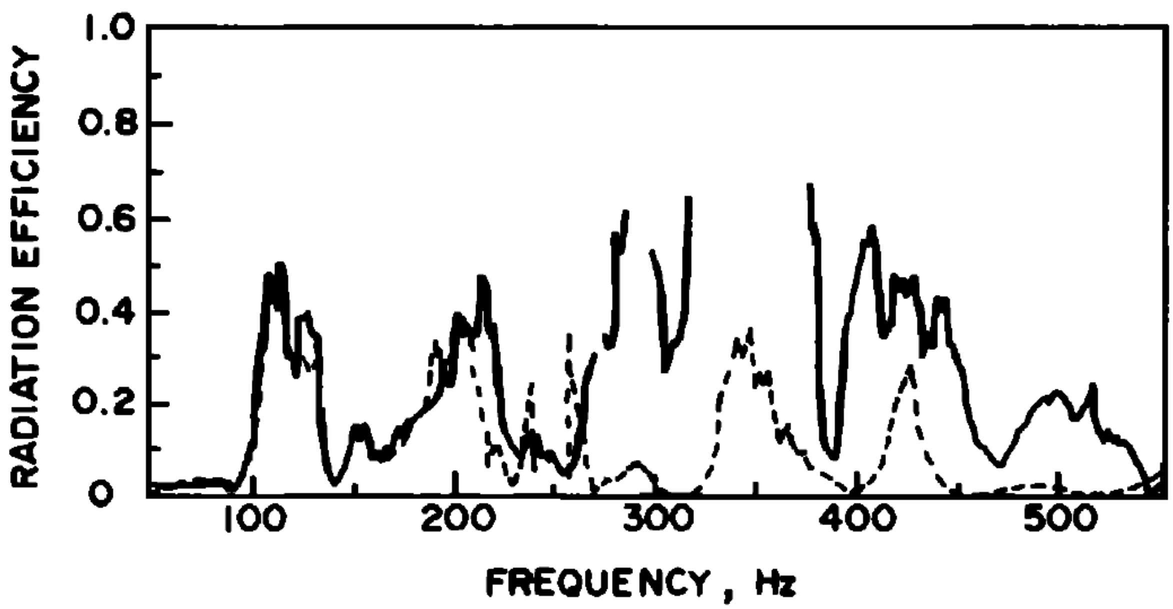

(b) η measured on one guitar, as normal (–) and η measured with mass loading (- -).

Figure 2.5: η measurements from Lai and Burgess (1990). Reprinted with permission from Lai, J. and Burgess M. (1990). Radiation efficiency of acoustic guitars, Journal of the Acoustical Society of America 88(3), 1222-1227. Copyright 1990, Acoustic Society of America.

the greatest values of η below 1000 Hz but the values of η did not correspond with the subjective quality of the guitars. As a result of using one-third octave excitation, it was not possible to study the values of η at specific frequencies; in particular, at or close to the resonance frequencies of the guitars' body modes.

Suzuki (1986) measured η on a piano soundboard at four different locations on the soundboard up to a frequency of 5.4 kHz. Below 80 Hz the radiation efficiency values were low and this was attributed to cancellation between the sound pressure produced by the upper and lower surfaces of the soundboard. The peak value of η was around 0.40 at 300 Hz. The greatest vales of η occurred below 500 Hz, while above 600 Hz the radiation efficiency remained stable with values varying between 0.1 and 0.2.

η is chosen as the definition of radiation efficiency used in this thesis. It is used because it directly relates the input and output from the same instrument without comparison to an external sound source as used to determine R_{eff}. If η is measured following an excitation on the bridge of an instrument then it shows how efficiently the power supplied to the body by the strings is converted into an acoustical power output. To determine the value of η at a known frequency, the power input and power output must be calculated separately.

2.6 Input Power

Input power is a measurement that can be made on most stringed instruments as it only requires the measurement of an applied force and the resulting velocity at the same point on the instrument's body. Realistically these measurements cannot be made at exactly the same point on the instrument without using an impedance head (a combined accelerometer and force transducer). However, impedance heads typically add a greater amount of mass to the instrument than an accelerometer and therefore alter its vibrational behaviour. Making force and acceleration measurements as close together as possible gives a good approximation of an input function. The force and velocity can be measured using a force transducer and an accelerometer. The velocity is obtained by dividing the acceleration signal by $i\omega$, where ω is the frequency and i is the imaginary unit. The input power at ω is then determined by calculating the cross-power spectrum between force and velocity as shown in equation 2.22.

$$P(\omega) = Re[F^*(\omega)V(\omega)]/2 \tag{2.22}$$

where Re is the real part of the square bracket, $F^*(\omega)$ is the complex conjugate of the force and $V(\omega)$ is the velocity. The division by 2 accounts for the time averaging of the velocity and force measurements. To gain a meaningful value of the power input, both the force transducer and accelerometer must be individually calibrated. The method for calibrating transducers is described in section 4.2.1. The velocity and force measurements can also be used to calculate the input admittance.

2.7 Output Power

Acoustical output power differs from input power in that the measurement is made at a distance from the point of excitation, typically not on the instrument's surface. An exception to this is the surface intensity method used by Suzuki (1986), which used a microphone positioned close to the surface of a piano soundboard. Meyer (1978) showed that sound fields produced by musical instruments are nearly always non-uniform in their profile with lobes of increased sound pressure output in some directions compared with others. Therefore careful consideration must be made when measuring the sound pressure and power output to account for the directional behaviour. There are several methods available for measuring acoustical power output and these are presented and compared here.

2.7.1 Sound intensity

For a plane harmonic wave propagating in a volume with zero reflections or additional sources present, it is possible to calculate the output power from an instrument using a single microphone to record sound pressure. First the sound intensity, I, of a plane wave is defined as

$$I = \frac{|p|^2}{\rho_0 c} \tag{2.23}$$

where p is the RMS sound pressure, ρ_0 is the air density and c is the speed of sound in air (Kinsler et al., 1980). The acoustical power output is calculated by integrating the sound intensity across the effective measurement area of the microphone. To use equation 2.23 to calculate I, only plane waves travelling outwards from the source must be present at the microphone's location. If anechoic conditions are used for sound pressure measurements then only outward moving sound waves will be measured. However, many objects that radiate sound do not radiate plane waves but instead can radiate spherical waves. In the near field these sound waves are spherical but in the far field (from the source), where $r \gg \lambda$, these waves can be assumed to be planar. For non-planar waves, two closely spaced microphones are required to measure the sound intensity, with I found by calculating the average sound pressure at the midpoint between the two microphones.

Radiated sound fields produced by musical instruments are typically non-planar in the near field. Instead they are either spherical or cylindrical in nature, or have even more complex shapes resulting from multi-pole sound radiation at higher frequencies. For most sound pressure measurements made on musical instruments it is not possible to measure in the far field due to constraints on room size, resulting from the longer wavelengths of the audio frequencies typically of interest. I can also be calculated by measuring the velocity and sound pressure at the same point. This is given as (Suzuki, 1986)

$$I = Re[p\left(\frac{a}{i\omega}\right)^{*}]/2 \tag{2.24}$$

where $a/i\omega$ is the expression of velocity calculated from the acceleration, a. The method of measuring I used by Suzuki involved first measuring the velocity on the soundboard from a known excitation force before measuring the pressure at the same point, close to the soundboard. This gave a measurement of the surface intensity of the instrument but equation 2.24 is valid at any distance from the instrument providing the velocity and sound pressure are measured at the same point. It is simplest to measure I on the surface of a instrument but at greater distances the issue of measuring velocity arises. To get a measurement of the sound intensity at a known distance from the instrument a sound intensity probe must be used.

Sound Intensity probes

Equations 2.23 and 2.24 suggest two different approaches to measuring sound intensity. The two different designs of sound intensity probe, p-p and p-u, are based on the measurements required by these two equations. A p-p probe measures sound pressure at two points close together in space and a p-u probe measures air velocity and sound pressure at the same point simultaneously (Fahy, 1989).

A p-u probe fulfils the requirements to calculate intensity using equation 2.24. The probe must be held in position with a velocity of less than 10^{-4} m/s so that the motion of the probe does not create an error in the velocity measurement (Fahy, 1989). The transducers used to measure the particle velocity rely on one of two principles. The first method of measuring particle velocity is to use ultrasonic beams near the acoustic centre of the microphone (Fahy, 1989). Two parallel ultrasonic beams are directed in opposite directions and convection of the waves occurs as a result of motion of the air particles. This convection results in a phase change in the ultrasonic beams which is then detected by a receptor and used to determine the particle velocity. This method of calculating particle velocity is susceptible to any air motion and so is not suitable for sound intensity measurements in turbulent environments.

The second type of p-u probe is the "microflown" which measures velocity with two closely spaced thin, short silicon wires coated with platinum heated to around 300°C (de Bree, 2003). These wires are cooled by the air flow and the change in the resistance of the wires is used to determine the particle velocity (Jacobsen and de Bree, 2005a). The velocity probes are not sensitive to background noise but errors are introduced in the reactive (the non–propagating energy) near field particularly if the probe is not phase calibrated to a high enough accuracy. To calibrate a p-u probe it must be placed in a sound field with a known relation between the particle velocity and sound pressure (Jacobsen and de Bree, 2005b). Examples of generated sound fields used for calibration of a p-u probe include a loudspeaker in the far-field region of an anechoic chamber (to approximate plane waves), the near field of a baffled monopole, or a standing-wave tube.

The other intensity probe configuration is a p-p probe which is constructed using two closely spaced pressure microphones, typically $10 - 12$ mm apart. p-p probes are subject to interference from extraneous noise and are best used in environments with minimally reflecting surroundings (Jacobsen, 1997). p-p probes are simpler to calibrate than p-u probes as they only require a known pressure signal and there are many commercially available devices that serve this purpose. Both p-p and p-u probes give comparable intensity measurements (Jacobsen and de Bree, 2005b) but the choice of probe will typically depend upon on the environment in which the measurements are made.

Using a p-p or p-u probe gives a measurement of the total sound intensity at a single point from all modes of vibration. However, it is not possible to calculate the contributions from monopoles, dipoles and other sound pressure sources to the total radiated sound intensity. A technique known as spherical-harmonic decomposition allows these contributions to the sound pressure to be calculated.

2.7.2 Spherical-harmonic decomposition

Spherical-harmonic decomposition requires two sets of pressure recordings made on two concentric measurement spheres with their centres located in the middle of the instrument of interest. The two measurement spheres are used to determine whether the recorded sound waves are moving away or towards the instrument. Measuring the sound pressure radiated outwards by the instrument means that the strengths of the sound sources that produce the radiated sound can be determined. The source strengths can then be used to calculate the power outputs from each polar source at a given frequency.

Spherical-harmonic decomposition has previously been used in Cardiff by Hill et al. (2004) and Richardson (2001) to calculate the "weights of the orthogonal radiation components", G_{lm}, at the resonance frequencies of known body modes of classical guitars. The lowest order weighting, G_{00}, has also been used previously to describe the effective area, A, of modes that radiate monopole sound fields (Christensen, 1984). To find the weightings for individual modes the instruments were driven at the anti-nodal regions of the body modes at their resonance frequencies. This reduced the level of excitation provided to the other modes but it does not completely prevent them from entering motion. If the excitation location is chosen correctly and the instrument is driven at a single frequency it can be assumed that the specific mode being driven dominates over all the others, effectively resulting in a single mode vibrating on the instrument.

In the work by Hill et al. (2004) the G_{lm} values were determined for the modes when driven at their anti-nodal areas. In order to calculate the values of G_{lm} as if the instrument were driven on its bridge (as is the case for the played instrument), two admittance values were determined. The first was an input admittance on the anti-nodal area of the mode where the instrument was driven and the second was a transfer admittance between the bridge and the anti-nodal region. The effective mass of the mode for both of these admittance curves was determined and the effective mass from the transfer admittance was divided by the effective mass of the input admittance. This gave a value which was called the ratio of effective masses, R. Multiplying G_{lm} calculated for the mode when driven at its anti-nodal region by R gives the value of G_{lm} as if the mode had been driven at the bridge.

Driving at the anti-nodal regions of modes gives the values of G_{lm} only for that particular mode. If the instrument is driven at the bridge rather than at an anti-nodal region of a mode the behaviour of the instrument at frequencies away from resonance can be studied. For an excitation on the bridge, several body modes will typically be set in motion at any frequency. The sound field will therefore not show a single mode's behaviour at resonance as clearly as the method used by Hill et al. (2004). By exciting many body modes at the bridge the vibrational behaviour is more similar to that of the instrument under normal playing conditions. The method for measuring G_{lm} depends on the results desired. If the experimenter is interested in the behaviour of the instrument's body modes under more normal playing conditions then G_{lm} should be calculated from an excitation at the bridge. However, if it is the behaviour of the individual body modes that are of interest then the ratio of effective masses should be used to determine the G_{lm} values of each mode.

Spherical-harmonic decomposition can also be used to calculate the source strength of each mode in terms of monopole and dipole contributions. The source strength can then be used to calculate the power output as shown later in section 3.9.2. Spherical-harmonic decomposition is the method used to calculate power output in this thesis because the contributions to the radiated sound power from monopoles and dipoles can be calculated. This technique has not previously been used to calculate the acoustical output power produced by stringed instruments but the theory is well established within the literature.

2.8 Visualising guitar mode shapes

There are several techniques which can be used to visualise the modes of vibration of stringed instruments or indeed of any vibrating object. The three main techniques are holographic interferometry, modal analysis and laser vibrometry. Prior to the development of holographic interferometry, one of the methods used to visualise the modes of vibration of objects was to develop Chladni figures. Waller (1961) produced Chladni figures from a series of plates by driving them at selected points and scattering sand across the plate. The sand gathers at the nodal lines of the body mode and produces a visualisation of the mode when it is driven at its resonance frequency at an anti-nodal area.

One of the first visualisations of the modes of vibration of the top plate of a guitar was made using holographic interferometry (Jansson, 1971). Richardson (1982) also used this technique to study the modes of vibration of a set of guitars up to 1000 Hz. Holographic interferometry is used to visualise the vibrating regions of an instrument when a single mode is driven in an anti-nodal area at its resonance frequency. The displacement of the plate produced by the motion of the mode is measured by recording the “light scattered by a diffusely-reflecting object” (Richardson, 1982). By driving at the resonance frequency of the mode at one of its anti-nodal regions, it is assumed that the mode is sufficiently separated from other surrounding modes and is the only one in motion. This is true providing the anti-nodal area does not coincide with the anti-nodal area of another nearby body mode. The criterion for the mode separation is that the mode shape should not change as the frequency of driving is swept through the resonance frequency (Richardson, 1982). The holograms show the displacement of the single mode. As it is the displacement that is measured, the measurements are highly susceptible to interference from any external noise sources. Real-time imaging of body modes can also be undertaken by using speckle interferometry, which is a similar technique to holographic interferometry. Moral and Jansson (1982) used speckle interferometry to measure the mode shapes of a violin.

Suzuki (1986) used an acoustical method to determine the mode shapes of a piano soundboard. The soundboard was excited at a single point and the sound pressure was recorded using a microphone. The microphone was moved across a mesh of measurement points just above the surface of the soundboard and the pressure levels were recorded. By taking the Fourier transform of the recorded sound pressure signals the mode shapes at the resonance frequencies of the body modes could be visualised. This technique has also been used with an array of microphones on a set of violins by Wang and Burroughs (2001). Another similar technique for visualising modes is the roving hammer technique where an accelerometer is fixed at a point on the guitar, such as the bridge, and the instrument is tapped at a series of points across the instrument (Elejabarrieta et al., 2000). This is also known as the modal analysis technique. As a result of the principle of reciprocity, the same result is achieved as if the instrument was excited at a single point and the response was measured at other points on the instrument. The response of the accelerometer following an excitation will provide an indication of the location of nodal lines. An excitation at a nodal line will result in no peak occurring in the FRF at the mode's resonance frequency.

The final, and most recently developed, method of visualising modes is to use a scanning laser vibrometer. Laser vibrometers use focused laser light to measure the velocity response following an excitation at a single point on the object. By measuring the velocity at a series of points across the body of an instrument, the mode shapes can be determined. This method is similar to the roving hammer method except the excitation is provided at a single point and the velocity is measured at a series of points across the surface. It has the advantage of adding no additional mass to the instrument. Some laser vibrometers can measure velocity in 2D or 3D so the motion of an object can be calculated in the x, y and z directions, producing both in-plane and out-of-plane velocity measurements. A Polytec PSV-500-3D-M scanning laser vibrometer has recently been purchased by Cardiff University and was used in this thesis to measure the 3D input admittance and the mode shapes of several stringed instruments. Laser vibrometers have also been used previously to measure the RMS velocity of the body of a violin (Bissinger, 2003b).

2.9 Psychoacoustics

Psychoacoustics is the study of a listener's perception of sound. There are many different experimental methods used to study a listener's perception of an instrument's sound under the umbrella term of psychoacoustics. An example of one study is that made by Meyer (1981), where the perceived quality of the radiated sound of several instruments was related to a set of criteria from the FRFs. Meyer found that the "3rd resonance (at about 400Hz)" had an important role in the perceived quality of an instrument[1]. The chosen criteria were listed in order of their importance to the perceived 'quality' of the guitar sound. The three factors that were deemed to have the greatest importance to the quality of a guitar were the peak level of the third resonance, the peak level of this resonance in comparison to those surrounding it and the Q value of the resonance.

Wright (1996) used listening tests to determine whether listeners could determine differences between pairs of synthesised guitar sounds and also to quantify these differences (on a scale of 0 - 3). The results of these listening tests showed that there are 'global' and 'local' parameters that affect the perceived sound. Examples of these global parameters included the values of A/m for the body modes, whereas the local parameters included the Q values and resonance frequencies of the modes. Changing the effective mass of a single mode at 220 Hz was found to affect the string partials at frequencies up to 2–3 kHz. Changing the resonance frequency of the mode only affected the string partials at surrounding frequencies.

Another method which has been used recently to study the sound produced by both violins (Fritz et al., 2007) and guitars (Woodhouse et al., 2012) is to determine the just noticeable differences (JNDs) in the radiated sound when a single element of its behaviour is altered. The JNDs are determined by presenting a listener with three synthesised string sounds and asking them to determine which of the three is different from the other two. This test is known as a three-alternative-forced-choice procedure (3AFC). The sounds were altered by changing either the amplitude, frequency or damping of either the string or body modes. For the first groups of three sounds presented, the modification of the different tone was set to be obviously noticeable. Following three correct answers the modification of the different tone was reduced and, if an incorrect answer was given, the modification was increased. Following 8 turning points (an incorrect answer following a correct answer for example) the experiment was stopped and the JND was determined.

For classical guitars, the damping of the string was found to have only a minimal

[1]It is possible that this mode corresponds with the $T(3,1)$ mode which is shown in chapter 5 to have an effect on the higher frequency η characteristic of classical guitars.

effect on the produced sound. It was determined that the smallest shift in body mode frequency that could be determined by a listener was 1%. The JND for a change in the damping of a body mode was a 20% shift, suggesting a lower importance to the "tonal perception" of the guitar sound (Woodhouse et al., 2012). Small changes to certain aspects of an instrument's sound can therefore cause noticeable changes to the radiated sound. This explains why seemingly similar instruments can be determined to be of vastly different quality despite there being only minor differences in their construction. Work in the area of psychoacoustics is currently being undertaken in the musical acoustics group at Cardiff University and was presented at the IOA conference in Nottingham by Roberts and Richardson (2013). Within this thesis comments are occasionally made to describe the 'quality' of several instruments but these are aimed to be a general guidance rather than a solid judgement.

Chapter 3

Experimental techniques

The effect of any experimental method on an instrument must be carefully considered when measurements of its behaviour are made. As guitars and violins have a lightweight construction, any additional mass or damping applied to the instruments will cause a change in their vibrational behaviour. The methods of exciting and supporting the instruments are therefore of considerable importance. In this chapter the methods for driving, suspending and studying stringed instruments are presented and compared. The theoretical and experimental methods used to measure the power output and radiation efficiency are also presented.

3.1 Instrument excitation

There are several techniques available for the excitation of stringed musical instruments each with their own advantages and disadvantages. The design of any excitation method should add as little mass as possible to the test object and cause minimal interference to its ability to vibrate. This also applies to any device used to measure the response produced by the excitation. For guitars, any object added to the vibrating area of the instrument should weigh a few grams at most, but a smaller mass will interfere less with the vibrations of the instrument. The addition of a 40 g mass to a top plate has been found to lower the resonance frequency of the second top plate resonance by up to 25 Hz, although the effect on any air resonance is minimal (Christensen and Vistisen, 1980). The addition of 8×15 g masses to the top plate of a guitar was found to reduce the radiation efficiency (power output / power input) of a guitar above 200 Hz but not below this frequency (Lai and Burgess, 1990). In both of these cases the additional mass affected the modes where the majority of the motion involved the body of the instrument rather than the enclosed air. As it is only the lowest frequency $T(1,1)_1$

mode which produces a strong motion of the air in the body, all other modes will have reduced amplitudes if extra masses are added to the instrument.

When making frequency response measurements it is important that the excitation method relates to how the instrument radiates sound (Jansson et al., 1986). The sound radiated to listeners by a stringed instrument results from the interaction between the string and the body, so the excitation point should be located near to the point where the strings couple to the bridge. The direction of the excitation is also of considerable importance and it should relate to the polarisation of the strings' motion when they drive the bridge. For classical guitars, the excitation is usually made in the out-of-plane direction because when the instrument moves in this direction it produces the greatest displacement of the surrounding air. The strings on violins are often excited using a bow across the strings. This produces an in-plane motion on the bridge and so an excitation should also be made in this direction.

Three of the main methods used for driving at a point on a stringed instrument are electromagnetic excitation, impulse excitation and the use of loudspeakers at a distance from the instrument.

3.1.1 Electromagnetic driving

Electromagnetic driving involves placing a magnet at the excitation location and placing an electromagnetic coil around it. The coil is driven by supplying it with a sinusoidally varying voltage. The coil drives the magnet and this in turn excites the instrument. This excitation method adds only the mass of the magnet to the instrument but, in order to make calibrated and accurate force measurements, a force transducer is also required. In a previous experiment involving electromagnetic driving of classical guitars, the mass of a magnet, force transducer and an accelerometer came to 3.5 g which fulfilled the requirement of a lightweight system (Richardson, 2001). Without a force transducer it is not possible to measure the force on the *instrument* from the applied voltage as it is only possible to determine the force on the *magnet* from the voltage signal (Ewins, 1984).

Electromagnetic driving allows an instrument to be driven at either a single frequency or across a range of frequencies by using a filtered white noise signal. When electromagnetic excitation is used there can be a small but noticeable level of second-order partial distortion, causing an excitation at an octave above the desired driving frequency (double the frequency) (Richardson, 1982). Second-order distortion can produce an excitation of higher frequency body modes if they share similar anti-nodal regions to the mode being studied. The motion of these other body modes can interfere with that from the mode of interest and give misleading results. If two modes are driven at the same time then the measured displacement at a point will be produced by motion of the two modes rather than the single mode that is of interest. To avoid the effect of second-order distortion the instrument should be driven with a low amplitude.

An application which involves using an electromagnetic driver to excite a single mode is holographic interferometry. Driving the mode at its resonance frequency on one of its anti-nodal regions allows the displacement it produces on the surface to be visualised using holographic interferometry (Jansson, 1971).

Electromagnetic driving can be used when measuring the admittance or sound pressure response of an instrument. Admittance is typically measured across a range of frequencies rather than at a single frequency. To excite an instrument across a range of frequencies there is a choice of two methods. The first is to use filtered white noise of a chosen bandwidth across the frequency range and the second is to make a sweep through increasing frequency voltage signals. Frequency sweeps produce a better signal-to-noise ratio (SNR) than filtered white noise but they are much more time consuming.

Mechanical shaker

Mechanical shakers work using a similar principle to electromagnetic driving except that the entire driving system is contained within a single unit. Mechanical shakers are typically placed at a distance from the instrument and are connected to the excitation point using a rod with stiffness only in the direction of excitation to prevent any off axis excitation. This system is often referred to as a stinger set up. It also requires a force transducer at the point of excitation or as near to it as possible. The increased mass and stiffness added to the instrument by the shaker system causes a larger shift in the resonance frequencies of lower frequency modes than if an impulse excitation were used (Griffin et al., 1998).

3.1.2 Loudspeaker excitation

The main principle of loudspeaker excitation is that a speaker, at a distance from the desired point of excitation, is driven with a known signal and radiates sound pressure. The sound pressure is measured at the excitation point, without the instrument present, and the applied force is derived from the pressure and pressure gradient (Weinreich, 1985). This excitation method adds no mass to the studied instrument. In order to measure the response of the instrument, the orientation of the speakers must be chosen carefully. If the aim of the experiment is to measure the out-of-plane response then the loudspeaker should face the instrument in this direction. This ensures that the response is measured in the same direction as the excitation. As with electromagnetic excitation, either a single frequency or a range of frequencies can be driven using loudspeaker excitation.

3.1.3 Impulse excitation using an impact hammer

By striking on the instrument with an impact hammer, an impulse excitation is generated. This impulse excites a range of frequencies, the upper limit of which is determined by the length of contact between the hammer and the surface. An ideal hammer strike can be approximated as being a delta function occurring at the time of impact. The Fourier transform of a delta function shows a flat distribution of excitation across *all* frequencies. In reality a hammer strike has a finite duration and can be approximated as a 'top hat' function in the time domain which is transformed into a sinc function in frequency space (Lynn, 1973). For a sinc function the amplitude reaches a minimum at a frequency of $\omega = \frac{\pi}{\tau}$ where τ is half the length of time that the hammer tip is in contact with the structure. The time of impact can be reduced by using a harder hammer tip or striking on a harder part of the instrument in question.

A major advantage of using impact hammers over other driving techniques is that they combine both excitation and force measurement by containing a force transducer within the hammer head. As no transducers are attached to the instrument to measure the applied force, this excitation technique adds no mass to the system. Impact hammers come in a variety of sizes for different applications, varying from testing lightweight structures such as guitars or circuit boards up to testing on large scale projects such as ships or bridges. A further advantage of impulse excitation is that the excitation point can be changed quickly without having to relocate any transducers. The mode shapes of the instrument can therefore be determined using the roving hammer technique (Carne and Stasiunas, 2006).

It is important when using an impact hammer to strike in only one direction at a time, particularly when comparing frequency response functions in several directions (Boutillon and Weinreich, 1999). A typical measurement made using impulse excitation is that of the response, normally velocity, of a guitar in the out-of-plane direction. This excitation direction is used because it is in the same orientation as the string polarisation which produces the greatest response of the instrument. If the impact angle lies between two designated directions of measurement then the excitation cannot be used to analyse a response in a single direction. Instead the excitation will drive the instrument in a combination of directions and the response in any single direction cannot be determined.

If a strike is made by hand, it is clear to see whether the hammer has rotated following the strike and the measurement can be ignored.

When striking an instrument with an impact hammer it is possible for a second strike to occur following the rebound from the initial strike. This double strike introduces interference in the recorded signals, which are most obvious when they are Fourier transformed into the frequency domain. A second strike shortly after the first introduces a sinusoidal variation in the frequency response. The rate of change (in Hz^{-1}) depends on the time between each hit and the level of variation depends on the amplitude of the second hit. For example, if a second hit occurs 0.1 seconds after the initial hit then the frequency response will pass through a maxima and minima every 10 Hz. To prevent double hits from occurring the hammer should be located at a distance that prevents a second strike following a rebound from the excited surface. When the force data is recorded by a computer it can automatically be rejected if a double strike is determined to have occurred.

Commercial impact hammer tips are often hard enough to cause damage to softer materials and may come with an optional rubber tip to prevent damage to the instrument (PCB, 2007a). However, the rubber tip lengthens the contact time between the hammer and the surface and reduces the frequency range of the hammer. While the increase in contact time is detrimental to the frequency range, it increases the level of energy supplied within the smaller range. An alternative to softening the tip is to attach a small piece of metal at the excitation location which prevents damage to the body while still maintaining the same frequency range. While this reduces the ease of making measurements at different locations, it protects the instrument and adds only a small amount of mass (around 100 mg) which is much lower than that of any commercial force transducer.

Impact excitation drives instruments over a short time period, typically $\sim \frac{1}{10000}$th of a second for a lightweight hammer with a hard tip. The actual excitation time is very short but recordings of the response must be long enough to allow the signal to decay to below the background noise level. Despite the requirement of additional recording time, impulse excitation drives the instrument across a wide frequency range much more quickly than frequency sweeps. This allows for quick repeats of FRF measurements. A disadvantage of using impulse excitation is that it cannot be used to excite a single body mode but instead any mode with no nodal line at the excitation point will be driven. If the behaviour of single modes is being investigated then electromagnetic or mechanical driving methods are more suitable.

Calibrating an impact hammer's response is possible if a correctly calibrated reference accelerometer is available. The calibration is undertaken by striking a known mass with the hammer and measuring the acceleration (Ewins, 1984). The full details of this method are shown in section 4.2.1.

3.1.4 Comparison

The choice of excitation technique is dependent on what results are required. If the behaviour of an instrument at an individual frequency or mode of vibration of an object is being analysed, then either a shaker or electromagnetic excitation provide the best results as a single frequency can be isolated and the level of driving controlled. For any measurement across a large frequency range, it is faster to take repeat measurements using an impact hammer. In this thesis the sound pressure response across a range of frequencies at over 300 measurement points was measured. This would be impractical in terms of time scale if the instrument were driven using an electromagnet, so impulse excitation using an instrumented hammer was the preferred technique

3.2 Velocity response measurement

The value typically measured to determine the response of an instrument is the velocity. If the velocity response is measured at the same point as the excitation then the input admittance and input power can be calculated. The velocity can be measured using either an accelerometer or a laser vibrometer.

Accelerometers directly measure the acceleration at a point on an instrument. The acceleration signal must be integrated to determine the velocity values from this measurement. As with impact hammers, accelerometers are available in a variety of sizes for different purposes. When making measurements on light structures, such as guitars, lightweight accelerometers should be used to minimise the transducer's interference with the motion of the instrument.

Accelerometers are best used at a single location (rather than continually moving them) as they must be fixed to a surface to give the most accurate measurements of the response (Ewins, 1984). Motion of the instrument, while the accelerometer is being used to determine velocity, should be kept to a minimum. However, a low-frequency motion (such as swaying) will have no effect on the body modes of the instrument which are at much higher frequencies.

Laser vibrometers provide no mass loading on the instrument and they directly measure the velocity at a point using laser light. They work using the principles of

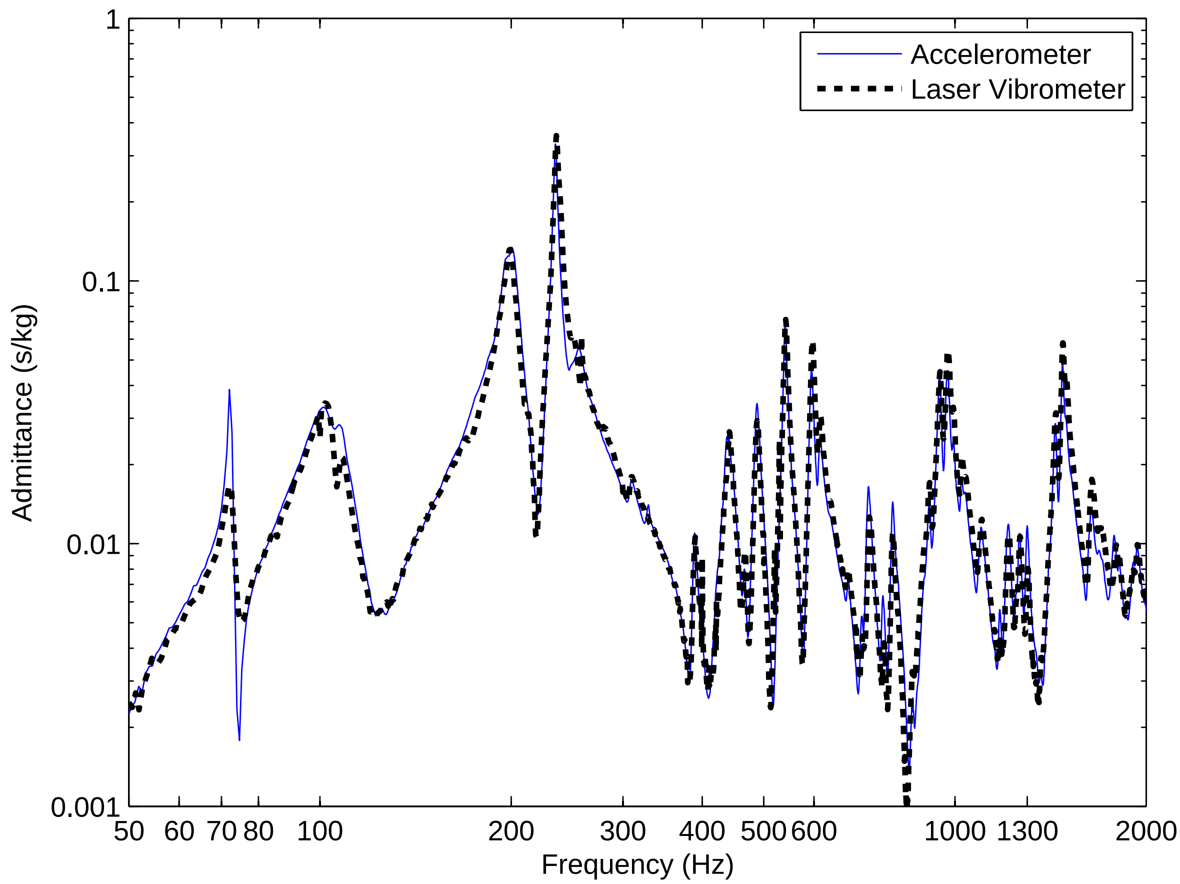

Figure 3.1: Admittance measurements made at the E_2 string of BR1 using an accelerometer and laser vibrometer (x direction).

Doppler shift and optical interference (Polytec, 2014). A laser is split using a beam splitter into a reference beam and a measurement beam. When the measurement beam is scattered from the surface of the instrument it is recombined with the reference beam and interference occurs between the two beams. The phase of the interference between the two laser beams provides a measurement of the displacement at the measurement point. By measuring the change in phase with time the velocity at the point can be determined.

3.2.1 Comparison of admittance measurement methods

The input admittance shown in figure 3.1 was measured on a classical guitar, BR1, using an impulse excitation to provide the input force. The velocity was measured both using an accelerometer and the laser vibrometer. In both cases the strings of BR1 were damped with felt and the instrument was suspended using elastic bands. For the laser vibrometer measurements, additional support was provided to the instrument by placing foam between its base and the floor and tying string between the metal support rack and its neck. The input admittance was determined from the complex average of 20 excitations for both measurement methods.

Despite the additional damping on the guitar when the laser vibrometer is used to measure velocity, the only significant difference in the input admittance curves in figure 3.1 is in the neck-bending mode at 72 Hz. The motion of this mode is restricted by the foam at the base of the guitar because it is a beam-bending mode that extends across the full length of the instrument. There are some slight differences in the peak values but all of the body modes are at the same resonance frequencies for both measurement methods. If it is only the input admittance in the out-of-plane direction that is of interest, then using a lightweight accelerometer to measure the velocity response provides accurate results within a shorter set up time than using a laser vibrometer. Using an accelerometer to measure the velocity is also more cost effective than a laser vibrometer. However, the laser vibrometer used in this work provides a major advantage over accelerometers because it can be used to measure the in-plane motion of the instrument at any point on its surface.

There are two possible methods for measuring the in-plane motion on the bridge of a guitar using an accelerometer. The first method is to attach accelerometers to a small block which is then attached to the instrument. The accelerometers are placed on the block facing in the x, y and z directions. This method was previously used by Boutillon and Weinreich (1999) to measure the 3D admittance on a violin bridge. The velocity of the block is measured rather than directly measuring the velocity of the instrument at that point. The other method for measuring the 3D admittance involves attaching an accelerometer to the edge of the bridge in the y and z direction. This method only allows the 3D admittance to be measured at the edge of the bridge and not on the surface of the instrument. The values obtained using this method cannot be said to be input admittances as the measurement points are separated from the excitation point. This method has been used previously by Lambourg and Chaigne (1993) to measure the 2D admittance on a guitar bridge.

Instruments must be kept still when the velocity is measured using a laser vibrometer. If the distance from the laser head to the test object is changed then the laser will become unfocused and produce incorrect results. In the experiments to measure the power input that are reported in this thesis, the guitar was continually being rotated so that the pressure response around it could be measured. For these experiments, therefore, a laser vibrometer was not suitable for performing the velocity measurements. To enable the power input and output to be calculated, the velocity and pressure responses produced by a given excitation must be measured simultaneously. Therefore an accelerometer was used to measure the velocity (which was then used to calculate the power input), despite the minimal effect of the small added mass on the instrument's response, for the purposes of determining radiation efficiency, η. A 3D scanning laser vibrometer was used in this thesis to measure the 3D admittance (out-of-plane and in-plane velocity) and the body mode shapes of several stringed instruments.

3.3 The physics of transducers

Force transducers and accelerometers are constructed using piezoelectric crystals. When a force is applied to a piezoelectric material it generates an electrical charge which is directly proportional to the size of the force, within its working frequency range. The generated electrical charge must be conditioned before the signal can be analysed. The two designs of signal conditioners are voltage and charge amplifiers. Both amplifiers require a high input impedance (Ewins, 1984) but their behaviours are different. Voltage amplifiers have a better SNR than charge amplifiers and have a simpler electronic design. However, the signal from a voltage amplifier degrades with cables of increasing length. Charge amplifiers allow for measurements to be made at lower frequencies than voltage amplifiers and any length of cable can be used.

There are two main designs of force transducer. The first, referred to as a force sensor here, has piezoelectric materials as the active component. Piezoelectric crystals can be used to measure an impact force but not an applied static force. This makes the force sensor ideal for use in an impact hammer where only impulse excitations are provided and recorded. The other force transducer design is known as a load cell. A load cell has two masses either side of the piezoelectric material which are known as the seismic mass and the base mass. Using a load cell makes it possible to measure a continual static force as well as dynamic or impulse forces. This makes it suitable for measurements of force under continual driving as well as impulse excitation.

As piezoelectric materials measure force directly, the acceleration must be determined from the force applied to the piezoelectric crystal. To measure the acceleration, a single mass is attached to the piezoelectric crystal. The force exerted on the crystal results from the inertial force of the additional seismic mass (Ewins, 1984) and this force is then used to calculate the acceleration. The main consideration with the design and use of an accelerometer is that the motion of the seismic mass, z, must be the same as that of the body, x. It should be noted that the distance z is the motion of the seismic mass relative to the body rather than the total motion of the seismic mass. If

x and z are not orientated in the same direction then transverse sensitivity will occur. Transverse sensitivity results in measurements in directions other than x being measured by the piezoelectric crystal. This can introduce errors in the measurements if the off-axis measurement is particularly large. However, if x and z are both orientated in the same direction then the acceleration values $\ddot{x}$ and $\ddot{z}$ will be directly proportional to one another. Therefore the accelerometer enables measurements of acceleration of instruments in one direction only.

The inclusion of a mass in the accelerometer introduces a resonance frequency into the system. The piezoelectric crystal behaves like a spring with stiffness, k, and with the addition of a mass, m, it becomes clear that the system will act like a mass on a spring. The accelerometer will therefore have a resonance frequency of $\omega = \sqrt{\frac{k}{m}}$. It is not only at resonance that the behaviour of the accelerometer will change. At 20% of the resonance frequency the difference between x and z will be 4% and at 33% of the resonance frequency the difference will be 12% (Ewins, 1984). To gain accurate results, measurements must therefore be made well below the resonance frequency. Depending on the size of the mass the sensitivity of the accelerometer will change. The sensitivity describes the voltage or charge output per unit acceleration. More massive accelerometers typically have higher sensitivities than lightweight accelerometers. If a transducer with too great a mass is attached to an instrument being studied then it will affect the vibrational behaviour of the instrument.

3.3.1 Accelerometer

The following explanations of the physics and workings of transducers, both mechanical and electrical, follow the work by McConnell (1995) and use the same terminology. By assuming that accelerometers behave like a mass-spring system with a damping element, c, then using Newton's second law of motion, the total motion of the system when a force, $f(t)$, is acting on it is

$$m\ddot{z} + c\dot{z} + kz = f(t) + m\ddot{x} \tag{3.1}$$

For factory constructed accelerometers, the value for $f(t)$ will be constant as the only force able to act on the seismic mass will be from gravity. The value of $\ddot{x}$ is the acceleration of the body and is the value that is measured by the accelerometer. z is the displacement of the seismic mass of the accelerometer relative to the motion of the body. By assuming solutions of $x = X_0 e^{-i\omega t}$ and $z = Z_0 e^{-i\omega t}$, and using them in equation 3.1, the following result is obtained

$$Z_0 = \frac{-m\omega^2 X_0}{k - m\omega^2 - ic\omega} \tag{3.2}$$

$-\omega^2 X_0$ is the magnitude of the base acceleration, a_0, so equation 3.2 can be rewritten as

$$Z_0 = \frac{m a_0}{k - m\omega^2 - ic\omega} = H(\omega) a_0 \tag{3.3}$$

where $H(\omega)$ is the mechanical FRF of the accelerometer. At frequencies well below resonance, the values of $m\omega^2$ and $ic\omega$ are negligible in comparison with k. This allows for a further simplification of equation 3.3 so that the magnitude of Z_0 is

$$Z_0 = \frac{m a_0}{k} \tag{3.4}$$

Therefore, at frequencies well below resonance the displacement of the seismic mass relative to the body is directly proportional to the acceleration. However, at frequencies nearing resonance, the proportionality no longer holds and differences begin to occur between the displacement and acceleration. Knowledge of the mechanical FRF is required in order to be able to make measurements at frequencies nearer to resonance, so that the change from a uniform response can be predicted thereby preventing erroneous results.

This is the mechanical model for an accelerometer but the accelerometers used for scientific measurements are typically constructed using a piezoelectric crystal in place of a spring or strain gauge. The piezoelectric crystal still acts like a spring so the mechanical FRF should still be included with the electrical FRF term. A piezoelectric crystal generates a charge, q, which is directly proportional to the displacement, z, of the crystal. The charge is converted into a voltage by passing it through an amplifier. The voltage can then be sent to a computer and recorded for later analysis. Piezoelectrics also allow for the design of accelerometers with certain resonance frequencies, weights and sensitivity characteristics. Elements of the mechanical model can be used to show the characteristics of a piezoelectric accelerometer.

Since the charge is proportional to the displacement, the generated charge will therefore also be directly proportional to the measured acceleration. The constant of proportionality between the charge and displacement is known as the displacement charge sensitivity, S_z, and its units are given as pC/m. There is also a constant of proportionality between the charge and acceleration which is called the transducer's charge sensitivity, S_q, and has units of pC/ms^{-2}. The charge sensitivities can be shown as

$$q = S_z z \tag{3.5a}$$

$$q = S_q a \tag{3.5b}$$

The charge is converted to a voltage using a charge amplifier which has a known capacitance, C_a. However, the amplifier is not the only source of capacitance in the system. There are also capacitances present within the transducer and the cable connecting the transducer to the amplifier. If cables of different lengths are used then the sensitivity of the transducer will change. The capacitances are parallel to each other so the total capacitance, C_f, is the sum of the three capacitances. PCB transducers, such as those in the impact hammer and accelerometer used in this work, contain the required charge amplifier circuit within the transducer itself (PCB, 2007a) as a microelectronic amplifier. This keeps the capacitance constant and allows for varying lengths of cable to be used without affecting the sensitivity of the transducer. A new term for the sensitivity is required when the charge is passed through a conditioner. This new sensitivity term is the voltage sensitivity, S_v, which is given as

$$S_v = \left[\frac{S_q}{b}\right]\left[\frac{1}{C_f}\right] \tag{3.6}$$

where b is a term to convert S_q to a standard charge sensitivity, S_q^*, which will typically be 1 pC/unit, 10pC/unit or 100 pC/unit. PCB transducers have a unity gain amplifier so in this case the value of b will result in S_q^* =1pC/unit. The voltage output, E_0, from the amplifier is given in terms of the voltage sensitivity as

$$E_0 = H_a(\omega) S_v a \tag{3.7}$$

where $H_a(\omega)$ is the combined mechanical and electrical FRF of the transducer. The voltage output from the accelerometer and the amplifier is therefore directly proportional to the acceleration of the body being studied, away from the resonance frequency of the transducer. For some transducers there is the possibility of triboelectric noise occurring. This noise occurs when cables generate an electric charge when the insulating material is compressed and produces a capacitance. If an inbuilt amplifier is used then the triboelectric effects do not occur as the signal has already been conditioned before being sent through the cable. The same piezoelectric principle used in the design of accelerometers is used to make force transducers.

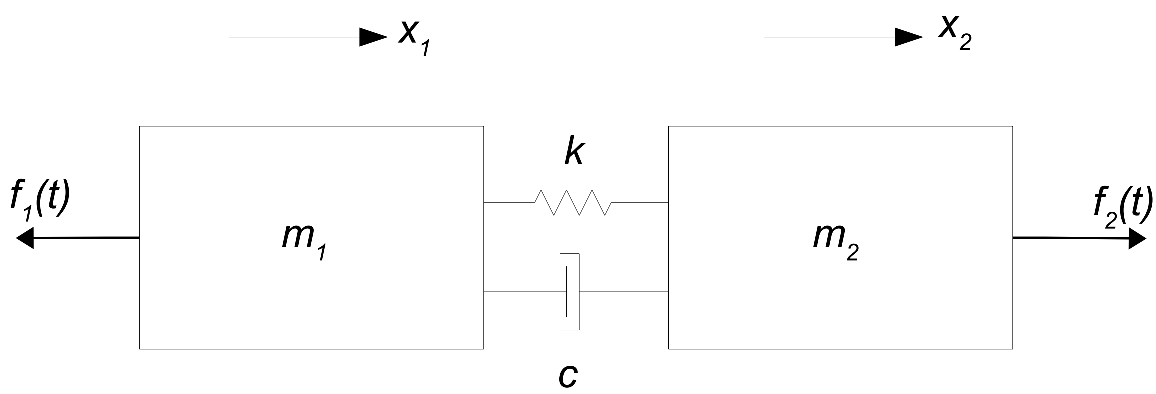

Figure 3.2: Model of a load cell force transducer.

3.3.2 Force transducer (load cell)

The load cell can be modelled as two masses, m_1 and m_2, connected by a spring of stiffness, k, with a damping factor, c, with separate external forces acting in opposite directions on each mass, $f_1(t)$ and $f_2(t)$. An example of a load cell is shown in figure 3.2. $f_1(t)$ is the force acting on the seismic mass, m_1, which is attached to the object being studied and it is this value which is of interest to the experimenter. $f_2(t)$ is the force acting on the base mass, m_2, and is included to allow for a correct measurement of $f_1(t)$ to be made. If the two masses are equal then either mass can be placed closest to the body of the instrument, if they are not then the seismic mass must be at the end attached to the body.

In the model shown in figure 3.2 the two masses are connected together by the same spring and therefore have the same values of k and c acting upon them. In a real force transducer the spring is the piezoelectric crystal with the two masses either side of it. The coupled system can be described as a pair of simultaneous equations.

$$\begin{aligned} m_1\ddot{x}_1 + c\dot{x}_1 - c\dot{x}_2 + kx_1 - kx_2 &= -f_1(t) \\ m_2\ddot{x}_2 - c\dot{x}_1 + c\dot{x}_2 - kx_1 + kx_2 &= f_2(t) \end{aligned} \tag{3.8}$$

The assumption is made that the forces and displacements vary sinusoidally. The terms $f_n(t) = F_n e^{-i\omega t}$ and $x_n = X_n e^{-i\omega t}$, where n is either 1 or 2, can be used in equation 3.8 to obtain the steady state response. By substituting $S = k - i\omega c$, where S is the apparent stiffness, into the expansion the simultaneous equations are reduced to

$$\begin{aligned} (S - m_1\omega^2)X_1 - SX_2 &= -F_1 \\ -SX_1 + (S - m_2\omega^2)X_2 &= F_2 \end{aligned} \tag{3.9}$$

The solution to equation 3.9 can be obtained by writing the simultaneous equations in matrix form.

$$\begin{bmatrix} (S - m_1\omega^2) & -S \\ -S & (S - m_2\omega^2) \end{bmatrix} \begin{bmatrix} X_1 \\ X_2 \end{bmatrix} = \begin{bmatrix} -F_1 \\ F_2 \end{bmatrix} \tag{3.10}$$

The determinant gives the characteristic frequency equation, $\Delta(\omega)$, which is

$$\Delta(\omega) = -[(m_1 + m_2)S - m_1 m_2 \omega^2]\omega^2 \tag{3.11}$$

By looking at the real part of $\Delta(\omega)$ it is possible to find the natural frequency, ω_0, of the transducer by setting $\Delta(\omega)$ to zero. The natural frequency is therefore

$$\begin{aligned} \omega_0 &= \sqrt{\frac{k}{m_e}} \\ m_e &= \frac{m_1 m_2}{m_1 + m_2} \end{aligned} \tag{3.12}$$

where m_e is the effective mass of the load cell. The effective mass in equation 3.12 shows that both the seismic mass and the base mass of the transducer will alter the resonance frequency of the transducer. The natural frequency is the lowest frequency resonance of the system. As for the accelerometer, at frequencies near to the resonance frequency the voltage output will no longer be directly proportional to force. By applying Cramer's method to equation 3.10 the steady state amplitudes of motion for the two masses are shown to be

$$\begin{aligned} X_1 &= \frac{SF_2 - (S - m_2\omega^2)F_1}{\Delta(\omega)} \\ \\ X_2 &= \frac{(S - m_1\omega^2)F_2 - SF_1}{\Delta(\omega)} \end{aligned} \tag{3.13}$$

Equation 3.5 shows that the piezoelectric charge is directly proportional to the relative motion of the transducer, which for a load cell is $z = X_2 - X_1$. Equation 3.7 can be rewritten to describe the behaviour of a force transducer, by replacing a with $z = X_2 - X_1$, to give the voltage generated by the displacement, E_f, as

$$E_f = H_f(\omega)\frac{S_z}{C_f}(X_2 - X_1) \tag{3.14}$$

where S_z is the displacement charge sensitivity and H_f is the combined mechanical and electrical FRF of the force transducer. Substituting the values of X_1 and X_2 from equation 3.13 into equation 3.14 gives

$$E_f = S_f H_f(\omega) \left[\frac{m_2 F_1}{(m_1 + m_2)} + \frac{m_1 F_2}{(m_1 + m_2)} \right] \tag{3.15}$$

where $S_f = S_z/C_f k$ and is described as the voltage sensitivity, which has units of volts/unit of force, and $H_f(\omega)$ is the combined mechanical and electric FRF of the transducer. The relationship between F_1 and F_2 must be found in order to calculate F_1. The relationship for an impact hammer is shown in section 3.3.3 as it was the only type of force transducer used in this work. Full details of the force relationships for a force transducer at a fixed foundation and a transducer in use with a vibration exciter are shown in the book 'Vibration Testing: Theory and Practice' by McConnell (1995).

3.3.3 Impulse hammer force measurement

As shown in section 3.3, the voltage output and therefore the calibration value of a force transducer is dependent on the seismic and base masses of the load cell along with the two applied forces. When a load cell is used in an impact hammer, the behaviour of the load cell is changed. The dominant force as a hammer strike occurs is the inertial force which allows the assumption to be made that $F_2 = 0$ in equation 3.15. This reduces the number of terms in equation 3.15 so that it may be given as

$$E_f = \left[\frac{m_2 S_f}{(m_1 + m_2)} \right] H_f(\omega) F_1 = S_f^* H_f(\omega) F_1 \tag{3.16}$$

The value S_f^* is the effective voltage sensitivity, which is the term contained within the square bracket. The square-bracket term shows that the effective voltage sensitivity will change depending on the masses m_1 and m_2, which for an impact hammer are the seismic mass and the effective mass of the hammer respectively. The effective mass of the hammer is defined as the mass of the hammer excluding the seismic mass of the force transducer. The hammer's effective mass can be increased by adding an extension mass to the hammer to allow for a greater level of force to be supplied by an excitation. It has been noted that differing hand mass can result in different calibration values with hand inertia being transferred to m_2, the effective mass of the hammer (McConnell, 1995). Calibration measurements should therefore be made by the same person who is making the experimental measurements.

The impact hammer used to make force measurements in this work was a PCB 086E80 impact hammer. The force transducer in the tip is a PCB miniature quartz force sensor which is a load cell type transducer. Unlike the typical behaviour for a load cell it is not possible, nor accurate, to measure a static force using this impact hammer. If a static force is applied to the transducer then a charge is generated but the electrostatic charge will eventually 'leak' away to zero through the "lowest resistance path" of the system (PCB). The time taken for the charge to decay to 37% of its original value is called the Discharge Time Constant (DTC) which for this particular hammer is $\geq 100s$.

3.4 Reading signals from transducers

For the purpose of analysing the measurements made using transducers, their output voltage signals must be digitised and read into a computer. One method for digitising the signals is to use a sound card which records samples of the analogue signal, thus converting into digital values. The accuracy of the reproduction of the signal in a digital form is determined by the sampling rate and the bit depth. The sampling rate determines how many samples are recorded by the sound card each second. The sampling rate is typically set at 44.1 kHz which results in a Nyquist frequency above the upper range of human hearing. The Nyquist frequency is the upper limit before aliasing effects begin to occur in the digitally recorded sound. The bit depth determines the dynamic range of the signal and the amplitudes that can be recorded. A bit depth of 16 bits allows for a dynamic range of 96 dB to be measured. The signals read into a sound card attached to a computer must be recorded for the purpose of analysis. Using software such as MATLAB the recorded signals can be stored in vector format so that FFTs and other signal analysis techniques may be used to study the recorded signals.

3.5 Attachment of transducers

Consideration must be made as to how transducers are attached to an instrument. The structure itself often dictates the possible methods. For large industrial objects, magnets or studs can be used to firmly attach transducers to objects. Attaching a transducer to an instrument using a stud would seriously damage the instrument and is therefore not a suitable option. The most common techniques used to attach transducers to stringed instruments are either to use glue, which can damage the finish of the instrument, or double-sided tape (Richardson, 2001). Double-sided tape is advantageous as it can be quickly applied and removed without damaging the instrument, providing care is taken when removing it. Double-sided tape also allows for the measurement location to be changed quickly. However, if the tape is not applied correctly then it may become detached from the surface and the transducer will no longer be in contact with the instrument.

In the case of instruments where only a small surface area is available for transducer attachment, it is not possible to use double-sided tape to hold the transducer in place. An example of such a location is on the bridge of a violin which consists of a thin piece of wood, only a few millimetres thick. For this case the solution is either to use a smaller transducer or to use glue to attach it in place.

The effect of the transducer attachment method can be determined by measuring the accelerance (acceleration/force = 1/mass) of a known mass. A light, simple mass will have a very high resonance frequency so between 0 Hz and 2000 Hz the accelerance should be flat. A PCB 352B10 accelerometer was attached to a 30 g aluminium block which was excited using a PCB 086E80 impact hammer. Five accelerance measurements were made and averaged for the accelerometer attached both with double-sided tape and glue.

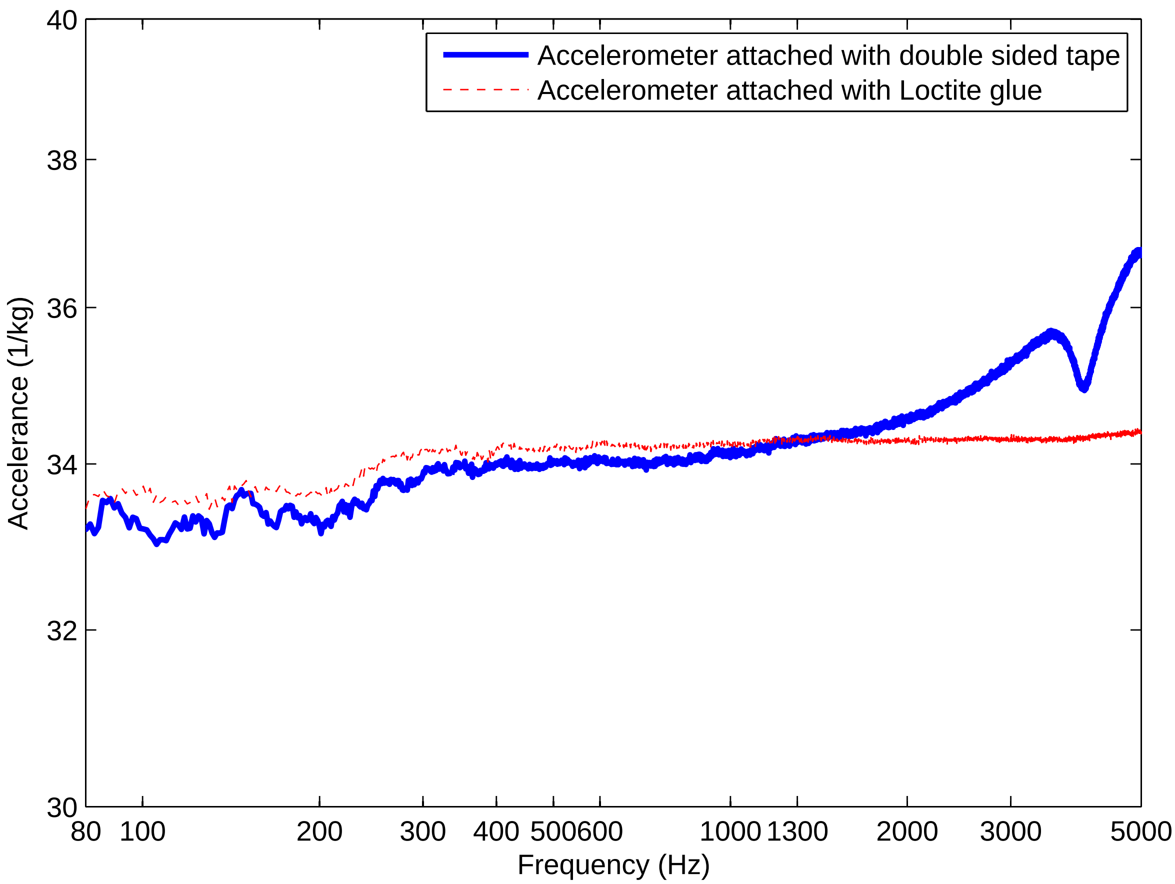

Figure 3.3: Accelerance measurement made on an aluminium mass of 0.03 kg.

Figure 3.3 shows some fluctuation in the value of accelerance for both attachment methods between 80 Hz and 2000 Hz. The standard deviation of the accelerance between 80 Hz and 2000 Hz is 0.9% when tape is used and 0.5% when glue is used. At frequencies above 2000 Hz there is a clear difference between the two attachment methods, the double-sided tape no longer provides a flat response but the glue attachment shows a flat accelerance up to 5000 Hz. The change in the response above 2000 Hz suggests that the layer of tape acts as a small additional spring in the system with a resonance frequency above 5000 Hz. The increase is not present below 5000 Hz for the Loctite glue as it is far stiffer and therefore the layer of glue will present a much higher resonance frequency than the tape. As a result of this added resonance, double-sided tape can only be used to attach accelerometers when the vibrations from an instrument are being studied below 2000 Hz. The transducers were attached to the guitars with double-sided tape restricting measurements to below 2000 Hz on the guitar. The violin studied had the accelerometer attached to it with Loctite glue and, as such, data up to 5000 Hz could be studied.

3.6 Suspension of the instruments

When making measurements on any object the method of supporting the object is of considerable importance. When studying guitars and other musical instruments it is typically a question of whether the instrument should be freely suspended or held in a manner similar to normal playing conditions. As has been stated in section 3.1, the addition of mass or any constraint to a system will affect its vibrational behaviour. If a test object is freely suspended it is also possible to calculate its behaviour under other conditions, such as with an additional mass or stiffness, from the data collected. It is not possible to 'remove' external constraints applied to the instrument (Ewins, 1984) from the measured response. Any external damping, mass or stiffness will change the behaviour of the instrument and its body modes. A general rule is that any method of suspension should have resonance frequencies "at least a factor of ten below the lowest structural resonance of the system under test" (Marshall, 1985).

Depending on the measurements being made it can be preferable to hold the guitar in normal playing conditions, an example being the examination of the modes of vibration of the neck of an electric guitar by Fleischer and Zwicker (1998). However, for the analysis of the modes of vibration of the guitar's body, the clearest data (i.e. sharp, well-defined peaks in FRF curves) is obtained when the guitar is freely suspended. This is typically achieved by suspending the instrument using elastic bands around the tuning pegs. While this technique does not accurately represent the instrument's behaviour under ordinary playing conditions, it does give the best measurement of how the guitar vibrates without any outside forces acting on it (Richardson, 2001). Freely suspending the instrument is easily definable and reproducible unlike support methods where the instrument is held at points on its body.

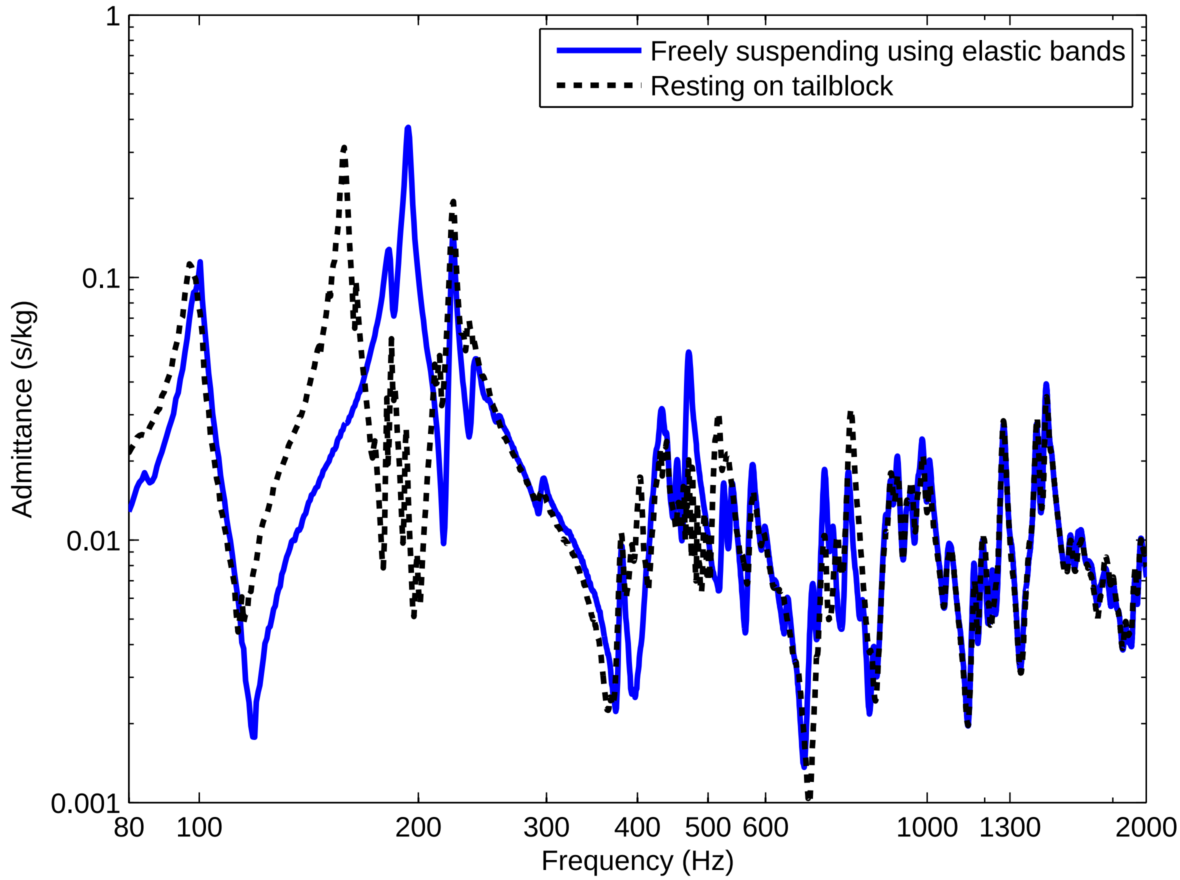

Figure 3.4: Admittance measured on the bridge of a classical guitar at the top E string using two suspension techniques.

Figure 3.4 shows that the input admittance, averaged from five measurements on the bridge of a classical guitar, is affected by the suspension method. The force was applied using an impact hammer and the velocity was measured using an accelerometer. When the instrument is freely suspended using elastic bands the peaks are clearly defined. When it is rested with the tail block on the floor, the lower-frequency response is altered considerably. There is an increased level of noise at 160 Hz and the resonance frequency of the second mode, $T(1,1)_2$, is lowered by around 40 Hz. Above 1000 Hz the two admittance measurements are close in value suggesting that the support at the tail block only effectively adds mass to the instrument's lower order body modes. However, it is the lower frequency range which has been studied considerably within the literature and is typically of most interest. Any contact between an instrument and its supports appears to affect the admittance measurement and alter the behaviour of the body modes. The instruments were suspended using elastic bands in this work to produce measurements that represent the behaviour of the instruments with no outside influence.

When suspending an instrument with elastic bands the only added interference to FRFs is produced by the instrument swaying after being excited by an impulse excitation. This swaying typically has a low amplitude and occurs at a frequency of the order of a few Hz, well below the resonance frequency of any modes of vibration that contribute to the radiated sound from any instrument. The total additional damping added to the instrument when it is freely suspended is less than 5% of the total damping (Bissinger, 2001).

A final consideration when considering how to support the instrument is the effect of the strings on the instrument. As the strings provide tension at the bridge, it is important to keep them attached and at normal playing tension when making measurements to best approximate playing conditions. If an excitation is made at the bridge the strings may be excited as well as the body modes of the instrument. String modes have considerably different characteristics to body modes. Body modes normally have Q values of < 100 (Christensen, 1984) but guitar strings have Q values of 1000 – 3000 when they are not attached to an instrument. As such, any string modes present in an FRF will be visible as a sharply defined peak in the spectrum. Due to the number of partials produced by each string some of the body modes of the instrument may be obscured by the string modes in the FRF. The presence of partials from the strings also makes the data far more complicated to analyse.

To reduce the presence of string modes in the FRF of the instrument, it was decided to dampen the strings so that only the body modes could easily vibrate. This was achieved by using a piece of soft felt wrapped between the strings towards the neck of the instrument. Admittance measurements were made with the felt in two different locations on the neck, between the 5th and 8th fret and also between the 10th and 15th fret. Figure 3.5 shows that the location of the felt damping on the strings does not have a considerable effect on the admittance. There are a few discrepancies in peak height of the body modes but these are most likely a result of slight differences of excitation location resulting from hand operation of the impact hammer. The placement of the felt can have an effect on the damping of the strings if the felt produces a termination at a node on the string, such as at the 12th or 7th fret. In this case an ‘artificial harmonic’ can be excited on the string resulting in a string mode vibrating. ‘Artificial harmonics’ are produced by placing a finger lightly at the node of a string. When the string is plucked the only string modes that vibrate are those that have nodes at that location. If the felt acts as a termination similar to a finger then an 'artificial harmonic' will be excited. This effect can easily be avoided by placing the felt so that it terminates the string away from any known nodal points.

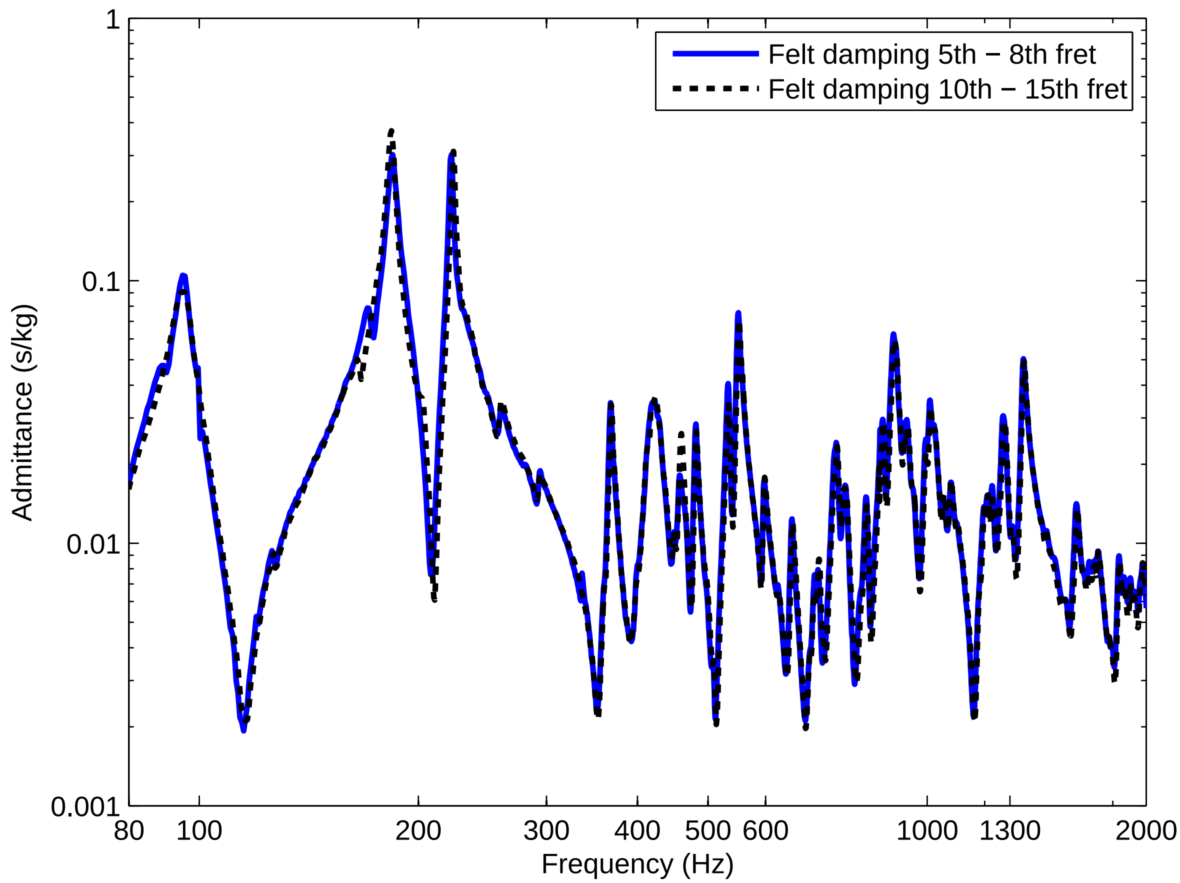

Figure 3.5: Admittance measured on a classical guitar with felt damping the strings at different locations on the neck.

3.7 Excitation locations

As an accelerometer and impact hammer were used to make input admittance and power input measurements, the force and velocity were measured at two points close together on the body rather than at the same point. The placement of the two transducers depends on the linearity of the instrument and also the desired measurement. In this thesis the behaviour of the instrument following an excitation similar to that provided by the strings was of most interest. To best approximate this excitation method, without driving the instrument through the strings, the instrument should be excited on the bridge. To measure the response produced by the impulse at the excitation point, the accelerometer was placed on the opposite side of the string. For example if the force was applied to the right of the E_4 string then the velocity was measured between the B_3 and E_4 strings. Due to the changing shapes of body modes at increasing frequencies, the response on the bridge will change depending on the which string is being studied. To best establish the change in behaviour of the instrument on the bridge, three excitation locations were used, two at the edge of the bridge and one in the centre. These three locations can be used to test where the instrument behaves symmetrically and also allows for the study of the instrument at the resonance frequencies of body modes with nodal lines down its centre.

The reciprocity of an acoustic guitar was shown in figure 2.1 in section 2.1 where the locations of an impact hammer strike and an accelerometer were swapped. It was found that the instrument produced the same values of admittance, both in terms of magnitude and phase. Swapping the locations of the transducers provides a simple test of the reciprocity of the instrument, but for confirmation of the instrument's linear behaviour the coherence function of the impulse and response must be calculated.

3.8 The coherence function

The coherence function is a statistical method used to analyse the similarities between two signals, x and y. Coherence is used to determine whether the same frequency components occur at the same time in two signals. If the value of coherence is 1 then the two signals are linearly related, lower values of coherence can indicate non-linearity but there are also other causes of lower values of coherence as shown in section 3.8.1. The typical form of the coherence function used for signal analysis is the magnitude squared coherence (Ewins, 1984). To calculate the coherence between two signals, the auto power spectral density (APSD) and the cross power spectral density (CPSD) of the two signals must first be calculated. The APSD describes the distribution of the power of a signal in the frequency domain (Kay, 1988) and is calculated by multiplying a signal, in frequency space, by its complex conjugate. The CPSD is a similar measurement except that one signal is multiplied by the complex conjugate of the other signal in frequency space. For both continuous and sampled signals the CPSD, $P_{xy}(\omega)$, between two signals, x and y, at a frequency, ω, is calculated using equation 3.17.

$$P_{xy}(\omega) = x(\omega)y(\omega)^* \tag{3.17}$$

The APSD of x, P_{xx}, is calculated by replacing $y(\omega)^*$ in equation 3.17 with $x(\omega)^*$ and the APSD of y is calculated by replacing $x(\omega)$ with $y(\omega)$. Using measurements of the APSDs and the CPSD of the two signals, the magnitude squared coherence, C_{xy}, can be calculated using equation 3.18

$$C_{xy} = \frac{|P_{xy}|^2}{P_{xx}P_{yy}} \tag{3.18}$$

where P_{xy} is the CPSD of x and y, P_{xx} is the APSD of x and P_{yy} is the APSD of y. Power spectral densities are typically used to describe long-term signals while the energy spectral densities are used for short-term signals. However, the power and energy spectral densities have "essentially similar properties" (Lynn, 1973) and can both be defined as P_{xy}, P_{xx} etc.

3.8.1 Calculating the CPSD and APSD using Welch's method

If equation 3.17 is applied to two signals then any peak in the CPSD spectrum indicates that the same frequency occurs in both signals (Golińska, 2011). If the Fourier Transform of the full signals is taken then it will not be possible to determine whether the frequency has occurred at the same time within both signals. To determine if the frequency component is present within the same time frame in both signals, the two must be separated into a series of shorter time segments. These short segments are then Fourier transformed, and equation 3.17 is used to determine the APSDs and CPSD. This is known as Welch's method (Welch, 1967). Two digitally recorded signals each with a total of N discrete points are used and each signal is separated into K overlapping segments each of length L.

The overlap between segments is important as it reduces the level of variance of any noise present in the signal. This makes it simpler to spot higher levels of coherence. By changing from no overlap to an overlap of 50% it has been shown that the variance of any background noise can be reduced to 31% of the non overlapped case (Carter et al., 1973). By reducing the variance of the background noise it is easier to locate true regions of higher coherence in the frequency spectra. The overlap between segments within each signal is typically chosen to be 50% or 75% (Kay, 1988). Increases in the number of overlapping points beyond a 75% overlap increases processing time and yields a smaller decrease in the error.

The fast Fourier transform (FFT) of each segment in the first signal is taken using a Hamming window to reduce the effects of spectral leakage, which can occur when using a simple rectangular window for short term FFTs (Thompson and Tree, 1980).

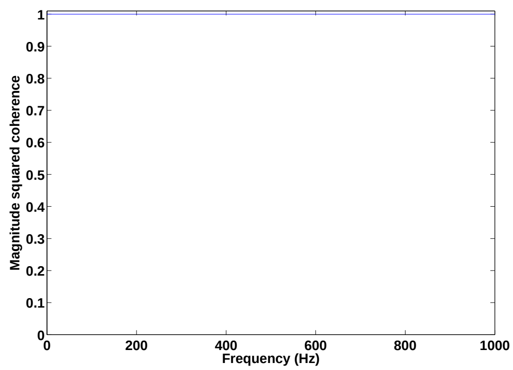

(a) C_{xy} calculated using one time segment.

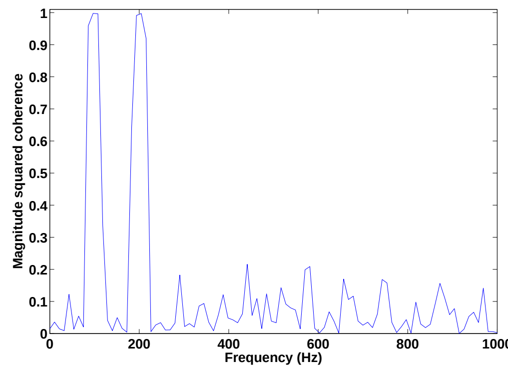

(b) X_{xy} calculated using twenty time segments.

Figure 3.6: Coherence measured on two signals with the same frequency components but different levels of white noise applied to them.

The FFT for each segment in the second signal is also taken and the CPSD of the first segment from each signal is then calculated using equation 3.17. This operation is repeated for each segment and the mean of all of the segment CPSDs is used to calculate the final value for the CPSD. Once the power spectral densities have been calculated, equation 3.18 is used to calculate the coherence of each segment. The coherence value for the complete signals is calculated by taking the mean of the coherence spectra of all of the time segments.

The number of segments and the number of samples in each segment must be chosen carefully. As with all FFT based calculations a compromise must be made between frequency resolution and the time taken to measure the signal. If only a single segment of the largest possible size is used to measure the coherence then the frequency resolution will be higher but it will not be possible to determine how the frequency spectra of the two signals change with time. Reducing the length of the segment shows the change in frequency spectra more clearly but reduces the resolution of the frequency points.

Figure 3.6 shows the coherence calculated for two signals each containing two sine waves of 100 Hz and 200 Hz, but with different phases and with white noise applied to both signals. White-noise signals contain all frequencies and this produces a characteristic hiss sound. If only a single time segment is analysed for both signals then they will both contain signals at all frequencies. This produces a coherence value of 1 across the entire frequency range as there is an exact match up for each frequency component in each signal as shown in figure 3.6a. Examining the coherence of a single time segment therefore reveals no information about whether a specific frequency component exists in both signals. Figure 3.6b shows the coherence when 20 overlapping time segments are used to calculate the coherence. There are two peak values of coherence which have values close to 1 at 100 Hz and 200 Hz, which are the frequencies of the two sine waves in the original signals. At all other frequencies the values of coherence are less than 0.2, so the two white noise signals clearly change with time. The presence of frequency components in two signals can only be determined if the signals are divided into many shorter overlapping time windows.

3.8.2 Coherence between real input and output signals

For an ideal linear system the coherence should equal 1 for all frequencies. This does not occur in real linear systems due to the effect of external noise and resonances within transducers at higher frequencies. However, values of coherence close to 1 show that the system can be assumed to be linear at those frequencies.

Force and acceleration measurements were made on a suspended mass, which is a simple linear system with no resonances in the frequency range of interest (80 Hz to 10,000 Hz). A force was applied, and measured, at one end of the mass using a hand-operated impact hammer and the acceleration was measured using an accelerometer at the opposite end. The response was recorded for 2 seconds after the impact at a sampling rate of 44.1 kHz (a total of 88,200 samples). The segment length was chosen to be 16,384 samples which allows for the use of FFT algorithms and the overlap for each segment was set at 50%. The coherence between the force and acceleration signals was measured to test the linearity between the two transducers.

Figure 3.7 shows the measured coherence plotted as a function of frequency. Between 80 Hz and 10,000 Hz the highest value of coherence is 0.999 and the lowest value is 0.977, which corresponds with the slight decrease at 140 Hz, which shows that the system is highly linear across a large frequency range. Below 80 Hz the coherence value is lower in value, but this region is of little interest for measurements on guitars as there are no body modes that radiate a significant amount of sound pressure. Also the lowest note playable on a classical guitar in standard tuning is E_2 which has a fundamental frequency of 82 Hz. The transducers used for the measurements are shown to be highly coherent and linear in behaviour for this simple linear system, with no resonances within the frequency range being studied. However, the coherence characteristics change depending on the linearity of the system being analysed.

The magnitude squared coherence was determined for a classical guitar and the coherence is shown in figure 3.8. The strings of the guitar were damped and an accelerometer was attached to the bridge of the guitar, between the B_3 and E_4 strings. A force was applied using a hand operated impact hammer to the right of the E_4 string.

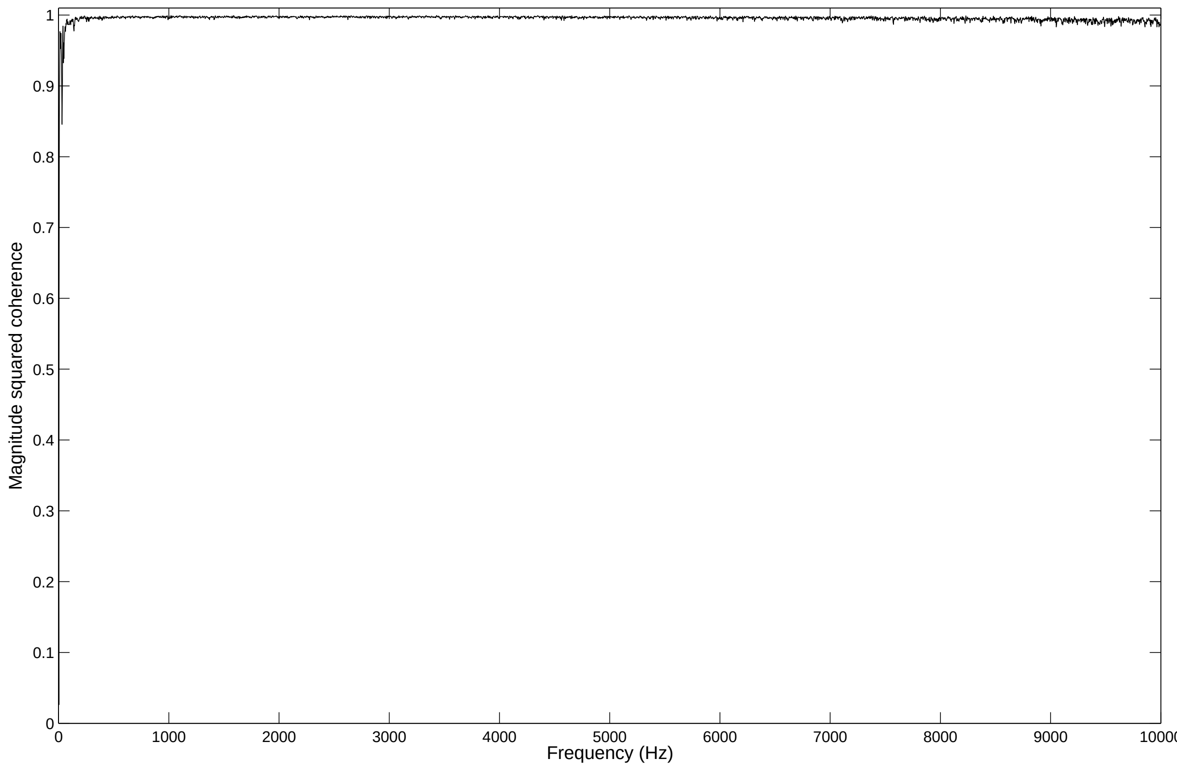

Figure 3.7: Magnitude squared coherence of force and acceleration signals measured on a suspended 0.03 kg mass.

The recording was made at a sampling rate of 44.1 kHz. The segment length was reduced to 8,192 samples for this coherence calculation but the overlap remained set as half the length of the segment. Above 1000 Hz the coherence is close to 1 but at lower frequency values there are several frequencies where the coherence value is considerably less than 1. The reduced values of coherence occur at the same frequencies as the anti-resonances in the admittance data also shown in figure 3.8. These anti-resonances correspond with frequencies where there is a low level of velocity output compared with the force input. The low level of output means that the signal can be affected by noise. This can lead to a decreased value of coherence due to the lower signal-to-noise ratio (SNR). Increasing the applied force improves the SNR, leading to the dips in the coherence values being reduced, so that the overall coherence frequency spectra is closer to 1. However, using impulse excitation on a classical guitar limits the force which can be applied because of considerations about damaging the instrument with too strong a strike. The lower output acceleration level will also lead to a lower value of the APSD and CPSD at that frequency which will result in an overall lower value of the coherence.

The other cause of reduced values of coherence is if the acceleration measurement decays more slowly than the applied force. In this case, the later time segments of

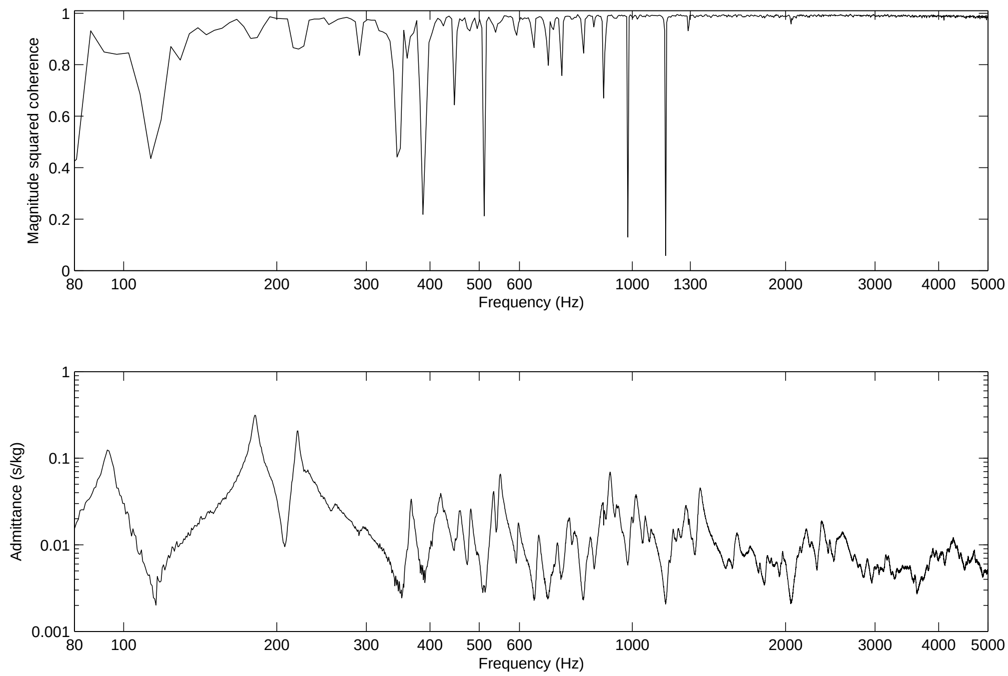

Figure 3.8: Magnitude squared coherence of force and acceleration signals measured on the bridge of a classical guitar either side of the top E string. The second graph shows the admittance measurement (velocity/force) measured from the same signals.

the recorded acceleration signal will still contain some frequency components that are no longer present in the force signal. This produces a low value in the CPSD and an overall lower coherence between the two signals. The issue of the acceleration decaying more slowly than the force only occurs if the instrument is excited using an impulse excitation. If the instrument is continually driven, for example using electromagnetic driving, the values of coherence will typically be higher than for an impulse excitation. It is preferable to determine coherence using continual driving, but impulse excitation still provides a good test of linearity between transducers and musical instruments in figure 3.8.

In figure 3.8 there are far fewer dips in the coherence above 1000 Hz than below 1000 Hz. A possible explanation for this is that the velocity decays much more quickly above 1000 Hz than at lower frequencies. As the impulse excitation results in the force decaying quickly, both the velocity and force signals will decrease to the background noise level quickly and give a greater value of coherence.

3.9 Calculating power output using spherical-harmonic decomposition

3.9.1 Sound Pressure

The sound pressure at a single point in space can be described as a combination of incoming and outgoing sound waves relative to the source of the sound waves. The sound sources are modelled as being simple sources with radii which are small in comparison to the wavelength of sound (Morse, 1948). The equation (previously shown in figure 2.17) to describe the sound pressure , $p(r, \theta, \phi)$, from a simple source at a distance r and angles θ (elevation) and ϕ (azimuth) from a vibrating object is (Weinreich and Arnold, 1980)

$$p(r, \theta, \phi) = \sum_{lm} [a_{lm} h_l(kr) + b_{lm} h_l^*(kr)] Y_{lm}(\theta, \phi) \tag{3.19}$$

where λ is the wavelength, k is the wave number $(\frac{2\pi}{\lambda})$, $h_l(kr)$ is the spherical Hankel function of the first kind, $Y_{lm}(\theta, \phi)$ is a spherical harmonic and a_{lm} and b_{lm} are the expansion coefficients describing the outgoing and incoming waves respectively. The values l and m describe the order of the spherical harmonic, where l takes values from $0 \to \infty$ and $m = -l ... 0 ... +l$. A monopole source is described when $l = m = 0$ and a dipole when $l = 1$ for all allowed values of m.

To calculate the incoming and outgoing coefficients, the sound pressure must be measured at two different radii on two separate concentric measurement spheres. For equation 3.19 to be true, there must be no sound sources or scatterers located between the two spheres of measurement. Therefore the measurement spheres must lie at a distance beyond the vibrating regions of the instrument being studied. If the measurements of sound pressure are made under anechoic conditions, with no external sources present, then the values of b_{lm} are kept to a minimum.

The pressure at a point in space can also be written more simply using the complex weighting factor of a spherical harmonic, C_{lm} (Williams, 1999). C_{lm} was calculated in this work using the same MATLAB script as used by Richardson (2001). The full details of calculating C_{lm} can be found in appendix A of the work by Richardson.

$$p(r, \theta, \phi) = \sum_{lm} C_{lm}(kr) Y_{lm}(\theta, \phi) \tag{3.20}$$

Using equations 3.19 and 3.20, the values of a_{lm} and b_{lm} can be calculated by measuring the sound pressure at the same angle (θ and ϕ) from the source but at two different radii, r_1 and r_2. As two pressure measurements are made at two different radii, a simultaneous equation can be solved to determine the values of a_{lm} and b_{lm}. The two coefficients should take the same values at any distance, ignoring heat losses as the sound wave travels through the air. The simultaneous equation can be expressed in matrix form as

$$\begin{bmatrix} a_{lm} \\ b_{lm} \end{bmatrix} = \begin{bmatrix} h_l(kr_1) & h_l^*(kr_1) \\ h_l(kr_2) & h_l^*(kr_2) \end{bmatrix}^{-1} \begin{bmatrix} C_{lm}(r_1) \\ C_{lm}(r_2) \end{bmatrix} \tag{3.21}$$

Using the calculated values of C_{lm} and $h_l(kr)$, the values of a_{lm} and b_{lm} are found. The outgoing coefficient, a_{lm}, alone is used to calculate the source strengths and the weights of the radiation components (Hill et al., 2004). As it is only the outgoing sound waves that are of interest, b_{lm} can be omitted from equation 3.19 and an expression for the source strength can be defined. The outgoing sound pressure is therefore

$$p(r,\theta,\phi) = \sum_{lm} a_{lm} h_l(kr) Y_{lm}(\theta,\phi) \tag{3.22}$$

Equation 3.22 shows the total outgoing pressure from all sources but the pressure contribution from the individual sources can be calculated by using values of l and m and ignoring the summation. For a monopole, l and m are both 0 resulting in an outgoing coefficient of a_{00}. The spherical Hankel functions of the first kind for $l = 0$ and $l = 1$ (for use in monopoles and dipoles) can respectively be written as (Williams, 1999)

$$\begin{aligned} h_0(kr) &= \frac{e^{ikr}}{ikr} \\ h_1(kr) &= -\frac{e^{ikr}(i+kr)}{(kr)^2} \end{aligned} \tag{3.23}$$

The final term in equation 3.22 is the spherical harmonic, Y_{lm}. These spherical harmonics are defined as

$$Y_{lm}(\theta,\phi) = \sqrt{\frac{2(l+1)}{4\pi}\frac{(l-m)!}{(l+m)!}} P_l^m(cos\theta) e^{im\phi} \tag{3.24}$$

The square root term is defined as a normalisation constant, N_{lm}, and $P_l^m(cos\theta)$ is the associated Legendre polynomial. The un-normalised spherical harmonics for $l = 0 \rightarrow 2$ are $Y_{00} = 1$, $Y_{10} = \cos\theta$, $Y_{1\pm1} = \pm\sin\theta e^{\pm i\phi}$, $Y_{20} = (3\cos^2\theta - 1)$, $Y_{2\pm1} = \sin\theta\cos\theta e^{\pm i\phi}$ and $Y_{2\pm2} = \sin^2\theta e^{\pm 2i\phi}$. The sound pressure from a monopole is shown in equation 2.13 and is repeated, for clarity, in equation 3.25

$$p = \frac{-ik\rho_0 c}{4\pi r} S_\omega e^{ikr} \tag{3.25}$$

An expression for a_{00} can now be determined, in terms of the source strength, S_ω, by setting equation 3.22 equal to equation 3.25 and using the definition of $Y_{lm}(\theta,\phi)$ from equation 3.24. a_{lm} is therefore give as

$$a_{00} = \frac{k^2 \rho_0 c S_\omega}{4\pi N_{00}} \tag{3.26}$$

Monopoles radiate sound pressure uniformly so they only have one orientation which is $l = m = 0$. For a monopole the source strength, S_ω, is the "rate of flow of air away from the surface" of the source (Morse and Ingard, 1968). The source is assumed to be a point source and as such spherical in shape. The source strength can therefore also be written as the effective area of the source, $G_{00} = A$, multiplied by its velocity, v, to give $S_\omega = Av$. For a monopole the source strength can therefore also be called the area velocity.

A dipole can have three orientations because $l = 1$ so m can take values of $-1, 0$ or 1. The three orientations of the dipole can be described as lying along the x, y and z axes of the chosen orientation. To calculate the three dipole a_{lm} values in terms of their source strengths, D_ω, the values of $l = 1$ and $m = -1 \rightarrow +1$ are used in equation 3.22 which is set equal to equation 3.27 (which is repeated from equation 2.16 for clarity). Equation 3.28 shows the value of a_{10}.

$$p = -k^2 D_\omega \frac{\rho c}{4\pi r} \cos(\theta) \left(1 + \frac{i}{kr}\right) e^{ikr} \tag{3.27}$$

$$a_{10} = \frac{k^3 \rho_0 c D_{\omega 0}}{4\pi N_{10}} \tag{3.28}$$

The dipole source strength, D_ω, can also be expressed as $S_\omega \mathbf{d}$. As $\mathbf{d}$ is the vector distance between the two monopoles, the dipole strength will therefore also be a vector quantity $\mathbf{D}_\omega$. The dipole strength is a volume velocity rather than an area velocity. For quadrupoles the source strength, $\mathbf{Q}_\omega$, is equivalent to $\mathbf{S}_\omega \mathbf{d^2}$, or $\mathbf{D}_\omega \mathbf{d}$. The G_{00} and source strength can no longer be described using simple geometry, such as effective area or volume, so instead an alternative description is used for higher order sources. The effective area or volume can be described as a weighting for each source, this weighting is written as G_{lm} (Hill et al., 2004).

The a_{lm} coefficients in terms of source strength can be calculated using the same methods as for equations 3.26 and 3.28, which results in a general formula for a_{lm} in terms of a generalised source strength. This was shown in Hill et al. (2004) as

$$a_{lm} = \frac{1}{N_{lm}} \frac{\rho_0 c k^{l+2}}{4\pi} G_{lm} v \tag{3.29}$$

where v is the velocity at the excitation point. The value $G_{lm}v$ in equation 3.29 is the source strength.

3.9.2 Source strength

Rearranging equation 3.26 gives the source strength, S_ω, for a monopole as

$$S_\omega = \frac{4\pi |a_{00}| N_{00}}{\rho_0 c k^2} \tag{3.30}$$

The magnitude of a_{00} is taken to account for the sign of the radiativity, that is to say whether the source is in phase or out of phase with the excitation force (Richardson, 2001).The source strengths, D_ω, for the three dipole orientations are

$$D_{\omega m} = \frac{4\pi |a_{1m}| N_{1m}}{\rho_0 c k^3} \tag{3.31}$$

where m takes values of either -1, 0 or $+1$. The source strengths, Q_ω, for the five quadrupole orientations are

$$Q_{\omega m} = \frac{4\pi |a_{2m}| N_{2m}}{\rho_0 c k^4} \tag{3.32}$$

where m takes integer values between -2 and $+2$. As equations 3.31 and 3.32 show, there are an increasing number of orientations possible for dipoles and quadrupoles. For dipoles the orientations lie along the Cartesian axes but quadrupoles have more complex orientations. The orientations of the dipole and quadrupole components from the spherical harmonics, Y_{lm}, (Blanco et al., 1997) are $Y_{1-1} = y$, $Y_{10} = z$ and $Y_{11} = x$ for dipoles and $Y_{2-2} = xy$, $Y_{2-1} = yz$, $Y_{20} = z^2$, $Y_{21} = xz$ and $Y_{22} = x^2 - y^2$. The quadrupole strengths, Q_ω, form a 3x3 symmetric tensor.

$$Q_\omega = \begin{pmatrix} Q_{xx} & Q_{xy} & Q_{xz} \\ Q_{yx} & Q_{yy} & Q_{yz} \\ Q_{zx} & Q_{zy} & Q_{zz} \end{pmatrix} \tag{3.33}$$

As the tensor is symmetric then for a linear system, $Q_{xy} = Q_{yx}$, $Q_{zx} = Q_{xz}$ and $Q_{zy} = Q_{yz}$ which reduces the total number of independent sources to six. These, in turn, are orientated such that they give five quadrupole wave sources (Morse and Ingard, 1968). To calculate the power output, the magnitudes of the dipole and quadrupole sources must be calculated. The magnitudes of the sources are given as (Morse and Ingard, 1968)

$$D_\omega = \sqrt{D_x^2 + D_y^2 + D_z^2} \tag{3.34}$$

$$Q_\omega = (Q_{xy} + Q_{yx})^2 + (Q_{xz} + Q_{zx})^2 + \frac{1}{3}(2Q_{zz} - Q_{xx} - Q_{yy})^2 + (Q_{xx} - Q_{yy})^2 \tag{3.35}$$

The magnitudes of the source strengths are used to calculate the power output for each component (Morse and Ingard, 1968) as shown in equations 3.36, 3.37 and 3.38.

$$\Pi_S = \frac{\rho\omega^2}{4\pi c} S_\omega^2 \tag{3.36}$$

$$\Pi_D = \frac{\rho\omega^4}{12\pi c^3} D_\omega^2 \tag{3.37}$$

$$\Pi_Q = \frac{\rho\omega^6}{60\pi c^5} Q_\omega^2 \tag{3.38}$$

where Π_S is the monopole power output, Π_D is the dipole power output and Π_Q is the quadrupole power output. To calculate the total power output from all sources it is simply a matter of summing the Π values expressed in equations 3.36, 3.37 and 3.38. A simple summation of the source powers is possible as there is "no power coupling between spherical harmonics of different orders" (Williams, 1999).

3.9.3 The half-wavelength problem

Using spherical-harmonic decomposition to determine the power output from an instrument reveals the individual contributions to the radiated sound but there is a limitation in the frequency range that can be studied. This limit is imposed by the spacing of the two microphones and is referred to here as the half-wavelength problem.

In previous work done using spherical-harmonic decomposition, body modes of classical guitars were studied at frequencies up to 600 Hz (Richardson, 2001). For the 0.26 m microphone spacing used (which is the same as that used in this work) the frequencies investigated had a half wavelength less than the spacing of the microphones. When an integer multiple of half the wavelength of the sound wave is comparable in size to the spacing of the microphones, the a_{lm} and b_{lm} coefficients calculated using spherical-harmonic decomposition increase rapidly and non-physically in size. Any reconstructed pressure field made with these values will show values of sound pressure far in excess of those measured using the microphones. As the incorrect pressure values are only present in the reconstructed sound pressure field, it must therefore be the method used to calculate a_{lm} rather than the placement of the microphones that produces the error. The incorrect values arise from the matrix of spherical Hankel functions shown in equation 3.21.

The equation for the spherical Hankel function of the first kind is shown in equation 3.23. The spherical Hankel function of the second kind is the complex conjugate of the spherical Hankel function of the first kind, $h_0^*(kr)$. When taking the inverse of the matrix of Hankel functions in equation 3.21 the determinant of the matrix is

$$\frac{k^2 r_1 r_2}{e^{ik(r_1-r_2)} - e^{ik(r_2-r_1)}} \tag{3.39}$$

When the separation of the microphones is equal to half the wavelength of the sound studied, λ, then $\lambda = 2(\Delta r)$, where $\Delta r = r_2 - r_1$. Using this expression for λ in k, equation 3.39 is then shown to be

$$\frac{k^2 r_1 r_2}{e^{i\frac{\pi}{\Delta r}(r_1-r_2)} - e^{i\frac{\pi}{\Delta r}(r_2-r_1)}} \tag{3.40}$$

Substituting Δr into equation 3.40 simplifies the denominator so that it is equal to $e^{-i\pi} - e^{i\pi}$. Euler's identity shows that both exponential terms are equal to -1. The denominator is therefore zero which means that the inverse of the matrix will be infinitely large when half the wavelength is exactly equal to the spacing of the microphone. The discrete nature of fast Fourier transforms means that it is not possible to measure a signal at frequencies where an integer number of half wavelengths is *exactly* equal to the microphone spacing. Instead the inverse of the matrix is unnaturally large rather than infinite around the half-wavelength frequency. The only option available to prevent these calculation errors is to reduce the spacing of the microphones. This increases the frequency where the inaccuracy arises and allows for a wider initial frequency range to be studied before the source strength appears infinitely large. However, Weinreich and Arnold (1980) stated the "numerical errors involved in solving for the coefficients will increase" if the microphones are very close together.

Data requiring the use of the reconstructed sound pressure field or source strengths, such as output power or radiation efficiency, will have data omitted at frequencies corresponding to integer multiples of $\lambda/2$. Incorrect a_{lm} and b_{lm} values are also found at frequencies surrounding $\lambda/2$ as the denominator becomes increasingly small. The microphone separation used in this work produced the smallest denominator at integer multiples of 660 Hz. Data is omitted 25 Hz either side of the integer multiples of 660 Hz and the output power from the instrument cannot be determined within these frequency ranges.

Chapter 4

Experimental Methods

4.1 Measuring radiation efficiency, η

To calculate the radiation efficiency, η, from a stringed instrument, four measurements must be made simultaneously. These are the force and velocity inputs at the bridge and the RMS sound pressure from two microphones on two concentric measurement spheres. A block diagram of the set up is shown in figure 4.1.

The strings of the instrument were under standard tuning tensions so that they applied the same amount of tension to the bridge as under normal playing conditions. To reduce the effect of the modes of vibration of the strings on any measurements, the strings were damped using a piece of felt wrapped between the strings. The instruments were suspended using elastic bands around the tuning pegs from the top of a column in the centre of an anechoic chamber (working dimensions of 2 m x 2 m x 1.5 m). The central column was fixed to a rotating stand which was connected to a motor that allowed the instrument and stand to be rotated. The instrument was also held lightly in place by a string of elastic bands across the neck and supported with soft foam on the lower bout of the back plate to reduce rotation and motion of the instrument after each impulse excitation. Suspending the instruments from elastic bands provides a support system that is the closest to freely suspending the instrument. The foam holding the instrument in place has only a small effect on an instrument's vibrational behaviour.

The force was both applied and measured using a PCB impact hammer (Model 086E80). To protect the surface of the instrument from damage a small metal disc (mass = 160 mg) was attached to the bridge using double-sided tape at the strike location. The acceleration was measured with a PCB accelerometer (Model 352B10) mounted on the bridge using double-sided tape for guitars. For each set of η measurements the accelerometer was removed and re-attached using a new piece of tape to ensure a strong

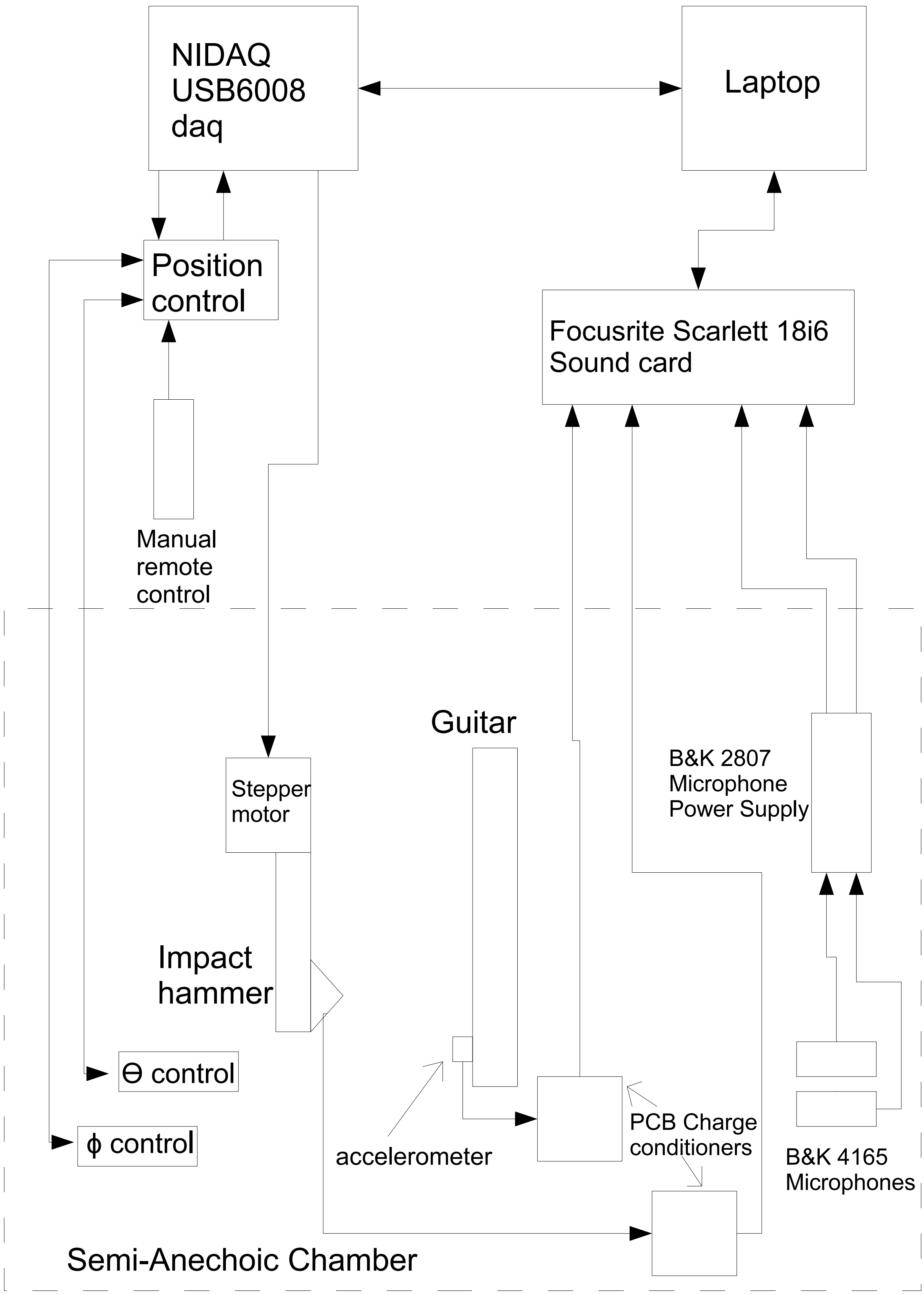

Figure 4.1: Block diagram of the apparatus used for η measurements.

connection between the accelerometer and the instrument.

The hammer was held in a specially constructed support pivoted on a ball bearing, which allowed the hammer to swing freely. The automated hammer set up is shown in figure 4.2. A stepper motor with a single 'tooth' was located above the impact hammer support to produce a repeatable, automated strike. The stepper motor turns clockwise and the tooth pushes the offset metal arm forwards, which results in the hammer moving back away from the instrument. As the tooth rotates it loses contact with the arm and the hammer swings forward and strikes the instrument. The hammer and accelerometer both have microelectronic amplifiers contained within their casing to act as charge amplifiers. The amplifiers in the transducers were powered using PCB 470C02 signal conditioners. The conditioners also send the output signal to the sound card for measurement.

The sound pressure was measured using two B&K 4165/2619 microphones, on two concentric spheres with radii of 0.45 m and 0.71 m from the centre of the guitar. The microphones are powered using a B&K 2807 microphone power supply. The microphones were mounted on a boom, attached to a motor, which allowed them to be moved through nine elevation angles determined using Gaussian quadrature. To measure the sound pressure on the two measurement spheres the motorised central column was rotated through 36 evenly spaced divisions (10°). The sound pressure levels were measured at 324 different measurement positions on a series of 9 (elevation) x 36 (azimuthal) points on the two measurement spheres. The sound pressure, force and velocity measurements were triggered from the signal produced by the force hammer. When the hammer struck the instrument the stepper motor was stopped and the measurements made. If the excitation was provided without any double hits then the microphones or instrument were moved to the next measurement location. Figure 4.3 shows a guitar suspended in the centre of the two measurement spheres determined by the microphone boom.

The two positioning motors (control of instrument azimuth angle θ and control of microphone elevation angle ϕ in figure 4.1) are both attached to separate metal discs. The discs have holes drilled through them around the circumference with angles from the centre corresponding to the measurement angles for the microphones. Either side of the disc are an IR emitter and a detector. As the motor turns, the disc rotates so that when the light from the emitter is detected through a hole an electrical signal is sent to the DAQ interface to show that the motor has reached a predetermined angle. The motors for microphone position and the stepper motor were controlled using a DAQ (Data Acquisition) interface, NI-USB 6008, which had instructions sent to it through a

Figure 4.2: The stepper motor and support for automated hammer excitation.

Figure 4.3: Guitar located in centre of anechoic chamber.

MATLAB program run on a laptop.

The force, acceleration and sound pressure signals were recorded at each measurement point using an external USB Focusrite Scarlett 18i6 sound card. This particular sound card has six 1/4" inputs, two with an adjustable gain and four without. The signals were sent to the four channels without adjustable gains so that the determined calibration values would not be affected by a slight change in the level of gain on one channel. Using a USB powered sound card and DAQ interface means that the laptop can be run on battery power rather than mains supply. This reduced the level of electrical noise present in the signals, in particular the microphone signals. The timings of the force, acceleration and sound pressure recordings were triggered by the impact hammer striking the guitar. The recordings were 2 s long and were made at a sampling rate of 44.1 kHz. A fast Fourier transform (FFT) of size 2^{16} samples was taken of all four signals at each of the 324 measurement points. The FFT window size and sampling rate result in a frequency resolution of 0.67 Hz. The window has a length of 1.49 s so the recording was sufficiently long to contain enough samples for the FFT to be taken of the data. This time window was also found to be of sufficient length for the sound pressure to decay away to zero.

Control signals were sent from the MATLAB program to the DAQ interface and to the positioning motors to move to the next measurement location after each successful strike. The total time to take a full set of 324 force, velocity and pressure measurements was around 2 hours, allowing for several repeat measurements on an instrument in a single day under similar atmospheric conditions.

The power output was calculated using a spherical-harmonic-decomposition algorithm in MATLAB at each frequency point. The power input was calculated across the frequency range for each of the 324 excitations. The power input used to determine η was averaged from the 324 power input measurements for the instrument.

The support structures for the instrument, microphones and automated impact hammer are of importance to the accuracy of the measured data. All of the supports are constructed using metal poles with dimensions designed to reduce the level of scattering and diffraction of the sound waves between 80 Hz and 2000 Hz. At higher frequencies diffraction of the sound waves from the support poles begins to occur so the support system would need to be changed. The poles are of diameter 20 mm and 15 mm which means that they are approximately an order of magnitude smaller than the wavelength of sound at 2000 Hz. The stepper motor dimensions are 30 mm x 40 mm x 40 mm, so the motor is also sufficiently smaller than the limit of the wavelength of sound studied.

4.2 Calibration

If measurements of FRFs are made without first calibrating the transducers then comparisons of measurements can only be made between instruments under the same conditions using the same equipment, as shown for a set of violins by Jansson et al. (1986). If the results are calibrated then it is possible to compare the same quantities from different instruments and different experimental set ups. Each element of the experimental set up must be calibrated so that meaningful measurements can be obtained.

4.2.1 Calibration of transducers

The two types of transducer used in this work were a force transducer and an accelerometer. In order to measure a true value of force, F, or acceleration, a, the voltages generated by the excitation and response, V_F and V_a, must be multiplied by a calibration factor, either S_F or S_a respectively (Ewins, 1984).

$$\begin{aligned} V_F &= S_F F \\ V_a &= S_a a \end{aligned} \tag{4.1}$$

The calibration factors in equation 4.1 are also known as the voltage sensitivities and the terms are interchangeable. For commercially constructed transducers, calibration values are provided but over time and use the values may change. The simplest method of checking the calibration values is to calibrate both an accelerometer and a force transducer together as a single system (Ewins, 1984). However, the calibration value obtained using this method is only suitable for input admittance measurements. The simplest way of checking the calibration values is to attach the accelerometer and the force transducer to opposite ends of a known mass, m. When a force is applied at the end where the force transducer is located, a voltage signal is measured by both the accelerometer and force transducer at their respective ends. Using Newton's second law ($F = ma$) and rearranging equation 4.1, the two calibration factors can be combined into a single factor, S, which is equal to $\frac{S_F}{S_a}$

$$\frac{V_F}{V_a} = Sm \tag{4.2}$$

This calibration value can be used for any measurement where the ratio between force and acceleration, or vice versa, is being measured. If calibration values are provided for both transducers then the combined calibration value should be the ratio of the two, confirming the accuracy of the individual calibrations.

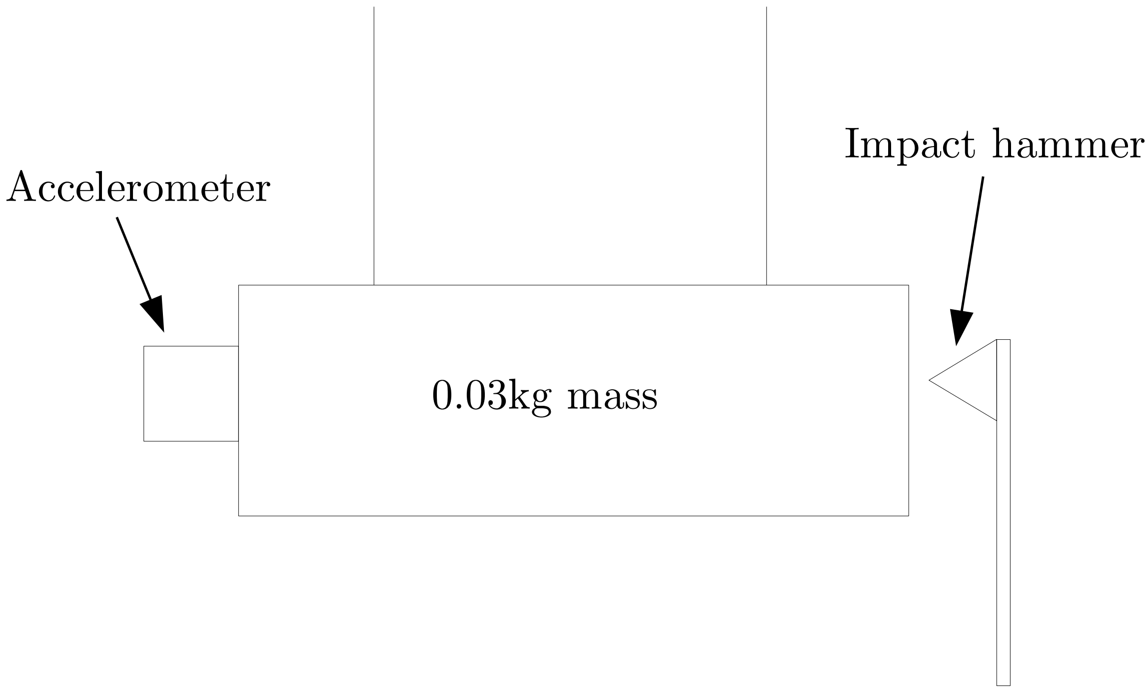

Figure 4.4: Diagram of calibration set up for a force transducer and accelerometer system.

In this work, the calibration value of a system using an accelerometer and impact hammer was determined by measuring the accelerance (a/F) of a cylindrical aluminium block of mass 0.03 kg, radius 9 mm and length 39 mm. A light mass was chosen so that the ratio of force to acceleration would result in a high SNR for the lightweight impact hammer. If the mass is too large then the level of acceleration generated at the opposite end to the excitation will be small and the calibration factor will be contaminated by noise. While the measurements made on the guitars were automated, the calibration was made by hand. The mass used for calibration was freely suspended to prevent any external damping affecting its behaviour. The mass was suspended using nylon fishing line which allowed it to swing freely back and forth. A diagram of the set up is shown in figure 4.4.

For calibration purposes, the accelerometer was attached to one end of the aluminium block with double-sided tape and the opposing end was struck with the impact hammer. The voltage signals were acquired using a sound card and were Fourier transformed and analysed using a MATLAB script to produce values of accelerance. Figure 4.5 shows the magnitude of the accelerance (before calibration) and figure 4.6 shows the phase of the accelerance (also before calibration). The magnitude is flat between 2 Hz and 10000 Hz and the phase has a value close to 0 radians. If an accelerometer with a reverse orientation was used then the accelerance would be in anti-phase by either $-\pi$

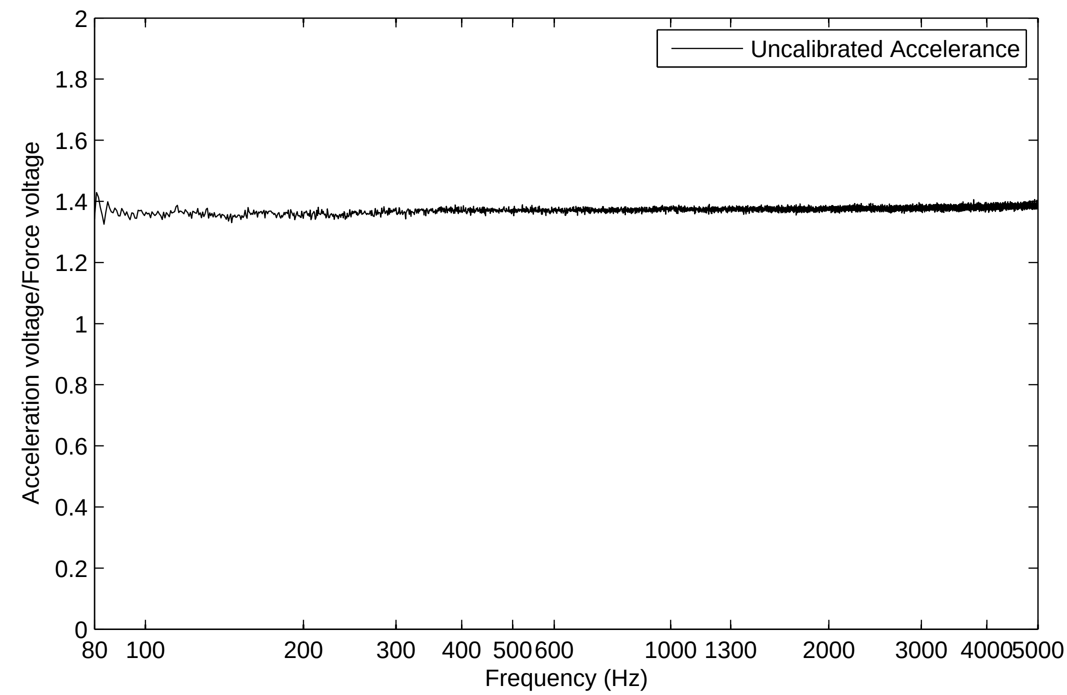

Figure 4.5: Uncalibrated accelerance measured on a 0.03 kg aluminium block.

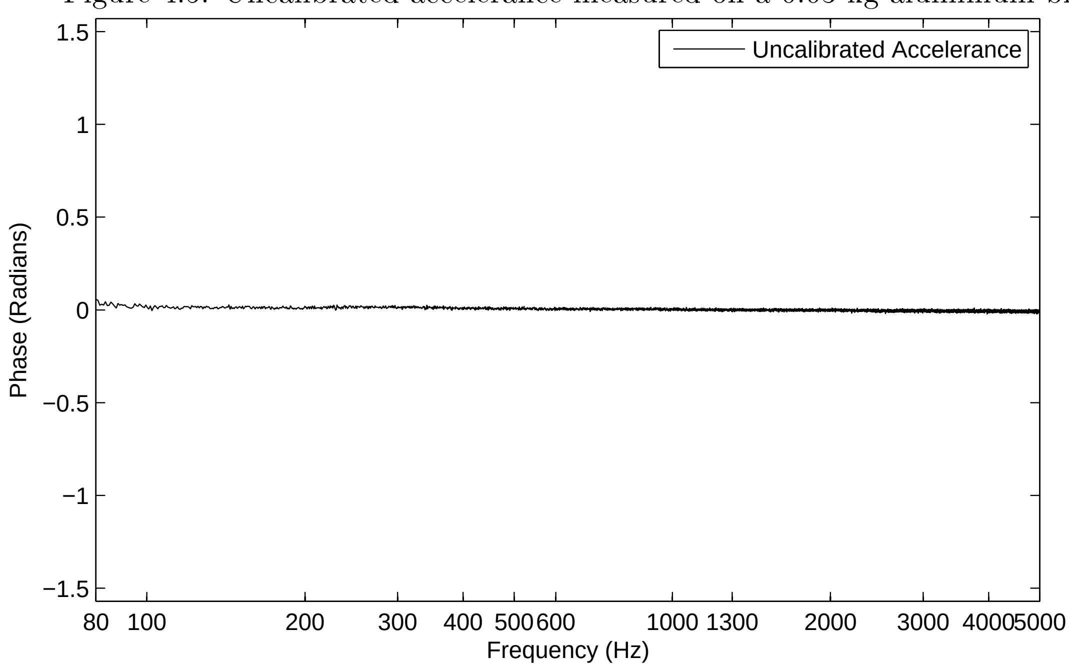

Figure 4.6: Phase of the uncalibrated accelerance measured on a 0.03 kg aluminium block.

or $+\pi$ radians. The uncalibrated accelerance is mainly dependent on the behaviour of the accelerometer which has a resonance frequency of 65 kHz and produces acceleration measurements that are accurate to within 5% from 2 Hz - 10000 Hz (PCB, 2007b).

The flat response of figure 4.5 and figure 4.6 shows that the method is suitable for calibrating the hammer and accelerometer system between 80 Hz - 10000 Hz. If the accelerance curve deviates from a flat line then it may indicate that the transducers are not functioning correctly or that they have a resonance frequency that affects the response within the studied frequency range. The combined calibration value, S, was found to be similar in value to that obtained by dividing the supplied factory calibration values by each other. The experimentally determined calibration value was (23.1 ± 0.2) kg^{-1} in comparison to the factory calibrated ratio of the sensitivities which is 22.2 kg^{-1}. The phase in figure 4.6 is slightly above 0 in the lower frequency range suggesting that the strike direction was not exactly parallel to the orientation of the accelerometer. Any off axis excitation will lead to the mass being excited in other directions which can 'contaminate' the acceleration measurement (Boutillon and Weinreich, 1999) so a true accelerance measurement cannot be made, which may explain the non-zero phase values.

4.2.2 Calibration of the sound card

When data is read from an external sound card in a MATLAB script the scale is automatically set so that the amplitude of input signals (in arbitrary units) is limited to between -1 and +1. Sound cards do not typically have voltage ranges between -1V and +1V so the voltage range of the card must be known before calibrated measurements can be made. To calibrate the input voltage to the sound card a sine wave was generated using a B&K Heterodyne Analyzer type 2010. The output voltage of the signal was sent to the Focusrite Scarlett 18i6 sound card and to a TTi 1604 digital multimeter. The peak RMS voltage value was acquired by the soundcard was measured using MATLAB and compared with the value measured using the multimeter. The factory calibration values were all provided in terms of units per volt, i.e. Pa/V, ms^{-2}/V etc. These values could be used in the MATLAB software once the sound card was correctly calibrated.

4.2.3 Microphone calibration

Using a calibrated sound card allows the microphones to be calibrated. B&K microphones of type 4165/2619 were used for all sound pressure measurements and were pre-calibrated. To check the factory calibration, and to calculate a new calibration value if necessary, a known sound pressure source was used. The sound pressure source was a B&K Sound Level Calibrator (Type 4230) which generates a sound pressure signal of 93.8 dB SPL (or 0.979 Pa) at 1000 Hz. The calibrator can be used on 1/2" and 1" microphones with an adaptor to firmly attach the calibrator to the microphones. The microphone signal is the voltage generated by 0.979 Pa sound pressure and should be equal to the calibration provided. Unlike the method for calibrating the transducers the microphone signal can only be examined in the time domain not the frequency domain.

4.2.4 Consistency of the automated hammer strikes

The automated hammer system shown in figure 4.2 produces a force impulse with a comparable magnitude for each excitation. There is a slight variation in the force applied depending on the position where the hammer is released to swing after it is pulled back. The calibrated admittance for each of the 324 excitations made on BR2 is shown in figure 4.7a. The anti-resonance at 113 Hz shows the most variation in the measured admittance and there is a small peak around 120 Hz. This frequency region is susceptible to noise as the anti-resonance has the lowest value of admittance between 80 Hz and 2000 Hz. Therefore at this frequency the instrument undergoes its lowest level of excitation. As such, small changes in the value will be visible on the log scale used in the graph. When the 324 admittance curves are averaged, shown in figure 4.7b, the anti-resonance is sharply defined, which suggests that it is produced by a natural variation in the behaviour of the instrument as it is rotated rather than by an external source. The peak at 120 Hz is present in the averaged (and unaveraged) admittance data for all of the guitars studied but it did not occur in the violin admittance. It is most likely to be produced as a result of a natural resonance within the experimental system for the study of guitars but as it takes a small value it can be ignored.

4.3 Experimental method for measuring velocity with a 3D scanning laser vibrometer

One-dimensional scanning laser vibrometers have previously been used to measure the out-of-plane motion of stringed instruments. Fleischer and Zwicker (1998) measured the out-of-plane velocity on the neck of two classical guitars to visualise the neck-bending modes and to find the locations of dead spots. Bissinger (2003b) measured the velocity response produced by an impulse excitation across the entire corpus (vibrating area) of a set of violins. These velocity measurements were used by Bissinger to calculate

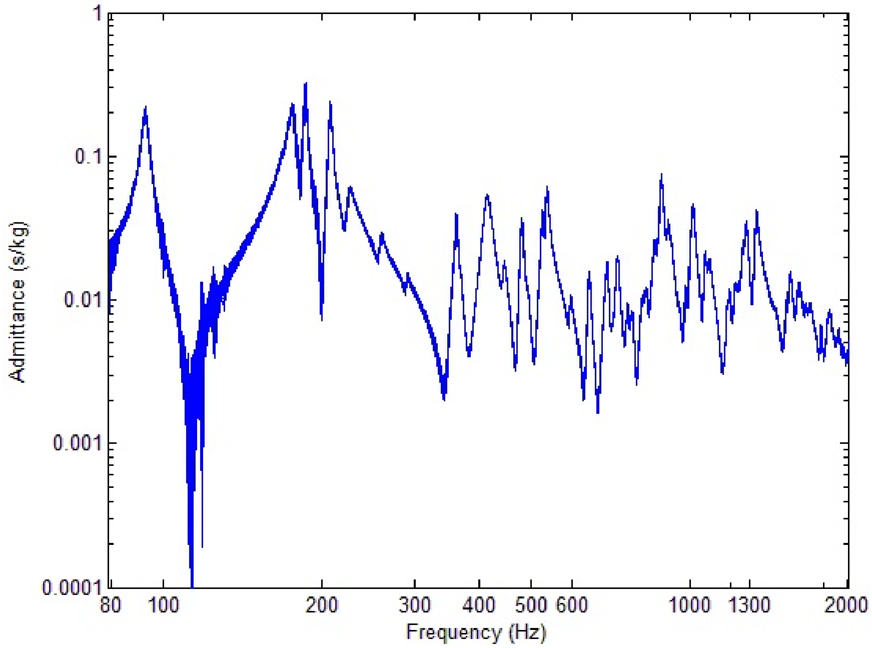

(a) 324 input admittance measurements.

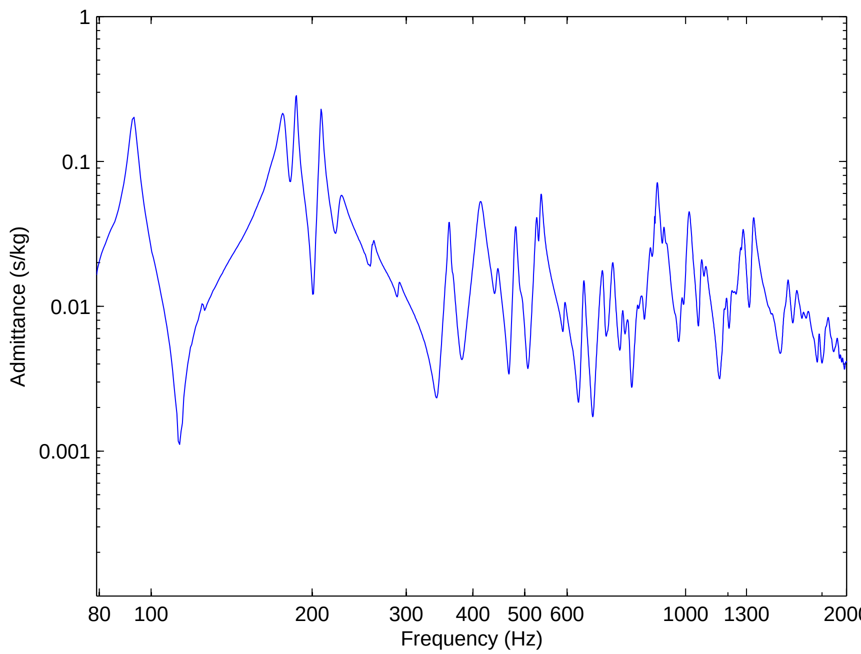

(b) Averaged of 324 input admittance measurements.

Figure 4.7: Admittance measurements from BR2 excited at the E_4 string.

the mean square velocity across the corpus and then to determine the value of R_{eff} described in section 2.5.1.

If the velocity response produced by an excitation on an instrument is measured at a sufficient number of points on its surface, the responses can be used to perform modal analysis on an instrument. A major advantage of measuring the velocity response of a stringed instrument is that the measurements are less susceptible to noise from any external motion than if the displacement is measured. Measurements of displacement using holographic interferometry are affected more by external noise and require the instruments to be heavily clamped. Clamping the instrument in place changes the behaviour of the modes of vibration of an instrument. Therefore a method which adds minimal additional support will produce velocity measurements which describe the behaviour of the instrument with only minimal external factors affecting it.

In this thesis a 3D scanning laser vibrometer, PSV-500-3D, was used to measure the out-of-plane and both orientations of in-plane velocity of several stringed instruments. The velocity in each of the three directions can be separated and studied individually or combined to study the total motion of the instrument at the measurement point. If an excitation is provided at a single frequency then the behaviour of the instrument at that frequency can be studied by measuring the velocity on a grid of measurement points. However, the velocity at each point on the grid can be measured across a wide range of frequencies by driving the instrument using an impulse excitation. The velocity response of the whole instrument at single frequencies can be determined by taking the FFT of the signal measured at each point and plotting the velocity of individual frequency components.

Using impulse excitation and laser vibrometry to measure the response means that the operating deflection shapes (ODS) of stringed instruments can be measured without having to drive individual body modes at their resonance frequencies on the anti-nodal regions. The broadband excitation provided by the impulse excitation means that many modes will be in motion and can be studied, providing the excitation is not made at the nodal lines of a particular mode. The measured response from an impulse excitation will result from motion of the mode of interest and the residual responses of body modes with lower resonance frequencies. As it is not the velocity produced by a single mode that is being measured it should be more accurately described as being an ODS. If the behaviour of a single body mode is to be studied then the mode must be driven at its anti-nodal regions at its resonance frequency. The driving location should also be placed at the nodal lines of the lower-frequency body modes as well if possible. The anti-nodal regions can be determined by measuring the ODS or by using techniques such as the roving hammer method.

The 3D scanning laser vibrometer was used to measure the 3D velocity response of four classical guitars, two steel-string guitars, a banjo and an oud. The strings of the instruments were tuned to their standard playing frequencies before being damped with a piece of felt. The instruments were suspended from their tuning pegs using elastic bands as shown in figure 4.8. To prevent extraneous motion, additional support was provided to the instruments by tying string between the support rack and its neck and by placing foam between the instrument's base and the floor. The foam at the base of the instrument prevented it from swaying after each impulse excitation. The instrument was excited at the bass side of the bridge (to the left of the E_2 string for guitars) using the same automated impact hammer used to drive the instruments for the radiation efficiency, η, measurements in this work. The hammer and its support obstructed the path of the lasers at certain points on the instrument which prevented velocity measurements being made across the entire surface. The support for the hammer was located in front of the neck so no velocity measurements could be made on the neck. In addition to the blocking of the laser pathway by the hammer support, velocity measurements could not be made on the neck because the strings were still attached to the instruments. If the laser was directed onto a string then the light was scattered and no velocity value could be measured. The grid of measurement points was defined automatically by the measurement software, so it was not possible to avoid defining measurement points which coincided with the locations of the strings.

Before making any velocity measurements, the three laser heads of the PSV-500-3D were aligned in both 3D and 2D. The 3D alignment was required so that the distance from the laser heads to the instrument were accurately measured. The 3D alignment was made by manually directing the three lasers so that they focused at the same point on the instrument. This first point was defined as the origin. This process was then repeated at locations in the z plane, the zy plane and the x plane. Determining the distance from the laser heads to these four points results in measurements of motion in the x, y and z directions that are accurately determined with no crosstalk between the three directions. This allows for correctly calibrated velocity values to be measured. The 3D alignment does not need to be repeated as long as the three laser heads remain at the same distance relative to each other. To prevent motion of any of the laser heads, and therefore maintain an accurate 3D alignment, they were attached to a rigid table tripod. No further calibration of measurements is required as the distances and changes of phase are determined using the known wavelength of the laser light.

2D alignment is performed so that the three lasers are all aimed at the same point

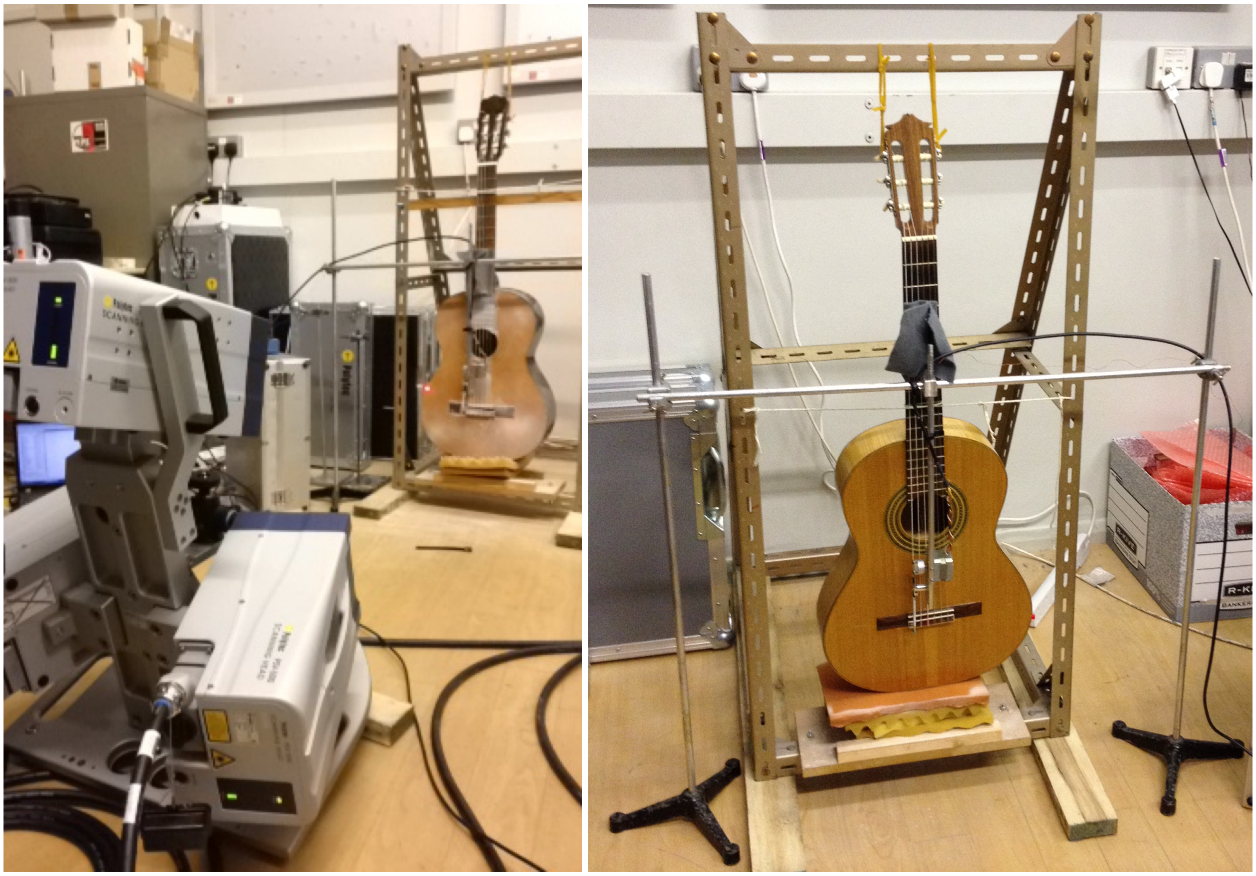

Figure 4.8: Experimental set up for suspending the instruments and measuring their velocity response with a 3D laser vibrometer.

on the instrument across the entire surface of the instrument. The 2D alignment is dependent on the distance from the laser heads to the instrument and any motion of the instrument will invalidate the alignment. If the three lasers are not all focused at the same point on the instrument then the values of velocity in the x, y and z directions will not be measured correctly. To perform a 2D alignment each of the three lasers must be manually directed to the four 'corners' of the instrument and also at a large number of points across the surface. This process takes around 30 minutes so the instrument was held in place with foam at the base to prevent any excessive motion.

Velocity and force measurements were made at a sampling rate of 5 kHz within a frequency range of 0–2000 Hz, which results in a frequency spacing of 0.625 Hz. The velocity was recorded at each point on the measurement grid for 1.6 seconds. The impact hammer used to provide the excitation was connected to the reference channel of the vibrometer and the force signal was recorded at the same time as the velocity in the x, y and z directions. The velocity measurements were triggered when the input to the reference channel passed a predetermined voltage level. A pre-trigger was used to record the velocity for 100 ms before the hammer strike. The velocity measurements were normalised with the applied force, resulting in a set of transfer admittances across the measurement grid. Normalising the velocity with the applied force reduces the effect of changes in the applied force. Recordings of the force for each excitation showed that the variation in the applied force for all of the measurements was $< 10\%$.

4.3.1 3D input admittance method

For 3D input admittance measurements, the three lasers were directed at a single point as close as possible to the location of the hammer excitation point. A small piece of reflective tape was attached at the measurement point on the bridge to ensure a maximum level of laser light was reflected back to the laser heads, rather than out to the room, therefore optimising the signal-to-noise ratio (SNR). The reflective tape was the only additional mass attached to the instrument and produced no measurable change on the velocity measurements. However, the instruments were still supported lightly at the foot of the instrument with foam which provided some additional damping. This could not be avoided but the effect of this support system on the measured response is discussed in section 3.2.1. The input admittance measurements were averaged from the complex frequency spectra produced from 20 excitations made at the same point, just to the left of the lowest string on the instrument. The impulse was only provided in the out-of-plane x direction as it was not possible to provide an excitation in the in-plane, y and z, directions using the automated impact hammer.

4.3.2 Background noise

The velocity measurements made in the y and z directions on the stringed instruments in this work were susceptible to noise away from the resonance frequencies of body modes. At the resonance frequencies of the body modes, the peak values of velocity in all three directions were clearly defined below 1500 Hz. As the measurements were only noisy away from the resonance frequencies, the noise in the signal must therefore result from the measured velocity being lower than the background noise level. The background noise of the system was determined by measuring the velocity to the left of the E_2 string on the bridge of BR2 with no excitation provided to the instrument. The velocity values in figure 4.9 are averaged from 20 measurements. Figure 4.9 shows that the noise decreases with increasing frequency and that the background velocity measurement decreases from from an average of 2μm/s to 0.1μm/s between 0 Hz and 2000 Hz. Away from the resonance frequencies of the body modes the recorded velocity in the y and z

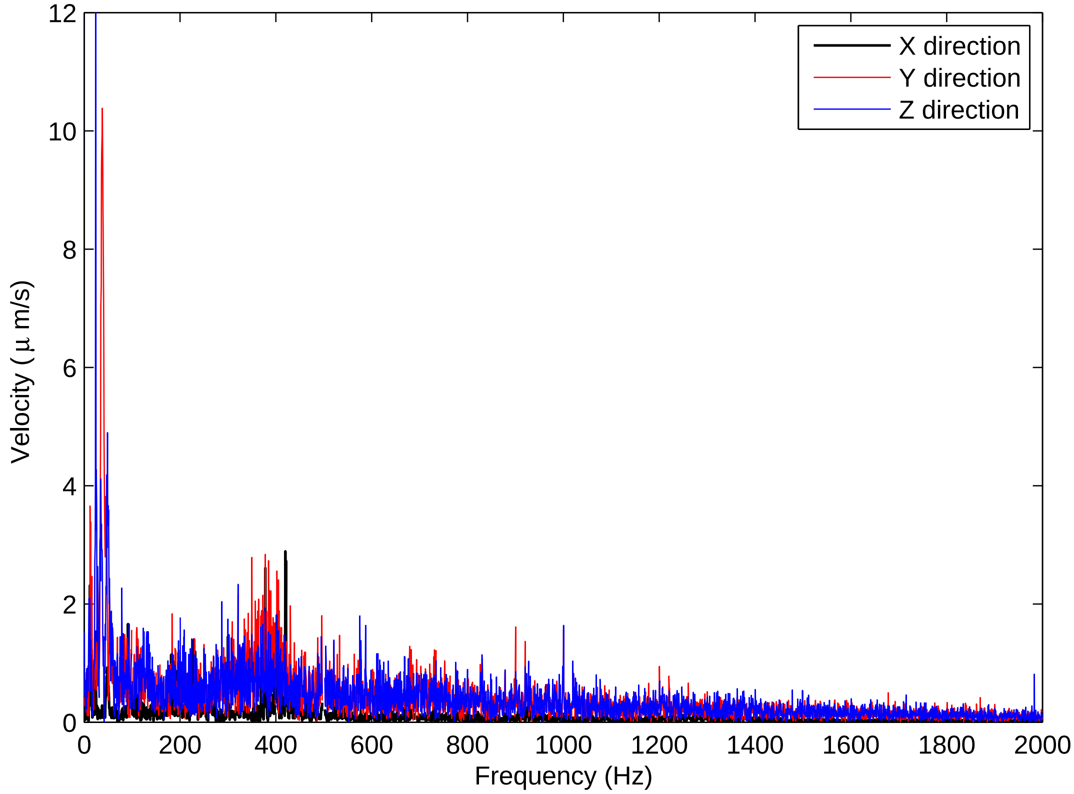

Figure 4.9: 3D velocity measured to the left of the E_2 string on BR2 with no excitation.

directions was $< 5\mu$m/s. The background noise of the system therefore contributes a considerable amount to the measured in-plane velocity away from resonance frequencies. The peak values of velocity were between 30-400 μm/s in the x direction,considerably larger than the background noise.

In addition to the broadband background noise across the frequency range there are two clear peaks in the data at 24 Hz and 38 Hz. As these peaks occur despite the averaging of 20 velocity measurements they must result from an external source within the room where the 3D scanning laser vibrometer experiments were made. These peaks are below the resonance frequency of any body modes of stringed instruments are can be ignored. There is also a greater amount of noise at 400 Hz which may also have resulted from external noise sources. The low level of background noise compared with the peak values of admittance at the resonance frequencies of body modes means that it is best to study the admittance values at the resonance frequencies. Away from the resonance frequencies of body modes care should be taken not to misinterpret the data if the velocity of the instrument is of a similar value to the background noise.

Chapter 5

Measurements on four classical guitars

In this chapter the sound radiation and vibrational characteristics of four classical guitars, between 80 Hz and 2000 Hz, are compared. Radiation efficiency, η, mechanical input power and acoustical output power from a set of four classical guitars (BR2, BR1, DLC and MAL) were measured using the method described in section 4. The radiated sound fields produced at different frequencies are also shown for BR2. The vibrational behaviour of the four classical guitars was also studied using a 3D scanning laser vibrometer using the methods described in sections 4.3 and 4.3.1. η data measured on BR2, a steel-string guitar (X10) and a violin have previously been published by Perry and Richardson (2014).

The acoustical power output and mechanical power input were calculated for each instrument between 80 Hz and 2000 Hz. The lower frequency limit was chosen as it is below the lowest frequency string on the guitar (E_2 = 82 Hz) in standard tuning. It is also below the resonance frequency of the lowest frequency body mode which radiates sound on any of the studied instruments. The upper frequency limit of 2000 Hz was determined as the frequency where the double-sided tape used to attach the accelerometer to the bridge began to affect the measured response (as described in section 3.5). Stringed instruments radiate sound that is perceivable by listeners up to a frequency of around 6000 Hz. However, preliminary studies showed that there were few clear features present in η measured on the guitars and violin at frequencies above 2 kHz. As is the case for input admittance measurements, the clearest features (high values of η and known body modes) in the η and power data occur below 2 kHz. The vibrational behaviour of the classical guitar is fairly well understood in this frequency range so it is a suitable range for study.

Spherical-harmonic decomposition was used to determine the acoustical power output. The power output and η are omitted in certain frequency ranges as a result of the half-wavelength problem described in section 3.9.3. Data is omitted at integer multiples of 660 Hz and at 25 – 50 Hz either side of these multiples. If η was greater than 1 at any frequency then the measurement at that frequency was omitted from the figure, as in the work by Lai and Burgess (1990). Data is also omitted at integer multiples of 50 Hz below 350 Hz because of the electrical noise present in the microphone signals. The electrical noise is only visible in the microphone signals if the instrument radiates a low level of sound pressure at that frequency. If the resonance frequency of a body mode coincides with an integer multiple of 50 Hz then the power output may be large enough to ignore the electrical noise and show the data. The electrical noise occurs within a very narrow band of frequencies so 1 Hz of data either side of the multiple of 50 Hz is omitted. As such there is only a minimal local effect on the overall power output from electrical noise.

The power output was determined from the source strengths, Γ_{lm}, of the monopole and dipole components at each frequency. Richardson (2001) determined Γ_{lm} of BR2's body modes up to the $T(3,1)$ mode and for $l = 0, 1$ and 2 (and the respective values of m). In that work the modes were driven at their anti-nodal regions rather than directly at the bridge. This required the values of Γ_{lm} to be scaled by a factor R, the ratio of effective masses, as described in section 2.7.2. In this thesis the instrument was directly driven at the bridge so more than one body mode was in motion at any frequency. The values of Γ_{lm} are therefore different to those found by Richardson (2001). However, the values of Γ_{lm} found in the current work had the same orders of magnitude and had the same values in relation to one another as those found by Richardson (2001). For example the Γ_{lm} values of the $T(1,1)_2$ mode of BR2, in decreasing size, were Γ_{00}, Γ_{1x}, Γ_{1z} and Γ_{1y} in both this work and the work by Richardson. The orientation of the instrument used to discuss the radiated sound fields and source strengths is the same as that used in the work by Hill et al. (2004) and is shown in figure 5.2.

Two locations in close proximity to one another were chosen for the force and velocity measurements on the instruments to measure the power input. The close proximity of the measurement points was found to give a good approximation to an input (rather than a transfer) measurement. The four excitation locations are shown in figure 5.1. Positions 1 and 2 were chosen to study the effect of the symmetry (or asymmetry) of the top plate's construction on its behaviour. Position 3 was used to minimise the excitation of modes with nodal lines at the centre of the bridge, such as $T(2,1)$ and $T(4,2)$. When the string is plucked the bridge is not the only termination for the string. There is also a transfer of energy at the nut or at the fret where the finger presses the string against the neck. Position 4 is on the 12th fret and was used to investigate whether the power input supplied to the neck is efficiently radiated as sound power.

The 3D admittance was measured at the bass side of the guitar's bridges, as close to the E_2 string as possible. Velocity measurements were also made across the top and back plates of some of these classical guitars using the 3D scanning laser vibrometer to produce visualisations of the body modes and to show the band data of the guitars. The band data is defined as being the rms of the admittance measured at each point on the instrument within the frequency range, 0 - 2000 Hz. This provides a visualisation of the areas of the instrument that undergo the greatest motion across the entire studied frequency range.

The resonance frequencies and body-mode shapes of BR1, BR2 and DLC were previously determined as part of a study of ten classical guitars funded by the Leverhulme Trust. The shapes of the body modes were determined using holographic interferometry. Data from several of the guitars studied was published by Richardson et al. (2002) but not all of the data has been published at this time. The resonance frequencies of guitar body modes, such as $T(1,1)_2$, are known to change over time by up to 5% (Wright, 1996). The resonance frequencies in the η figures were determined from the peaks in the input admittance measured on the instruments using the previously determined resonance frequencies as an estimate. The shapes of the top- and back-plate modes of MAL were measured using a 3D scanning laser vibrometer. Data measured with the 3D scanning laser vibrometer is shown using a reverse-rainbow colour bar where dark red shows a minimum in the data and dark blue shows a maximum.

The normalised sound fields (sound pressure/applied force) of the instruments were studied by plotting the amplitude of the normalised sound pressure measurements for each angle (azimuth and elevation) on a single measurement sphere. Normalising the sound pressure with the applied force means that the effect of variations in the applied force can be ignored providing that the instrument behaves in a linear fashion. The measurements of coherence in section 3.8 show that the instrument is expected to behave linearly between 80 Hz and 2000 Hz. The sound pressure values used to produce the sound field figures were those measured on the inner of the two concentric measurement spheres, at a distance of 0.45 m from the centre of the instrument. The inner measurement sphere was chosen because the recorded sound pressure values were greater than those on the outer sphere. This reduces the effect of external noise and low signal level on the sound fields.

Using an impulse excitation to drive the instrument means that the sound fields can be studied away from the resonance frequencies of the body modes. The simplest method for studying the changing sound field is to produce a video where each frame

Figure 5.1: Excitation and response locations on a classical guitar.

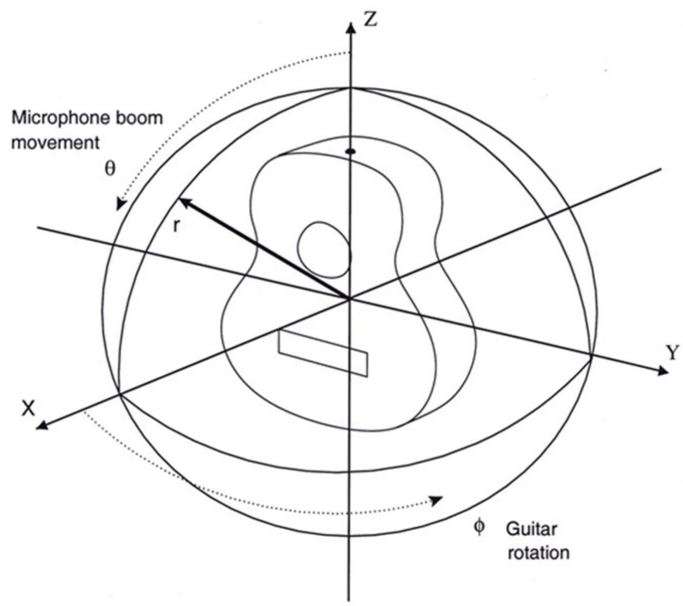

Figure 5.2: Measurement directions for the classical guitar (from Hill et al. (2004)). Reprinted with permission from Acta Acustica United with Acustica.

shows the sound field produced by the instrument at a single frequency. I presented videos of the sound fields of BR2 across several frequency ranges at the ISMA 2014 conference in Le Mans (Perry and Richardson, 2014). The changing sound fields presented in this section are snapshots taken at selected frequencies (surrounding the resonance frequencies of body modes) from these videos. The sound fields show the sound radiated by all of the excited body modes at a single frequency.

The η figures in this thesis show the total radiation efficiency, monopole radiation efficiency and dipole radiation efficiency on the same figure. The individual radiation efficiencies are shown on separate figures for closer study in appendix A for all of the measurements made.

5.1 Classical guitar, BR2

BR2 is a traditionally designed classical guitar with Torres bracing made by Dr Bernard Richardson of Cardiff University. It has been previously studied as part of research into the physics of guitars by both Hill et al. (2004) and Richardson (2001). In these previous studies the weights of the orthogonal radiation components, G_{lm}, and the normalised source strengths, Γ_{lm}, of the top- and back-plate modes were determined at frequencies below 600 Hz. G_{lm} is the equivalent of the effective area, $G_{00} = A$, for monopole sources and the effective volume, $G_{1m} = V$, for dipole sources. The mode shapes discussed in this section are shown in table 1.1 on page 15.

5.1.1 BR2 excited at position 1

Figure 5.3 shows the radiation efficiency, η of BR2 measured at position 1. The monopole radiation efficiency, η_m, is the ratio of the monopole output power to input power and the dipole radiation efficiency, η_d, is the ratio of the dipole output power to input power. The power output produced by quadrupole sources was also calculated but it was found to be negligible in comparison with the monopole and dipole output powers for all of the studied instruments. There are several similarities between η measured on BR2 in this work and η measured on two other classical guitars by Lai and Burgess (1990). In both studies the peaks in η do not correspond with the resonance frequencies of the body modes of the instruments. The peak values of η are also not necessarily as sharply defined as those in the 1D admittance curve shown in figure 5.5. Below the resonance frequency of the lowest frequency body mode, Lai and Burgess found that η was close to 0. This was also found for BR2 but is not shown in figure 5.3. In the lower frequency range η is dominated by monopole power output and at higher frequencies the dipole power output produces the greatest contribution to the radiated sound power.

In figure 5.4, the mechanical power input and the acoustical power output are shown for BR2 when it was excited at position 1. The acoustical power output is the summation of the monopole and dipole power outputs. The resonance frequencies of the body modes correspond with a peak in the power input but there is not always always a corresponding peak in the power output. For example, the $T(1,2)_1$ mode has a low value of η and produces a peak in the power input but there is no corresponding clear peak in the power output. When the instrument is driven at position 1, the mode is easily driven by an excitation (high input power) on the bridge but it radiates a low level of acoustical output power. $T(2,1)$ also has a low value of η but it produces a peak in the power output data. However, the peak in output power is considerably smaller than the power input for the $T(2,1)$ mode, which has the second largest power input within the studied range.

Figure 5.6 shows the 3D admittance (Y_{xx}, Y_{xy} and Y_{xz}) measured at the E_2 string of BR2 with the instrument driven in the x direction (out-of-plane) using an impact hammer. The first letter in the subscript describes the excitation direction and the second letter describes the response measurement direction, so Y_{xy} has an excitation provided in the x direction and the response measured in the y direction. No excitation

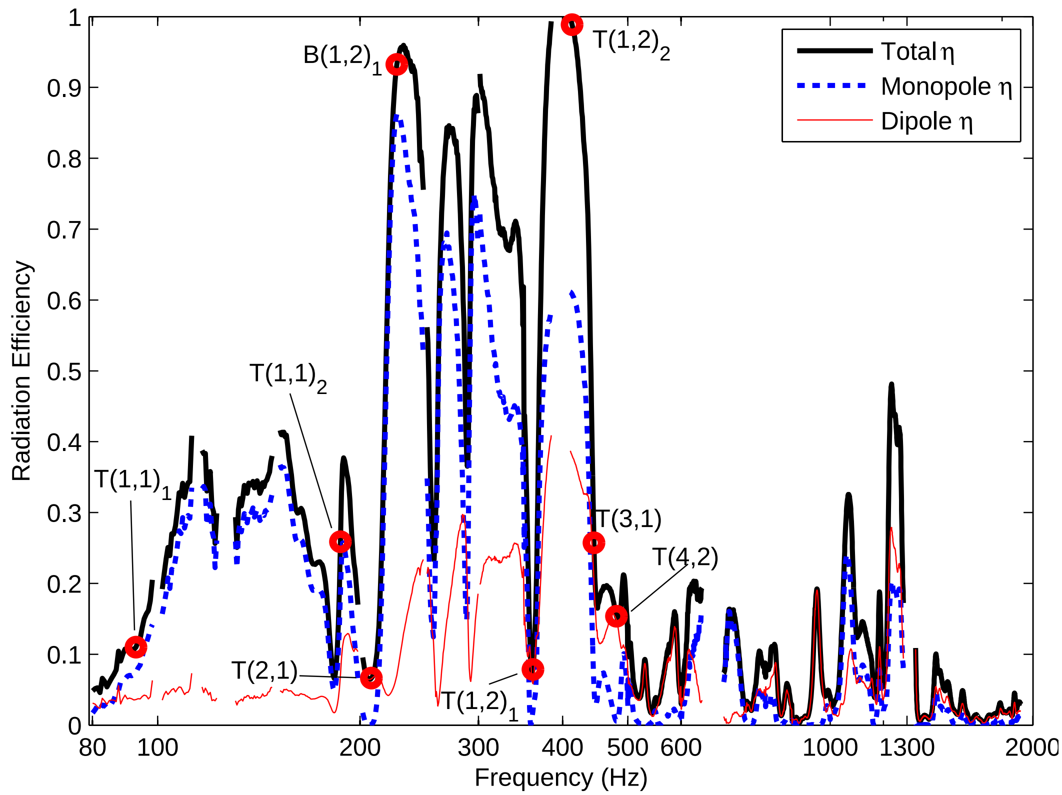

Figure 5.3: Radiation efficiency measured at position 1 on BR2.

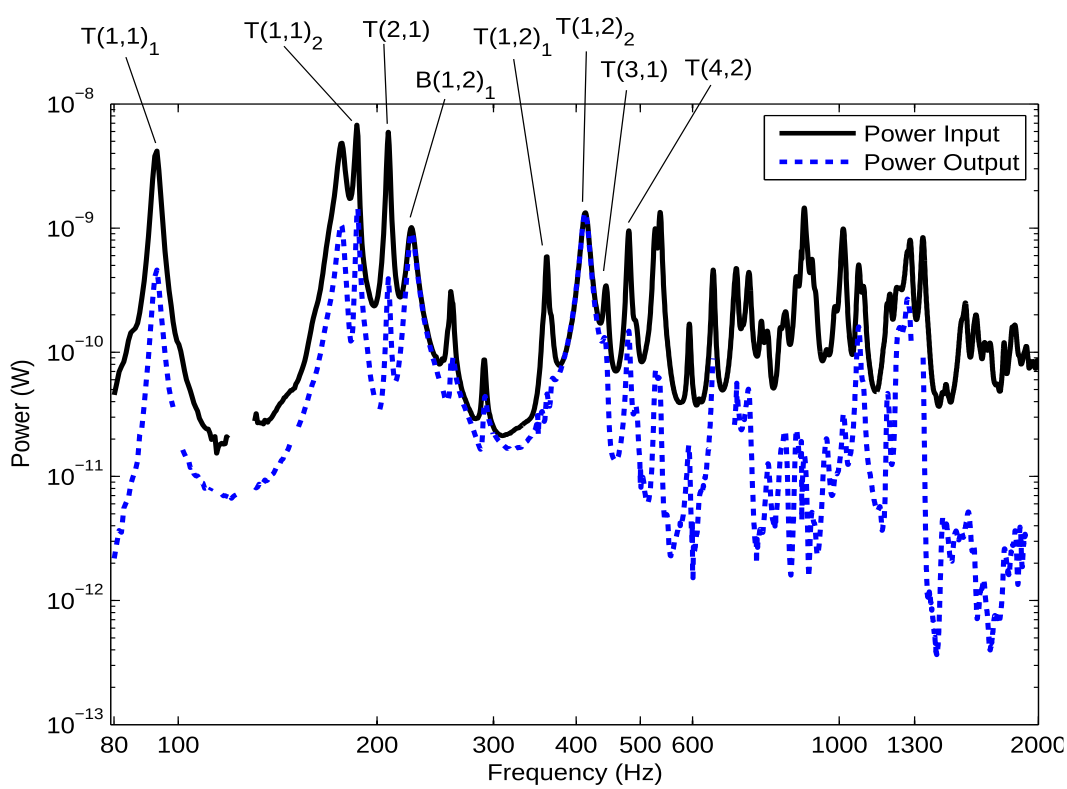

Figure 5.4: Mechanical power input and acoustical power output for BR2 excited at position 1.

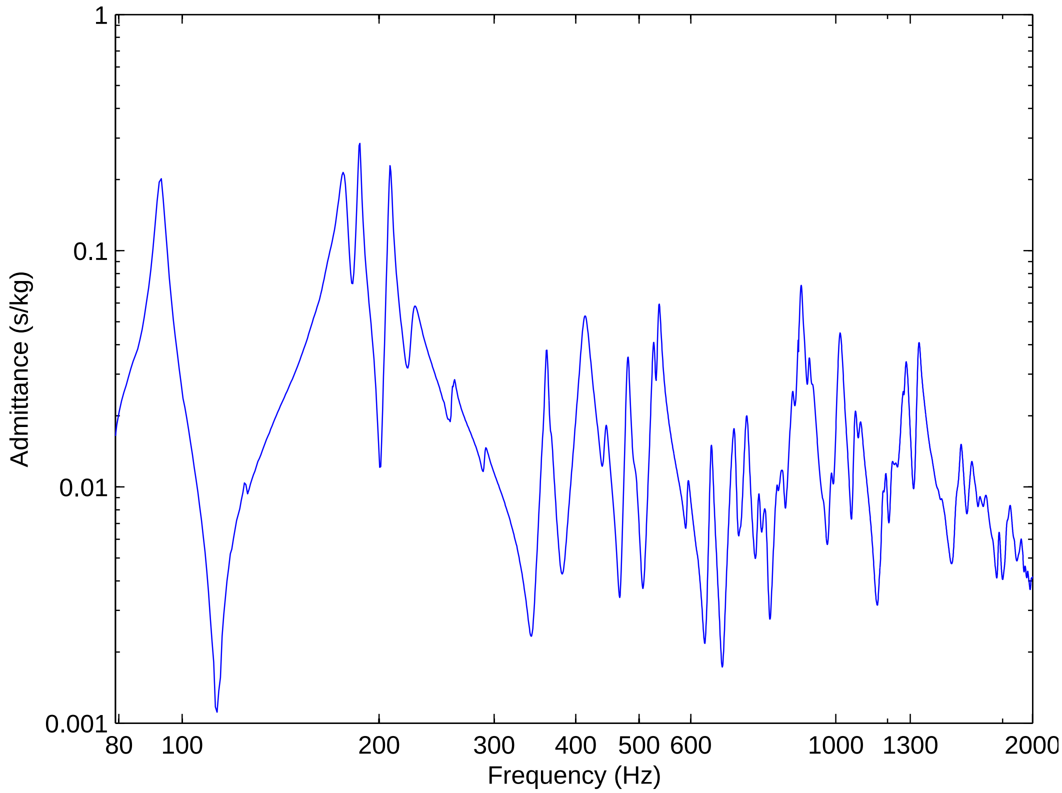

Figure 5.5: Input admittance measured at position 1 on BR2.

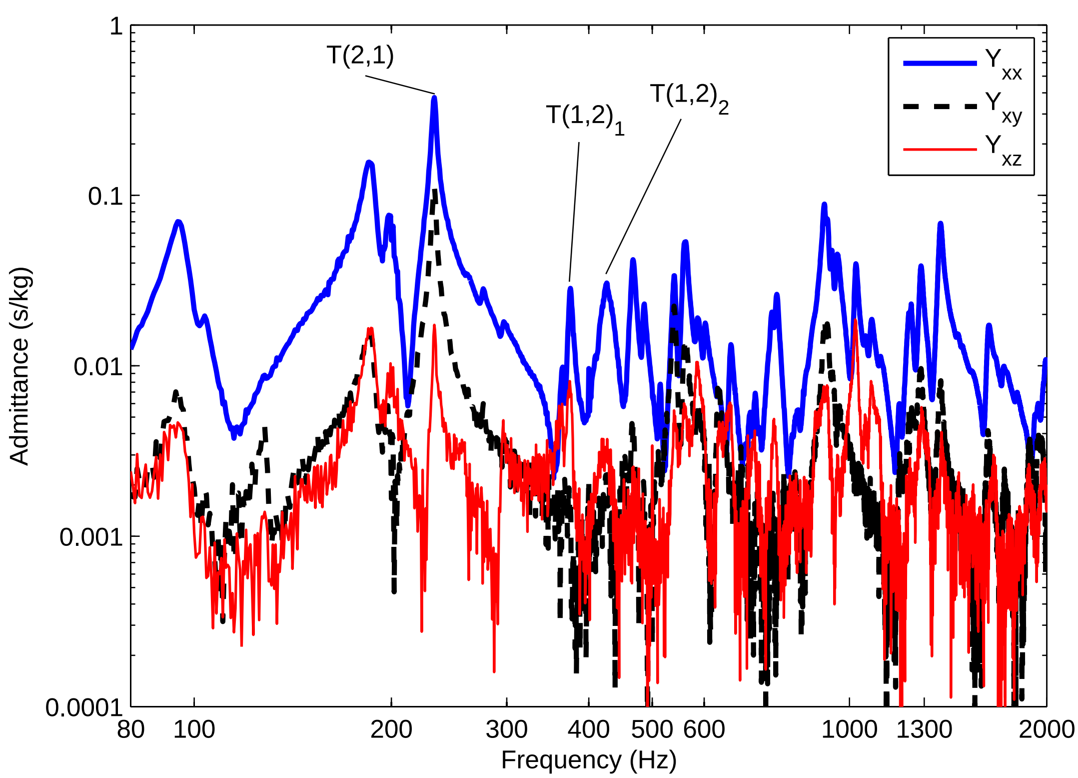

Figure 5.6: 3D admittance measured to the left of the E_2 string of BR2.

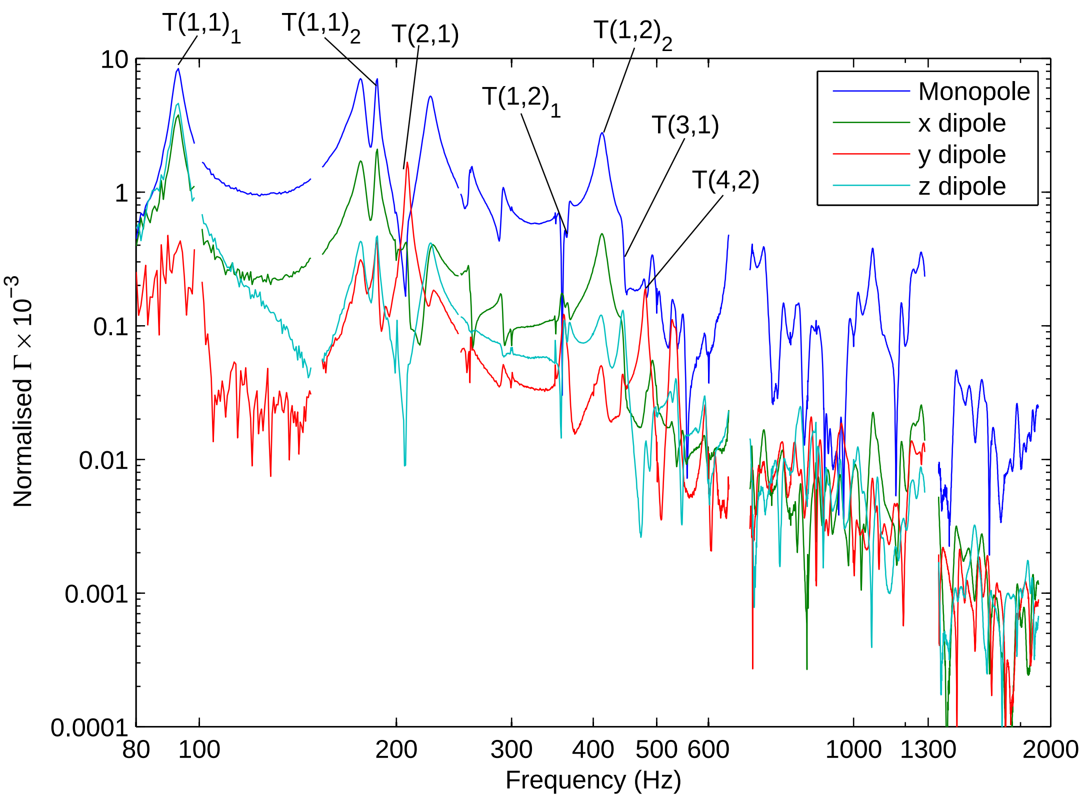

Figure 5.7: Γ_{lm} values for BR2 excited at position 1.

could be provided to BR2 in the y or z directions so no comparison can be made between Y_{xy} and Y_{yx} or Y_{xz} and Y_{zx}. Between 80 Hz and 2000 Hz the greatest values of admittance are produced in the out-of-plane, Y_{xx}, direction and the lowest values in the in-plane, Y_{xz}, direction. This is an expected result as the instrument is driven in the x direction when a force is applied by the strings, so it should also produce the largest values of Y in this direction. The radiated sound pressure is produced by a displacement of the surrounding air and this is most efficiently achieved by an out-of-plane motion. As such the instruments are designed to undergo the greatest level of motion in the out-of-plane direction with less consideration to the in-plane direction. The mean values of admittance in the three directions between 80–2000 Hz for BR2 are $Y_{xx} = 0.017$ s/kg, $Y_{xy} = 0.003$ s/kg and $Y_{xz} = 0.002$ s/kg. For the y and z directions, modes with even numbers of anti-nodal areas, with similar sizes, produce greater values of y and z velocity than modes with odd numbers of anti-nodal areas.

Figure 5.7 shows the source strengths, Γ_{lm}, for BR2 measured at position 1. Figure 5.3 has already shown that, in the low frequency range, monopole power output produces the large contribution to the radiated power. Figure 5.7 shows that the x-dipole typically contributes the most to the magnitude of the dipole source strength,

D_ω across the entire frequency range. Γ_{1x} is the greatest of the dipole Γ values because it corresponds with an out-of-plane motion from the top plate of the guitar. Motion of the top plate in an out-of-plane direction displaces a greater amount of air than an in-plane motion. A larger displacement of air results in a greater power output from the instrument and also a greater value of Γ. The impulse excitation was also provided in the x direction which would therefore drive the instrument more easily in x than in either the y or z directions.

The radiation efficiency, η, of BR2 can be described as having three different regions of behaviour in frequency space. The first is between 80 Hz and 200 Hz and is bounded at its upper frequency limit by the $T(2,1)$ mode. The second region is between the $T(2,1)$ mode and $T(3,1)$ and the third region is above $T(3,1)$.

The first frequency region (80 Hz - 200 Hz)

The greatest values of η do not coincide with the resonance frequencies of the body modes within the first frequency region but instead lie between the two $T(1,1)$ modes. The anti-resonance in the input admittance curve, shown in figure 5.5, between $T(1,1)_1$ and $T(1,1)_2$ occurs at the frequency where a Helmholtz oscillator would be expected to occur. If this motion was produced by a Helmholtz oscillator, the only motion would be the air moving through the sound hole and no motion would occur on any of the walls of its cavity (front plate, back plate or ribs). The motion of air through the sound hole produces an acoustical power output. A Helmholtz oscillator would produce a zero power input measurement on the top plate following an excitation because it would produce no velocity response and result in $\eta > 1$. This result cannot occur as it would be impossible to drive completely rigid walls with an excitation on their surface. The flexible ribs and plates allow for motion of the bridge and top plate to occur but it is reduced in comparison with the motion at either of the two $T(1,1)$ modes. The reduced power input at the bridge and the power output produced by the Helmholtz oscillator-like motion results in an increase in η.

Despite the main contributions to η being produced by monopole sources within the first frequency region, there is a dipole power output below 200 Hz. Body modes are not easily excited below their resonance frequencies so it is unlikely to be the $T(2,1)$ mode producing the dipole power output in this frequency range. The sound hole sum rule states that at frequencies below the resonance frequency of a Helmholtz oscillator-like motion, a stringed instrument will behave like a dipole (Weinreich, 1985). The dipole behaviour results from the force applied at the instrument moving the top plate inwards towards the air enclosed within the cavity. As the enclosed air is incompressible the only way that a net change of volume can be prevented from occurring is for air to flow through of the sound hole. The air flows outwards through the sound hole as the plate moves inwards and vice versa. The motion of the air through the sound hole and the motion of the plate have opposite phases so the radiated sound will produce a dipole sound pressure field. The dipole strength decreases in proportion to ω^2 but dipole power is still produced according to the sound hole sum rule between 80 Hz and 200 Hz.

In the first frequency region there are three body modes which radiate sound pressure, $T(1,1)_1$, $T(1,1)_2$ and $T(2,1)$. The $T(1,1)_1$ and $T(1,1)_2$ modes result from a coupling between the top plate, back plate and air cavity. There is also a $T(1,1)_3$ mode but its resonance frequency and mode shape have not been found on BR2. $T(1,1)_1$ and $T(1,1)_2$ have similar shapes with one large anti-nodal area, which is constrained in the lower bout of the plate, in motion (Richardson, 1982). As there is only a single area of the instrument in motion the surrounding air is mainly displaced either in front or behind the instrument. These two coupled modes both produce monopole-like sound fields. However, the instrument radiates a greater level of sound pressure in front of the top plate than behind it, resulting in a directional characteristic for both $T(1,1)$ modes, which is shown in the sound fields in figure 5.8. In terms of the total power output, the dipole source contributes 32% of the total radiated power produced by the $T(1,1)_1$ mode so it exhibits some directionality. For the $T(1,1)_2$ mode, the dipole components produce 18% of the power so there is less directionality and the contribution from dipole sources to the radiated sound produced by the sound hole sum rule has decreased.

The source strengths, from figure 5.7, for the $T(1,1)_1$ mode are $\Gamma_{00} = 8.4 \times 10^{-3} m^3 s^{-1} N^{-1}$ and the Γ_{1m} values for the x, y and z orientations are $3.78 \times 10^{-3} m^4 s^{-1} N^{-1}$, $0.40 \times 10^{-3} m^4 s^{-1} N^{-1}$ and $4.60 \times 10^{-3} m^4 s^{-1} N^{-1}$ respectively. The motion in the z direction is parallel to the strings and must therefore result from the sound hole sum rule producing a motion in both the upper *and* lower bouts of the top plate. The opposite phases of the two areas causes a rocking motion about the nodal line which produces a velocity response in the z direction.

The $T(1,1)_2$ mode has a greatly reduced value of Γ_{1z} compared with $T(1,1)_1$, which suggests that the effect of the sound hole sum rule is reduced at frequencies above the $T(1,1)_1$ mode. This is agreement with the sound hole sum rule theory. Between these two coupled modes, the monopole output is still the greatest contributor but the value of Γ_{1z} shows a much more rapid decrease in value. The effect produced by the sound hole sum rule decreases with ω^2 and this is shown in the decrease in Γ_{1z}. The other two orientations of dipole are not related to the motion produced under the sound hole

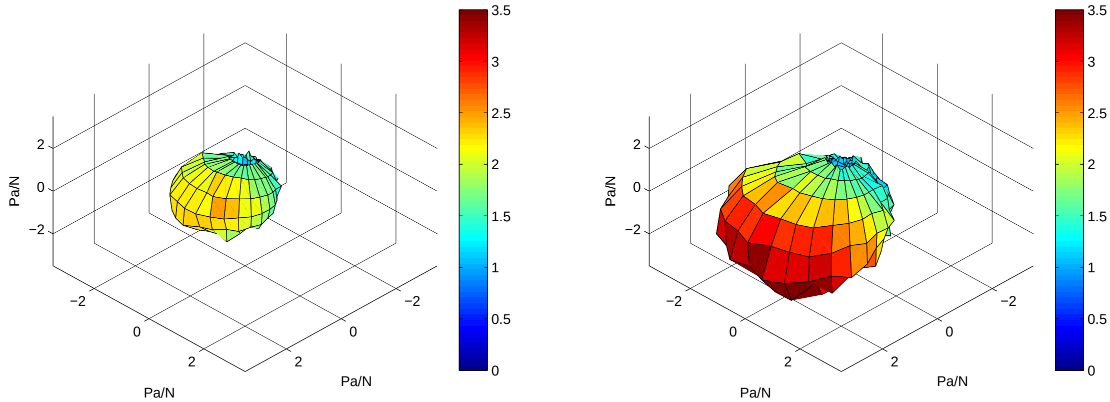

(a) BR2 $T(1,1)_1$ - 92.9 Hz.

(b) BR2 $T(1,1)_2$ - 176.3 Hz.

Figure 5.8: Normalised sound fields of the $T(1,1)$ modes of BR2.

sum rule but instead relate to the directionality of the two modes. The Γ_{1x} values have the same characteristic as Γ_{00}. The values of Γ_{1x} must therefore be produced by the $T(1,1)$ modes rather than the sound hole sum rule.

The $T(2,1)$ mode has a low value of η because a cancellation of the radiated sound pressure occurs between the two anti-nodal regions. This cancellation occurs because the two anti-nodal regions have similar sized areas but opposite phases. The shape of this mode is shown in figure 5.9. The opposite phase sound pressures produce the cancellation in the radiated sound power. As there are two areas with opposite phases the radiated sound power will also have a dipole-like characteristic. This is confirmed by the η data at the mode's resonance frequency where $\eta_m = 0$ and $\eta_d = \eta$. Dipoles are less efficient radiators of sound than monopoles so a lower level of power output is produced by $T(2,1)$ than modes with more monopole-like characteristics.

Figure 5.6 shows that the greatest in-plane motion admittance between 80 Hz and 2000 Hz is produced at the resonance frequency of the $T(2,1)$ mode in the Y_{xy} direction. The motion is produced in the y direction because of the orientation of the two opposite phase anti-nodal areas produced by this mode. In-plane motion displaces a smaller volume of air than out-of-plane motion as it cannot easily displace the air contained within and also surrounding the cavity. Therefore only a small amount of power output is produced by in-plane motion of the top plate and there is a lower value of η. This mode also produces the greatest value of Y_{xx} across the frequency range as the two anti-nodal areas are also moving in the x direction. However the opposite-phase motion does not radiate a large amount of sound pressure, as previously discussed.

Figure 5.10 shows the evolution of the guitar's sound field at frequencies surrounding

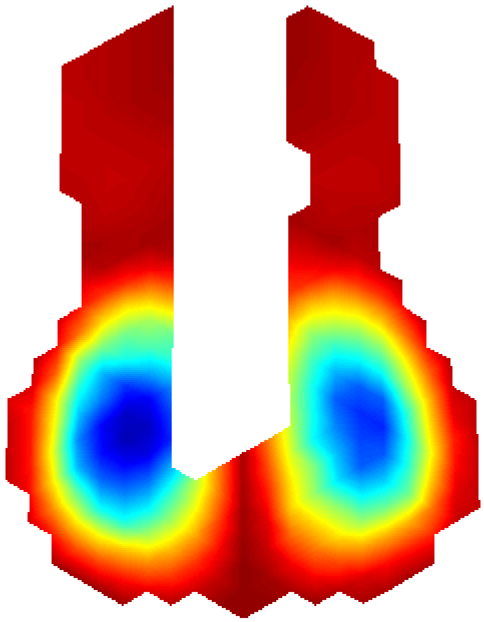

Figure 5.9: BR2 $T(2,1)$ mode - 208 Hz. Measured using a 3D scanning laser vibrometer

the $T(2,1)$ mode. At the resonance frequency of the $T(2,1)$ mode, 208 Hz, a dipole-like sound field with a y orientation is clearly visible. At frequencies either side of the resonance frequency the dipole appears to rotate in an anti-clockwise direction. This is a result of the phase relationship between the $T(2,1)$ mode and the residual pressure response of the low frequency resonance triplet. In figure 5.10a the nearer lobe from the instrument is in phase with the residual response and the further lobe is out of phase. Above the resonance frequency, in figure 5.10c, the phase relationship is reversed and the further lobe has the greater pressure values. If the mode was driven at both of its anti-nodal regions at the resonance frequency and with the correct phase relationship then the $T(1,1)$ modes would not be excited. In this case the radiated sound pressure would be more equal for both sides of the instrument either side of the resonance frequency.

Below 600 Hz, there are only two modes with resonance frequencies where the largest value of Γ_{lm} is not Γ_{00}. The first of these is the $T(2,1)$ mode, in the first frequency region, where there is a clear peak in Γ_{1y} which is not present in Γ_{00}. This large value of Γ_{1y} produces the y-orientated dipole-like field shown in figure 5.10b. There is no peak in Γ_{00} as very little monopole output is produced by the motion of two equal-sized anti-nodal areas with opposite phases. The strong dipole component results in a low value of η for this mode. The other mode where the greatest value of Γ_{lm} is not Γ_{00} is the $T(1,2)_1$ mode in the second frequency region, which is discussed in the next section.

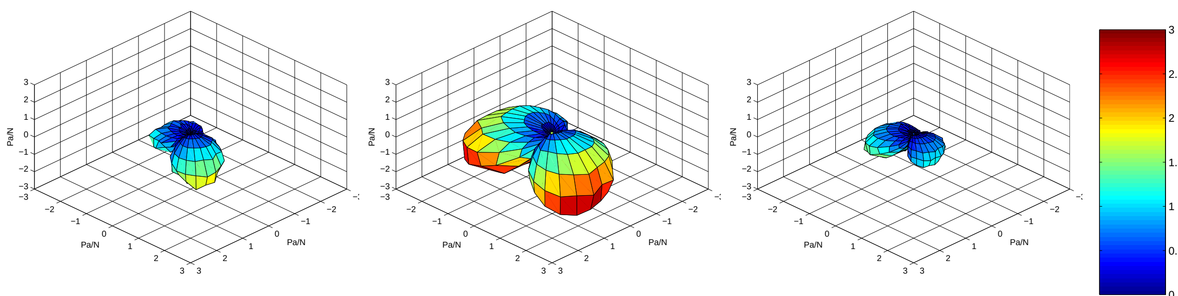

(a) 206 Hz. (b) 208 Hz. (c) 211 Hz.

Figure 5.10: Sound fields produced by BR2 at frequencies surrounding the $T(2,1)$ mode.

The second frequency region (200 Hz - 450 Hz)

The second region of η behaviour, between 200 Hz and 450 Hz, shows an increase in the level of dipole sound radiation in comparison with the first region but the total power output is still dominated by monopole contributions. This frequency range also produces the greatest values of η on the instrument. Christensen (1983) found that "an overwhelmingly large part of the acoustic energy radiated from the guitar" is produced at frequencies below 600 Hz in a study of the acoustical energy produced by played guitars. It would therefore be expected that the instrument would be most efficient below 600 Hz. Many of the body modes within the second frequency range produce dipole-like sound fields as they typically have two vibrating areas of opposite phase. An exception to this is the $T(3,1)$ mode. This mode has three vibrating regions, the outer two are in phase and displace a large volume of air in comparison with the central anti-phase region. All three of these anti-nodal areas are in the lower bout of the top plate. There is some cancellation between the two outer anti-nodal areas and the inner anti-nodal area of $T(3,1)$ which produces some dipole power output. However, as the volumes of air displaced by the opposite-phase regions are not equal there will be a monopole-like contribution to the radiated sound in addition to the dipole component.

Despite the presence of many dipole-like modes in the second frequency region there is still a considerable monopole power output. The most likely source of this monopole power output is from the residual response produced by the low frequency coupled modes, $T(1,1)_1$ and $T(1,1)_2$, as predicted by the three mass model (Richardson et al., 2012). This residual response acts to strengthen the response of the instrument at frequencies above the resonance triplet. There will therefore be a monopole power component at frequencies where the body modes typically produce dipole sound fields. Another source of monopole power output is from modes which have unequal sized anti-nodal areas, such as the $T(3,1)$ mode. Monopole power can also be produced by (2,1) and (1,2) shaped modes if the two anti-nodal regions, of opposite phase, have different sizes. If the two anti-nodal areas have different sizes then they will each radiate a different level of sound pressure with opposite phase. There will be some cancellation between the two opposite phases but if one area is larger it will radiate somewhat like a monopole as the opposite-phase motions will not completely cancel one another out.

The first clear peak value of η in the second region is close in frequency to the $B(1,2)_1$ mode. $B(1,2)_1$ has two anti-nodal areas which are unequal in size and are separated by one of the struts on the back plate. The lower of the two anti-nodal regions has a greater level of velocity across a greater area of the plate than the upper anti-nodal region. The two vibrating areas have opposite phases so some cancellation will be produced by this mode. However, as the two areas are unequal in size the lower, larger area will still be able to radiate sound despite the cancellation produced by the opposite phase motion of the smaller upper area. The vibration from the lower bout of the back plate will therefore produce a monopole-like sound field but with some directionality as a result of the opposite phase of the upper anti-nodal area.

The next two body modes in the second frequency region have $T(1,2)$ shapes but opposite phase and η characteristics. These two $T(1,2)$ modes occur as a result of a coupling between a top-plate mode and a higher frequency air mode within the instrument. The lowest frequency air mode is the Helmholtz oscillator-like mode in the resonance triplet but there are higher frequency air modes in classical guitars (Elejabarrieta et al., 2002b). The different phase relationships between the air motion and the plate results in the different η characteristics of the $T(1,2)$ modes. $T(1,2)_1$ produces $\eta = 0.08$, whereas $T(1,2)_2$ has an η of almost 1. The $T(1,2)_1$ mode has a lower value of η because the anti-nodal region in the lower bout is smaller than the one in the upper bout. The lower region is directly excited by driving on the bridge. This produces a smaller excitation of the mode than if it were driven in the upper, larger, region. It also produces a peak value of Y_{xz} which results in a low value of η because the strong in-plane motion does not displace a significant amount of air. The $T(1,2)_2$ mode at 426 Hz has a lower value of Y_{xz} and produces the greatest motion of the instrument in the out-of-plane direction. This results in a greater power output and η. Both of these $T(1,2)$ modes have greater values of Y_{xx} than the admittance in the in-plane directions. This is similar to the $T(2,1)$ case as the two anti-nodal areas move primarily in the x direction, however cancellation between the motions can result in a lower power output.

The $T(1,2)_1$ mode shows a decrease in the monopole source strength, Γ_{00}, at the resonance frequency of the mode. For this mode all three dipole orientations produce

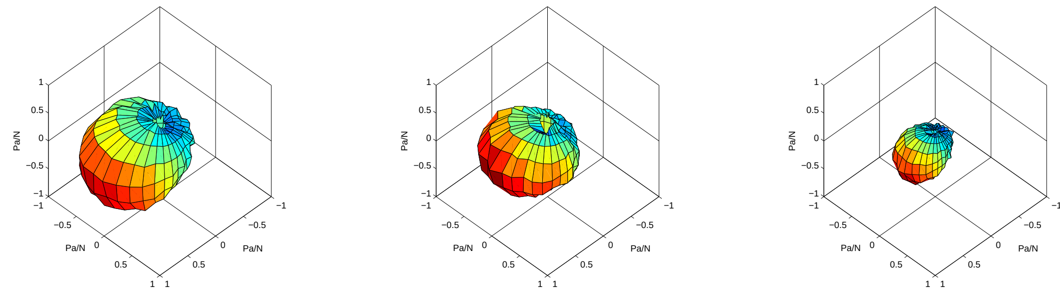

(a) 241 Hz. (b) 260 Hz. (c) 281 Hz.

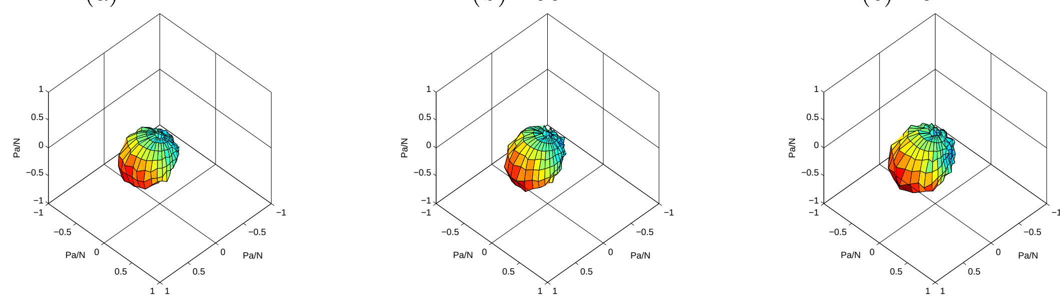

(d) 308 Hz. (e) 328 Hz. (f) 341 Hz.

Figure 5.11: Sound fields produced by BR2 between 241 Hz and 341 Hz (0 - 1.2 Pa/N).

greater values of Γ than the monopole. The sudden decrease in Γ_{00} may result from the y-orientated nodal line which runs across the bridge of BR2 which prevents the mode from being driven efficiently by an excitation at the bridge. Another contributing factor to the reduction in Γ_{00} is the fact that the mode has two anti-nodal areas which would naturally produce a dipole motion. Away from the resonance frequency of this mode the value of Γ_{00} is much higher so the decrease is a localised effect produced by the mode shape at its resonance frequency. The two modes with greater dipole Γs than Γ_{00} ($T(2,1)$ and $T(1,2)_1$) are the least efficient modes of the instrument. This corroborates with the knowledge that dipoles are less efficient radiators of sound than monopoles.

Across a frequency range of 20 Hz either side of the resonance frequency of $T(1,2)_2$ (413 Hz), the power input and power output are nearly equal which results in the high value of η across the range. A possible explanation for the high values of both power output and power input of the $T(1,2)_2$ mode is that the closest frequency body mode below it is the $T(1,2)_1$ mode. This particular mode has an opposite phase to the higher frequency $T(1,2)_2$ mode but it radiates very inefficiently and does not produce a peak in the power output. The mode will therefore not radiate a considerable amount of output power above its resonance frequency and there will only be a small amount of out-of-phase motion between the two modes. This will allow the higher frequency mode to radiate sound with minimal interference from the lower frequency mode.

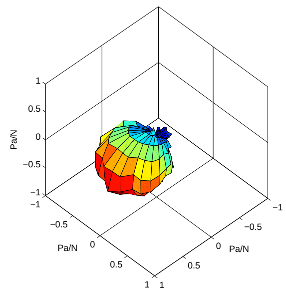

(a) 256 Hz.

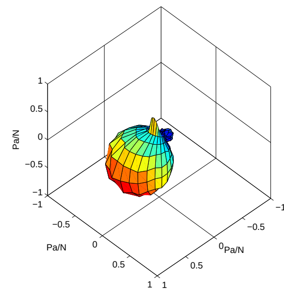

(b) 289 Hz.

Figure 5.12: Dipole sound fields of BR2 (0 - 1.2 Pa/N).

In the second frequency region there are several large rounded η peaks which are interspersed with sharp decreases. The sharp decreases in η coincide with an increase in η_d but a decrease in η_m. As dipoles are less efficient radiators of sound power than monopoles both the total power output and η decrease. The increase in dipole power output is produced by the increasing number of body modes with more complex shapes, such as the $T(1,2)_1$ mode, within this frequency range.

Between 250 Hz and 350 Hz the radiated sound field typically has a monopole-like shape with an average normalised sound pressure of 0.5 Pa/N radiated in front of the instrument. Six sound fields within this frequency range are shown in figure 5.11. The lack of a y-orientated dipole characteristic in the sound field between 250 Hz and 350 Hz shows that the $T(2,1)$ mode does not produce a significant residual pressure response above its resonance frequency. However, there is a greater pressure response in front of the instrument than behind it which results in a dipole power output. The most likely cause of the monopole-like sound fields in this region is from the residual response of the low-frequency resonance triplet.

At frequencies where there is a strong dipole power output, such as 256 Hz and 289 Hz, there is only a very small amount of pressure radiated behind the instrument (< 0.2 Pa/N) and a much greater amount (1 Pa/N) radiated in front of the instrument. The sound fields at these frequencies are shown in figure 5.12 where there are two unevenly sized lobes. The monopole component in the acoustical power output therefore makes BR2 a more efficient radiator at these frequencies than at the resonance frequency of the $T(2,1)$ mode. The sound fields at 256 Hz and 289 Hz correspond with the sharp decreases in η seen in figure 5.3, which follow the rounded peaks produced by the more monopole-like sound fields.

Lai and Burgess (1990) found that, on both of the guitars that they studied, the region between 300 Hz and 400 Hz produced values of $\eta > 1$. The vibration exciter used in that experiment was unable to provide a large enough level of power input to study the behaviour of the guitars in this particular frequency range. When BR2 was excited at position 1, η was greater than 1 at 400 Hz but between 300 and 350 Hz there are η values between 0.6 and 1. As the values of η are typically less than 1 between 300 Hz and 400 Hz for BR2, it can be assumed that the instrument is in fact highly efficient within this frequency range and that the impact hammer typically provides a great enough level of power input at the bridge to measure η.

The third frequency region ($>$ 450 Hz)

The third frequency region, above the $T(3,1)$ mode at 450 Hz, is characterised by a much lower average level of η than the two lower frequency regions. The decrease in η starts between the $T(1,2)_2$ mode and the $T(3,1)$ mode. Between the resonance frequency of the $T(4,2)$ mode and 2000 Hz, η is less than 0.2, aside from two peaks. In this third region the main contribution to the power output is from body modes with a more dipole-like characteristic, but there are still peaks in η where the power output is nearly entirely produced by monopole sources. A possible explanation for the reduction in the monopole power output compared with dipole power at higher frequencies is provided by the shapes and the phase relationships of the higher frequency modes. The higher frequency body modes have greater numbers of anti-nodal areas which produce cancellation effects and dipole-like sound fields.

The $T(4,2)$ mode has a low value of η because it has four pairs of anti-nodal areas with opposite phase which act like dipoles, similar to $T(2,1)$. The even number of areas of opposite phase with similar sized areas also results in a cancellation of the sound pressure output, and therefore they radiate a lower amount of sound power. The dominance of dipole power output in the higher frequency regions results from the increasing complexity of the modes of vibration occurring on the top plate. As the number of smaller vibrating areas increases it is difficult for monopole-like sound fields to be produced by the instrument as the top plate is not able to move in a single uniform direction. Dipoles typically produce a smaller amount of acoustical power output than monopoles so η will therefore decrease at higher frequencies. There is a strong monopole output at 700 Hz that coincides with the resonance frequency of the $T(5,1)$ mode. It has an anti-nodal region that is located in the centre of the bridge and extends to its edges and behaves in a similar fashion to $T(3,1)$; there is a cancellation between four of the five vibrating regions leaving the other area free to vibrate and produce a monopole-like output.

The sound field produced by the $T(3,1)$ mode, 455 Hz, was previously measured by Hill et al. (2004) and is shown in figure 5.13b. In that experiment, the instrument was driven at two of its three anti-nodal regions using two electromagnetic exciters with signals of the same frequency but with opposite phase. Exciting the instrument at the anti-nodal regions of the mode with the correct phase relationship between the drivers kept the excitation of other body modes to a minimum and only the $T(3,1)$ mode was assumed to be radiating sound. In the current work, where the instrument was excited using the impact hammer system, it was not possible to separate and individually drive single body modes. As a result of this, the $T(3,1)$ mode shows a greater level of normalised sound pressure in the upper half of the sound field in figure 5.13a than in the lower half.

Holographic interferometry studies of the $T(3,1)$ mode of BR2 have previously shown that there is a low level of displacement produced in the upper bout for this mode (Hill et al., 2004). $T(3,1)$ is around 40 Hz higher in frequency than the $T(1,2)_2$ mode which has a large vibrating area in the upper bout of the instrument. The low level of sound pressure in the lower half of the sound field is a result of the $T(3,1)$ mode acting out of phase with part of the lower vibrating area of the $T(1,2)_2$ mode. In the upper half of the sound field, the large level of sound pressure must therefore result from the residual response from the $T(1,2)_2$ mode. The $T(1,2)_2$ mode undergoes a greater level of motion in the upper bout than the $T(3,1)$ mode, particularly near to the sound hole. Therefore this upper bout motion must also occur as a residual response above the mode's resonance frequency and produce the sound field in figure 5.13a.

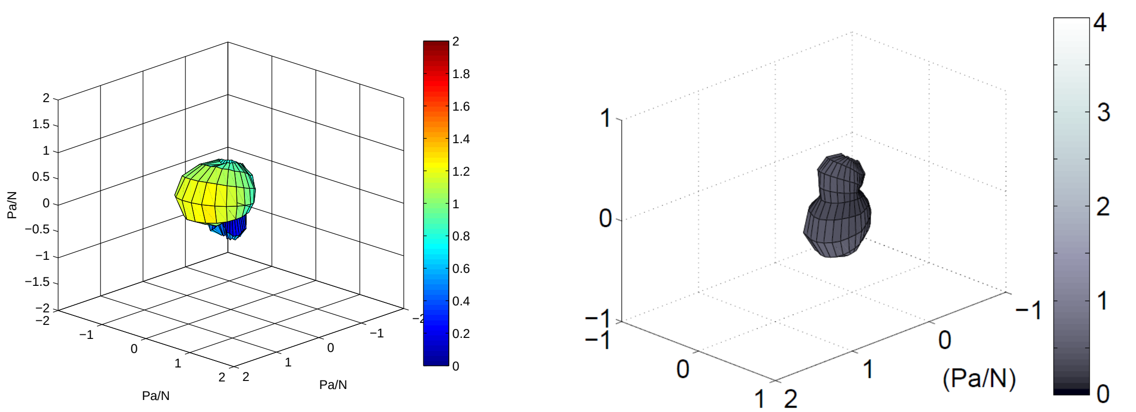

(a) Normalised sound pressure field of BR2's $T(3,1)$ mode.

(b) Normalised sound pressure field of BR2's $T(3,1)$ mode measured by Hill et al. (2004). Reprinted with permission from Acta Acustica United with Acustica.

Figure 5.13: $T(3,1)$ measured on BR2.

At higher frequencies there are two body modes which produce values of in-plane velocity which are almost equal in value to the out-of-plane velocity. At 540 Hz the value of Y_{xy} is almost the same as Y_{xx}. This is the resonance frequency of the $T(2,2)$ mode which has equal-sized anti-nodal areas and nodal lines in the z and y directions passing through the bridge. This mode is within the lower η frequency region for BR2. There is a peak in Y in the z direction at 1024 Hz which does not produce a clear ODS but appeared to be a $T(1,5)$-like mode which produces the strong Y_{xz} measurement seen in figure 5.6.

The peak values of power input and output occur at frequencies below 450 Hz which corresponds with a previous study by Christensen (1983). Christensen found that 80% of the acoustic energy produced by a classical guitar was found to be below 600 Hz and over 60% of the energy was below 400 Hz. At frequencies above the highly efficient $T(1,2)_2$ mode, the peak values of power output are at least an order of magnitude smaller than that of the $T(1,2)_2$ mode. Above 1300 Hz, the peak values of power output are another order of magnitude smaller than those between 450 Hz and 1300 Hz. The power input is fairly consistent between 450 Hz and 1300 Hz with the values lying within one order of magnitude. The difference in the power input and output shows that while the body of the instrument may be set into motion fairly easily this does not necessarily correspond with a large power output. This shows the importance of measuring both the response on the instrument's body and the radiated sound produced by the excitation. The lower level of power output above 1300 Hz is the result of the higher frequency body modes having greater numbers of small anti-nodal areas.

At frequencies above the $T(3,1)$ mode, no monopole-like sound fields are produced by the instrument. Instead the sound fields become increasingly complex due to the larger number of smaller vibrating regions in motion for individual modes. Some of these higher order modes produce values of normalised sound pressure which are comparable with those produced by lower frequency modes. However, the Γ data in figure 5.7 and the η data in figure 5.3 show that a large dipole component in one orientation does not necessarily mean that the mode will radiate sound efficiently. At higher frequencies the magnitude of the radiated sound pressure also decreases making it more difficult to visualise the sound pressure fields without background noise affecting the data.

The three modes with the greatest values of Γ_{00} are the $T(1,1)_1$, $T(1,1)_2$ and $T(1,2)_2$ modes. The last of these three modes is the most efficient mode on this instrument. The $T(1,2)_2$ mode produces the largest value of Γ_{00} between 400 Hz and 2000 Hz showing that this is the last of the modes that is able to easily radiate monopole sound power. Across the entire frequency range the greatest contribution to D_ω is typically produced by the Γ_{1x} component which radiates sound in an out-of-plane direction. Above 600 Hz the contributions to the dipole source strength from the x, y and z directions show a

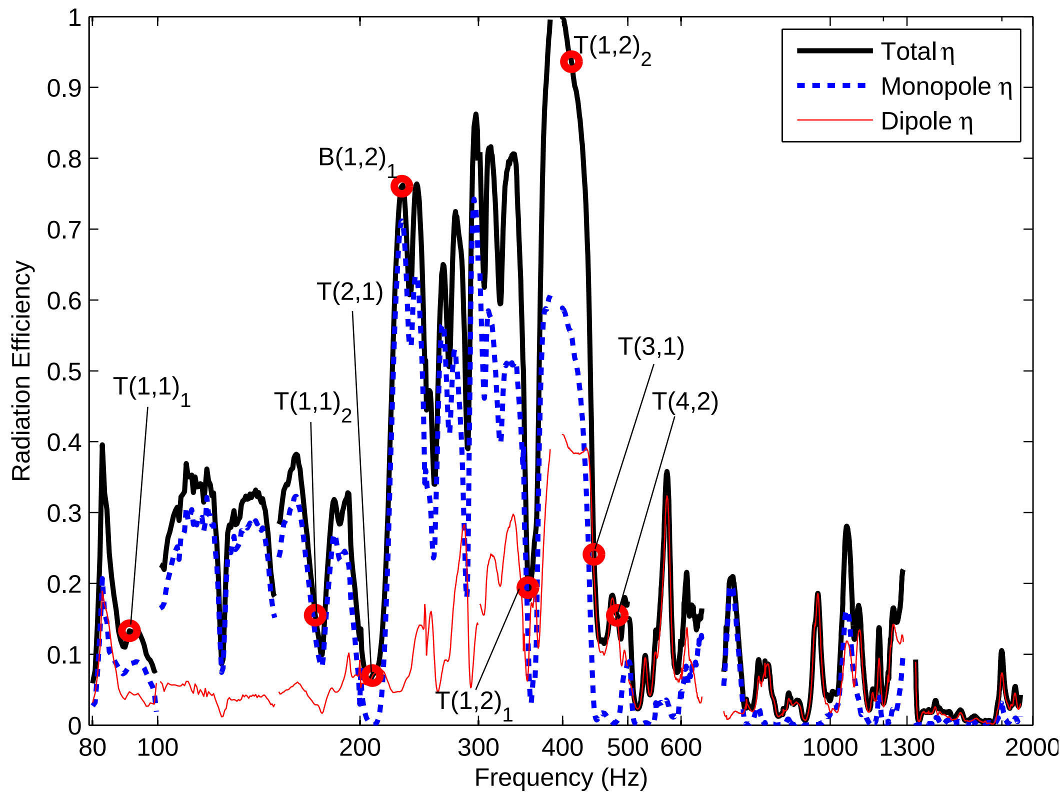

Figure 5.14: Radiation efficiency measured at position 2 on BR2.

greater amount of overlap and have more similar values. The radiated sounds fields will therefore not produce the same clear orientation as the more dipole-like modes such as $T(2,1)$.

5.1.2 BR2 excited at position 2

The vibrational behaviour of stringed instruments is known to change when excitations are made at different points on their bridges (Richardson, 2001). The measurements reported in this section were made at position 2, near to the E_2 string, on the opposite side of the bridge to position 1. Position 2 is shown in figure 5.1 on page 99.

Figure 5.14 shows that when BR2 is excited at position 2 it produces a similar η profile to when it is excited at position 1 (see figure 5.3). There are still the three regions of η behaviour which occur within the same frequency ranges. Below 200 Hz the η behaviour is different but the peak values are similar and also do not occur at the resonance frequencies of the body modes. On average, η is slightly lower in the second region, between 200 Hz and 450 Hz, than for the excitation made at position 1. The slight difference in the values of η is most likely to result from the instrument not having an entirely symmetrical construction. The asymmetry will result in a different vibrational behaviour depending on the excitation point.

Below 200 Hz the radiated sound power is still dominated by monopole contributions with an increase in dipole contributions at frequencies above the $T(2,1)$ mode. The dipole contribution from the sound hole sum rule is present below 200 Hz and the peak values of η are still located between the two $T(1,1)$ modes. The peak value of η at 80 Hz is presumed to be noise as there are no body modes present at this frequency. The value of η for the $T(2,1)$ mode was the same for both position 1 and position 2 ($\eta = 0.07$) despite the fact that the opposite anti-nodal region was excited. This shows that the two anti-nodal areas have similar sizes which are located on either side of the bridge.

Between 200 Hz and 450 Hz, the same η behaviour is observed for position 2 as for position 1, with the sharp decreases in η between the rounded peaks corresponding with a decrease in η_m and an increase in η_d. The $T(1,2)_1$ mode is still comparatively inefficient, producing $\eta = 0.19$ in comparison with the $T(1,2)_2$ mode which produces $\eta = 0.94$. However, the $T(1,2)_1$ mode is more efficient when the instrument is excited at position 2 than when it was excited at position 1. That said, this mode is still inefficient in comparison with η at other frequencies. As this mode shows the greatest difference in η of the top plate modes, between excitations at positions 1 and 2, it must therefore exhibit a greater level of asymmetry across the bridge than the other body modes.

Above the resonance frequency of the $T(3,1)$ mode, η is typically lower for position 2 than for position 1. Several of the same features occur within η at these higher frequencies for both positions. At 710 Hz there is an η peak with an almost entirely monopole characteristic and at 960 Hz there is a peak with a strong dipole-like characteristic in the η data. The first of these peaks is close in frequency to the $T(5,1)$ mode and the second has a $T(6,1)$ shape with two of the six anti-nodal regions located on the bridge. These two areas on the bridge have opposite phases but similar sizes and therefore the mode will be driven by an excitation at either position 1 or position 2.

Figure 5.15 shows that the power input to the $T(2,1)$ mode produces the largest peak between 80 Hz and 2000 Hz. However, the power output is considerably smaller than the input power. This is the same result that occurred for position 1. $T(1,2)_1$ does not radiate a large level of output power compared with its input power but there is a small peak in output power visible for position 2. This is the same as for the excitation made at position 1, showing that the $T(1,2)_1$ mode is an inefficient radiator of sound even though it does take a large power input. According to the holographic

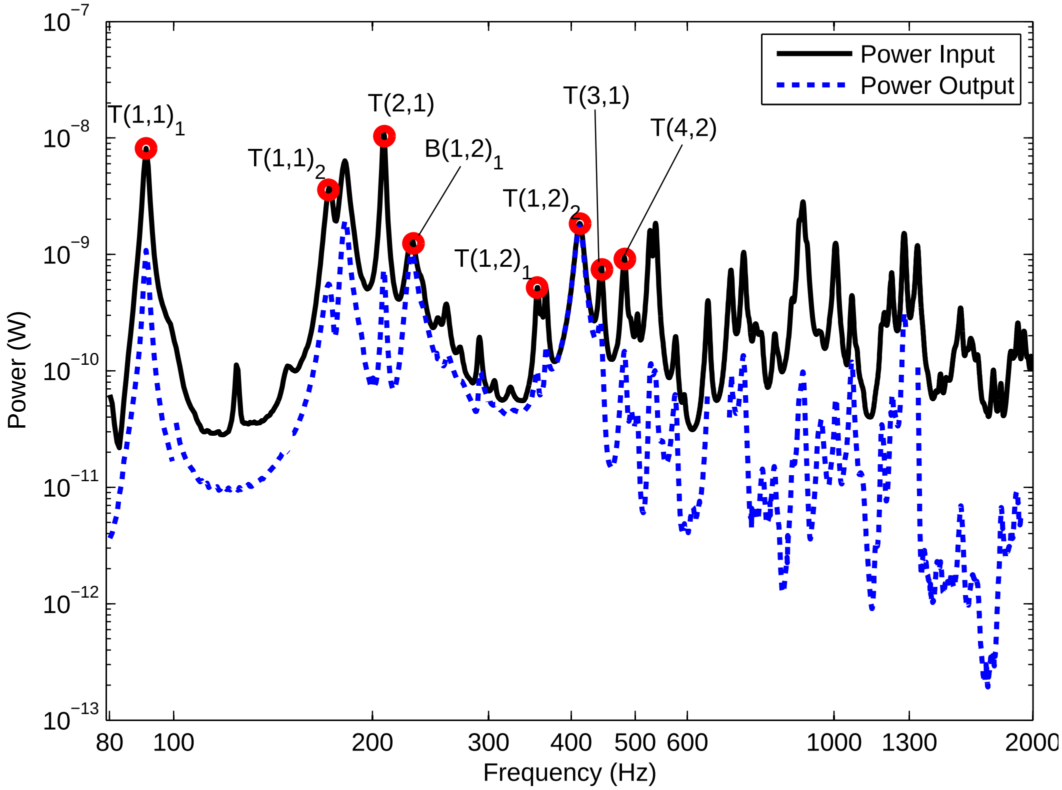

Figure 5.15: Mechanical power input and acoustical power output for BR2 excited at position 2.

interferometry pictures of the modes of BR2 (Hill et al., 2004) the nodal line of $T(1,2)_1$ is located on the bridge. As η is greater at position 2, the bass side of the bridge must be closer to the lower anti-nodal area than the treble side. A greater asymmetry in guitar construction could result in a greater difference in the power output and a different value of η.

Position 1 and position 2 both show similar η and power properties between 80 Hz and 2000 Hz as both locations are an equal distance from the centre of the bridge and top plate. Therefore the symmetrically shaped modes would be expected to behave in a similar fashion for both points, providing that they have similar sized anti-nodal areas. The simplest way to determine the effect that modes with y-orientated nodal lines through the bridge have on η and power is to excite the instrument at the centre of the bridge. This reduces the level of excitation provided to modes which have their nodal lines through the centre of the bridge.

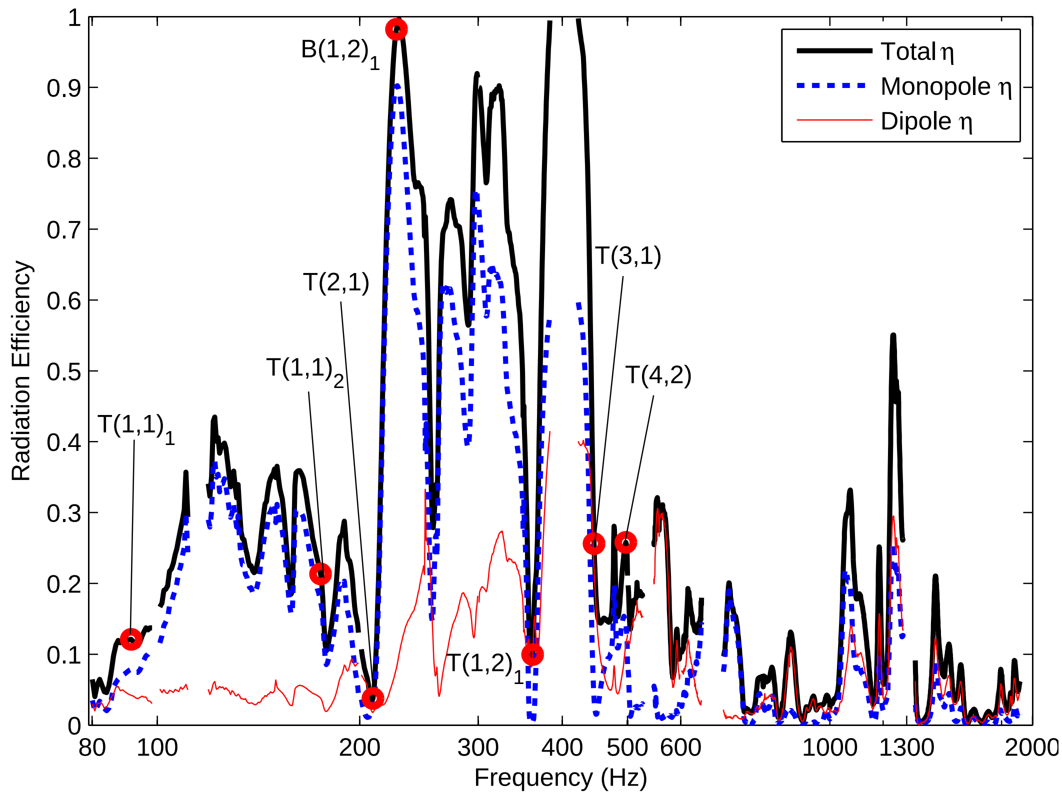

Figure 5.16: Radiation efficiency measured at position 3 on BR2.

5.1.3 BR2 excited at position 3

Positions 1 and 2 are both located on the far sides of the bridge and the previous sections have shown the effect of the symmetry of the instrument's construction on η. There are many body modes which have their nodal lines at the centre of the bridge, such as the $T(2,1)$ and $T(4,2)$ modes. If the instrument is excited at the centre of the bridge then these modes will be driven at their nodes and will produce a lower response. Position 3 is shown in figure 5.1 on page 99.

Figure 5.16 shows that BR2 produces similar η behaviour between 80 Hz and 2000 Hz when excited at position 3 as that produced when the excitations were made at positions 1 and 2. The greatest values of η lie between 200 Hz and 450 Hz and this region still appears 'bounded' by the $T(2,1)$ and the $T(3,1)$ modes. The $T(1,2)_2$ mode is not shown in figure 5.16 as it corresponded with a value of $\eta = 1.05$ as a result of an insufficient amount of input power being supplied to the instrument for this mode. The power output in figure 5.17 shows that, at the frequencies surrounding this mode, the instrument is highly efficient at radiating acoustical power. The $T(2,1)$ mode produces $\eta = 0.04$ which is less than that for either positions 1 or 2 but it is still comparable in size. The cause of this η result is shown in the power input and output in figure

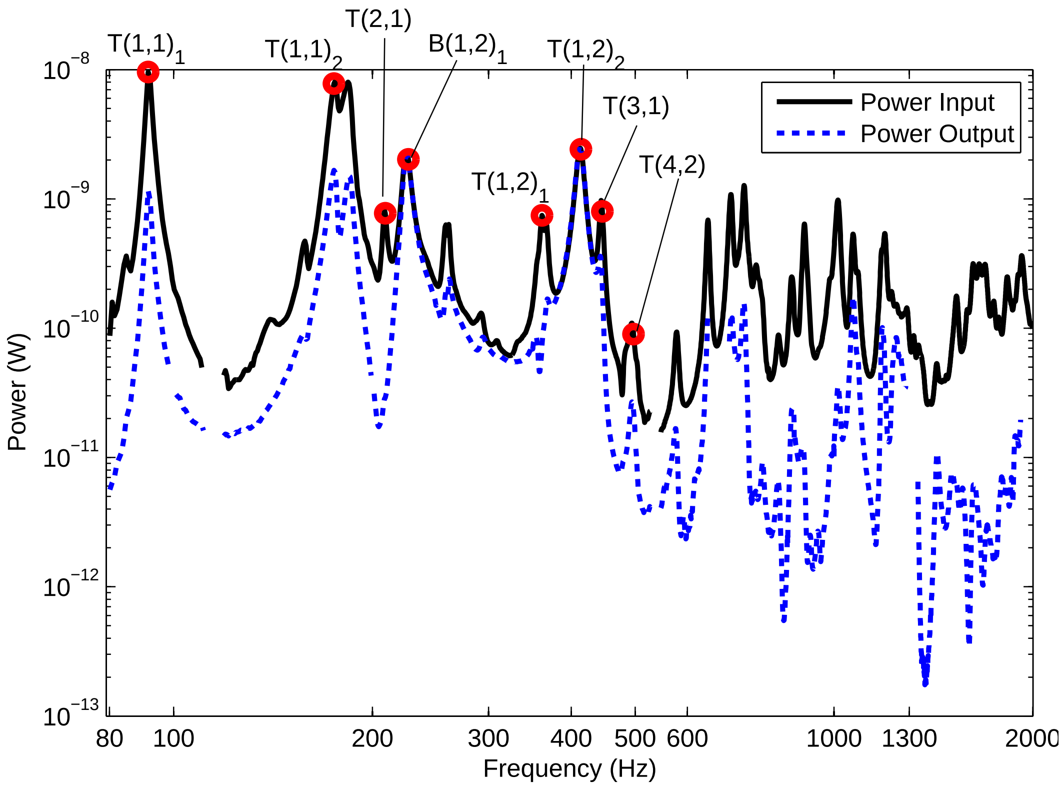

Figure 5.17: Mechanical power input and acoustical power output for BR2 excited at position 3.

5.17 where there is no longer a peak in the output power measurement as there was for positions 1 and 2. However, the peak in the power input is also much smaller than for the measurements made at positions 1 and 2. The peak in power input for $T(2,1)$, at position 3, occurs because the velocity was not measured on the nodal line. There is therefore a greater level of velocity measured, which results in a greater power input than if the velocity and force were measured exactly in the centre of the bridge. The value of η when the instrument is driven at the centre of the bridge may in fact be greater than that measured because the level of input power will be lower. This could not be checked as there was no method available for providing an impulse excitation at the same location as the velocity measurement for the η measurements.

The low level of η of the $T(2,1)$ mode for all three excitation locations shows that the mode does not generate a large level of output power relative to the input power regardless of the driving location. This is despite the fact that large areas of the body are in motion for this mode. As a result, η of this mode is consistent across the bridge and therefore the input power from any of the strings should be expected to result in a similar level of output power at its resonance frequency. The $T(2,1)$ mode is not a

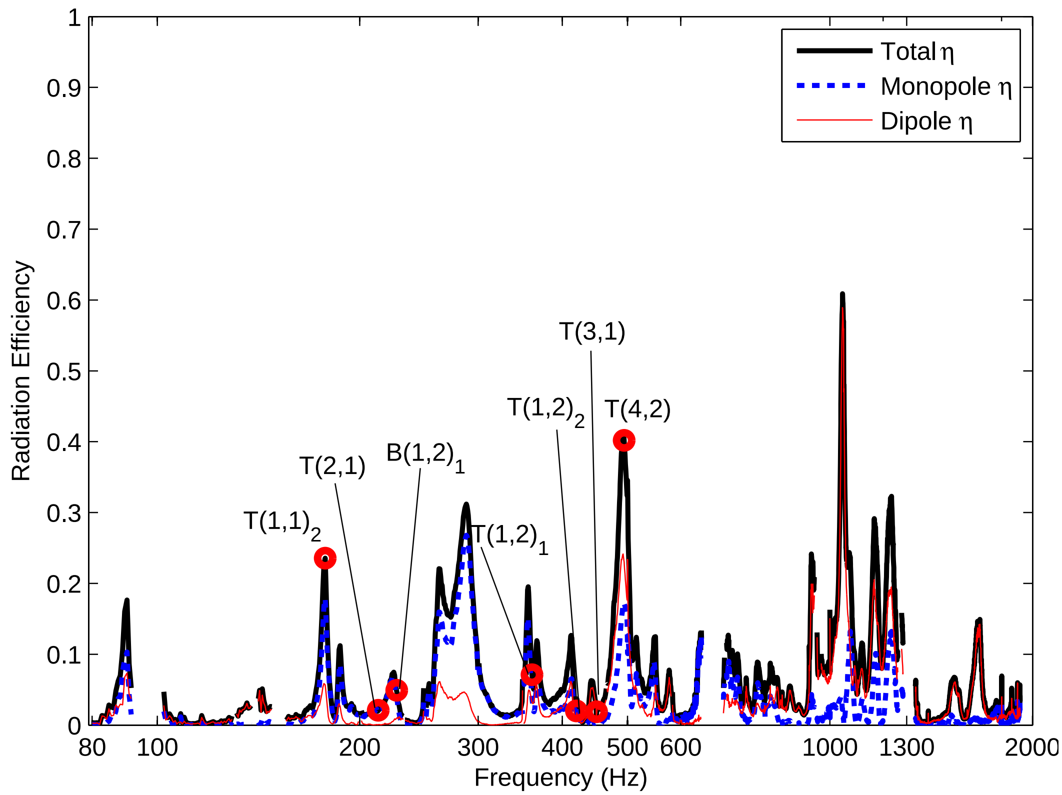

Figure 5.18: Radiation efficiency measured at position 4 on BR2.

large contributor to the radiated sound either at or above its resonance frequency.

It should be noted that at 960 Hz, the strongly dipole-like mode is no longer present in the η data for position 3 as it is corresponds with the $T(6,1)$ mode. The nodal line at the centre of the $T(6,1)$ mode must therefore lie at both the excitation and the response measurement locations of position 3.

5.1.4 BR2 excited at position 4

The results in the previous sections have shown the behaviour of BR2 when it was excited on the bridge. The bridge provides one termination for the string and the other is provided either by the nut (for an open plucked string) or by the finger on a fret, so the behaviour of the instrument should be studied at this termination as well. The sound pressure produced by an excitation at the nut has previously been studied and it was found that a “significant amount of acoustically active resonance ... coupled to the nut” (White, 1981). However, in the study by White, the measurements of the pressure response produced from the excitation at the nut were not calibrated. The input admittance has also previously been measured along the neck of a classical guitar.

Boullosa (2001) found that higher values of input admittance were measured next to frets located on the body compared with those on the neck. The radiation efficiency, η, of a guitar resulting from an excitation on the neck has not previously been studied.

As a result of constraints produced by the size of the anechoic chamber and measurement spheres, it was not possible to measure η produced by an excitation at the nut or at frets on the body of the instrument. The strings were damped and the D_3 and G_3 strings were held apart close to the nut using a small piece of wood of mass 5 g. The wood was held in place by tension from the strings and did not touch the neck of the instrument. Separating the strings in this way allowed for the excitation and response measurement to be made on the neck. The excitation and response were measured close together at the 12th fret at position 4 (shown in figure 5.1 on page 99).

Figure 5.18 shows that BR2 radiates sound power far less efficiently when excited on the neck of the instrument than when driven on the bridge. The $T(1,1)_1$ mode is not labelled in figure 5.18 because the microphones were not sensitive enough to measure the low pressure response as the sound radiated by the instrument was lower than the background noise level. The majority of the motion of the $T(1,1)_1$ mode occurs in the lower bout and it is therefore less easily excited by an excitation on the neck than the $T(1,1)_2$ mode.

Below 200 Hz there is no significant dipole power output component. The effect produced by the sound hole sum rule is no longer present because the instrument was excited at a point on the neck which is not located on the top plate of the instrument. Therefore the top plate was not driven by the impulse and the enclosed air was not excited. The lack of a plate or air motion means that the sound hole sum rule cannot produce a dipole sound field. The frets on the top plate of the instrument may produce the sound hole sum rule effect as they can directly drive the plate, but η on these frets could not be studied. There is also no clear peak between the resonance frequencies of the two $T(1,1)$ modes, which is consistent with the prediction that it is the Helmholtz oscillator-like motion between the two modes which causes an increase in η. The air within the guitar cavity cannot be easily driven by an excitation provided at the neck of the instrument and this reduces the values of η across the entire frequency range.

$B(1,2)_1$ and $T(1,2)_2$ both produced peak values of η when BR2 was driven on the bridge but have very low values of η at position 4 because the motion of these modes does not extend as far as the neck of BR2. The two greatest values of η below the $T(4,2)$ mode, when BR2 is driven at position 4 occur at 262 Hz and 288 Hz with $\eta = 0.22$ and $\eta = 0.31$ respectively. When BR2 was excited at the bridge these two frequencies produced minima in η with $\eta_d > \eta_m$. When the excitation was provided at the neck the opposite case occurs with $\eta_m > \eta_d$. At these two frequencies the instrument has two back plate modes with $B(1,2)$ shapes which have a larger anti-nodal region in the upper bout of the back plate than the lower bout. As the larger of the two anti-nodal areas is closer to the neck than the bridge, the $B(1,2)$ modes are therefore more likely to be driven more easily at position 4. If the larger area is excited there will be a smaller amount of cancellation between the two anti-nodal regions and this will result in a greater amount monopole power output than dipole power output.

Below the resonance frequency of the $T(4,2)$ mode, the body modes of BR2 undergo the majority of their motion in the lower bout of the guitar. Unlike the excitations made at the bridge, when the instrument is driven at the neck there are several modes which show a peak in η at their resonance frequencies, such as $T(1,1)_2$ and $T(4,2)$. The motion of these body modes must therefore extend into the upper bout of the instrument and can thus be set into motion by an excitation at the 12th fret. At 1044 Hz there is a peak in η which corresponds with a large dipole power output.

When BR2 was excited at position 4, η was lower than when it was measured at any measurement point on the bridge. The conclusion is that the instrument does not effectively radiate sound when driven at the 12th fret. Energy transferred from the string to the neck at this point will therefore not be efficiently radiated as sound and will be 'lost' to the instrument, most likely as heat.

5.2 BR1, DLC and MAL classical guitars

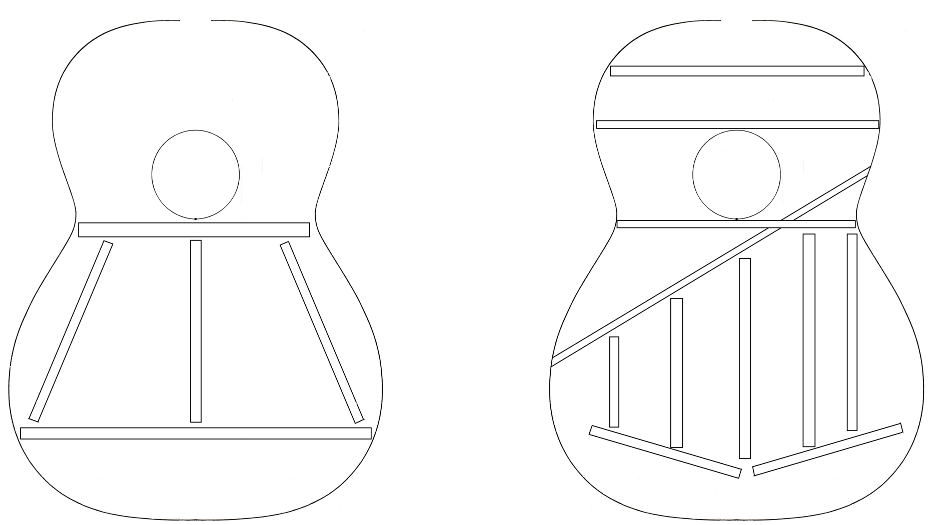

(a) MAL. (b) DLC.

Figure 5.19: The bracing patterns of the top plates of MAL and DLC.

The radiation efficiency, η, and 3D input admittance was also measured on three other classical guitars in this work; named BR1, DLC and MAL. Both BR1 and DLC have been previously investigated as part of a study of ten classical guitars funded by the Leverhulme Trust but MAL was not part of that study. The resonance frequency, effective mass, spherical harmonic weighting (G_{lm}), Q value and mode shape for all body modes below 500 Hz were determined for the ten classical guitars. The data from some of the instruments in the Leverhulme Trust study have been previously published (Richardson et al., 2002), but the data for BR1 and DLC has not been published at the time of writing. In this thesis BR1, DLC and MAL were all excited at position 1 on their bridges.

BR1 has a similar construction to BR2 and was also built by Dr Bernard Richardson. It has a spruce top plate with Torres bracing and maple back and sides.

The De La Cruz guitar, DLC, has a different strutting pattern to BR1 and BR2. This pattern is based on the Ramirez strutting previously shown in figure 1.2. The strutting of DLC's top plate is shown in figure 5.19b. The most noticeable difference in the strutting of DLC in comparison with the other three classical guitars is the diagonal strut running from the upper bout to the lower bout. This introduces an asymmetry to the design which is not present on the other instruments.

MAL is a Kyoto brand acoustic guitar which was built in Korea. Unlike most classical guitars it has a steel rod inside the neck. The bracing design is based on Torres bracing but the top plate has far fewer struts (see 5.19a). When playing MAL the lowest three strings, even when new, produce a very small initial attack as perceived by the listener in the radiated sound and it has been determined to be the lowest quality instrument of the four classical guitars. This is admittedly a subjective judgement but it is one that seems apt.

The resonance frequencies of the labelled body modes on all of these instruments do not typically coincide with peaks in η, as was the case for BR2. However, there are some exceptions, such as the $T(1,1)_2$ mode on MAL. Often peak values of η occur close to the resonance frequencies of the body modes but not actually at the same frequency, such as the $T(1,2)_2$ modes for BR1, BR2 and DLC. The peaks in η typically occur between the body modes as the power input decreases more rapidly than the power output either side of a resonance frequency. This is the same result as was seen on BR2. However, as noted above, the peaks in η can occur at the resonance frequency of a body mode.

Figures 5.20, 5.22 and 5.24 show that the greatest values of η for these three guitars occur between 200 Hz and 450 Hz in what was described as the second frequency region

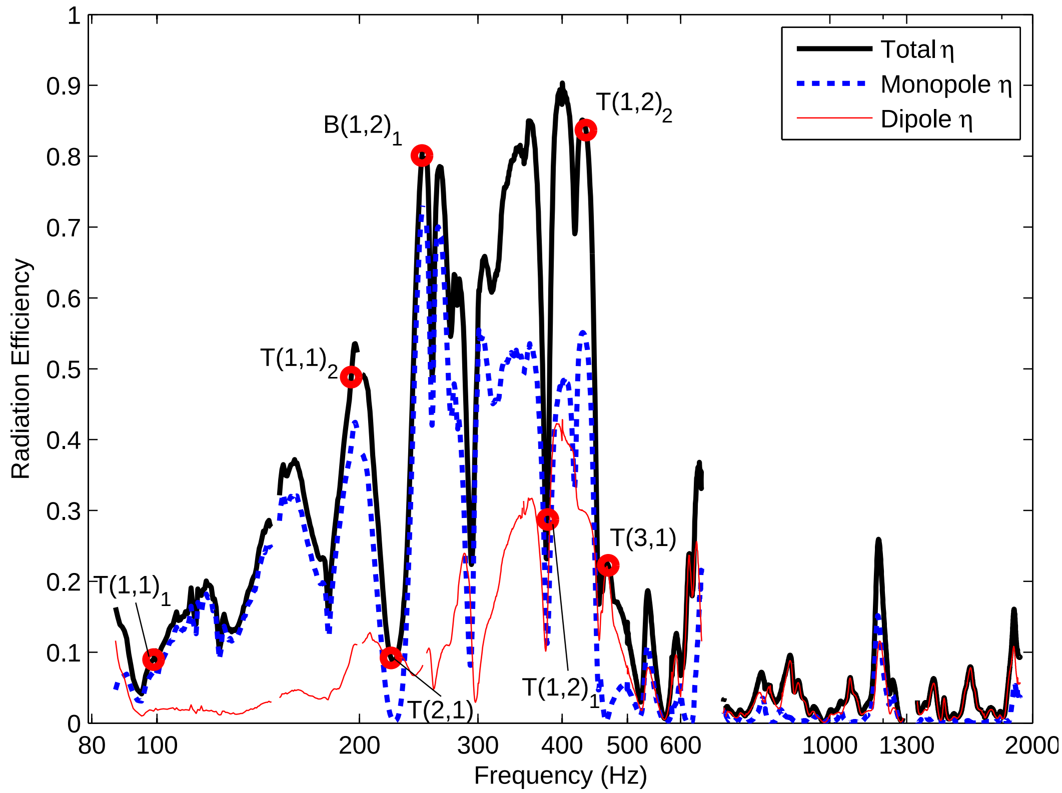

Figure 5.20: Radiation efficiency measured at position 1 on BR1.

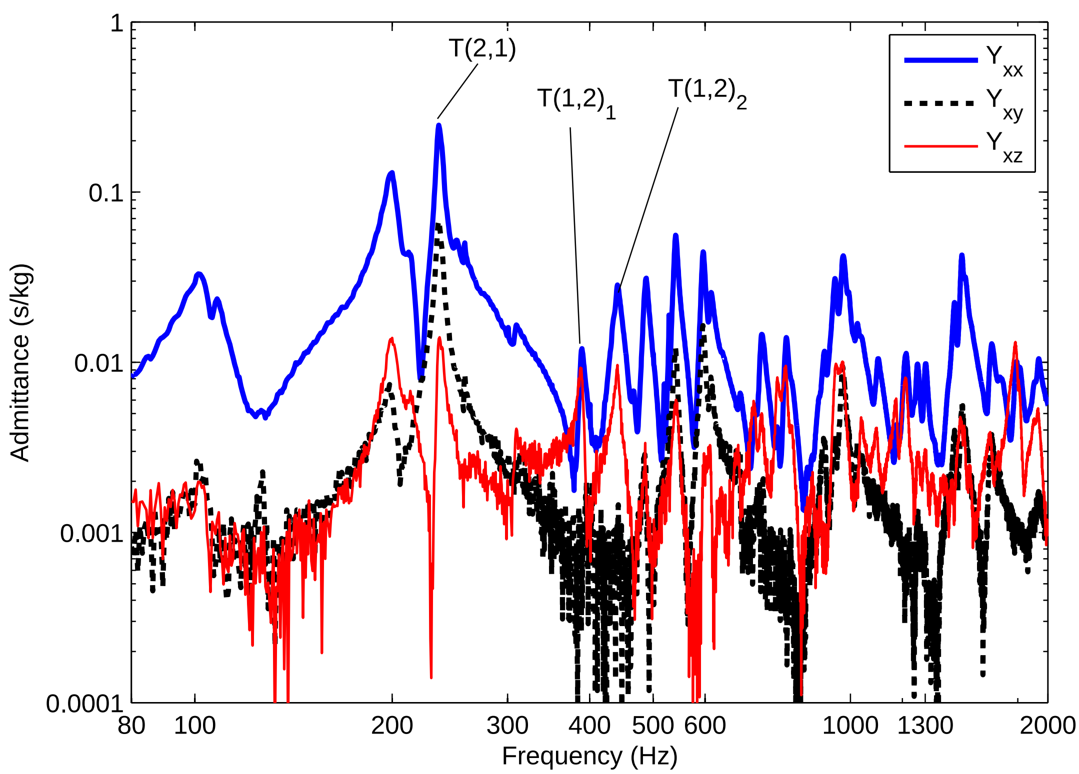

Figure 5.21: 3D input admittance measured at position 2 on BR1.

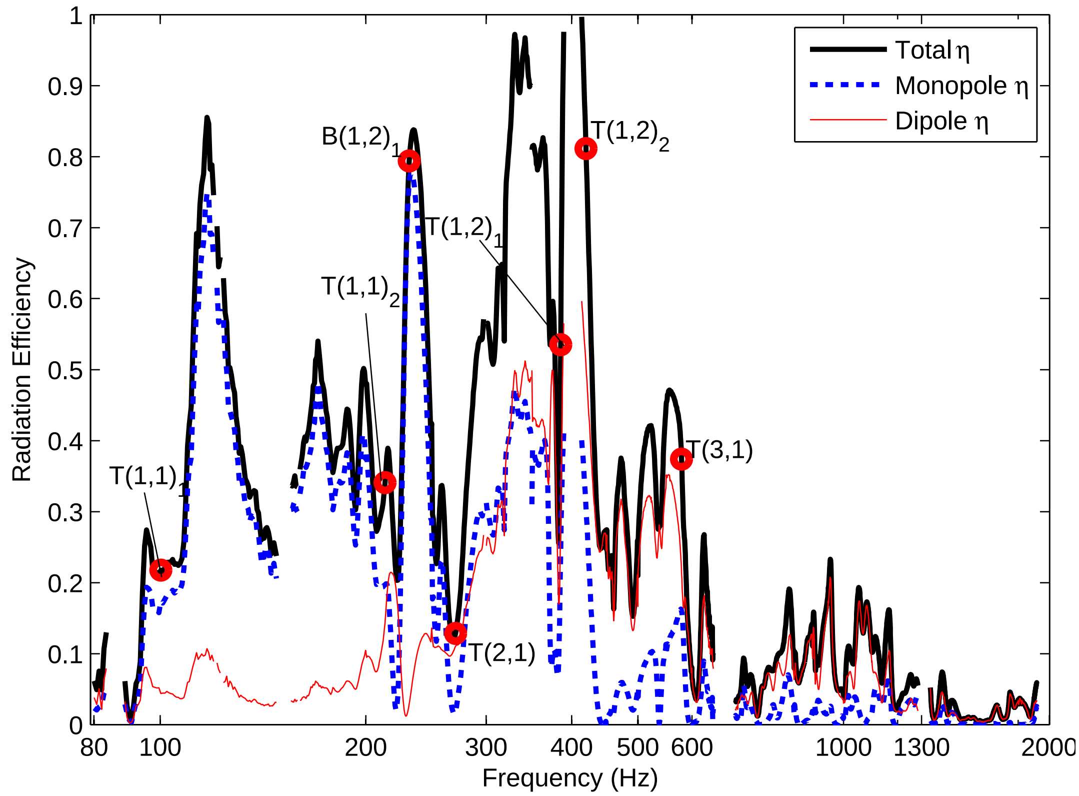

Figure 5.22: Radiation efficiency measured at position 1 on DLC.

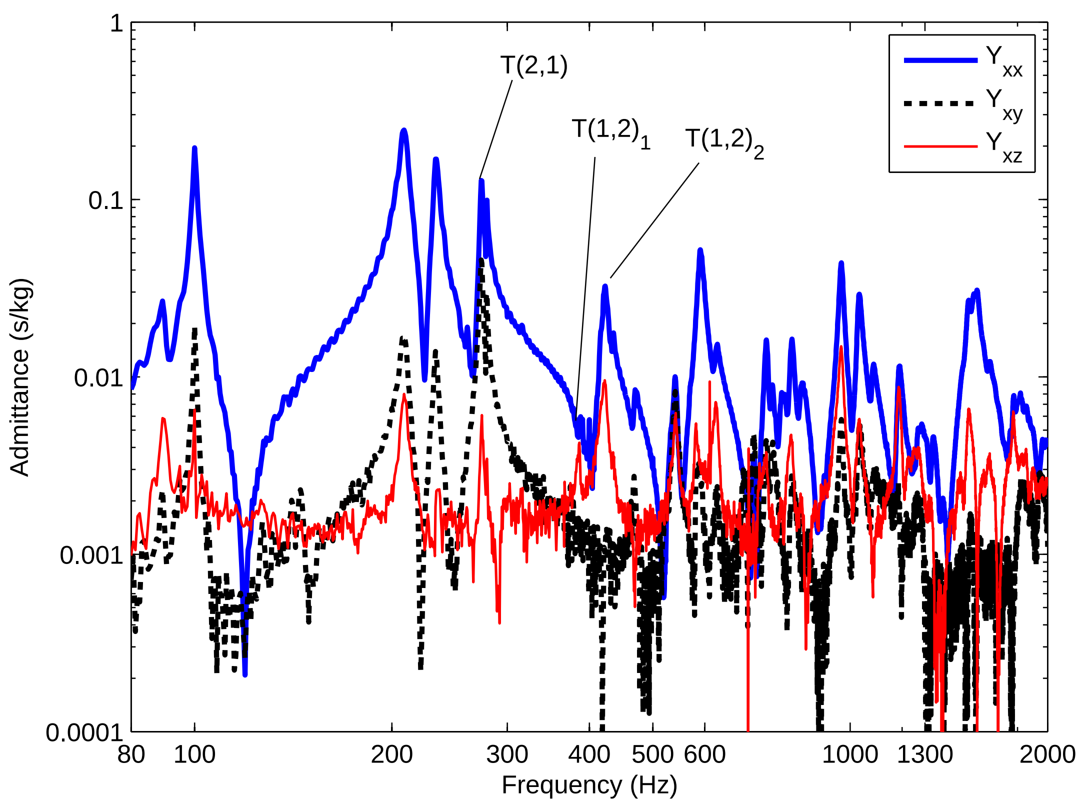

Figure 5.23: 3D input admittance measured at position 2 on DLC.

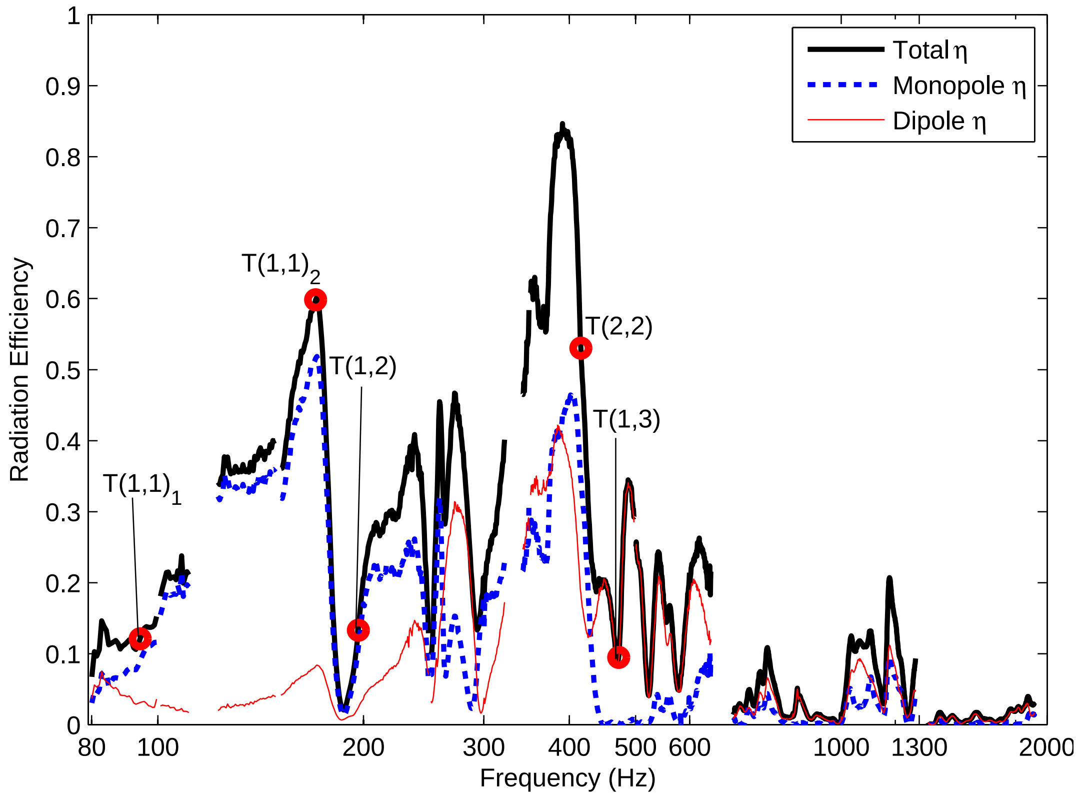

Figure 5.24: Radiation efficiency measured at position 1 on MAL.

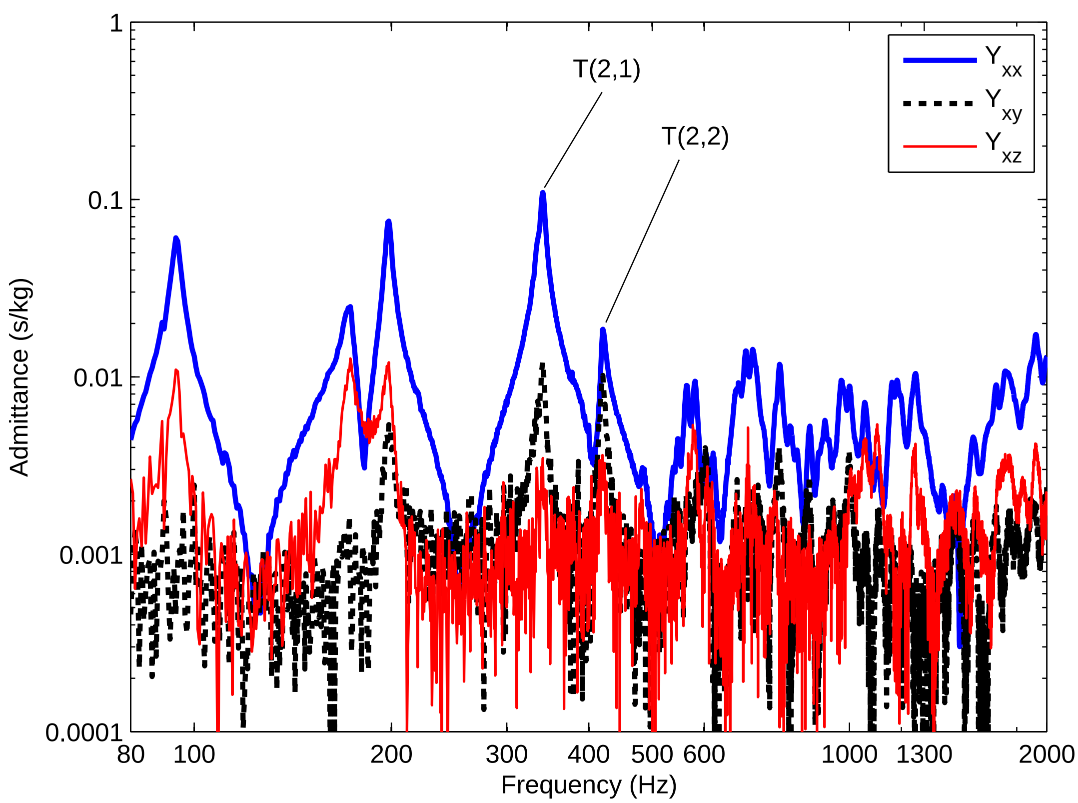

Figure 5.25: 3D input admittance measured at position 2 on MAL.

for BR2. Above this second frequency range the values of η decrease. All of the classical guitars have body modes with an increasingly large number of anti-nodal areas on them at higher frequencies and this results in the lower values of η. In addition, all of the instruments showed low values of η below 80 Hz as this frequency range is below the resonance frequency of the $T(1,1)_1$ mode.

Between 1500 Hz and 2000 Hz, the average value of η for the four classical guitars excited at position 1 are as follows. $\eta_{BR2} = 0.020$, $\eta_{BR1} = 0.040$, $\eta_{MAL} = 0.015$ and $\eta_{DLC} = 0.019$. There is only a small difference between the η values of the four instruments at this frequency which suggests that the construction of the instruments has only a limited effect on the radiation efficiency at higher frequencies. Subjectively, MAL is the lowest quality of the four guitars and has the lowest average value of η but this is only slightly lower than the averages for BR2 and DLC which are much 'better' instruments.

The 3D admittance was also measured at the E_2 strings of three other classical guitars; BR1, DLC and MAL (see figures 5.21, 5.23 and 5.25). As was the case for BR2, the velocity for all three guitars in the x direction was far greater than in either y or z. Away from the resonance frequencies of body modes, the in-plane velocity for all three instruments was similar in value to the background noise of the measurement system. All of the studied classical guitars produced the greatest value of Y_{xy} at the resonance frequency of their $T(2,1)$ modes. The $T(1,2)$ shaped modes produce the greatest values of Y_{xz} as a result of the orientation of their anti-nodal areas.

MAL is the lowest quality of the four instruments and produces the lowest values of velocity in the y direction (as shown in figure 5.25). The three higher quality classical guitars have thinner plates than MAL which allow for a greater level of in-plane and out-of-plane motion. The increase in the in-plane motion is therefore a by-product of thinning the plates to allow for a greater level of out-of-plane motion. This requires a fine balance when deciding on the plate's thickness. Aside from the structural issues, if the plate is too thin then a greater amount of in-plane motion will occur which does not produce much output power. Conversely if the plate is too thick then it will not be able to undergo much out-of-plane motion and will therefore not radiate acoustical power efficiently.

For all four of the studied classical guitars, the top plate modes with nodal lines at the centre of the bridge produce a greater in-plane velocity than the modes which have their nodal lines elsewhere on the bridge. The modes which produce this effect most clearly are the $T(2,1)$ and $T(2,2)$ modes. The $T(1,2)_1$ mode of BR1 was previously shown in section 5.2 to be an inefficient mode. Figure 5.21 shows that this mode, at 380 Hz, produces a large value of Y_{xz} but the higher frequency, 434 Hz, $T(1,2)_2$ mode produces a negligible in-plane motion. This mode, with only a small in-plane motion, is a much more efficient radiator than $T(1,2)_1$.

5.2.1 Comparison with BR2

BR1 has a similar construction to BR2 and produces similar values of η across the frequency range as expected. However, differences are present as a result of the differences in the material properties of the wood used to build the instruments. BR1 shows the same three divided regions of radiation efficiency as BR2. These regions are bounded by the same body modes as BR2 despite the differences in their resonance frequencies. The first region is bounded by $T(2,1)$, the second region lies between the $T(2,1)$ mode and the $T(3,1)$ mode and the final region is above the $T(3,1)$ mode. Above the resonance frequency of $T(3,1)$ for BR1 the values of η are typically less than 0.2. While the second region still contains the greatest values of η, the peak values are lower than those for BR2. Within this second frequency region there are also rounded peaks with sharp decreases coinciding with increases in dipole power output and decreases in monopole power. This behaviour occurs because the body modes are similarly spaced in frequency and have similar mode shapes to those on BR2.

DLC has a different η profile from BR1 and BR2 and has greater values of η between 80 Hz and 600 Hz than any of the three other classical guitars. One of the clearest differences for DLC is that the values of η are far greater between 80 Hz and 200 Hz than for any of the other instruments. However, the greatest values of η still lie between 200 Hz and 450 Hz as they did for BR1, BR2 and MAL. The equivalent of the second frequency region for DLC starts at around 200 Hz but extends to around 600 Hz which is 150 Hz higher than for BR2 or BR1. η is greater across a wider frequency range because the resonance frequencies of the body modes of DLC are much higher than those on BR1 or BR2. $T(3,1)$ on DLC is at 579 Hz compared with 453 Hz for BR2 and 484 Hz for BR1. As the modes with greater numbers of anti-nodal regions are at higher frequencies there is a reduction in the level of cancellation with the residual response present at lower frequencies. This extends the upper frequency limit of the region of greater values of η. Between 600 Hz and 1500 Hz the values of η are less than 0.20 just as for BR2 but there are a greater number of small peaks and no single larger peaks in η like those for BR2 shown in figure 5.3.

The start of the frequency region of greatest η values is not as clearly defined for DLC as it was for BR1 and BR2. It can be described as starting either at the $B(1,2)_1$ mode or the $T(2,1)$ mode. The resonance frequency of the $B(1,2)_1$ mode on DLC is lower than that of the $T(2,1)$ mode. This arrangement of body modes is different from that of the three other instruments discussed in this chapter. $T(2,1)$ is 55 Hz higher on DLC than BR2, although DLC's $B(1,2)_1$ mode has a comparable resonance frequency to both BR1 and BR2. By placing the back plate mode below the resonance frequency of the $T(2,1)$ mode, the first peak value of η, which was associated with the start of the second region for BR1 and BR2, is also shifted in frequency. For these classical guitars the start of the second region is therefore not directly related to the placement of the $T(2,1)$ mode as it is the *back plate* mode which produces the first large value of η. Therefore it is the mode placement, in frequency, that determines the η characteristic around it.

MAL has a different η characteristic to the other instruments but the greatest value of η occurs within the same range as for the other instruments. The mode placement on this instrument is considerably different from the other classical guitars and therefore changes the values of η. The $T(2,1)$ mode, 339 Hz, is not shown in figure 5.24 as a result of a low power input measurement (which is explained by its mode shape and is discussed in section 5.2.2). MAL produces much lower values of η across the studied range. This can be explained by the fact that its plates are thicker and stiffer than the other instruments as MAL is a factory-built, plywood instrument. Factory-produced instruments are typically overbuilt to prevent damage to the guitar as it is being shaped by machines. As a result of the instrument being overbuilt, the body modes cannot undergo as great a displacement when they are driven. This means that the total power output is reduced as the instrument cannot drive the surrounding air as efficiently, and consequently η is also reduced.

No clear $T(3,1)$ mode could be found for MAL but at frequencies above the $T(2,2)$ mode the values of η are less than 0.30. The only other higher frequency mode that could be determined for MAL was a $T(1,3)$ mode which is a highly inefficient radiator of sound. Again, this shows that at frequencies where there are increasing numbers of anti-nodal areas, η decreases.

Top plate band data

It has previously been shown by Richardson (1982) that the low frequency body modes undergo the majority of their motion in the lower bout of the instrument. These modes also produce the greatest values of input admittance on the bridge of guitars. Figure 5.26 shows the band data of three classical guitars (BR2, DLC and MAL). The band data is defined as being the RMS of the admittance measured between 80 Hz and 2000 Hz. The figure demonstrates that, over the frequency range 80 – 20000 Hz, the largest values of admittance occur below the sound hole. The peak values of transfer

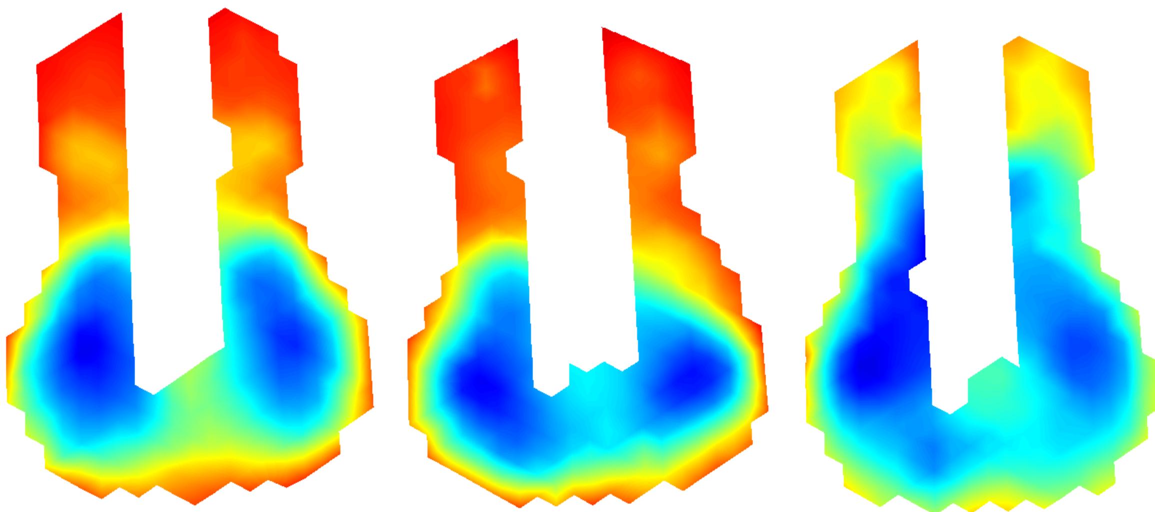

(a) BR2 top plate band data, range (0 - 1.8 s/kg). (b) DLC top plate band data, range (0 - 1.5 s/kg). (c) MAL top plate band data, range (0 - 0.7 s/kg).

Figure 5.26: Top plate band data from classical guitars.

admittance and their locations differ for each instrument depending on the construction of their top plates.

Figure 5.26 shows that BR2, DLC and MAL have their maximum total admittance values across the entire frequency range in a $T(2,1)$-like shape which is contained within the lower bout. This shape occurs in the band data because the $T(2,1)$ has the greatest value of admittance on all of the instruments. BR2 shows the clearest division between the two regions of peak total admittance in the (2,1) shape. MAL has more uniform band data values across the top plate with similar values of band data in the upper bout and the lower bout. BR2 and DLC are higher quality, 'better' sounding instruments and they both have greater peak values of band data admittance than MAL. This is an expected result as MAL has a thick plywood top plate and produces a lower level of sound output than either BR2 or DLC. The maximum values in the band data for BR2 and DLC are all located below the strut on the top plate placed just beneath the sound hole. There is a strut located just below the sound hole of both instruments and its presence appears to reduce the ability of the instrument to vibrate in the upper bout following an excitation at the bridge.

The $T(2,1)$-like shape of the band data from DLC has a greater asymmetry than the other two instruments. The area of peak total admittance on the treble side of the instrument is smaller than that on the bass side of the instrument. This is a result of the bracing design of the instrument which was shown in figure 5.19 to have a diagonal strut crossing the top plate from the upper bout to the lower bout. The edge of the area of higher band data corresponds with the location of this strut. The peak values of admittance are located below the strut beneath the sound hole on DLC. It would therefore appear that the strut location defines the areas of the top plate in which the instrument can easily vibrate between 0 Hz and 2000 Hz.

Back plate band data

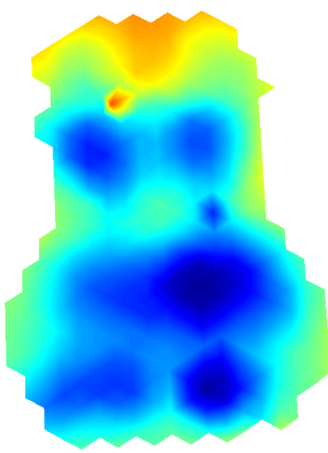

(a) BR2 back plate band data range (0 - 0.7 s/kg).

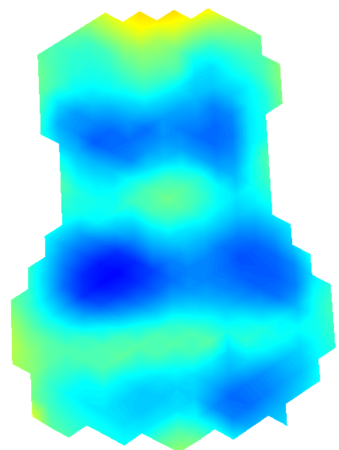

(b) MAL back plate band data, range (0 - 0.4 s/kg).

Figure 5.27: Back plate band data from two classical guitars.

The back plate band data was measured by exciting the instruments to the left of the E_2 string on the top plate and measuring the velocity response across the back plate. The excitation was provided on the top plate to provide a comparable excitation to the instrument to that provided by a vibrating string. An additional advantage of providing the excitation on the top plate and measuring the velocity on the back plate is that there is no obstruction produced by the hammer support between the laser heads and the back plate. The velocity response produced by the excitation was lower for the back plate than the top plate and was therefore more susceptible to noise. The strutting pattern on the back plate of guitars is typically simpler than the bracing pattern on the top plate, as shown in figure 1.1. It was not possible to gather mode data on the back plate of DLC as its surface was highly reflective. This prevented velocity measurements being made at many points on the plate and the NDT developer spray could not be used on the instrument.

Figure 5.27 shows that BR2 and MAL both have three separated regions of higher total admittance values which correspond with the areas of the back plate between the struts. The peak value of band data on the back plate of BR2 (0.7 s/kg) is greater than that measured on MAL (0.4 s/kg). This is the same behaviour as noted for the top plate for these two guitars. Both the top and back plate of MAL are much stiffer than the plates of BR2 and would be expected to produce a smaller value of admittance. The strut placement appears to determine the regions where the maximum admittance values can occur for the back plate as well as the top plate.

5.2.2 Individual mode behaviour

Section 5.2.1 showed that the η characteristic for all four of the studied guitars was determined by the resonance frequencies and shapes of their body modes. The body modes of these instruments have different resonance frequencies and source strengths but they can result in similar η characteristics, albeit with different absolute values of η. For example the $T(2,1)$ mode produces the lowest value of η amongst surrounding frequencies for all four of the studied classical guitars.

Low-frequency resonance triplet

All three instruments (BR1, DLC and MAL) produce dipole output power at frequencies well below the resonance frequencies of any of the modes which produce distinct dipole-like sound fields. Therefore the dipole power output within this frequency range is produced according to the sound hole sum rule. BR1, DLC and MAL have a lower value of η for $T(1,1)_1$ than for $T(1,1)_2$. Richardson (2001) found that the effective mass, m_{eff}, of $T(1,1)_2$ measured on four guitars (including BR2) was several times smaller than m_{eff} of $T(1,1)_1$. The reduction in m_{eff} results in a greater level of velocity being produced by the instrument and therefore a larger power input. As the sound pressure and sound power output have a G_{lm}/m_{eff} relationship the level of sound power output will also increase. Data from the Leverhulme Trust study showed that, between the two $T(1,1)$ modes, the m_{eff} of BR1 decreases from 401 g to 84 g and DLC's m_{eff} decreases from 575 g to 123 g. The values of Γ_{lm} for $T(1,1)_2$ are typically smaller than those for $T(1,1)_1$ but the equivalent decrease is much smaller than the decrease in m_{eff}. This results in a greater power output for the higher frequency coupled mode.

The peak in η between the two $T(1,1)$ modes occurs for all four guitars and results from the Helmholtz oscillator-like motion between the two modes, visible as a minimum in input admittance curves. At frequencies surrounding this Helmholtz-like motion, the motion of air through the sound hole is greater than the motion of the top plate. This results in an increase in power output and a decrease in power input as the top plate moves less. The values of η therefore increase between the two $T(1,1)$ modes for all of the instruments as they all have sound holes.

The $T(2,1)$ mode

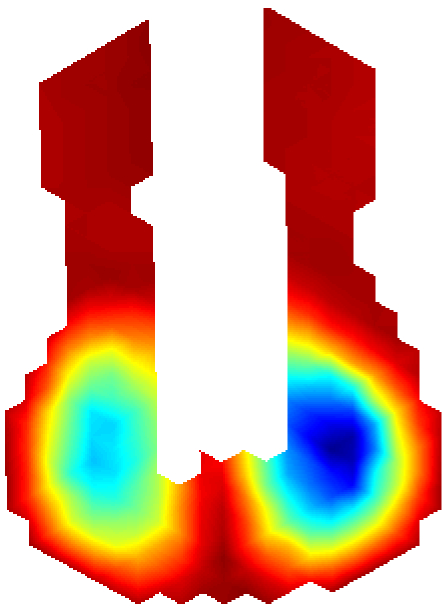

(a) The $T(2,1)$ mode at 274 Hz measured on DLC at position 1, range = 0 – 0.40 s/kg.

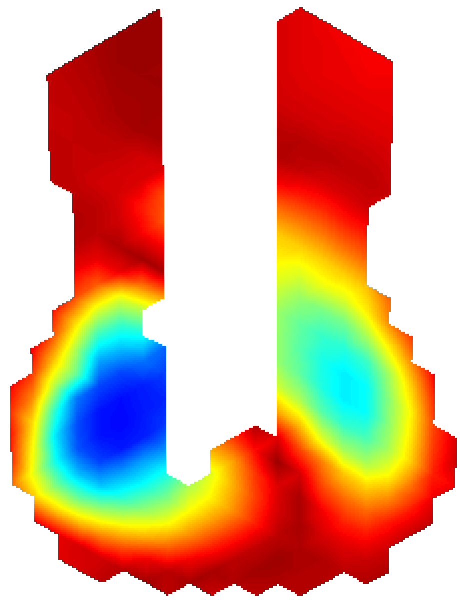

(b) The $T(2,1)$ mode at 340 Hz measured on MAL at position 1, range = 0 – 0.18 s/kg.

Figure 5.28: The $T(2,1)$ modes of DLC and MAL

All of the studied classical guitars produce a low value of η at the resonance frequency of the $T(2,1)$ mode, in comparison with frequencies surrounding this mode. DLC produces the greatest value of η for this mode of any of the classical guitars. The cause of the difference in the values of η for the $T(2,1)$ mode on different instruments does not relate to its resonance frequency but instead to the shape of the mode. The $T(2,1)$ mode of DLC has two anti-nodal areas with different sizes which results in a greater value of η. Figure 5.23 shows that this mode, at 268 Hz, still produces a large values of Y_{xy} despite this asymmetry.

The $T(2,1)$ mode could not be shown in figure 5.24 for MAL as the power input was found to decrease by a considerable amount at frequencies surrounding the resonance frequency, sometimes result in $\eta > 1$. Figure 5.28b shows the ODS (operating deflection shape) of the $T(2,1)$ mode on MAL. This figure shows that the peak values of motion produced by this mode occur on the bass side of the bridge. Therefore a low level of velocity is produced on the bridge between the top B and E strings which produces the low level of power input. As the driving location is closer than the response measurement position to the anti-nodal region, the excitation can produce a motion in the instrument that results in the production of acoustical power but a low value of power input. For this particular mode the placement of the hammer and accelerometer are important for determining the power input to the mode as both locations are close to its nodal line.

Figure 5.9 showed that the $T(2,1)$ mode on BR2 has two equal-sized anti-nodal areas separated by a z-orientated nodal line through the bridge. This mode has a low value of η for these two instruments. This is not the case for DLC which, as shown in figure 5.19b, has a strut running diagonally across its top plate. This strut produces an asymmetry in the instrument and the two anti-nodal areas that form the $T(2,1)$ mode are no longer equal in size, as shown in figure 5.28a. The difference in the size of the anti-nodal areas of the $T(2,1)$ mode of DLC is less pronounced than in figure fig: MAL T21 The unequal size results in a reduction in the level of cancellation between the opposite phase areas because there is a greater amount of sound pressure radiated with one phase than with the opposite phase. This results in the production of a net monopole contribution from the larger of the two areas. As monopoles are more efficient radiators of sound power there will be a greater value of η. Unequal-sized anti-nodal areas produce a greater level of power output, providing the excitation can be made on one of the anti-nodal areas rather than a nodal line. If the excitation is made on the nodal line, like for MAL, then the mode will not radiate efficiently even if it is asymmetric.

The $B(1,2)_1$ mode

DLC and BR1 have $B(1,2)_1$ modes which produce large values of η. As the main motion of this mode is located on the back plate, the instruments must therefore couple strongly through the top plate, ribs and the enclosed air in order to drive this mode following an excitation at the bridge. The frequency region between 200 Hz and 400 Hz contains several back-plate modes which correspond with increases in η for BR1, BR2 and DLC. However, on MAL the top plate and air cavity do not couple as strongly with the back plate. The result is that the back-plate modes are reduced in their power output and there is a lower value of η.

The $T(1,2)$ modes

BR1, BR2 and DLC all have two $T(1,2)$ type modes with opposite phase relationships to one another. The measurements on BR2 showed that the different phase relationships of the two modes produce two different η values, with the lower frequency mode having a lowη and the higher frequency mode having a greater value of η. This relationship occurred for all three excitation points on the bridge of BR2, but not when the instrument was driven on the neck. BR1 and BR2 both have $T(1,2)_1$ modes with low values of η and $T(1,2)_2$ producing some of the highest values of η for the instrument. The value of η for the $T(1,2)_2$ mode is greater because the lower of the two anti-nodal regions of this mode extends across the bridge to a greater extent than for BR1 or BR2. This mode is more easily driven by motion of the bridge and is therefore a more efficient radiator of power output. The $T(1,2)$ modes can produce a large value of Y_{xz} but this is dependent on whether the areas of the anti-nodal regions are equal in size and how they are orientated about the centre of the bridge. If the nodal line is at angle to the bridge then the two anti-nodal regions will also produce a motion in the z direction as well as the y direction

There is an air mode with a similar resonance frequency to the $T(1,2)$ plate mode. The air mode couples with the plate mode to produce the two $T(1,2)$ modes. The $T(1,2)_2$ mode has a greater value of η suggesting that it must work in phase with the air mode while the $T(1,2)_1$ mode will be out of phase with it.

Only one $T(1,2)$ mode could be found on MAL. It has a low value of η and the power output is nearly entirely monopole in nature. This mode on MAL is at a considerably lower frequency than for the other instruments so it cannot couple with any of the higher frequency air modes to produce a $T(1,2)_1$ and $T(1,2)_2$ mode. DLC has two $T(1,2)$ modes and, while the higher frequency of these two modes does produce a greater value of η, the difference is not as great as for BR1 and BR2.

Higher order body modes

The $T(3,1)$ mode is the last mode to exhibit a large value of η on three of the guitars (BR1, BR2, DLC) and at frequencies above this mode the values of η are typically less than 0.2. Despite the different resonance frequencies of the $T(3,1)$ modes, all three instruments have similar behaviours, with greater values of Γ_{00} than dipole source strengths. The $T(3,1)$ mode has an odd number of vibrating regions so there will be a lower level of cancellation than for modes with even numbers of vibrating regions, such as $T(2,1)$ or $T(4,2)$. There will be some cancellation between the regions of opposite phase on $T(3,1)$ but there will still be a monopole component. The values of Γ_{lm} for $T(3,1)$ on BR1, BR2 and DLC are shown in table 5.1.

There is no clear $T(3,1)$ mode for MAL but η decreases at frequencies above the $T(1,3)$ mode which is the first of the body modes with a greater number of anti-nodal

Guitar	Frequency (Hz)	$\lvert\Gamma_{00}\rvert$ $(m^3s^{-1}N^{-1})$ $\times 10^{-3}$	$\lvert\Gamma_{1x}\rvert$ $(m^4s^{-1}N^{-1})$ $\times 10^{-3}$	$\lvert\Gamma_{1y}\rvert$ $(m^4s^{-1}N^{-1})$ $\times 10^{-3}$	$\lvert\Gamma_{1z}\rvert$ $(m^4s^{-1}N^{-1})$ $\times 10^{-3}$
BR1	468	0.291	0.110	0.021	0.258
BR2	446	0.345	0.066	0.040	0.120
DLC	579	0.951	0.123	0.084	0.101

Table 5.1: Source strengths for the $T(3,1)$ modes of BR1, BR2 and DLC excited at position 1.

areas on this instrument. The $T(1,3)$ mode radiates sound power inefficiently as one of the nodal lines of the mode lies across the bridge.

Above the resonance frequency of the $T(3,1)$ mode, the mode shapes of all of the classical guitars have increasingly large number of anti-nodal areas and BR1, BR2 and DLC have lower values of η than those exhibited at frequencies below this mode. This shows that the presence of more complex modes reduces η on all of the studied classical guitars. As this is the first of the modes with more than two anti-nodal areas it will act out of phase with the residual response from the resonance triplet. Therefore this will be one of the last modes that can radiate efficiently. The higher resonance frequency of the $T(3,1)$ mode on DLC appears to extend the region of greater η values up to 600 Hz in comparison with BR1 and BR2 where the upper limit is at 450 Hz. The effect of changing the behaviour of the $T(3,1)$ mode on the η characteristic is shown in chapter 6.

Chapter 6

η measurements on an experimental guitar

6.1 The experimental guitar

The η data from the four classical guitars in chapter 5 suggested that the resonance frequency of the $T(3,1)$ mode determines the upper limit of the frequency range where the greatest values of η lie. The $T(3,1)$ mode of DLC has the highest resonance frequency of all four instruments and DLC produced greater values of η up to around 600 Hz. BR1 and BR2 have lower frequency $T(3,1)$ modes and the greatest values of η were below 450 Hz. The peak values of η existed between 200 Hz and the resonance frequency of the $T(3,1)$ mode for all three of these instruments. The $T(3,1)$ mode could not be found on MAL where the first body mode with a greater number of anti-nodal areas was a $T(1,3)$ mode.

A specially designed guitar top plate was used to investigate whether the resonance frequency of the $T(3,1)$ mode has an effect on the radiation efficiency of classical guitars. The top plate was constructed as part of a study into the physics of the classical guitar by Lewney (2000). In the work by Lewney a top plate was constructed with eight different bracing patterns including Torres bracing, lattice bracing and asymmetric bracing. The mode shapes, effective mass and Q values of the modes of the top plate were studied both on the separated plate and on an experimental guitar rig. The experimental guitar rig consisted of a thick slab of wood with a guitar cavity carved out of it. This produced a fixed volume and rigid sides when the top plate was attached to it.

The final bracing pattern of the top plate used in the work by Lewney is shown in figure 6.1a and it is this plate which was used for study in this section. The plate is

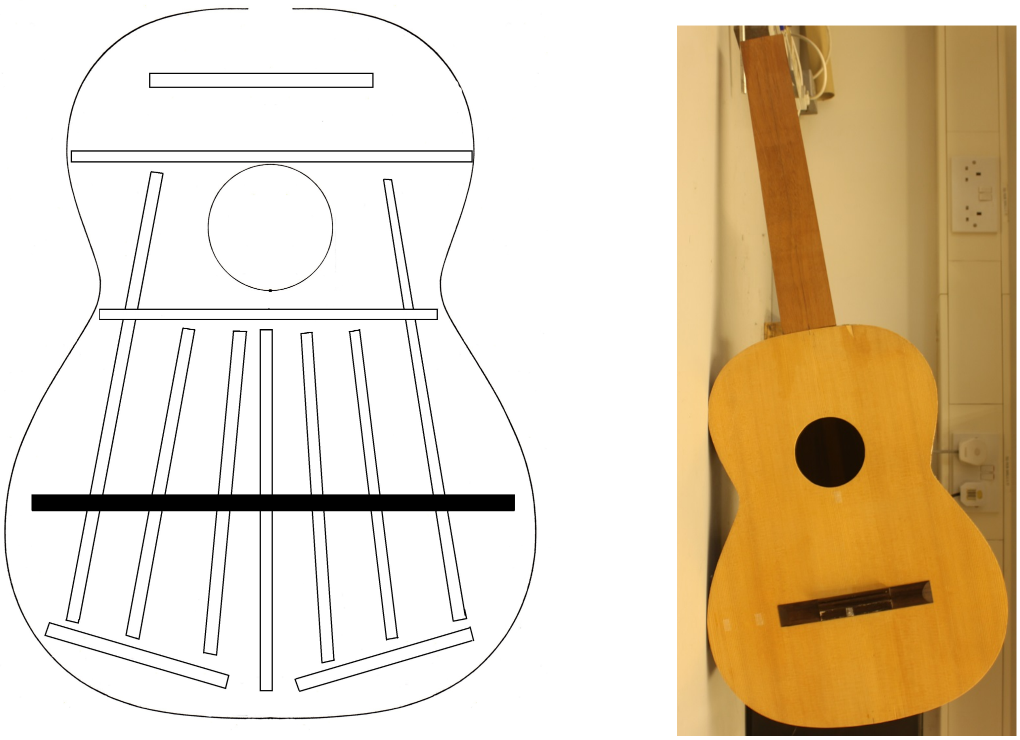

(a) Bracing pattern of the experimental top plate (bridge bar marked in black).

(b) Experimental top plate attached to ribs, back plate and neck.

Figure 6.1: The experimental guitar.

2.5 mm thick and the fan braces are 6 mm tall and 6 mm wide. The main difference between this plate design and more traditional bracing patterns is the addition of a horizontal bar, called the bridge bar here, across the width of the instrument under the bridge from left to right. The fan bracings are glued on to the top plate with the bridge bar glued in place on top of them. The bridge bar has a series of notches so that it is in contact with the fan bracing and the top plate. The horizontal strut just below the sound hole also has notches to allow the two longer fan braces to pass underneath it, however, the braces are not in contact with this horizontal strut. The bridge bar is not typically used in guitar construction but adding it to the top plate increases the resonance frequencies of modes such as the $T(2,1)$ and $T(3,1)$ modes by increasing the stiffness across the grain.

η was measured on the top plate under four different conditions with the excitation and response measurements made at position 1 each time. The first measurement was made on the free top plate. The top plate was then glued onto a set of ribs attached to a back plate to form an enclosed air cavity. A neck, without a headstock, fretboard or strings, was attached to the ribs of the instrument in the usual location. This instrument

	Resonance Frequency (Hz)		
Mode shapes	11.5 mm high bridge bar	7 mm high bridge bar	No bridge bar
$T(1,1)_1$	111	109	107
$T(1,1)_2$	232	228	221
$T(1,1)_3$	253	246	244
$T(2,1)$	367	328	268
$T(1,2)_1$	330	344	339
$T(1,2)_2$	430	429	426
$T(3,1)$	667	609	574

Table 6.1: Resonance frequencies of the body modes of the plate attached to an instrument with different values of bridge bar height.

is shown in figure 6.1b. η was then measured for this relatively complete instrument. The top plate was then removed from the ribs and the bridge bar was thinned from 11.5 mm tall to 7 mm, before the top plate was reattached to the ribs and back plate to make a third η measurement. The final step was to completely remove the bridge bar from the top plate and remeasure η on the complete instrument.

The mode shapes of the top plate were determined by using the roving hammer method described in section 2.8. The resonance frequencies of the body modes are shown for the full instrument with different bridge bar heights in table 6.1. The back plate modes were not determined as the back plate was not altered as part of this experiment and the top plate modes, in particular the $T(3,1)$ mode, were the focus of study. The resonance frequencies of the $T(2,1)$ and $T(3,1)$ modes change by the greatest amount but there is also a shift in the $T(1,1)$ modes. The $T(1,1)_2$ mode undergoes the largest frequency shift of the three coupled modes because the greatest motion of this mode is produced by the top plate.

6.2 η of an isolated top plate

The top plate was suspended in an anechoic chamber using string tied around the sound hole. This gives an approximation to freely suspending the plate. Figure 6.2 shows η measured on the isolated top plate. The resonance frequencies and mode shapes of the isolated plate were not determined. At frequencies below 200 Hz it was not possible to supply a sufficient power input to measure η accurately. Repeat measurements of power input, without measuring power output, showed that the input is much greater than the power output in this frequency range which results in $\eta < 0.01$.

η is far lower for the isolated plate than for any of the studied classical guitars as

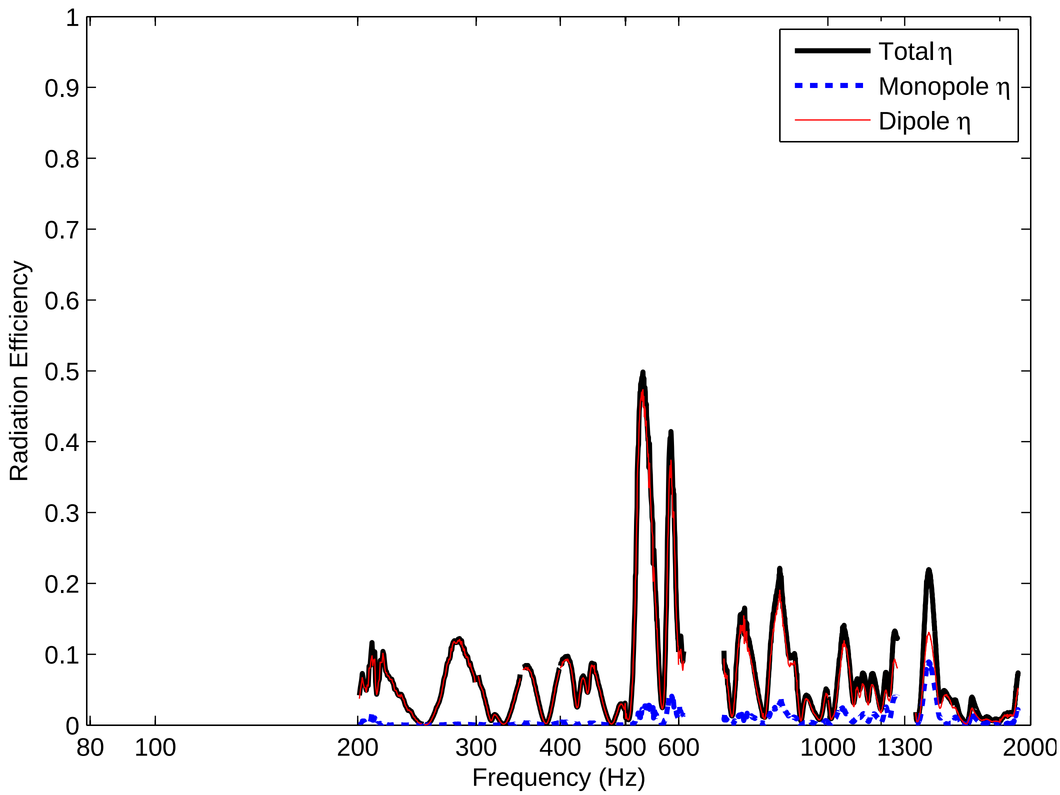

Figure 6.2: η of an isolated top plate excited at position 1.

there is no back plate or air cavity to couple with the top plate modes. The reduction in η will also result from the sound radiation being produced by dipole sources. As air is displaced both in front and behind the instrument by the top plate modes, the greatest contribution to the power output across the entire frequency range is produced by dipole components. Figure 6.3 shows that there is a similar level of sound pressure and a similar sound field shape radiated both in front and behind the isolated plate. This shows that the ribs and back plate are required for the instrument to produce a monopole power output.

There are two peaks in η between 500 Hz and 600 Hz. These values of η are greater than those on the completed instruments studied in this section. The lower values of η on the completed instrument are most likely to be produced by coupling between the higher frequency plate and air modes in the complete instrument. An opposite phase motion between the air mode and the plate mode would reduce the radiated sound power. The values of η between 700 Hz and 1300 Hz on the isolated plate are greater than those on the studied classical guitars but it produces a similar η characteristic to the studied instruments above 1300 Hz.

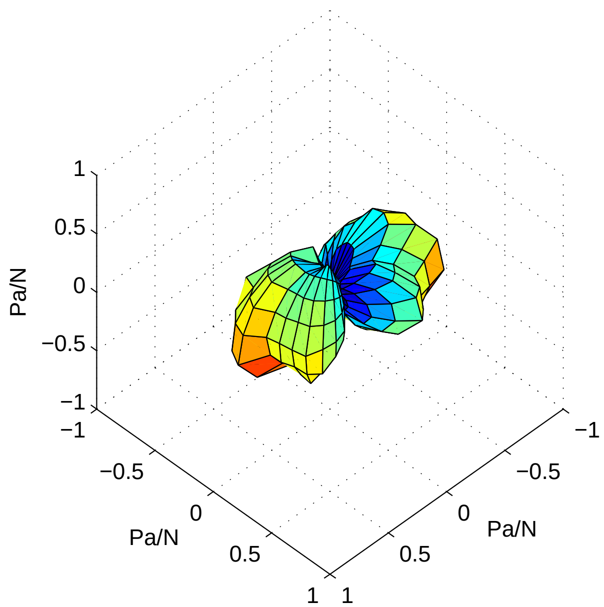

Figure 6.3: Normalised radiated sound field at 468 Hz.

6.3 η of the experimental guitar with an 11.5 mm high bridge bar

The top plate was attached to a body, ribs and neck. The neck had no headstock or fretboard but instead had two screws at its top to facilitate hanging the instrument in the anechoic chamber. Figure 6.4 shows η measured on the complete instrument with an 11.5 mm high bridge bar. There is a large decrease in η at frequencies around 150 Hz which coincides with the resonance frequency of the neck-bending mode. The neck-bending mode would normally have a resonance frequency below 100 Hz but because there is no headstock on the instrument it occurs at a much higher frequency. This mode produces a very small dipole power output but requires a much larger power input which results in values of η close to 0.

For BR1 and BR2 the frequency range where the largest values of η occurred typically extended from around 200 Hz to 450 Hz. The upper limit of this frequency range corresponded with the $T(3,1)$ mode. DLC showed peak values of η up to around 600 Hz and this guitar had a higher frequency $T(3,1)$ mode. For the instrument with a bridge bar on the top plate, the upper limit of this frequency range extends to above 600 Hz. The resonance frequency of the $T(3,1)$ mode on this plate, attached to the instrument, is 667 Hz. η cannot be shown at this frequency because of the half-wave

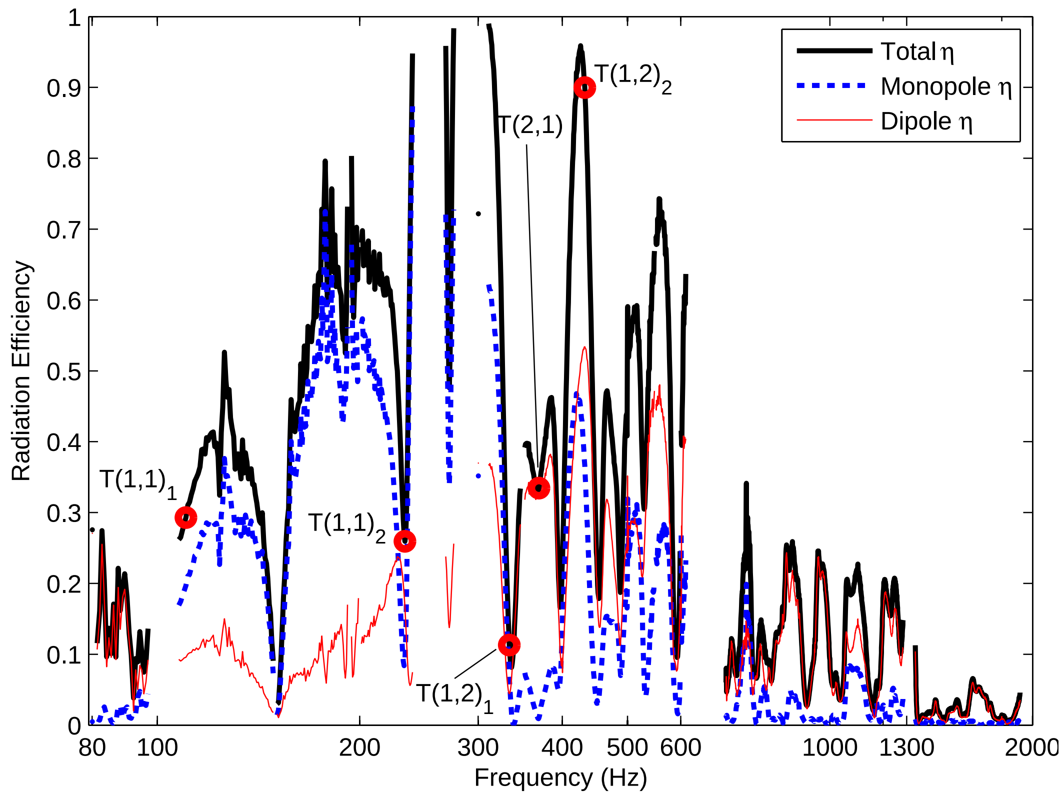

Figure 6.4: η of a complete instrument with an 11.5 mm high bridge bar

problem preventing the use of spherical-harmonic decomposition. This suggests that the higher resonance frequency of the mode extends the frequency range where the peak values of η occur. $\eta = 0.5$ at 600 Hz for the experimental guitar with 11.5 mm high bridge bar, which is far greater than for any of the other classical guitars which had $T(3,1)$ modes with lower resonance frequencies.

Between 700 Hz and 1300 Hz there are many frequencies where $\eta > 0.2$ so this instrument is much more efficient up to a higher frequency than the other classical guitars. However, at frequencies above 1300 Hz the values of η are comparable to those of the other studied guitars. Between 200 Hz and 300 Hz it was not possible to supply a great enough power input to the instrument to produce values of $\eta < 1$. This may result from the excitation location lying closer than the response location to an anti-nodal area. This would result in a larger power output but a smaller measured power input.

While the top plate has a considerably different construction to the top plate of BR2 and BR1 there is still the same η characteristic produced by the two $T(1,2)$ modes. The lower frequency $T(1,2)_1$ mode has a lower η than the higher frequency $T(1,2)_2$ mode. These modes are assumed to couple with one of the higher frequency air modes. The

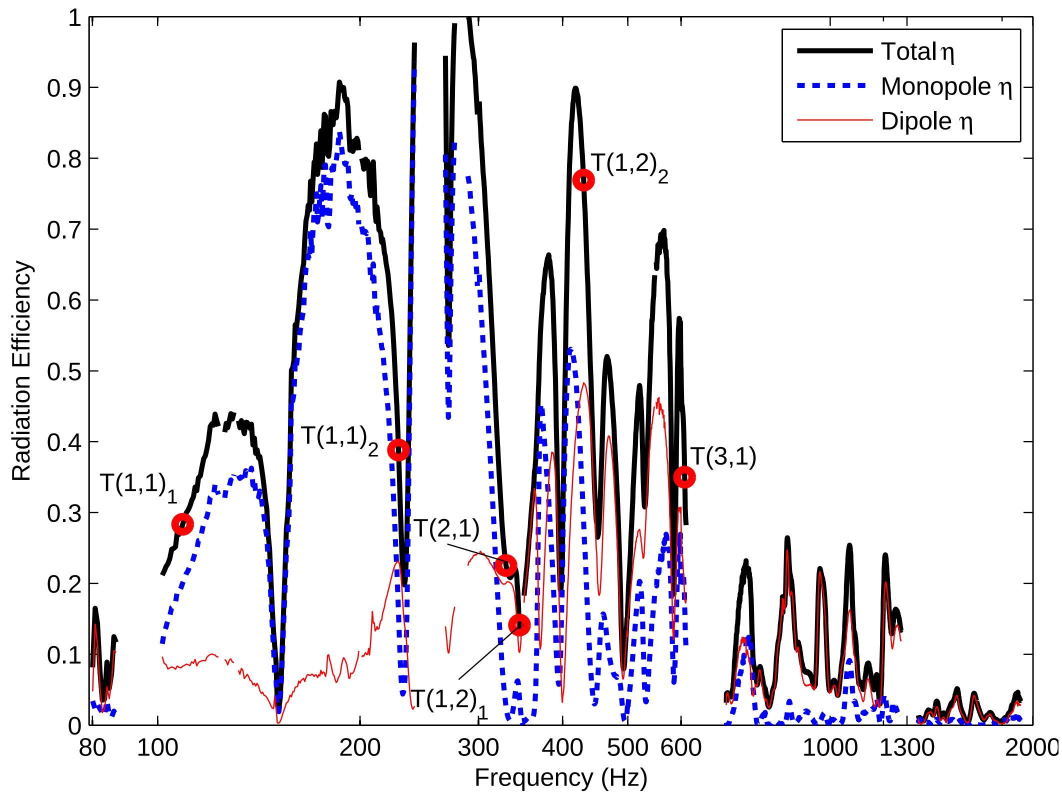

Figure 6.5: η of a complete instrument with an 7 mm high bridge bar

phase relationship between the plate mode and the air mode produces the difference in η.

6.4 η of the experimental guitar with a 7 mm high bridge bar

Table 6.1 shows that reducing the height of the bridge bar shifts the resonance frequencies of the $T(2,1)$ and $T(3,1)$ modes downwards. With a 7 mm tall bridge bar, the resonance frequency of the $T(3,1)$ mode was reduced to 609 Hz and can therefore be studied in the η data as this frequency is not affected by the half-wavelength problem. η of the instrument with a 7 mm high bridge bar is shown in figure 6.5. There is still a sharp decrease in η at 150 Hz produced by the neck-bending mode. The fact that the neck-bending mode reduces η so drastically in comparison with the surrounding values shows that the placement of this mode is important if no sudden decreases in η are desired. Electric guitars and bass guitars, such as those constructed by Steinberger, can be constructed without heads and as such it is likely that there will be a large power input at frequencies within the instrument's playing range which may result in 'dead notes' which decay very quickly.

The $T(2,1)$ mode has a lower resonance frequency than the $T(1,2)_1$ mode when the bar is thinned to 7 mm. The $T(2,1)$ mode is also less efficient when the bar is thinned to 7 mm. The thinning of the bridge bar must therefore affect the mode shape of the $T(2,1)$ mode. The guitars with the most efficient $T(2,1)$ modes had mode shapes with unequal sized anti-nodal areas, such as the $T(2,1)$ mode on DLC. If the value of η decreases then the mode must have more similar shaped anti-nodal areas when the bridge bar is thinner. While the resonance frequency of the $T(3,1)$ mode is now 58 Hz lower than when the bridge bar was 11.5 mm high, the largest values of η still extend as far as 600 Hz.

The η characteristic between 700 Hz and 1300 Hz is similar for both the 11.5 mm and 7 mm bridge bar with several peaks of $\eta < 0.3$. The frequencies of these peaks are not shifted by a significant amount by thinning the bridge bar but the radiation efficiency is reduced. The shift in the frequency of the $T(3,1)$ mode must therefore result in a change in the η values above its resonance frequency. Between 1300 Hz and 2000 Hz the values of η are similar for both bridge bar heights. Changing the resonance frequency of the $T(3,1)$ mode therefore does not have a significant effect on the η characteristic above 1300 Hz.

6.5 η of the experimental guitar with no bridge bar

Figure 6.6 shows η measured on the guitar with no bridge bar attached. The $T(3,1)$ mode now had a resonance frequency of 574 Hz and the peak values of η are contained within a smaller frequency range. When the bridge bar was present, values of $\eta > 0.5$ were measured at frequencies up to 600 Hz but without the bridge bar $\eta = 0.2$ at this frequency. Reducing the resonance frequency of the $T(3,1)$ mode on the experimental guitar resulted in a decrease of the upper frequency limit of the frequency range where the largest values of η occurred. These experiments suggest that a higher resonance frequency of the $T(3,1)$ mode increases the upper limit of the frequency range where large values of η can occur.

The frequency region between 700 Hz and 1300 Hz shows a similar η characteristic as the measurements made with the bridge bar attached to the top plate. However, the values of η are smaller than those measured with the bridge bar in place. The reduction in the resonance frequency of the $T(3,1)$ mode may reduce the values of η but it does not significantly affect the frequencies of the peaks in η within this frequency range.

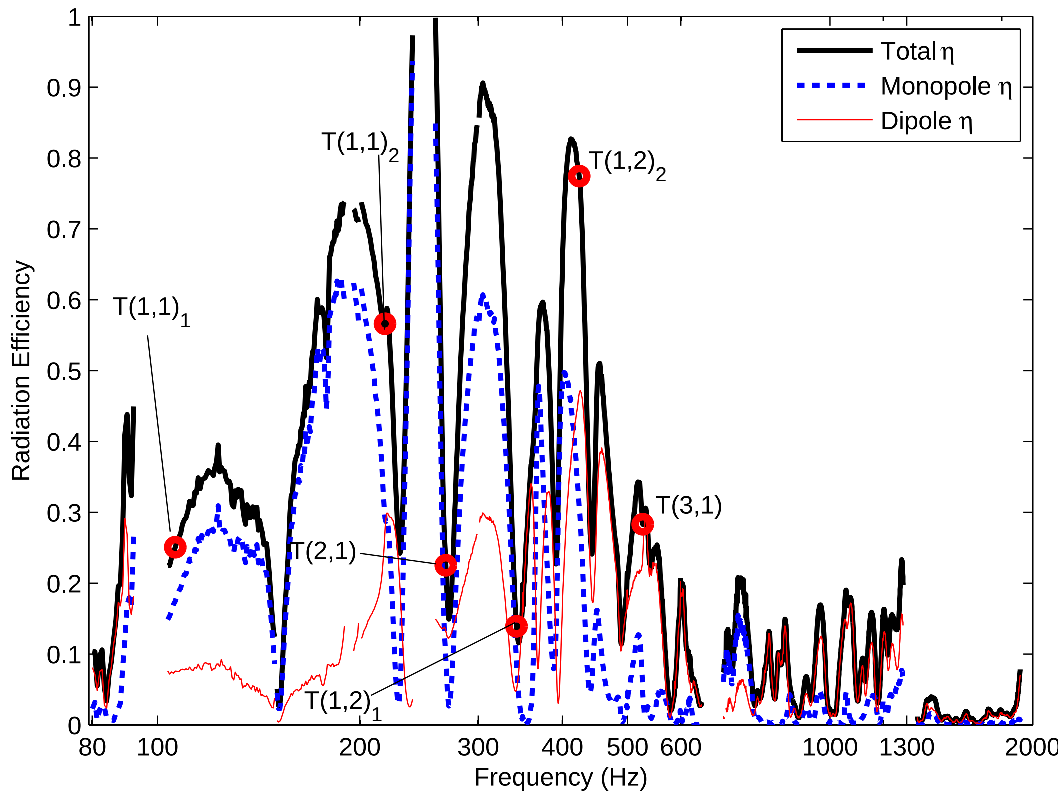

Figure 6.6: η of a complete instrument with no bridge bar

The frequencies of the peak values of η in the higher frequency range must therefore result from the behaviour of other higher frequency body modes.

The response below 450 Hz showed little change irrespective of the presence of the bridge bar, although there is a slight change in the amplitudes of η. Within this range it is only the $T(2,1)$ mode than has undergone a large change in frequency as the bridge bar is thinned. This mode therefore does not have a large effect on the η characteristic of the instrument.

Chapter 7

A case study on blocking the sound hole of two classical guitars

7.1 The effect of blocking the sound hole on BR2

7.1.1 Vibrational behaviour of BR2

The effect of the sound hole on the input admittance and radiated sound pressure of classical guitars has been well documented (Christensen and Vistisen, 1980). If the sound hole is blocked the $T(1,1)_1$ mode cannot be set into motion and the resonance frequency of $T(1,1)_2$ is shifted downwards by several Hz. These effects are shown in the input admittance curves in figure 7.1 for BR2 with its sound hole both open and blocked with non-porous foam. The two input admittance curves in figure 7.1 were produced from the averages of the 324 force and velocity measurements made to determine the power input. Above 500 Hz the peak values of admittance occur at the same frequencies and there is only a small difference in their amplitudes. This suggests that the residual response from the low-frequency resonance triplet is less important to the motion of these higher frequency body modes than to the lower frequency modes. There are also higher frequency air modes (Elejabarrieta et al., 2002b) which are affected by the blocking of the sound hole. The higher frequency air modes do not push as much air through the sound hole as the lower frequency Helmholtz-like motion. As there is less motion of the air through the sound hole, these air modes will be less affected by blocking the sound hole than the Helmholtz oscillator-like mode.

Blocking the sound hole affects the vibrational behaviour of the entire instrument, not just that of the bridge. The velocity across the top and back plate of BR2 was measured using a laser vibrometer and the ODS were measured for BR2 on both its top

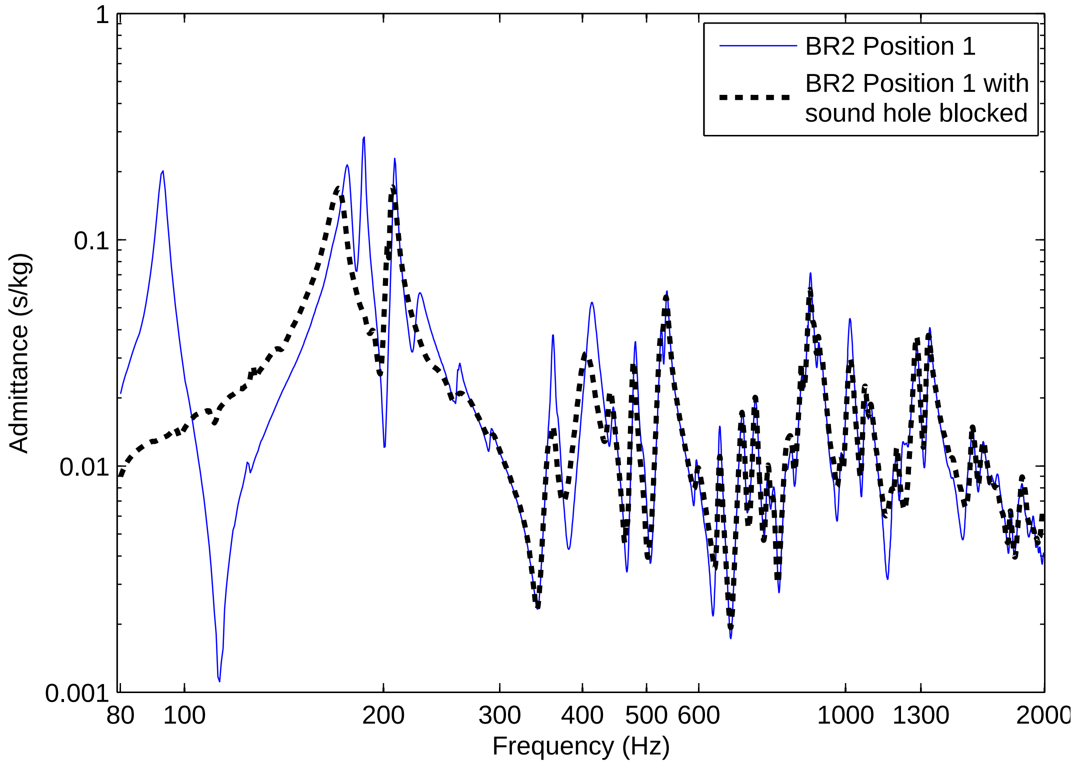

Figure 7.1: Comparison of input admittance for BR2 excited at position 1 with and without the sound hole blocked with foam.

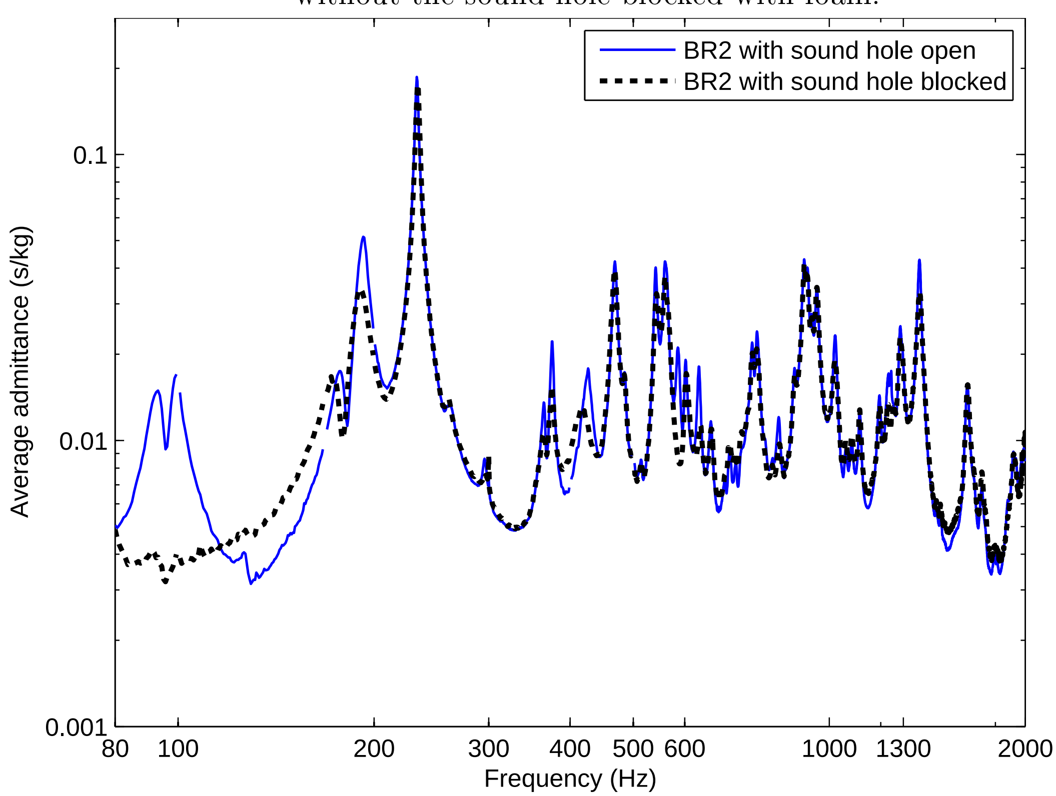

Figure 7.2: Average admittance measured across the top plate of BR2 with and without its sound hole blocked produced by an excitation at position 1.

and back plates with the sound hole open and with it blocked. The average spectrum in figure 7.2 is the average of all of the admittance measurements made across the studied plate. Figure 7.2 shows the transfer admittance averaged across all of the measurement points on BR2 when the sound hole was open and when it was closed. The same effects are seen across the entire top plate as for the measurements of input admittance shown in figure 7.1. The $T(1,1)_1$ mode is no longer visible and the $T(1,1)_2$ mode is at a lower frequency. At higher frequencies the admittance is less affected by the sound hole but there are some peaks which are shifted because the higher frequency air modes can no longer enter motion.

7.1.2 ODS of the $T(1,1)$ modes

By blocking the sound hole, the $T(1,1)_1$ mode of a classical guitar is assumed to no longer undergo motion as there is no coupling between the top plate and the motion of air through the sound hole. The averaged admittance when the sound hole was blocked, in figure 7.2, showed no peak at the expected resonance frequency of the $T(1,1)_1$ mode. Figure 7.3 shows the ODS of BR2 at 93 Hz both with the sound hole open and the sound hole blocked. The maximum value of transfer admittance measured on the top plate at the frequency where the $T(1,1)_1$ mode would be expected to occur is 0.05 s/kg when the sound hole is open compared with 0.015 s/kg when the sound hole is blocked. The $T(1,1)$ shape shown in figure 7.3b is actually produced by the $T(1,1)_2$ mode below its resonance frequency. We can tell that the motion is produced by the higher frequency mode because the phase is the same at both this frequency and the resonance frequency of $T(1,1)_2$ when the sound hole is blocked. This means that the $T(1,1)_2$ mode is entering motion over 90 Hz below its resonance frequency. Blocking the sound hole with foam therefore prevents the $T(1,1)_1$ mode from entering motion and the small response produced by the instrument is produced by the $T(1,1)_2$ mode operating below its resonance frequency.

Figure 7.4 shows that the shape of the $T(1,1)_2$ mode does not change considerably when the sound hole is blocked. The resonance frequency of this mode changes from 193 Hz to 190 Hz and the peak value of admittance decreases from 0.20 s/kg to 0.15 s/kg. The reduction in the peak value of admittance occurs because this body mode is also coupled with the motion of air through the sound hole.

The first back plate mode on classical guitars is the $B(1,1)_1$ mode. The $T(1,1)_1$ and $B(1,1)_1$ modes occur at the same frequency because both of their motions are produced by the same body mode. Figure 7.3 showed that when the sound hole was blocked there was a response at the $T(1,1)_1$ mode's resonance frequency on the top plate produced

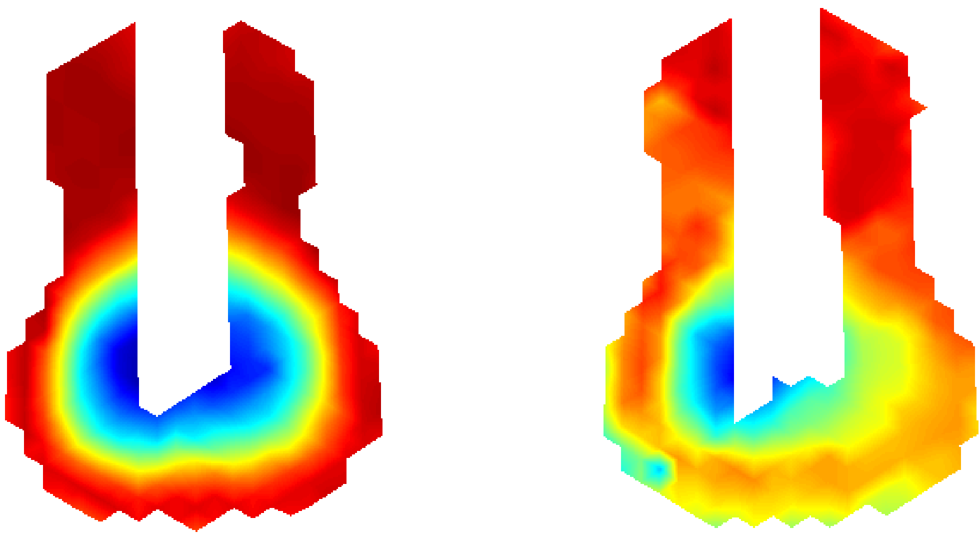

(a) BR2 with sound hole open, range (0 - 0.05 s/kg).

(b) BR2 with sound hole blocked, range (0 - 0.015 s/kg).

Figure 7.3: ODS of BR2 at the resonance frequency of the $T(1,1)_1$ mode - 93 Hz.

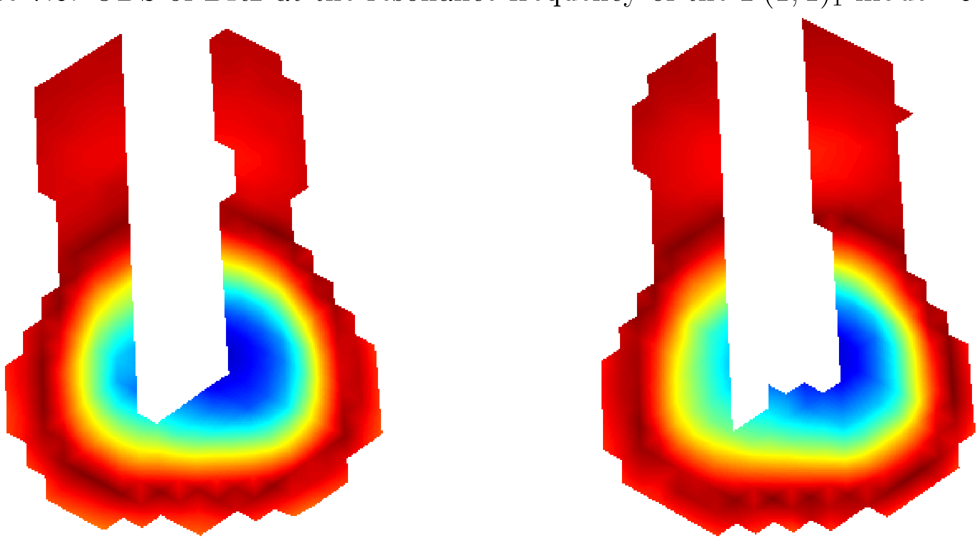

(a) BR2 with sound hole open, range (0 - 0.2 s/kg) - 193 Hz.

(b) BR2 with sound hole blocked, range (0 - 0.15 s/kg) - 190 Hz.

Figure 7.4: The $T(1,1)_2$ modes of BR2.

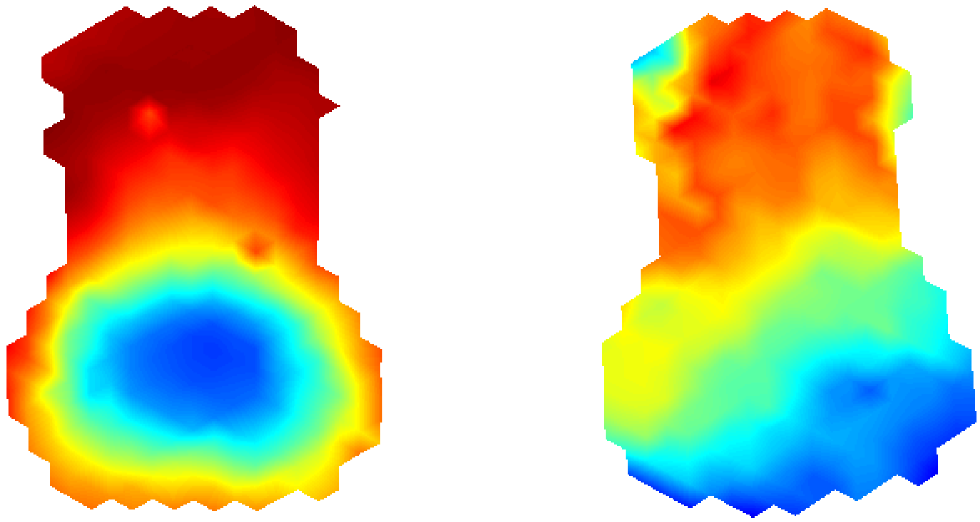

(a) BR2 with sound hole open, range (0 - 0.006 s/kg).

(b) BR2 with sound hole blocked, range (0 - 0.003 s/kg).

Figure 7.5: The $B(1,1)_1$ modes of BR2 - 93 Hz.

by the much higher frequency $T(1,1)_2$ mode. Figure 7.5 shows that the back plate does not undergo motion at this frequency because the motion of the top plate is no longer coupled to the back plate via the lowest frequency air mode. When the sound hole is open the area of maximum admittance is at the same point on the back plate as on the top plate in figure 7.3a. When the sound hole is blocked the mode shape is changed considerably with the peak values of admittance occurring at the bottom of the back plate and minima occurring at the top of the plate. This is a similar motion to the neck-bending mode of the top plate but not to the $B(1,1)_1$ or $B(1,1)_2$ modes. The back plate is therefore not easily driven below the resonance frequency of its first body mode.

When the sound hole is open, the $T(2,1)$ mode couples with the enclosed air to produce a motion on the back plate. The peak values of admittance occur only on one side of the back plate rather than as the two opposite phase anti-nodal areas present on the top plate. When the sound hole is blocked, the motion of the $T(2,1)$ mode cannot couple to the back plate through the enclosed air and a different ODS is formed. This suggests that the top plate couples with the enclosed air and back plate at the resonance frequency of the $T(2,1)$ mode. The values of admittance are greater at either side of the plate when the sound hole is blocked, with a nodal line running down the centre of the instrument. The $T(2,1)$ mode has a strong y component which transfers energy more easily into the ribs in the lower bout than a motion in either the x or z directions. This motion in the ribs would drive the back plate and produce the greater values of admittance on the edges of the back plate for the blocked sound hole case.

Figure 7.7 shows the admittance averaged from all of the measurements made on the back plate of BR2, measured in the Y_{xx} direction. All of the back plate modes below 650 Hz have lower average admittance values when the sound hole is blocked. The most noticeable difference in admittance occurs for the first five peaks in the data. This reduction in the average velocity response means that the coupling between the air cavity motion and the back-plate is of importance to the generation of back plate motion, particularly in the low-frequency range. At higher frequencies the admittances become increasingly similar and the air coupling is of less importance. Between 1300 Hz and 2000 Hz the average admittance when the sound hole is blocked is 0.002 s/kg and when it is open the average admittance is 0.003 s/kg. For both cases the standard deviation of the admittance is 0.001 s/kg.

7.1.3 Band data measurements

Figure 7.8 shows the band data measured on the top and back plates of BR2 when its sound hole was blocked. The maximum values of band data on the top plate (shown in figure 5.26a) are reduced from 1.8 s/kg to 1.6 s/kg when the sound hole is blocked. On the back plate (shown in figure 5.27a) the maximum value in the band data is reduced from 0.7 s/kg to 0.6 s/kg. The reduction of the motion of the $T(1,1)_1$ mode also changes the overall behaviour of the band data. The peak values of band data of the top plate are more clearly divided into a $(2,1)$ shape when the sound hole is blocked than when it was open. This occurs because the $T(1,1)_1$ mode can no longer enter motion so the $T(2,1)$ mode provides a greater proportion of the overall motion at the centre of the plate. The centre of the bridge therefore moves with a lower velocity between 80 Hz and 2000 Hz when the sound hole is blocked. This is an expected result as the $T(1,1)_1$ mode produces a large velocity in the centre of the lower bout.

The velocity response of the back plate is more uniform than the top plate but there are three clear areas of the plate where the level of motion is greater. These are separated by lines of lower band data which correspond with the bracing on the back plate. The effect of the bracing is clearer when the sound hole is blocked as there is no coupling between the Helmholtz-like motion of the air and the back plate which would produce a motion across the struts.

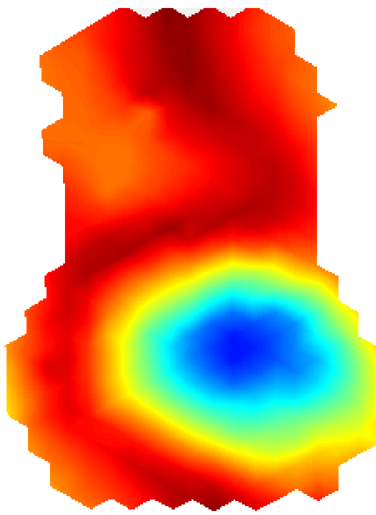

(a) BR2 back plate with sound hole open, range (0 - 0.15 s/kg).

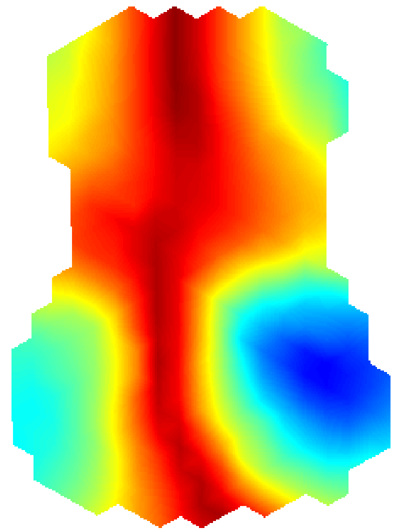

(b) BR2 back plate with sound hole blocked, range (0 - 0.07 s/kg).

Figure 7.6: BR2 back plate mode coupled with $T(2,1)$ - 234 Hz.

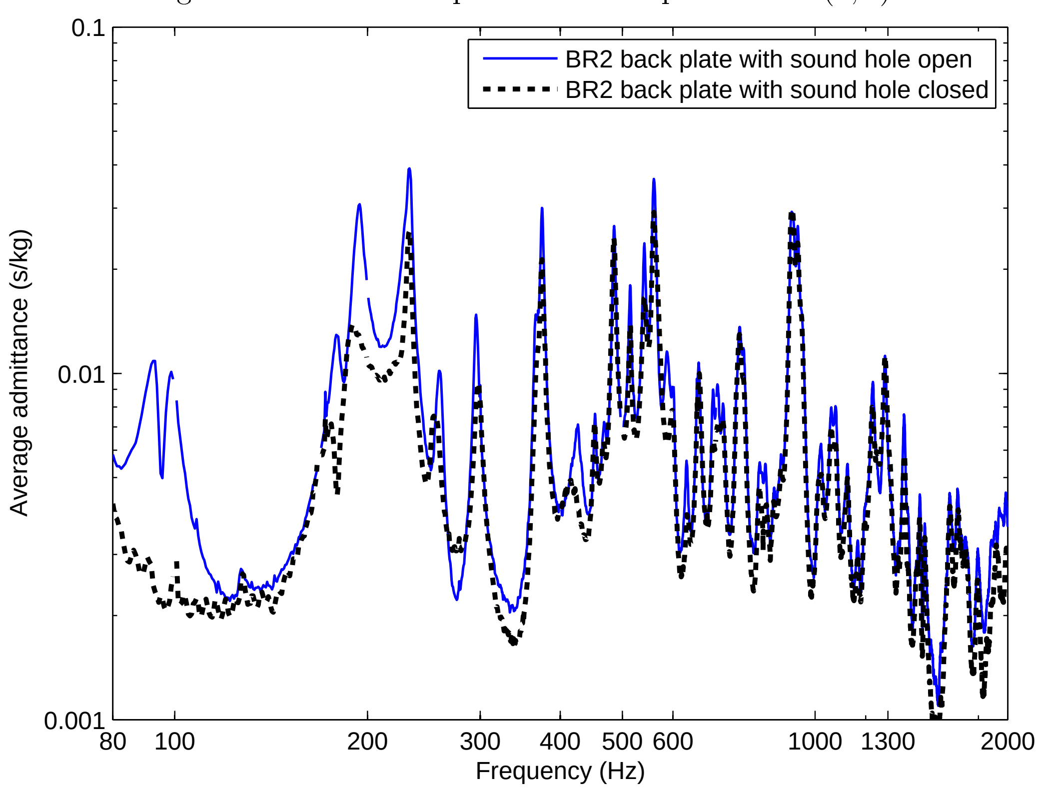

Figure 7.7: Average admittance measured on the back plate of BR2 with the sound hole open and blocked

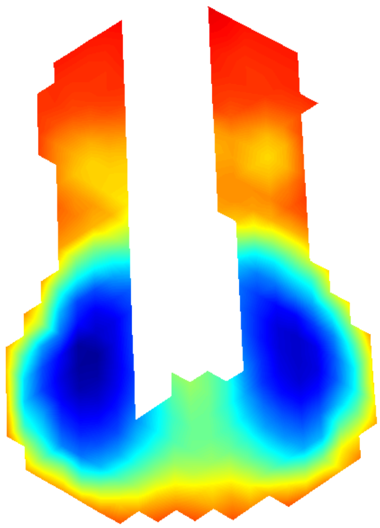

(a) BR2 top plate band data (0 - 1.6 s/kg).

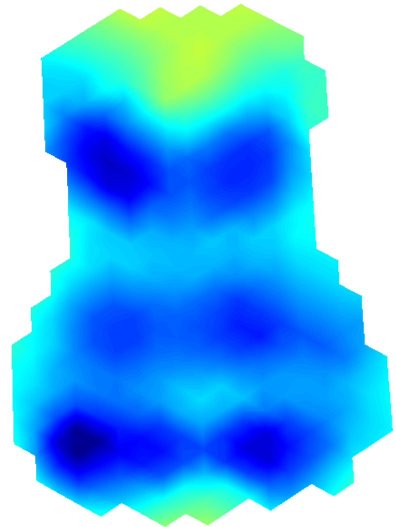

(b) BR2 back plate band data (0 - 0.6 s/kg).

Figure 7.8: Band data for BR2 with its sound hole blocked.

7.1.4 η for BR2 excited at position 1 with the sound hole blocked

Power input, power output and η have not been measured on any stringed instruments with their sound holes blocked previously. The sound hole of BR2 was blocked using soft non-porous foam and was excited at position 1 with its strings damped as in section 5.1.1.

When the sound hole is blocked there are still the three separate frequency regions for the η behaviour of BR2 in figure 7.9. The three regions are 'bounded' by the same body modes as when the sound hole was open but the η characteristic within these regions are changed. At frequencies below 200 Hz, η is much lower when the sound hole is blocked than when it is open. The $T(1,1)_2$ mode is now the lowest frequency mode on the instrument, as shown in figure 7.1, and body modes cannot be easily excited below their resonance frequencies. This results in a lower response from the instrument below 200 Hz and a near zero value of η below 100 Hz followed by a steady increase in η at frequencies approaching the $T(1,1)_2$ mode. The peak value of η between 80 Hz and 200 Hz is 0.13 which is at 197 Hz. This frequency does not correspond with any of the known body modes. This is the same behaviour as when the sound hole was open.

When the sound hole is blocked, the sound hole sum rule described by Weinreich (1985) no longer applies. The enclosed air cannot flow through the sound hole and a dipole motion does not occur between the sound hole and the lower bout of the top plate. The neck-bending mode at 75 Hz is still set into motion but this does not radiate any sound. The lack of dipole sound radiation from the motion of the top plate and the

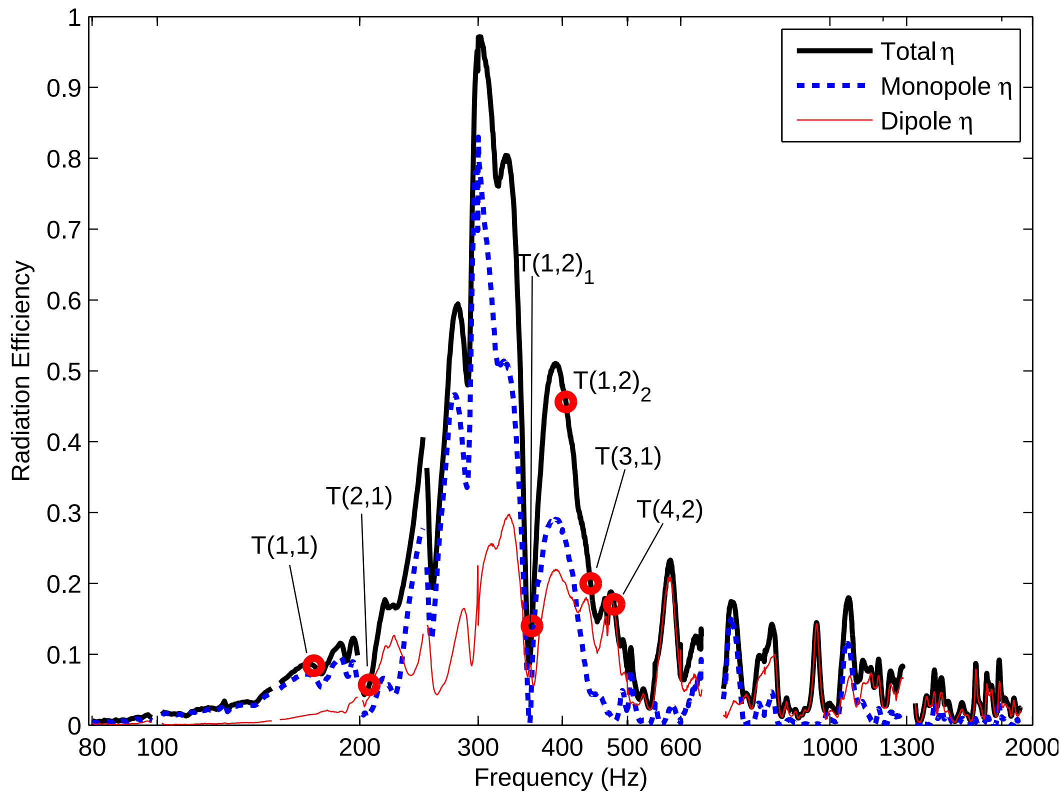

Figure 7.9: Radiation efficiency for BR2 excited at position 1 with the sound hole blocked with non-porous foam.

enclosed air results in the low level of η_d in figure 7.9 below 150 Hz.

In chapter 5 figure 5.8 showed that there is a dipole component in the $T(1,1)_2$ mode and figure 5.10b showed that a clear dipole-like sound field is produced by the $T(2,1)$ mode. Figure 7.9 shows that the $T(1,1)_2$ mode produces the dipole power at frequencies between 150 Hz and its resonance frequency. The dipole contribution from this mode decreases above its resonance frequency and the $T(2,1)$'s y-orientated dipole provides the greatest contribution to the power output. The $T(2,1)$ mode is still highly inefficient when the sound hole is blocked so the motion of air through the sound hole has no effect on its η behaviour.

The second region is still 'bounded' by the $T(2,1)$ and $T(3,1)$ modes but the peak values of η are reduced, with the maximum in η at 300 Hz rather than 400 Hz. At 300 Hz, the peak values of η are similar for both the blocked and open sound hole cases so this frequency region of the instrument is not affected by the presence, or lack, of the air modes. The $T(2,1)$ and $T(1,2)_1$ modes still have low values of η which suggests that their radiativity behaviours are also not significantly altered by the air modes. The power input and power output values do change and are shown in figure 7.10. In the second frequency region, the mean value of η between 200 Hz and 450 Hz is 0.65 when the sound hole is open and $\eta = 0.43$ when the sound hole is closed. The residual response from the low-frequency coupled modes must therefore still contribute to the total power output between 200 Hz and 450 Hz. Despite the $T(1,1)_1$ mode no longer being able to contribute to the radiated sound, the power output is still dominated by monopole radiation below 400 Hz so the $T(1,1)_2$ mode must still be making a considerable contribution to the power output above its resonance frequency.

Above the resonance frequency of the $T(3,1)$ mode, η is less than 0.2 with no peaks above this value. The strong dipole peak at 954 Hz still occurs when the sound hole is blocked but the value of η is reduced. The monopole peak at 707 Hz, which corresponds to the $T(5,1)$ mode, is also still present so this mode does not couple with a motion of air through the sound hole and can therefore still radiate sound pressure and power efficiently. Between 1500 Hz and 2000 Hz, the average η was 0.03 when the sound hole was blocked and 0.02 when the sound hole was open. The sound hole therefore has a negligible effect on the radiation efficiency above 1500 Hz.

Both η_m and η_d are lower across the whole frequency range (80 Hz - 2000 Hz) when the sound hole of BR2 is blocked. A possible reason for this is that the air contained within the cavity acts as an additional mass on the top plate, back plate and ribs of the guitar. The additional mass of the air lowers the amplitude of the body modes and they therefore radiate a lower level of sound power. Another possible explanation is that the removal of the $T(1,1)_1$ mode reduces the residual pressure response from the low-frequency resonance triplet and therefore reduces the power input and power output at higher frequencies. The higher frequency air modes are also affected by blocking the sound hole and any modes which couple with them will produce a smaller output. The effect on the higher frequency air modes will produce a more localised change than the reduction in the low-frequency resonance triplet.

In figure 7.10, the power input is flat with only small deviations below 150 Hz before increasing towards the resonance frequency of the $T(1,1)_2$ mode. The flat input shows that there are no significant body modes that radiate sound vibrating below the single $T(1,1)$ mode. There is in fact a neck-bending mode below 80 Hz but this does not radiate a significant level of sound pressure. However, the power output increases steadily towards the $T(1,1)$ mode from 80 Hz. Peaks in the power output between 200 Hz and 300 Hz that were sharp and well defined when the sound hole was open are flattened and have a much lower amplitude when the sound hole is blocked. Blocking the sound hole must therefore reduce the Q value of the body modes in this frequency range. According to the simple harmonic oscillator model proposed by Christensen

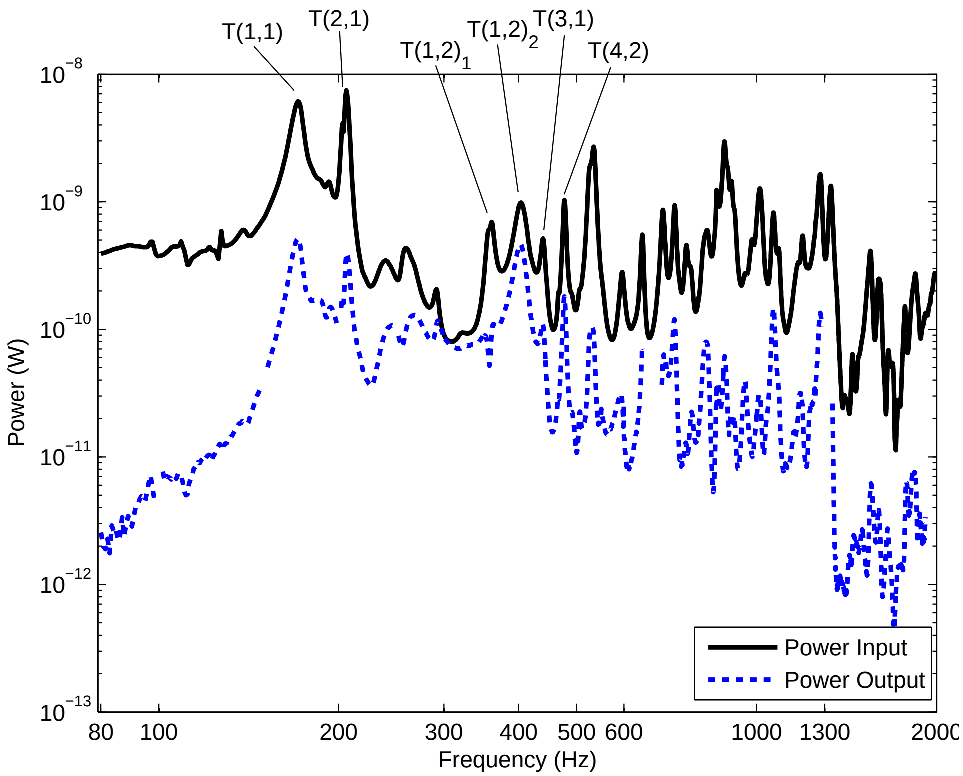

Figure 7.10: Mechanical power input and acoustical power output for BR2 excited at position 1 with the sound hole blocked.

(1984), $Q = \frac{m\omega_0}{R}$ where ω_0 is the resonance frequency of the mode, m is its effective mass and R is the resistance coefficient. Blocking the sound hole must therefore increase R in this system and flatten the peak values of power input.

When the sound hole was open, there was no peak in the power output at the resonance frequency of the $T(1,2)_1$ mode. When the sound hole is blocked there is actually a large decrease in the output power at this frequency. The reduction in the power output when the sound hole is blocked suggests that $T(1,2)_1$ couples with an air mode that pushes air through the sound hole. The second air mode is known to occur at a frequency near to the $T(1,2)_1$ mode (Elejabarrieta et al., 2002b). This air mode does not result in a large volume of air passing through the sound hole but it is affected by blocking the sound hole and appears to have an effect on the $T(1,2)_1$ mode.

The power output decreases above 400 Hz and above 1300 Hz it decreases by a further order of magnitude. This is similar to the power output characteristic for BR2 when the sound hole is open.

7.2 The effect of blocking the sound hole on BR1

A comparison with η on BR2 with its sound hole blocked is provided in this section. Classical guitar BR1 was excited at position 1 on the bridge with the sound hole open and also with it blocked with non-porous foam. It has already been shown for BR2 in section 7.1.4 that blocking the sound hole reduces η at frequencies below 200 Hz.

Figure 7.11 shows that the first peak value in admittance is no longer present when the sound hole is blocked which is the same as the result shown in figure 7.1 for BR2. As the lowest frequency body mode can no longer enter motion it cannot radiate sound which explains the low values of η below 200 Hz when the sound hole is blocked.

Figure 7.12 shows that blocking the sound hole reduces η between 80 Hz and 2000 Hz for BR1. Preventing the $T(1,1)_1$ mode from vibrating reduces η to close to 0 at frequencies below the $T(1,1)_2$ mode and removes the dipole power output produced according to the sound hole sum rule. As the Helmholtz oscillator-like motion between the two $T(1,1)$ modes cannot occur there is also no increase in η between where the two modes should be. This is the same result as for BR2 so the sound hole plays an important role in the radiation efficiency of classical guitars below 200 Hz.

Between 200 Hz and 450 Hz the values of η are reduced in comparison with the case where the sound hole was unblocked. The peak values of η occur between 300 Hz and 350 Hz indicating that within this frequency range there is minimal coupling between the motion of the top plate and the air modes. This is the same result as for BR2. On BR1 the behaviour of the two $T(1,2)$ modes is similar to that of BR2 but more pronounced. Table 7.1 shows the η values of the two $T(1,2)$ modes of BR1 and BR2. The value of η for the $T(1,2)_1$ mode of BR1 is greater than for BR2 both when the sound hole is open and closed. This suggests that there is less coupling between this mode and the higher frequency air mode than there was on BR2.

	η			
	BR1 open	BR1 closed	BR2 open	BR2 closed
$T(1,2)_1$	0.29	0.45	0.08	0.14
$T(1,2)_2$	0.84	0.47	0.99	0.46

Table 7.1: η for the $T(1,2)$ modes of BR1 and BR2

η_m and η_d are reduced across the entire frequency range (80 Hz - 2000 Hz). Without the motion through the sound hole the main monopole contribution is produced by the $T(1,1)$ mode on the top plate. The reduction in η is most likely to be produced by the reduction in the residual response of the low-frequency resonance ‘triplet’ which cannot now be produced. This will affect the behaviour of the instrument across a large range

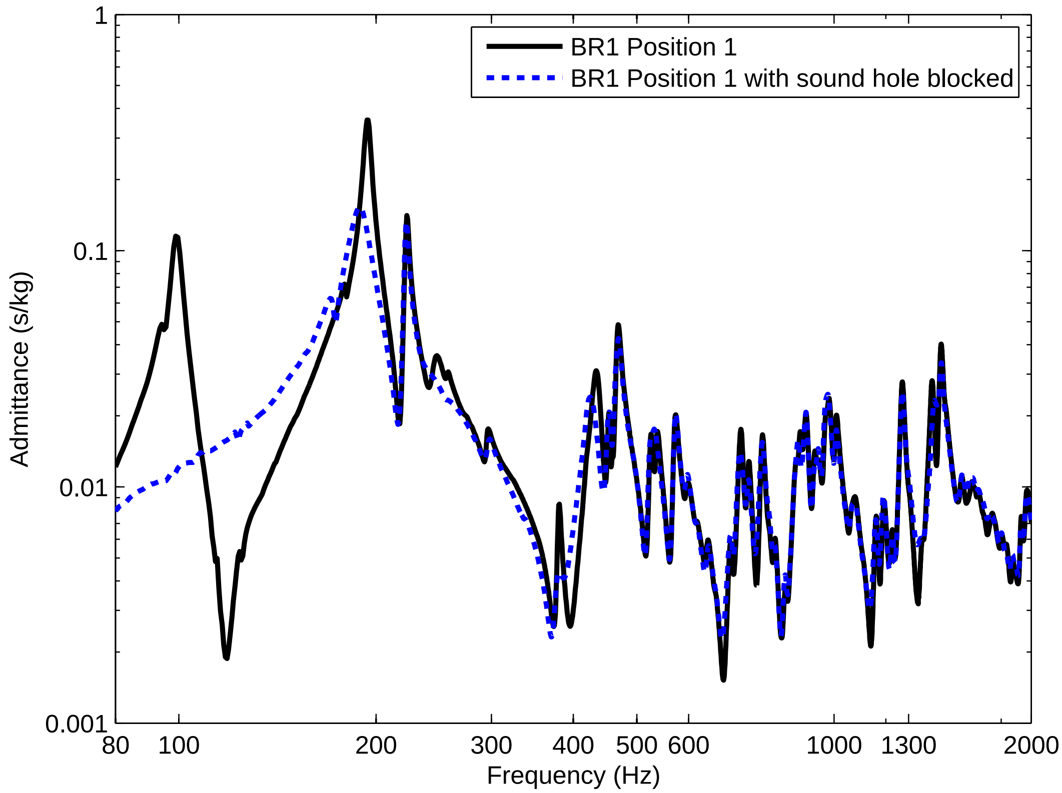

Figure 7.11: Input admittances measured on BR1 at position 1.

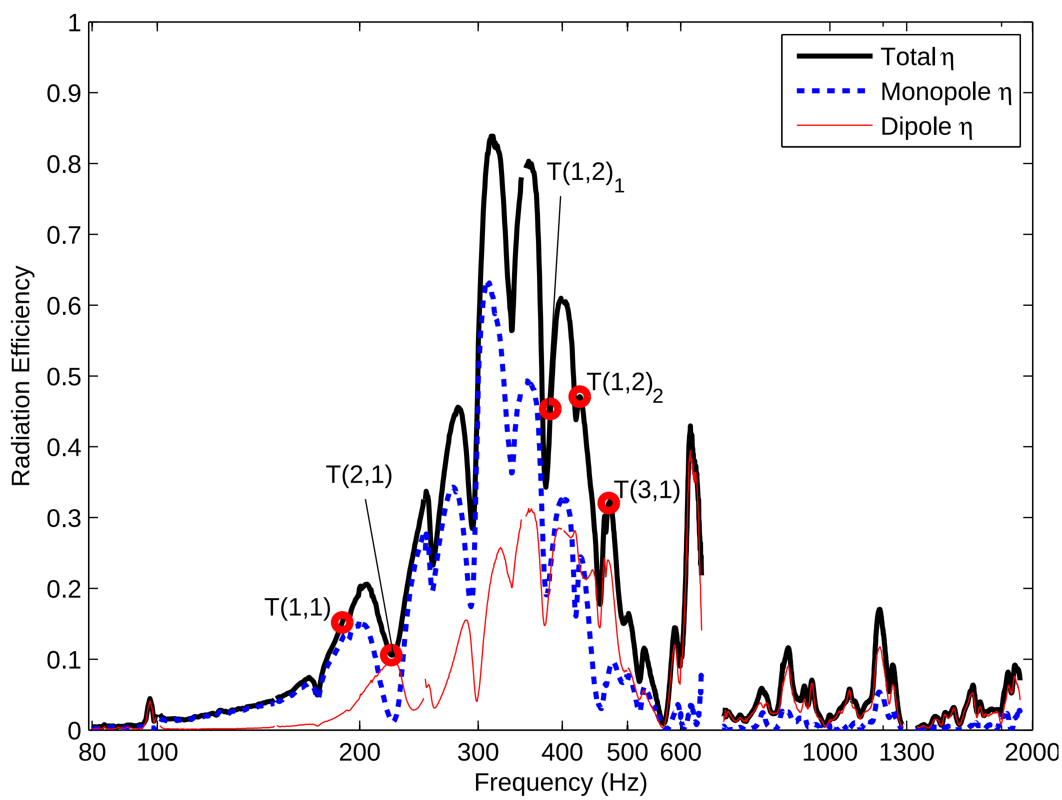

Figure 7.12: η measured from BR1 with its sound hole blocked.

of frequencies. Above 600 Hz the large peaks in η are reduced in magnitude but the η characteristic is more similar to the unblocked sound hole case than the lower frequency range. The air modes must therefore have a smaller effect on the radiated sound power at higher frequencies.

Chapter 8

Measurements on other stringed instruments

In addition to the four classical guitars studied in chapter 5, the radiation efficiency η, power input and power output were measured on a carbon-fibre steel-string guitar, X10, and a violin. X10 was studied because it was constructed using completely different materials from standard classical and steel-string guitars. It also has no struts on the top or back plates which results in a different vibrational behaviour to traditional wooden instruments. The violin was studied so that a comparison between the two definitions of radiation efficiency described in section 2.5, R_{eff} and η, could be made. R_{eff} was previously studied on a set of violins by Bissinger (2003b) but η has not been measured on a violin. The vibrational behaviour of X10, the violin, a banjo, an oud and another steel-string guitar, S&P, was also studied using a 3D scanning laser vibrometer.

8.1 Steel-string guitars

8.1.1 Studied instruments

Two steel-string guitars, X10 and S&P, were studied in this work. X10 is shown in figure 8.1. It was built using carbon-fibre composites for the top plate, back plate, ribs and neck. As such, it has no strutting on either the top or back plate; instead the thickness of the carbon-fibre plates is altered to change their stiffness characteristics. The bridge has an asymmetric design and is glued to the top plate. The top and back plates of the guitar are noticeably curved unlike the flatter plates of the other guitars studied in this thesis. The vibrational behaviour of the top and back plates of X10 were also studied using a 3D scanning laser vibrometer.

Figure 8.1: Carbon-fibre steel-string guitar, X10. The instrument has been painted white for the purposes of holographic interferometry and 3D laser vibrometry.

The other steel-string guitar studied in this section is S&P. S&P is a Simon & Patrick songsmith folk guitar with a spruce top plate and red wild cherry back plate and ribs. This instrument was unavailable for η measurements but its more traditional wooden construction provides a useful comparison with the vibrational response measured on X10. S&P has a considerable amount of strutting, the design of which is shown in figure 8.2. S&P also has flatter top and back plates than X10.

8.1.2 3D input admittance measured on X10 and S&P

Figure 8.3 shows the 3D input admittance measured on X10 and S&P when excited at position 2 (on the bass side of the bridge, see figure 5.1). S&P was not available for η measurements and so the effect of the in-plane motion on η cannot be determined for this guitar. It has already been shown that steel-string guitars have lower values of input admittance when out-of-plane measurements are made on the instrument. 3D input admittance has not been previously measured on steel-string guitars.

The peak values of admittance in the x direction, Y_{xx}, have lower amplitudes, for both of these instruments, than those normally present in classical guitars. This is a result of the stiffer top plate construction (which is required to support the steel strings which have a greater level of tension than nylon strings). The first peak in the admittance curves is produced by the $T(1,1)_1$ mode. The resonance frequency of this mode is higher for X10 than S&P because it has a cutaway body shape which reduces the volume of the air cavity and therefore increases the resonance frequency of the Helmholtz oscillator-like motion. The second body mode, $T(1,1)_2$, has a slightly higher

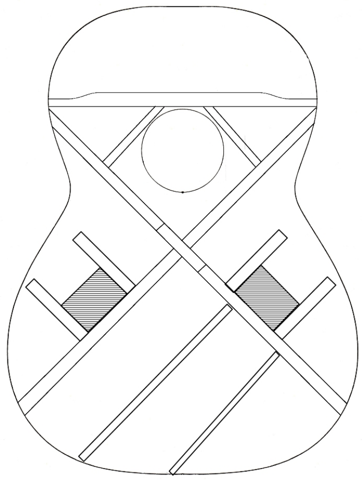

Figure 8.2: Strutting for the top plate of S&P, the cross-hatched sections are thin pieces of wood.

resonance frequency on X10 than S&P. The higher frequency resonance may result from a weaker coupling between the top plate and the air motion through the sound hole on X10 or because the top plate of X10 is stiffer than that of S&P.

The resonance frequencies of S&P's body modes are different from those of X10. Figure 8.3 shows that X10 produces strong peaks in admittance up to 1300 Hz including a peak at 1281 Hz which has a comparable magnitude to the $T(1,1)_1$ mode. The two greatest values of Y produced by X10 are at the resonance frequencies of the $T(2,1)$ and $T(2,2)$ modes whereas the greatest Y values occurs at the $T(1,1)_2$ mode for S&P. S&P behaves more like a classical guitar than X10 in that the peak values of admittance decrease at frequencies above the $T(2,1)$ mode and are typically an order of magnitude lower than this peak. X10 behaves more uniformly between 80 Hz – 2000 Hz and this is speculated to result from the carbon-fibre construction of X10.

The in-plane admittances, Y_{xy} and Y_{xz}, are lower for S&P than X10 across the entire studied frequency range, indeed the velocity was nearly always obscured by noise away from the resonance frequencies of the body modes for S&P. The most obvious explanation for the difference in the admittance for all three directions is the construction of the carbon-fibre plates. Wooden top plates are anisotropic but have a grain that is orientated so that it runs parallel with the strings. The level of anisotropy in carbon-fibre plates is dependent on the orientations of the layers of carbon fibre used in the plate construction. The orientation of the particular carbon-fibre composite used to build X10 is not known, but the admittance characteristics show that it clearly has

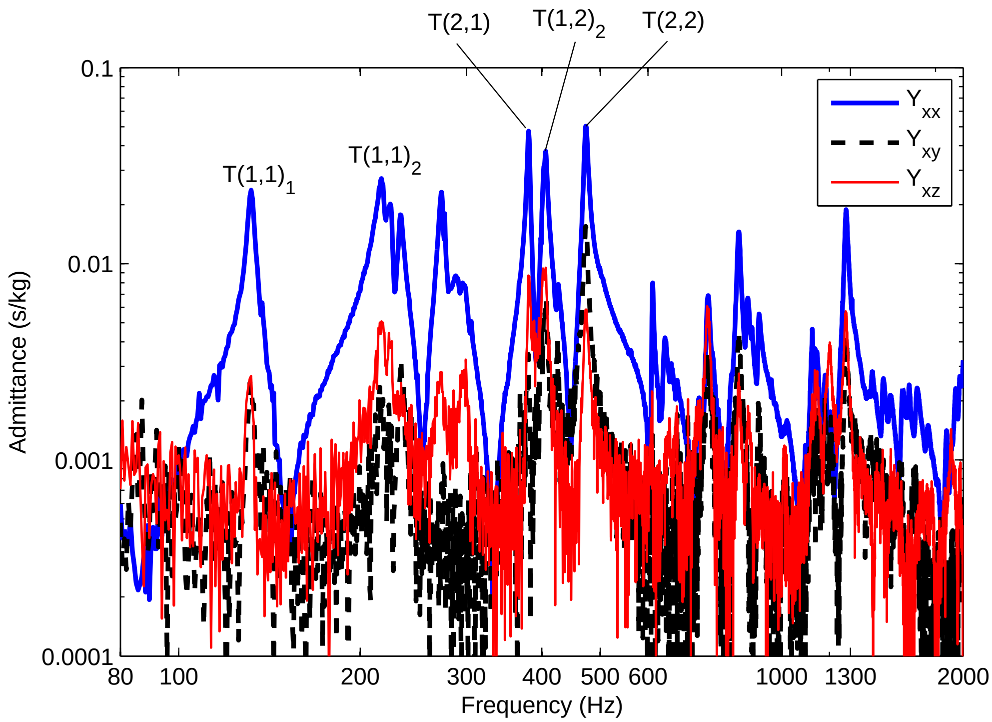

(a) X10.

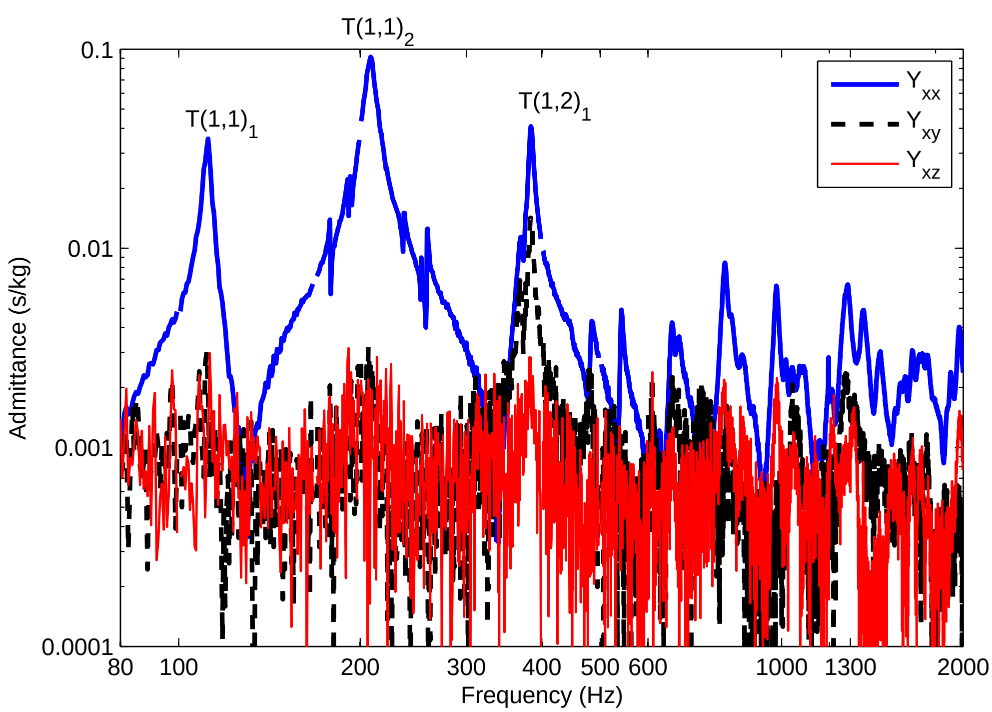

(b) S&P.

Figure 8.3: 3D input admittance measurements on two steel-string guitars at their E_2 strings.

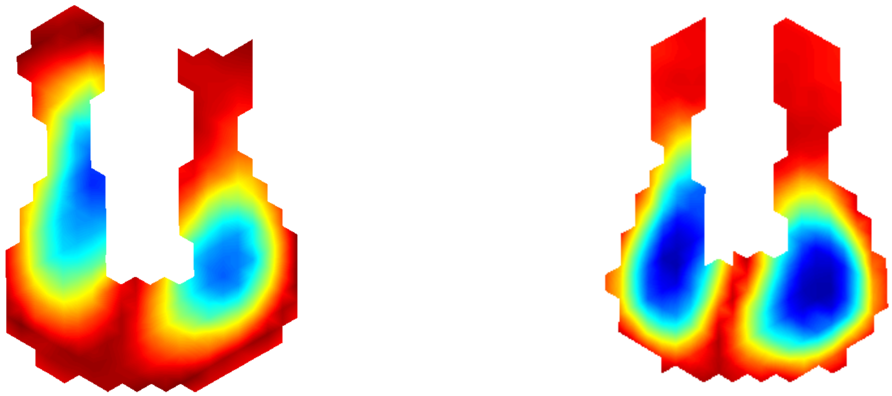

(a) X10 $T(2,1)$ mode - 378 Hz.

(b) S&P $T(2,1)$ mode - 384 Hz.

Figure 8.4: The $T(2,1)$ modes of X10 and S&P measured using a lser vibrometer

a different characteristic from spruce. S&P has smaller values of Y_{xy} and Y_{xz} than X10 which shows that X10 is less stiff in the in-plane directions than the more traditionally built wooden instrument. The carbon-fibre plate therefore has a more uniform stiffness than the strutted wooden plate as the in-plane velocity is greater for X10 than S&P.

Despite the low average values of Y_{xy} and Y_{xz} for both instruments, there are still some body modes which produce large values of Y_{xy} (for X10 and S&P) and of Y_{xz} (X10). It is the body modes which have equal-sized anti-nodal areas with opposite phases which produce the greatest values of Y_{xy}. This is the same behaviour as for the classical guitars. The $T(2,1)$ mode of X10, with a resonance frequency of 381Hz, is not symmetrical (shown in figure 8.4a). For X10's $T(2,1)$ mode, the value of Y_{xz} at the bridge is greater than Y_{xy} because the mode's nodal line is at an angle to the bridge. The angle of the nodal line means that the motion of the two opposite phase anti-nodal areas will produce a motion in the z direction as well as the y direction. The $T(2,2)$ mode on X10, at 475 Hz, is more symmetrically orientated about the centre of the instrument and therefore shows a greater value of Y_{xy} than the $T(2,1)$ mode.

Figure 8.4b shows that the $T(2,1)$ mode of S&P is slightly asymmetrical but it is at a smaller angle to the bridge than the $T(2,1)$ mode of X10. As such this mode shows a larger value of Y_{xy} for S&P than for X10 and is the only body mode to produce a large in-plane velocity on S&P. The additional stiffness provided across the grain by the bracing on S&P, combined with the thicker wooden top plate, reduces the level of motion in the plane of the top plate. X10 is less heavily reinforced across its 'grain' and as such shows a greater level of in plane motion, particularly for the more symmetrical body modes such as $T(2,1)$ and $T(2,2)$.

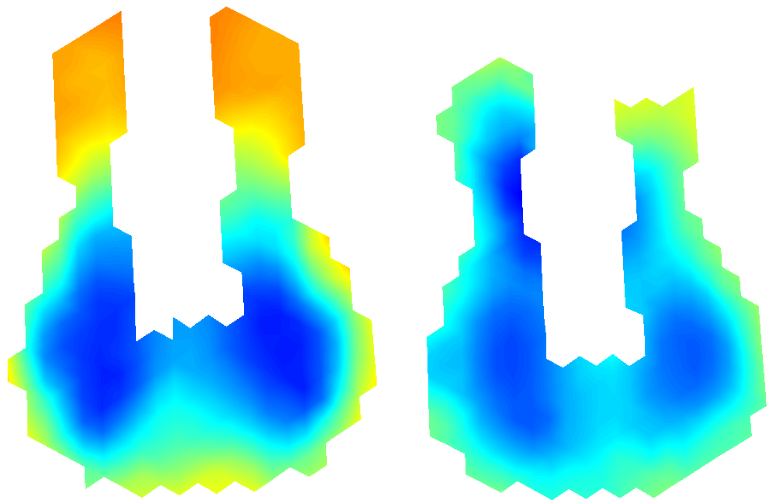

(a) S&P top plate band data, range (0 - 0.5 s/kg).

(b) X10 top plate band data, range (0 - 0.5 s/kg).

Figure 8.5: Top plate band data from steel-string guitars.

8.1.3 Top plate band data

Figure 8.5 shows that both of the steel-string guitars, X10 and S&P, produce maximum values of band data in a $T(2,1)$ shape. This is the same result as seen for the classical guitars in section 5.2.1. However, the motion of X10 extends into the upper bout rather than being constrained to the lower bout. As X10 has no struts attached to its top plate, the surface waves produced by the excitation at the bridge are not interrupted by the increases in stiffness produced by top plate strutting. This allows for a more even distribution of admittance values across the plate with more motion in the upper bout on X10 than for S&P. Both of the steel-string guitars have similar peak values in the band data (0.5 s/kg) but these peak values are lower than any of the classical guitar top plates. The peak admittance values are lower for the steel-string guitars as they have stiffer top plates to support the greater tension of the steel strings.

8.1.4 Back plate band data

The back plate band data of X10 was measured using the same technique as described in section 5.2.1. The back plate of S&P was too reflective to make measurements of its velocity and NDT spray could not be applied to this instrument without damaging its appearance.

Figure 5.27 showed that the classical guitars BR2 and MAL both had three separated regions of higher total admittance values which correspond with the areas of the back

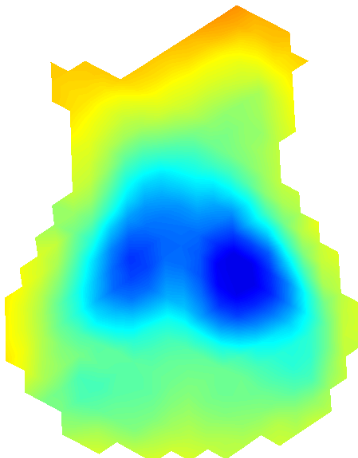

(a) X10 back plate band data, range (0 - 0.5 s/kg).

Figure 8.6: Back plate band data from X10.

plate between the struts. This effect is not present for X10 which has no struts on either the top or the back plate. On X10 the maximum values of total admittance lie within the centre of the back plate and decrease towards the edges. The area of maximum band data does not correspond with the location of the sound hole on the top plate, so maximum band data is produced by the motion of the plate rather than a coupling between the back plate and a motion of air through the sound hole.

X10 has the same peak total value of Y (0.5 s/kg) on the back plate as on the top plate. For classical guitars the top and back plates are made of different woods with different characteristics, but the two plates of X10 are constructed from carbon-fibre in. As such the carbon-fibre top and back plates appear to have more similar characteristics than top and back plates made of different woods.

8.1.5 X10 η

η was measured on X10 using an excitation close to the E_4 string at position 1 (as defined in figure 5.1 on page 99). X10 has a considerably different η characteristic to the four classical guitars studied in chapter 5. Unlike the classical guitars, X10 has its maximum value of η at 200 Hz, between the two $T(1,1)$ modes, as shown in figure 8.7. The next highest peak in η is between 400 Hz and 500 Hz which was towards the upper frequency limit of the region of high η values for the classical guitars. The instrument is much more efficient below 200 Hz than any of the classical guitars but is not as consistently efficient between 200 Hz and 450 Hz. It also exhibits greater values

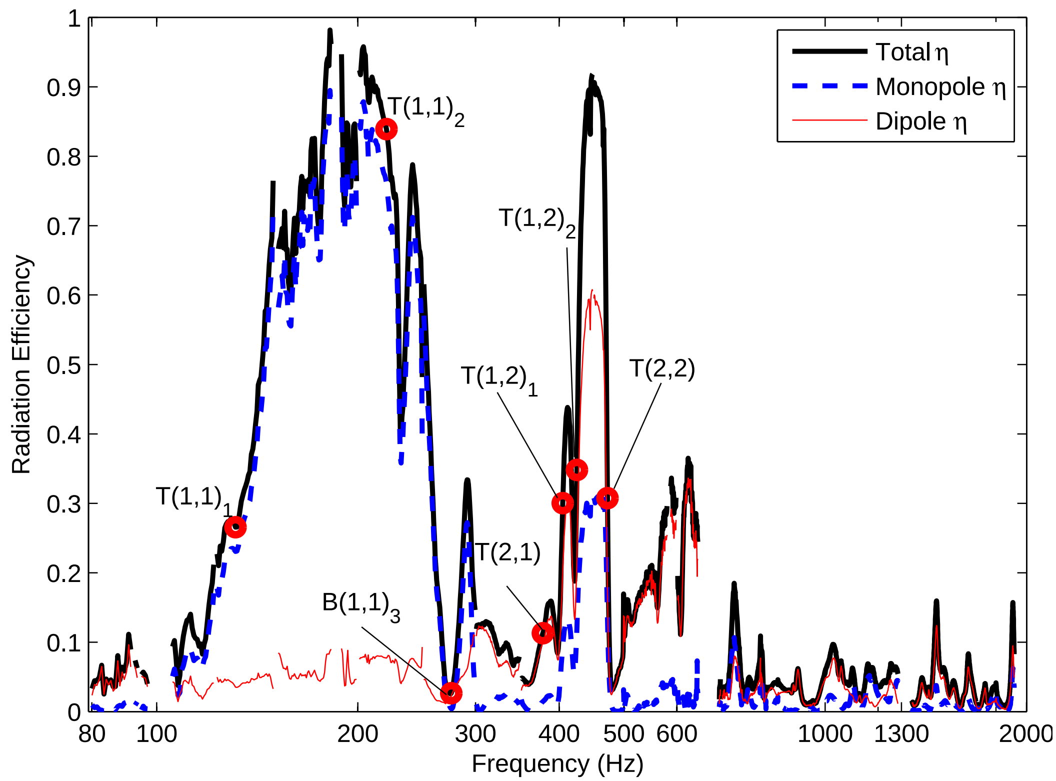

Figure 8.7: Radiation efficiency measured at position 1 on X10.

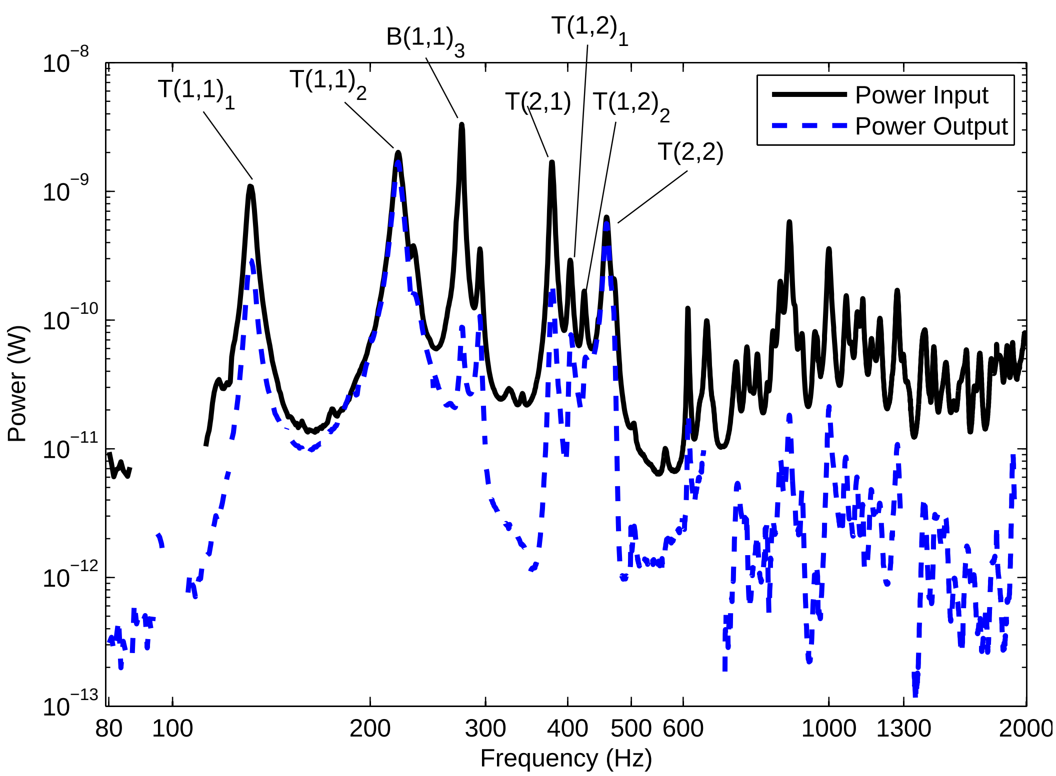

Figure 8.8: Mechanical power input and acoustical power output for X10 excited at position 1.

of η between 450 Hz and 600 Hz than BR1, BR2 or MAL and the power output within this range has a strong dipole component, similar to DLC.

At frequencies below 300 Hz, the power output is mostly produced by monopole sources. Unlike the classical guitars, the dipole power output is nearly always greater than the monopole contribution above 300 Hz except for a peak at 731 Hz. The sound power produced by monopole components was much greater than from dipoles for classical guitars up to frequencies between 400 Hz and 500 Hz. Dipole components are responsible for the majority of the power output from a lower frequency for X10 than for the classical guitars. Therefore the residual response from the lowest frequency monopole-like body modes must be reduced for this instrument as there is a smaller monopole contribution to the steel-string guitars power output. If the top plate is stiffer then the residual response from the low-frequency resonance triplet will be lower and there will be a smaller contribution to the power output from monopole sources than dipole sources. The amplitudes of the peaks in the of input admittance curve are lower for X10 than for any of the classical guitars because of the stiffer plate construction. The increased stiffness of the top plate does not affect the behaviour of the $T(1,1)_1$ mode (which is produced by a coupling with a Helmholtz oscillator-like motion) but if the top plates are stiffer, then the resonance frequencies of the $T(1,1)_2$ mode and the other higher frequency modes will increase.

The $B(1,1)_3$ mode produces the lowest value of η of any of the X10 body modes. The cause of this reduced value of η is the shape of the mode rather than its resonance frequency. This mode has one large anti-nodal area in the centre of the back plate and an opposite motion motion surrounding it that extends onto the edges of the plate and the ribs. As there is a motion being produced on the ribs by this mode there is a smaller amount of displacement of the surrounding air than if the motion was constrained to the plate. As the greatest velocity values are present in the centre of the back plate, this anti-nodal region is easily driven by an excitation at the bridge. However, as this motion does not displace a considerable amount of air it will produce a small power output in comparison with the power input, as shown in figure 8.8.

The $T(2,1)$ mode on $X10$ has a higher value of η than on any of the classical guitars. Figure 8.8 shows that the power input and output of this mode are more similar in value than on the classical guitars. This results from the shape and angle of the $T(2,1)$ mode on the top plate. The nodal line of this mode is at an angle to the bridge and has unequal sized anti-nodal areas as shown in figure 8.4a. This results in a smaller amount of cancellation between the two anti-nodal regions than if the anti-nodal areas were of the same size. The reduction in cancellation produces a greater amount of power output and a higher value of η. There is also a greater amount of monopole power output than would normally be expected as a result of this asymmetry.

Even though the output power is nearly entirely produced by monopole sources below 200 Hz, there is a clear dipole component in this region below the resonance frequencies of the body modes which predominantly radiate dipole sound power. X10 therefore also follows the sound hole sum rule in the same way as the classical guitars as outlined by Weinreich (1985). The increase in η between the two $T(1,1)$ modes is also a result of the Helmholtz oscillator-like motion between the two modes which also occurs on classical guitars. This was previously shown to occur on BR2 in section 5.1.1.

X10 has a similar η characteristic to the studied classical guitars at frequencies above 600 Hz where $\eta < 0.2$ despite the considerable difference in the construction of X10. The last mode to produce a high value of η is the $T(1,3)$ mode which occurs near to 600 Hz (not shown in figure 8.7). Above the resonance frequency of this mode the values of η decrease and remain less than 0.2. The mean value of η between 600 Hz and 2000 Hz is 0.050 for X10 when excited at position 1. The average values of η between 600 Hz and 2000 Hz for the four classical guitars and X10 are shown in table 8.1. X10 has a lower average η than the three higher quality classical guitars but greater than MAL. MAL is the lowest quality instrument and therefore it would be expected that it would have the lowest value of η because of its over-constructed nature. X10 also has a stiffer top plate than BR1, BR2 and DLC and would be expected to have a lower value of η. However, the difference in the total variation of η across this frequency range for all five guitars is only 0.037 which is a much smaller difference than at lower frequencies.

Guitar	η average
BR1	0.068
BR2	0.080
DLC	0.060
MAL	0.043
X10	0.050

Table 8.1: Average η between 600 Hz and 2000 Hz of five guitars.

8.2 Violin

The violin was constructed in a violin making school, in Abertridwr, to a standard design. Unlike the guitars, which were excited by the hammer perpendicular to the plane of the top plate, the violin was driven on the side of the bridge. This excitation

Figure 8.9: Excitation direction for η measurements on the violin's bridge.

applies a force to the violin in the bowing direction. The excitation and measurement locations are shown in figure 8.9

A small metal disc was attached to the top of the treble side of the bridge with the accelerometer just below it. The hammer excitation was made on the metal disc to provide a larger area for the impact to strike. The disc only weighs 80 mg and was slightly larger than the width of the bridge. The accelerometer was attached to the side of the bridge next to the metal disc using Loctite glue. This ensured that the accelerometer and disc remained in contact with the bridge. The blue wire seen on the bass side of the bridge in figure 8.9 is connected to a force transducer which was not used in this experimental work.

Radiation efficiency η, power input and power output were all measured using the technique described in section 4. The same suspension system was used but with longer elastic bands to suspend the instrument, so that it was located at the centre of the two measurement spheres. This suspension method meant that the instrument moved a greater distance following an excitation than the guitars and, as such, a rocking motion may be more apparent in the admittance and power input data than for the studied guitars. The rocking motion will appear in the data as a peak at low frequency. Any rocking from the suspension system occurred well below the body mode with the lowest resonance frequency. The mode shapes of this particular violin are not known but the mode shapes of another violin have previously been measured and will be used as the basis for the discussions that follow (Moral and Jansson, 1982).

Figure 8.10 shows the input admittance averaged from 324 excitations at the treble side of the bridge on the violin. The peak values of admittance are greater on the violin than on the steel-string guitars, but they are smaller than those of the classical guitars shown in chapter 5. As violins are considerably smaller than guitars, the violin's body modes have much higher resonance frequencies. There are several small peaks around

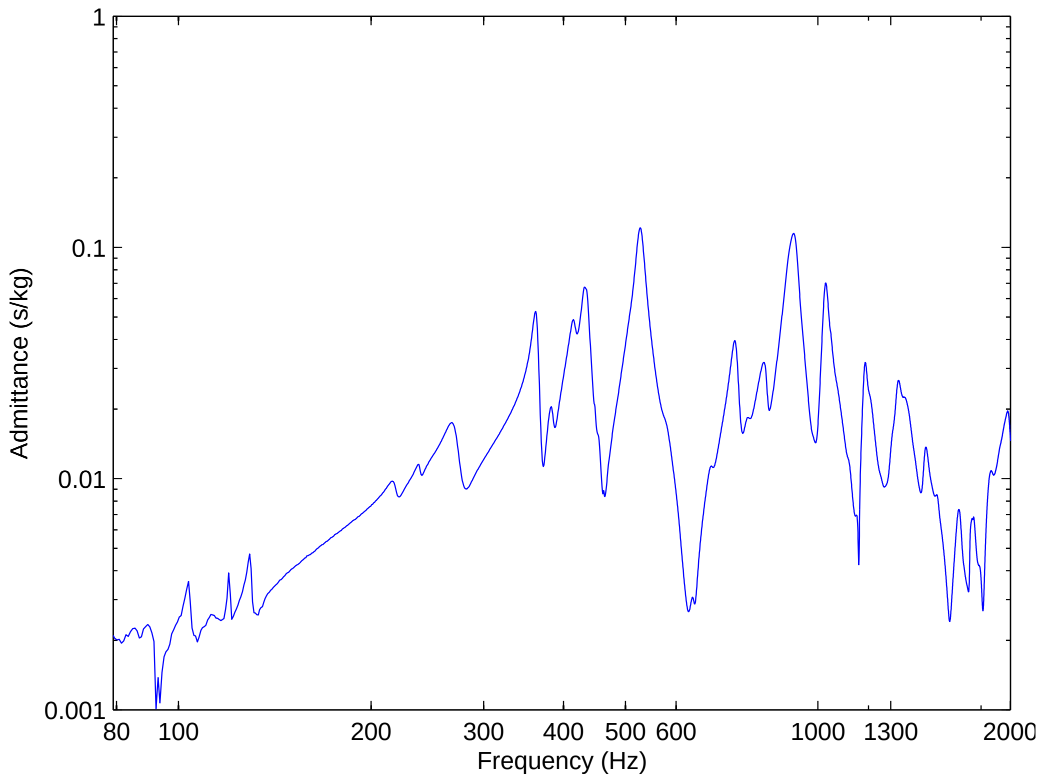

Figure 8.10: Input admittance measured on a violin from an excitation at the treble side of the bridge.

100 Hz but these are most likely to result from a neck bending mode rather than any body mode which radiates sound. Unlike the classical guitars, the lowest frequency body modes do not produce the greatest values of admittance. Instead the greatest value occurs at 527 Hz and the first clear resonance frequency which corresponds to a body mode is at 267 Hz.

8.2.1 Violin η

Figure 8.11 shows that, below the resonance frequency of the first body mode the violin, behaves in a similar way to the five studied guitars. η is less than 1% below 200 Hz and the first body mode has a resonance frequency of 216 Hz, although this mode does not radiate sound power very efficiently. The first clearly defined peak in the input admittance is at 267 Hz which is close in frequency to the first peak in η. This mode has been named $A0$ within the literature and it is produced by a Helmholtz resonator-like motion coupling with the top plate, like the $T(1,1)_1$ mode on classical and steel-string guitars. The Helmholtz resonator-like motion results from air motion through the f-holes on the top plate of the violin. As η only begins to increase just

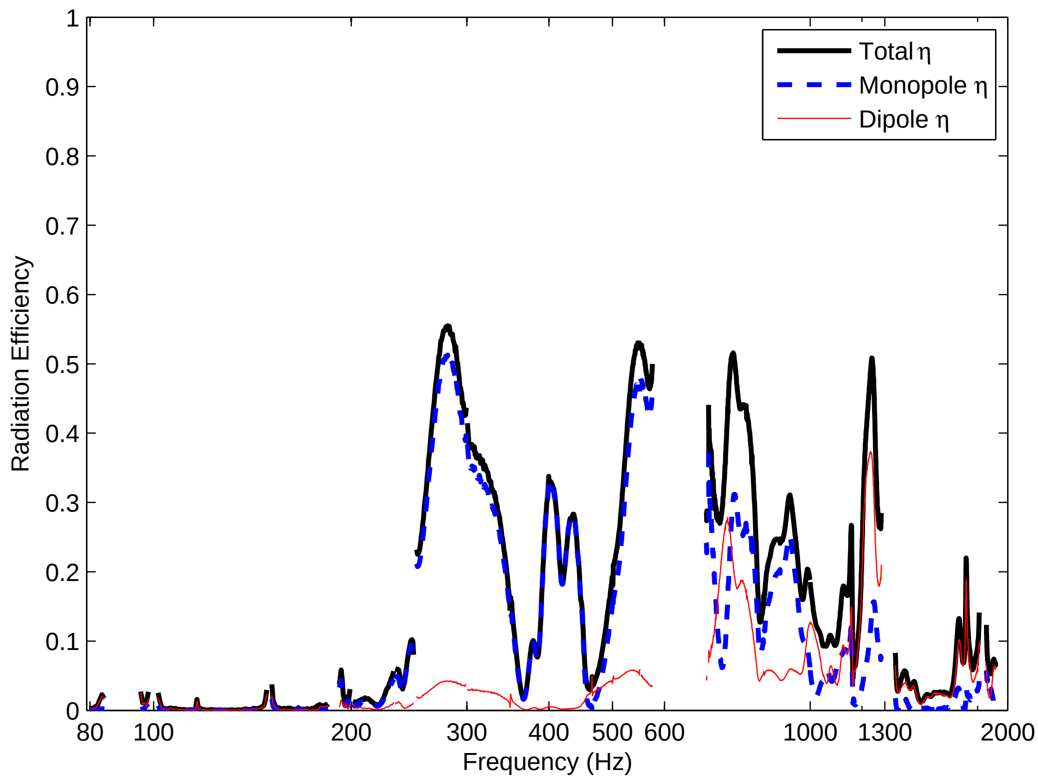

Figure 8.11: Radiation efficiency measured at the treble side of the bridge of a violin.

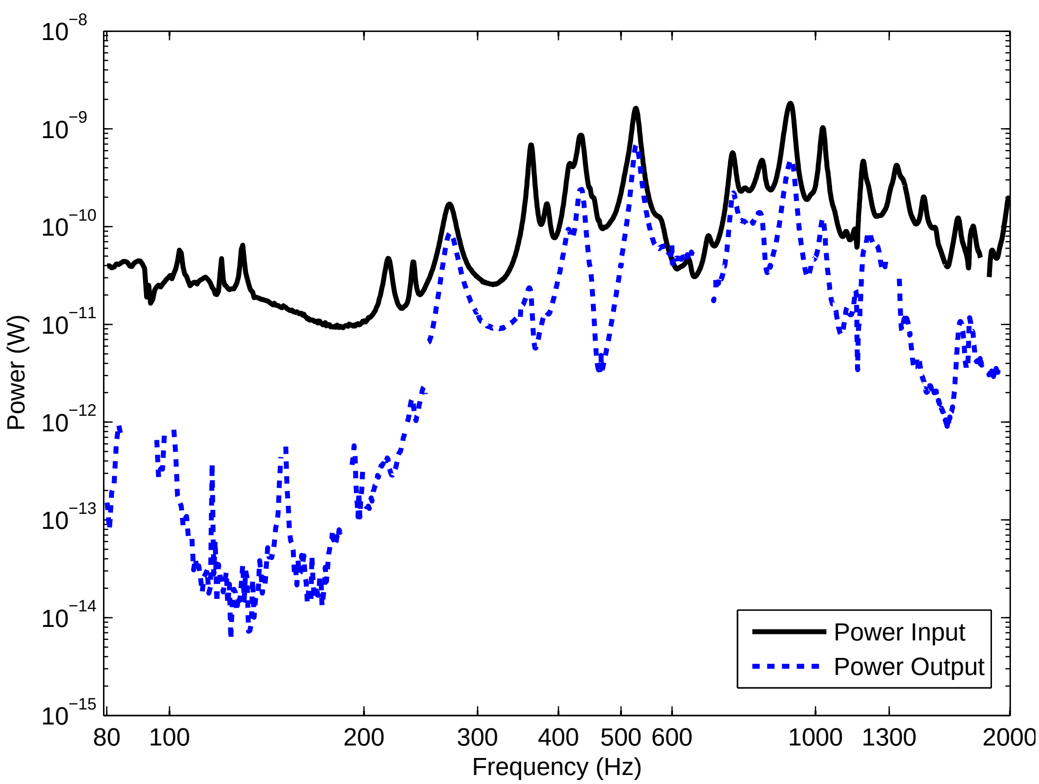

Figure 8.12: Mechanical power input and acoustical power output for a violin excited at the treble side of the bridge.

below the resonance frequency of $A0$ it is clear that it is the first mode to radiate sound power efficiently on the instrument. The lower frequency peaks in admittance do not radiate any significant level of power output despite the greater level of power input. As $\eta < 0.1$ below 250 Hz, the fundamental frequencies of the notes between G_3 to B_3 will radiate inefficiently. However, the higher frequency partials of these notes may radiate more efficiently. There is a dipole component produced at frequencies around the resonance frequency of the $A0$ mode despite the strong monopole behaviour of this mode. The contribution of this dipole component decreases with increasing frequency which also suggests that it is produced according to the sound hole sum rule. However, the effect of the sound hole sum rule is smaller on the violin than on any of the classical guitars. This occurs because the resonance frequencies of the Helmholtz oscillator-like mode and the first plate mode are a greater distance apart than those on the classical guitar. This reduces the coupling between the two modes and therefore reduces the effect produced by the sound hole sum rule.

Between 200 Hz and 1000 Hz, the monopole contributions to η are greater than the dipole contributions. Monopole sources contribute most to the power output across a much wider frequency range on the violin than on any of the studied guitars. The body modes of the violin have increasing numbers of anti-nodal regions at higher frequencies, just like those of the classical guitar. The nodal lines of violin body modes are typically curved and cannot be described using the $T(m, n)$ nomenclature used to describe the shapes of the body modes of guitars. Moral and Jansson (1982) showed that at frequencies up to 1000 Hz many of the body modes of a violin have nodal lines which lie underneath the feet of the bridge. There is a greater amount of motion on the bass foot of the bridge in comparison with the treble foot when the instrument is excited. This occurs because the sound post under the treble foot restricts the motion of the top plate. As the bridge excitation drives the bass foot to a greater extent, modes with nodal lines at the bass foot will not be driven by this motion. There will be some excitation of the anti-nodal areas by the treble foot but this will produce a small output. This reduces the level of dipole power output and the monopole output produced by the residual response of the lowest frequency body modes will dominate the radiated sound at higher frequencies.

Figure 8.12 shows that at frequencies between 200 Hz and the resonance frequency of the $A0$ mode there are two peaks in the power output but these are difficult to distinguish from the general trend of the power output increasing towards A0. For an excitation provided perpendicularly to the strings on the treble side of the bridge, it can be assumed that the A0 mode is the first body mode to produce an appreciable level of power output. The peak in η occurs 4 Hz above the A0 mode as the power output decreases more slowly above the peak than the power input. However, the power output decreases across a wider frequency range than the power input which results in the low value of η at 368 Hz.

The average value of η between 600 Hz and 2000 Hz is 0.158 which is considerably greater than that observed for the classical guitars. Figure 8.11 shows that the violin is more efficient at higher frequencies than any of the classical guitars. This is a result of the more complex body modes having higher resonance frequencies on the violin than on the classical guitars. A similar effect was also present on the classical guitar DLC.

As the accelerometer was attached to the bridge using Loctite glue, the frequency response of the instrument could be measured over a much wider frequency range than the classical guitars. Attaching the transducer to the instrument with glue gives a much more stable response than if it were attached using double sided tape (as shown in section 3.5). It was therefore possible to measure η up to 5000 Hz on the violin. Figure 8.13 shows that, between 2000 Hz and 5000 Hz, η is always less than 0.05 and has an average value of $\eta = 0.015$. There are no clear peaks or features present in the η data like those below 2000 Hz. Even at the peak in the admittance known as the bridge hill (Woodhouse, 2005) at around 3000 Hz, the values of η are still much lower than those those below 2000 Hz.

The η definition of radiation efficiency produces a considerably different profile to R_{eff} used by Bissinger (2003b). R_{eff} for 12 violins was shown in figure 2.3 and is repeated in figure 8.14 for comparison with η. The values of R_{eff} steadily increase towards a value of 1 at the critical frequency. The values of η are greater at lower frequencies but decrease as the mode shapes become more complex. The violin is therefore more efficient than a baffled piston at higher frequencies but the amount of power output produced from an input decreases.

8.3 The banjo and oud

8.3.1 Banjo and oud top plate band data

While the banjo and oud were not the main focus of this work the 3D vibrational behaviour of the two instruments was studied to provide a comparison with the behaviour of classical and steel-string guitars. The oud is of a traditional design, built in Bahrain, with eleven strings which are arranged with one drone string and five pairs of equally tuned strings. The oud resembles a lute. It has a flat top plate but a half-pear shaped

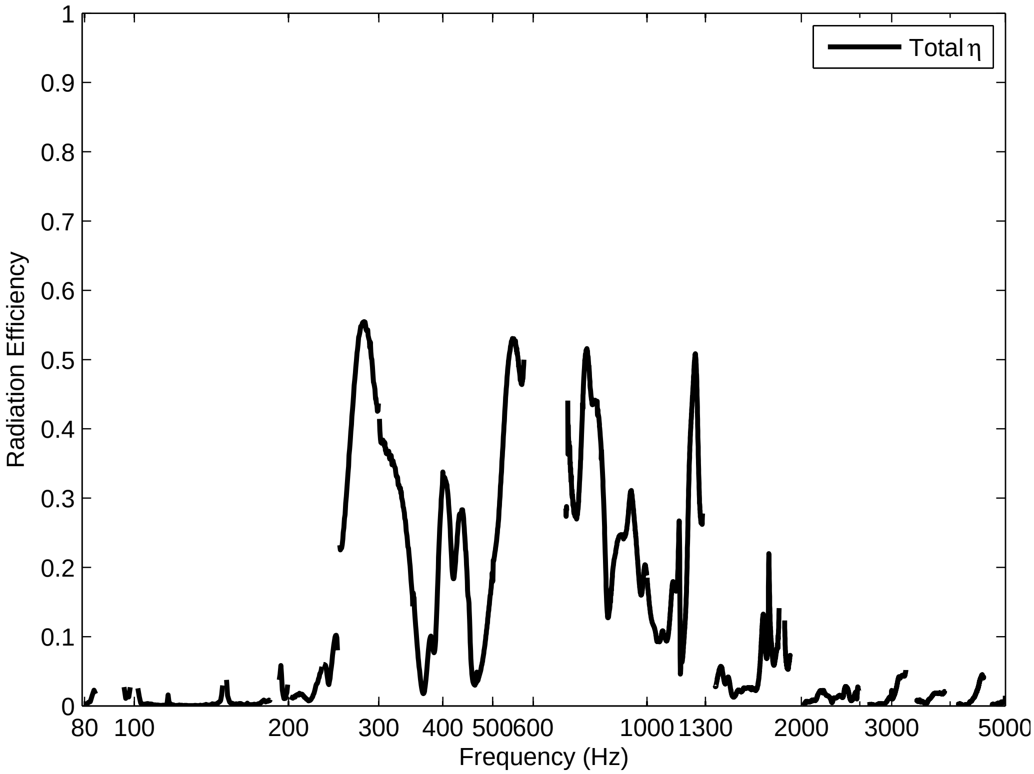

Figure 8.13: Total radiation efficiency measured on a violin between 80 Hz and 5000 Hz.

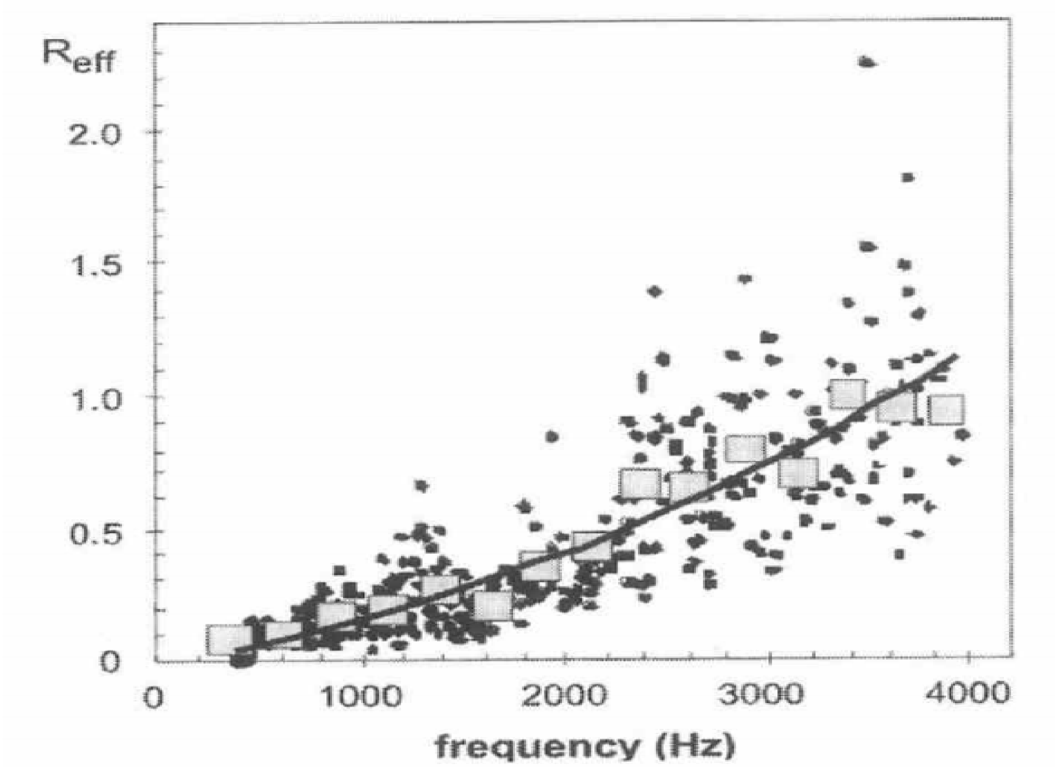

Figure 8.14: R_{eff} determined from 12 violins by Bissinger (2003b). Reprinted by permission of the Catgut Acoustical Society.

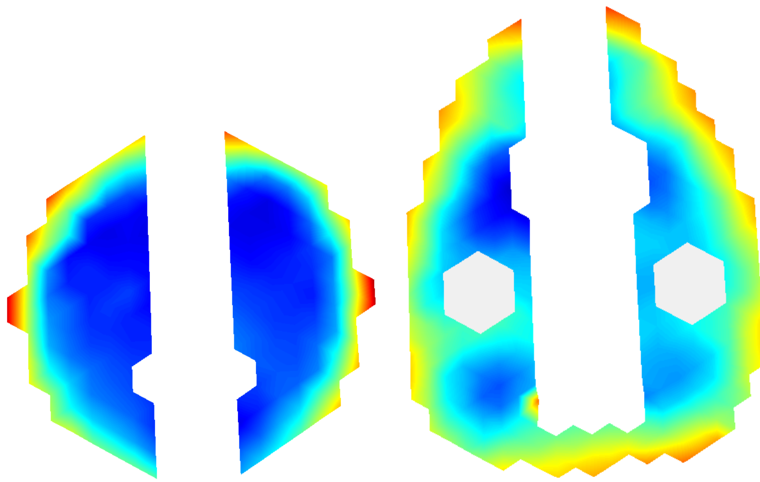

(a) Banjo membrane band data, range (0 - 14 s/kg).

(b) Oud top plate band data, range (0 - 1.2 s/kg).

Figure 8.15: Top plate band data from a banjo and an oud.

back plate with a large air cavity. The top plate has three sound holes which are each covered with a wooden lattice, known as a shams or rose. There are no frets on the neck or top plate and the headstock is sharply angled inwards towards the player. The banjo was built by Ozark and has 5 strings with one string terminated at half the length of the neck rather than at the headstock. There is only a single circular membrane with no sound hole, so there is no air cavity and no Helmholtz resonator-like motion is produced by the instrument. Some banjos have detachable resonators that can be attached to the back of the instrument to create an enclosed air cavity. However, the banjo studied in this chapter did not have one of these resonators. Neither the oud nor the banjo were suitable for η measurements as they were both too large to be placed at the centre of the two measurement spheres in the anechoic chamber.

The banjo produces much larger values of admittance across the 0 – 2000 Hz range than the classical and steel-string guitars. Figure 8.15a shows that the largest total values of admittance across the frequency range on the banjo are at the centre of the membrane. The banjo produces values of band data up to 14 s/kg which is an order of magnitude greater than the band data measured on the guitars. High values of admittance result in a large amount of coupling between the strings and the membrane, leading to a characteristic 'thud' when the strings are plucked. Very strong coupling can also lead to 'wolf notes' being produced when the string vibrates (Roberts and Richardson, 2014). Wolf notes produce an unpleasant sound with a large amount of beating and, while most prevalent in cellos, sometimes occur in classical guitars. They can be suppressed by adding a small weight to the string.

The admittance values on the banjo decrease radially and uniformly outwards from the centre of the membrane. The bridge on the banjo visibly distorts the shape of the membrane but the velocity response on the membrane is not affected by its placemenet. As there are no struts attached to the membrane of the banjo there are no increases in stiffness on the plate and as such the instrument vibrates more uniformly than the plates of the guitars. The decrease in velocity towards the edges of the plate suggests that it behaves in a similar fashion to a clamped circular membrane.

The oud produces values of band data across its top plate which are similar in range to those produced by the classical guitars BR2 and DLC with a peak value of 1.2 s/kg (see figure 8.15b). In the traditional oud design the braces are all orientated horizontally across the top plate, perpendicular to the strings, with no struts running parallel to the strings. As there are no struts running in the same direction as the grain, the summed admittance for the oud does not have the $T(2,1)$-like shape seen on guitar top plates. The strut between the two lower sound holes and the bridge appears to reduce the values of admittance within this area of the instrument. The band data shows peak values of summed admittance across the entire frequency range near to the largest of the three sound holes and also surrounding the bridge of the instrument.

8.3.2 Operating Deflection Shapes of the oud

Operating deflection shapes (ODS) show the levels of motion (displacement, velocity or acceleration) on an instrument at a single frequency. In the following descriptions of the ODS measurements on the oud, the horizontal direction is parallel with the bridge and the vertical direction is parallel to the strings.

The top-plate modes of a 'typical' classical guitar are well known but there is less data available for ouds. Luthiers have informally studied the top-plate modes of the oud by producing Chladni patterns. However, no measurements of the velocity across the surface can be determined using this technique.

The top plate ODS of the oud, between 129 Hz and 738 Hz, are shown in figure 8.16. The excitation was provided to the left of the low-frequency drone string using an impact hammer and the velocity response was measured using the 3D scanning laser vibrometer. As the instrument was excited using an impulse excitation the shapes shown in figure 8.16 are actually the operating deflection shapes. This is because it is not only the mode of interest that is in motion at its resonance frequency; body modes with lower resonance frequencies are also excited as a result of their residual responses. Using impulse excitation to drive the instrument means that there is a greater overlap between the higher frequency body modes than if each mode were driven individually

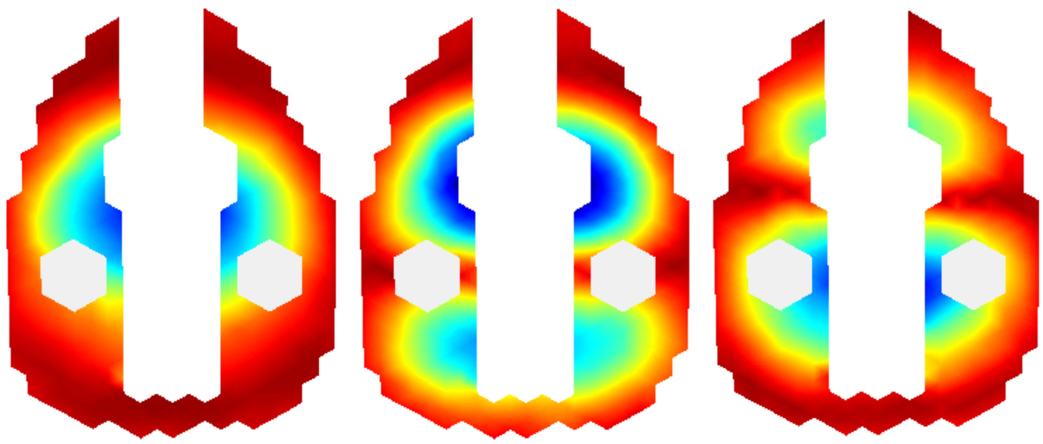

(a) $T(1,1)$ - 129 Hz (0 - 0.05 s/kg).

(b) $T(1,2)_1$ - 175 Hz (0 - 0.07 s/kg).

(c) $T(1,2)_2$ - 222 Hz (0 - 0.07 s/kg).

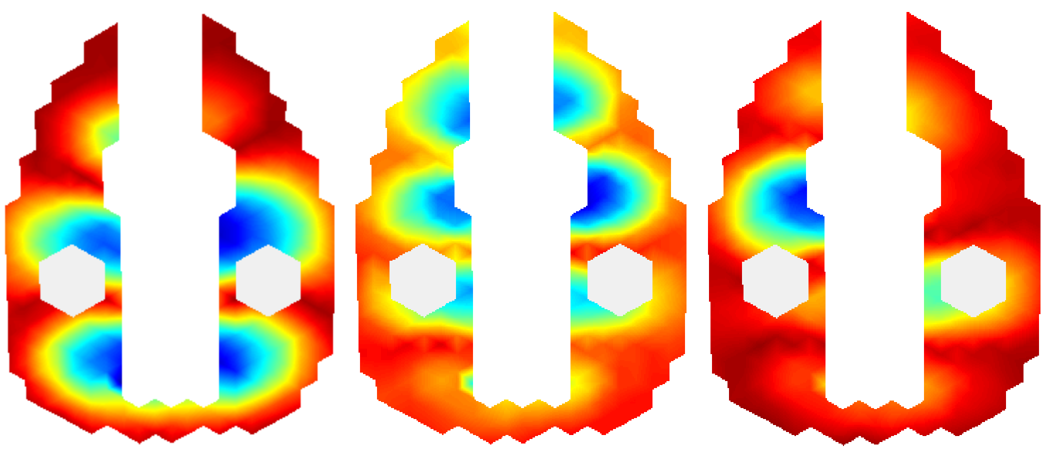

(d) $T(1,3)$ - 263 Hz (0 - 0.16 s/kg).

(e) $T(1,4)_1$ - 382 Hz (0 - 0.1 s/kg).

(f) $T(1,4)_2$ - 398 Hz (0 - 0.25 s/kg).

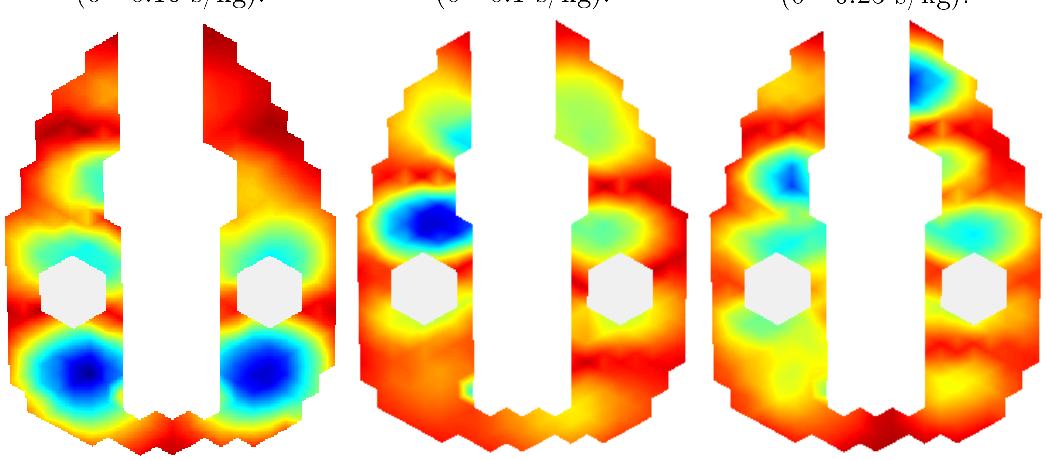

(g) $T(2,3)$ - 534 Hz (0 - 0.2 s/kg).

(h) $T(2,4)$ - 664 Hz (0 - 0.06 s/kg).

(i) $T(2,5)$ - 738 Hz (0 - 0.07 s/kg).

Figure 8.16: Top plate ODS of the oud.

at their resonance frequencies. As a result of this overlap, the highest frequency mode which could be determined was the $T(2,5)$ mode at 738 Hz. Above this frequency the anti-nodal areas became increasingly small and could not be measured with the chosen grid spacing.

The first clear difference between the ODS measured on the oud and those measured on classical guitars is that there is only a single $T(1,1)$ mode. Below this $T(1,1)$ mode, the only visible mode of the instrument is produced by a neck bending motion rather than a single motion in the lower bout. This suggests that the rose (shams) on the three sound holes reduces the ability of the instrument to produce a Helmholtz oscillator-like motion (due to the considerably reduced area of the sound holes). It was not possible to remove the shams from the instrument to determine the amount that the Helmholtz oscillator motion is reduced by when they are in place. Without the Helmholtz oscillator-like motion, the top plate cannot couple to the back plate and the resonance triplet, described in section 1.4.2, cannot be produced. It is also possible that the Helmholtz oscillator-like motion occurs at a frequency where it is unable to couple with the $T(1,1)$ mode. The highly curved back plate is also unlikely to produce a resonance frequency within a similar range as the $T(1,1)$ mode. Therefore it is unlikely that a back-plate mode will couple with the top plate.

On a classical guitar the number of anti-nodal areas usually initially increases both horizontally and vertically with increasing frequency rather than in a single orientation. Within the frequency range shown in figure 8.16, on a classical guitar the $T(2,1)$, $T(3,1)$, $T(4,2)$ and possibly $T(2,2)$ modes would be expected to occur. However ,the number of anti-nodal regions on the oud increase vertically from $T(1,1)$ to $T(1,4)$ before any increase in the number of horizontally orientated anti-nodal regions occurs. The $T(2,3)$ mode at 534 Hz is the first mode to show more than a single anti-nodal region orientated horizontally. The explanation of the orientation of the oud's modes lies with the bracing of the instrument. The braces on the oud are orientated horizontally except for two short, vertically-braced struts either side of the largest sound hole. This is the standard bracing pattern used by luthiers. The lack of any substantial vertical bracing reduces the number of horizontally-placed anti-nodal regions.

Chapter 9

Conclusions

The research for this thesis developed a new method to determine the radiation efficiency η (the ratio of acoustical power output to mechanical power input) of stringed musical instruments. Previous research has determined η across a range of frequencies for several classical guitars and a piano sound board. The methods developed here used spherical-harmonic decomposition to determine the contributions to the total acoustical power output from monopole and dipole sources. While the method also enables the contribution to the power output from higher order sources to be determined, the research demonstrated that their impact was negligible. The method used impulse excitation to drive the instruments, which enabled η to be measured across a range of frequencies and not only at the resonance frequencies of body modes. The spherical-harmonic decomposition was performed on the sound pressure signals measured on two concentric measurement spheres, with the instrument in their centre. These sound pressure values were also used in the research to visualise the radiated sound fields produced by the instruments at different frequencies.

η was measured from excitations on five classical guitars at different locations on their bridges and also under different conditions. The classical guitars typically produced the greatest values of η at frequencies below 450 Hz. One of the five classical guitars, DLC, had greater values of η up to around 600 Hz because its body modes had higher resonance frequencies than those of the other classical guitars. Measurements on an experimental guitar reduced the resonance frequency of the $T(3,1)$ mode without considerably altering the behaviour of the other body modes. The $T(3,1)$ mode is the highest frequency body mode which still displaces large volumes of surrounding air. Lowering the resonance frequency of this mode reduced the upper frequency limit of the range where the maximum values of η occurred. At frequencies above the $T(3,1)$ mode the body modes have increasing numbers of smaller anti-nodal areas. These modes do not displace as large a volume of air as the lower frequency body modes and therefore produce lower values of η.

When the input admittance and radiated sound pressure produced by a stringed instrument are measured, the peaks in the data correspond with the resonance frequencies of body modes. This is not the case with η where the resonance frequencies of body modes do not correspond with either a large or small value of η. Instead it is the shapes of the anti-nodal areas of the body modes that determine the η value. An example of this is the $T(2,1)$ mode on classical guitars. The instruments in which the $T(2,1)$ mode was more symmetrical (i.e. equal-sized anti-nodal areas) produced a lower value of η than those with unequal-sized anti-nodal areas. There is a greater amount of cancellation in the pressure output produced by modes with equal-sized anti-nodes because the amount of pressure radiated with each phase is more equal than if the anti-nodal areas had different sizes. This results in a lower power output and a low value of η. Another example of a large peak visible in the power input and input admittance but which does not produce a peak in power output is the neck-bending mode, which typically occurs below 100 Hz. This mode produces a dipole-like sound field but a negligible level of power output in comparison with the supplied power input.

Measurements of the in-plane velocity were made on several classical guitars in chapter 5. These showed that the level of in-plane velocity was similar in value to the background noise of the measurement system away from the resonance frequencies of the body modes. The greatest in-plane velocity was produced at the resonance frequencies of body modes with pairs of more equally-sized anti-nodal areas. On the classical guitar, BR2, these included the $T(2,1)$ and $T(1,2)_1$ modes which produced comparatively large values of velocity both across the grain and along the grain respectively. It is also the modes with the greatest in-plane motion that are among the least efficient on the instrument. This results from a power input being supplied to produce a motion which does not displace a considerable amount of air. As only a small amount of air is displaced by an in-plane motion the power output is lower than if an out-of-plane motion occurred.

In the low-frequency region of all of the studied instruments, including a steel-string guitar and a violin, the monopole sources produced the greatest values of power output. At higher frequencies the dipole source begin to contribute more to the radiated power output before eventually becoming the main source of power output. For the classical guitars the monopole sources produce the greatest values of power output even at frequencies where modes with dipole characteristics begin to develop, for example between 200 Hz and 450 Hz. On the violin, which has body modes with higher resonance frequencies, the monopole source produces the greatest contribution to the power output up to 1000 Hz. The steel-string guitar, X10, had the largest contribution from monopole sources below 300 Hz. Between 200 Hz and 450 Hz on the classical guitars the body modes showed $T(2,1)$ and $T(1,2)$ shapes, which have dipole-like sound fields, but the monopole sources still provided the greatest contribution to the power output. The most likely source of the monopole power output is from the low-frequency resonance triplet. This is theorised because the amount of monopole power output decreases when the $T(1,1)_1$ mode, the lowest frequency mode of the resonance triplet, is prevented from entering motion by blocking the sound hole. Above 1300 Hz the values of η were around 0.01 for all of the classical guitars studied. The values of η are greater in this frequency range on the violin because its body modes have much higher resonance frequencies than those of the classical guitar.

9.1 Further work

The method used to measure η, described in chapter 3, is applicable for stringed instruments in general as well as guitars and violins. The requirement of this method is that the entire instrument must be located within the smallest measurement sphere. Only classical guitars, a steel-string guitar and a violin were studied in this work but if all of the vibrating parts of an instrument can be contained within the 0.45 m radius sphere then they can be studied. This would allow for studies of banjos, violas and lutes if they could be made available for experimental purposes.

Classical guitars are often constructed to be as symmetrical as possible, in particular using the Torres bracing pattern on the top plate. Symmetrical construction results in modes such as $T(2,1)$ and $T(1,2)$ having more equal-sized anti-nodal areas than occurs with more asymmetric designs. The instruments with a more asymmetric construction had more efficient $T(2,1)$ and $T(1,2)$ modes. This provides the basis for further studies into the extent that changes in the bracing pattern affect the η characteristic of classical guitars.

A future area of study is to use physical models to determine the η characteristics for an instrument. By altering elements within these models, such as the resonance frequencies of certain modes, the η values across the frequency range could be changed. By using these different η characteristics in conjunction with listening tests the effect of η on the perceived sound could be determined.

Appendix A

η data from all instruments

In this appendix graphs of the total radiation efficiency, η, monopole radiation efficiency, η_m and dipole radiation efficiency, η_d, are shown in separate figures for each of the instruments studied.

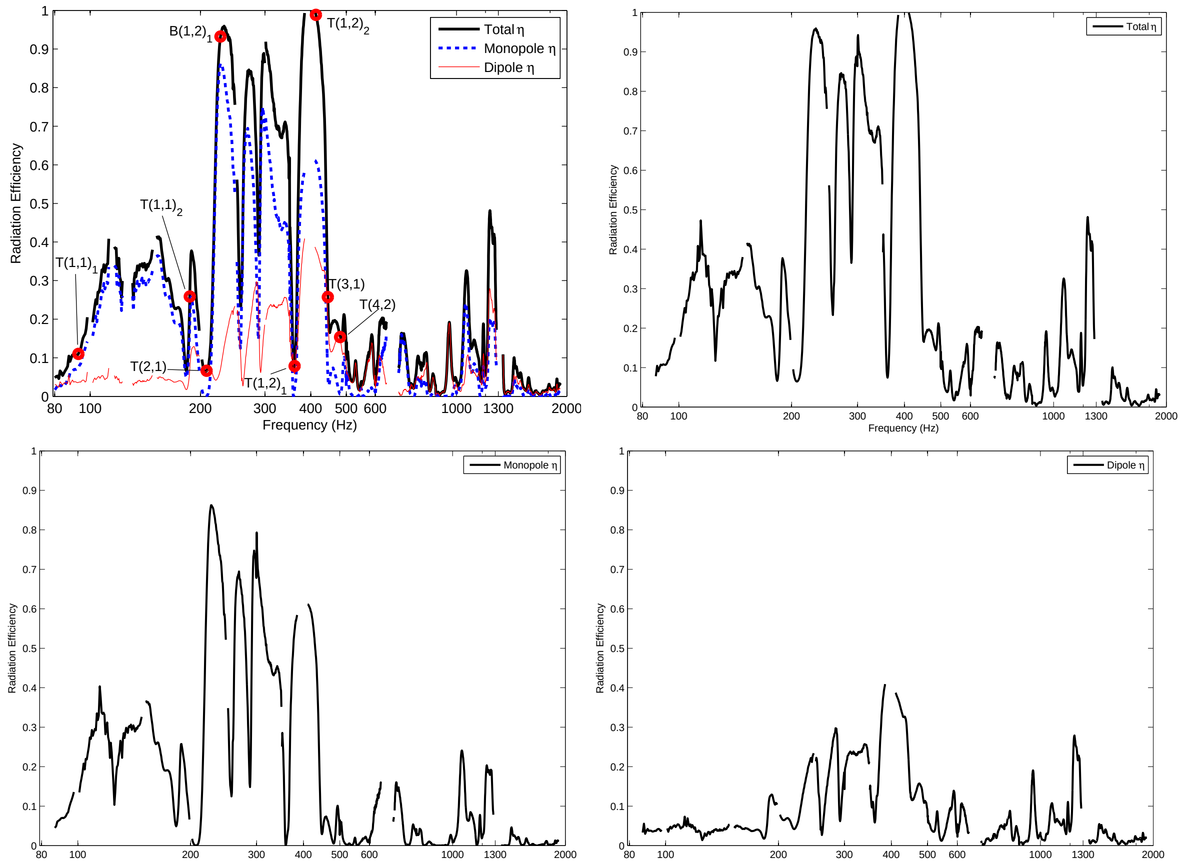

Figure A.1: η measured at position 1 on BR2.

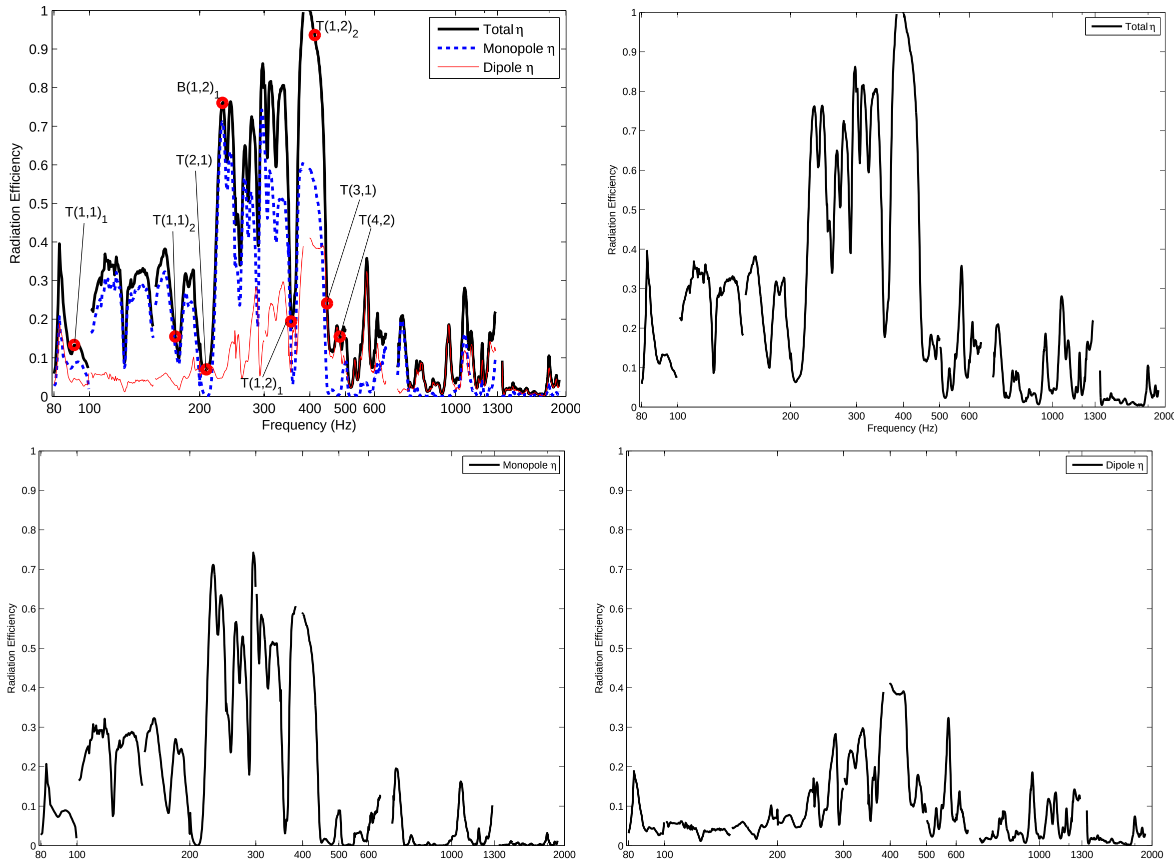

Figure A.2: η measured at position 2 on BR2.

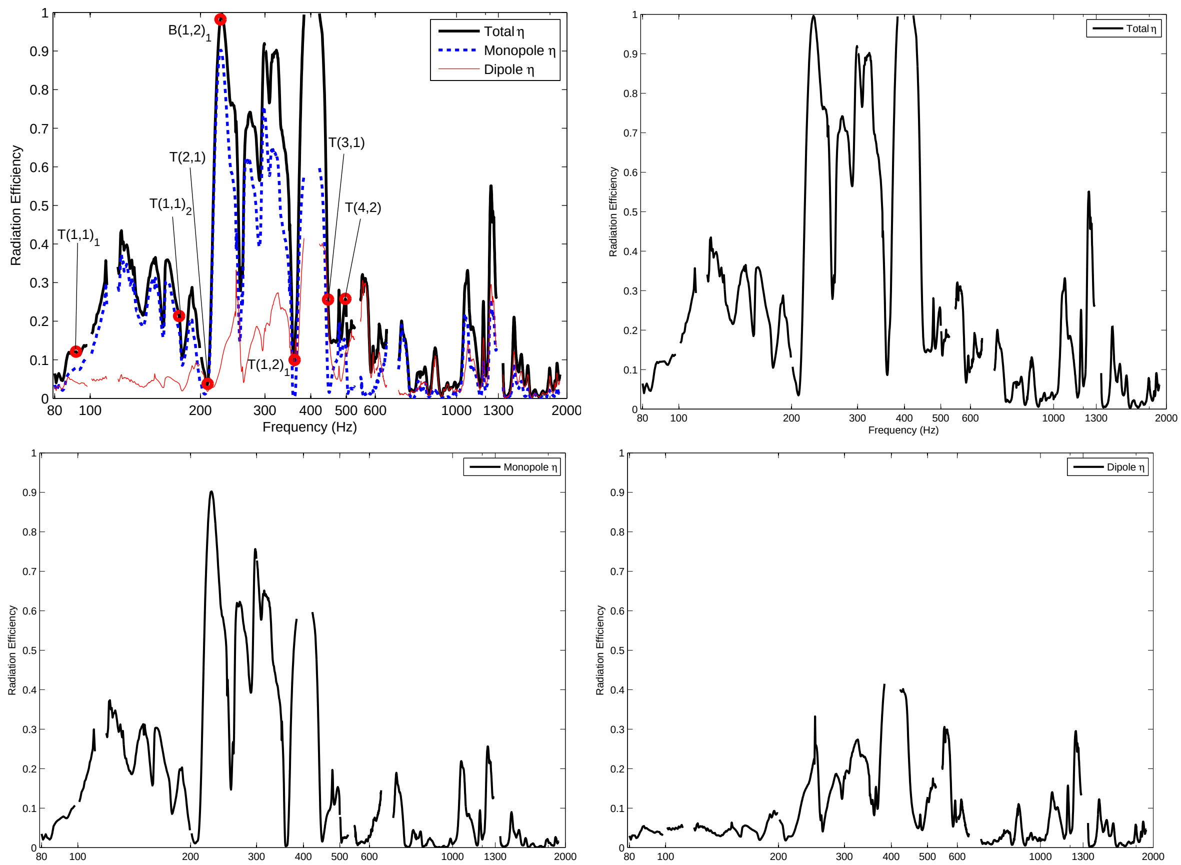

Figure A.3: η measured at position 3 on BR2.

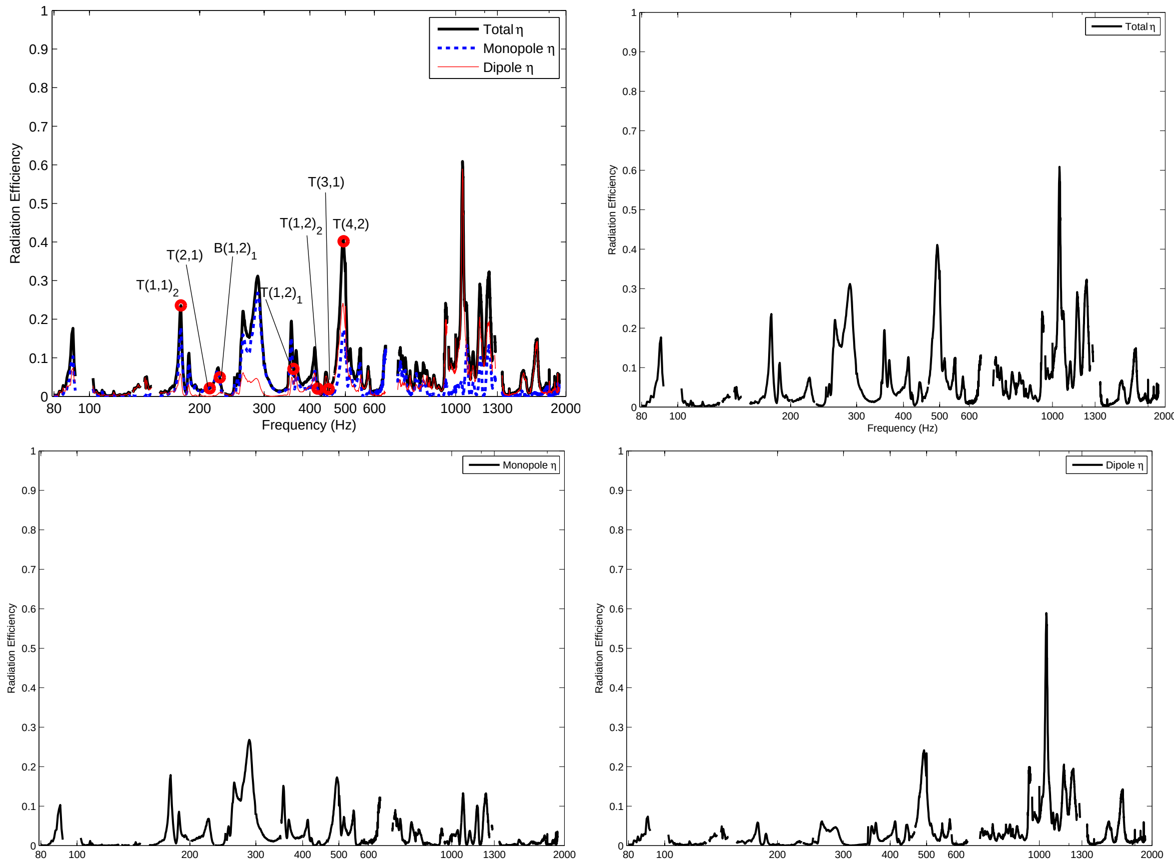

Figure A.4: η measured on the 12th fret on BR2.

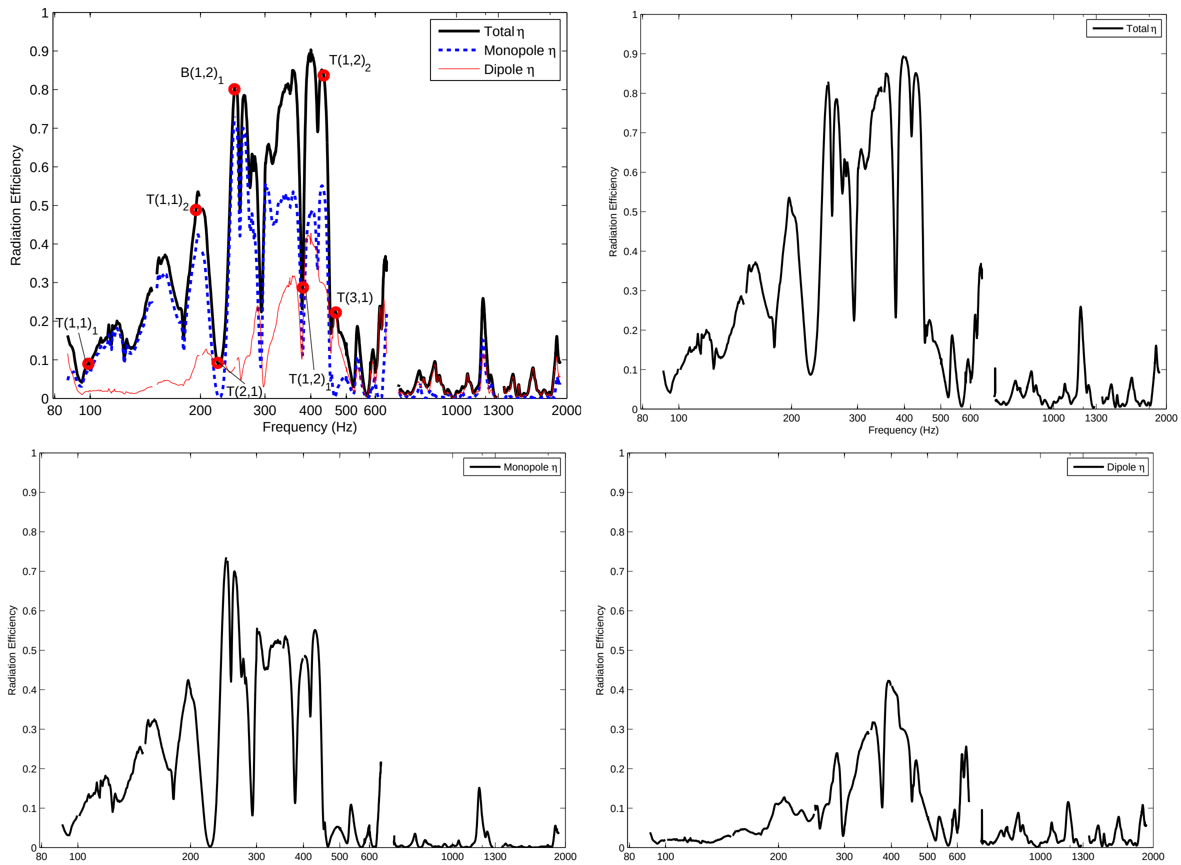

Figure A.5: η measured at position 1 on BR1.

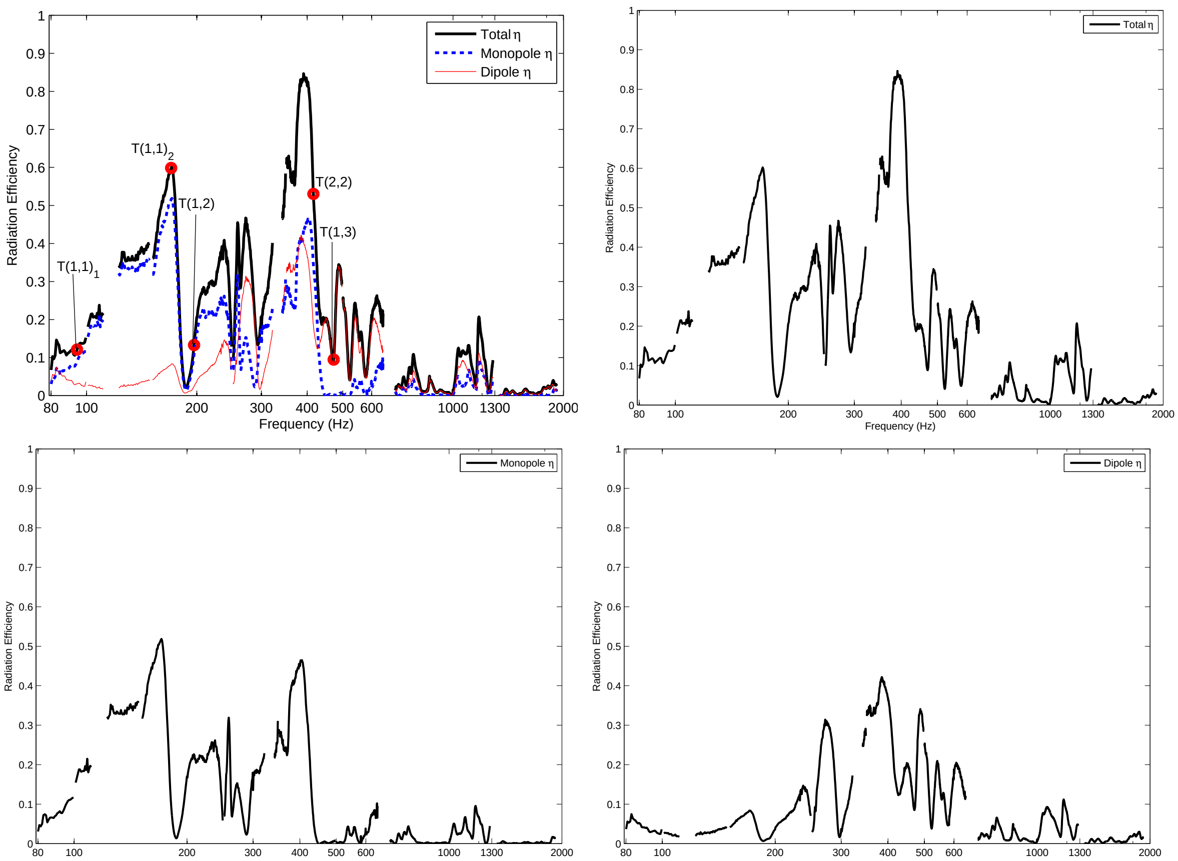

Figure A.6: η measured at position 1 on MAL.

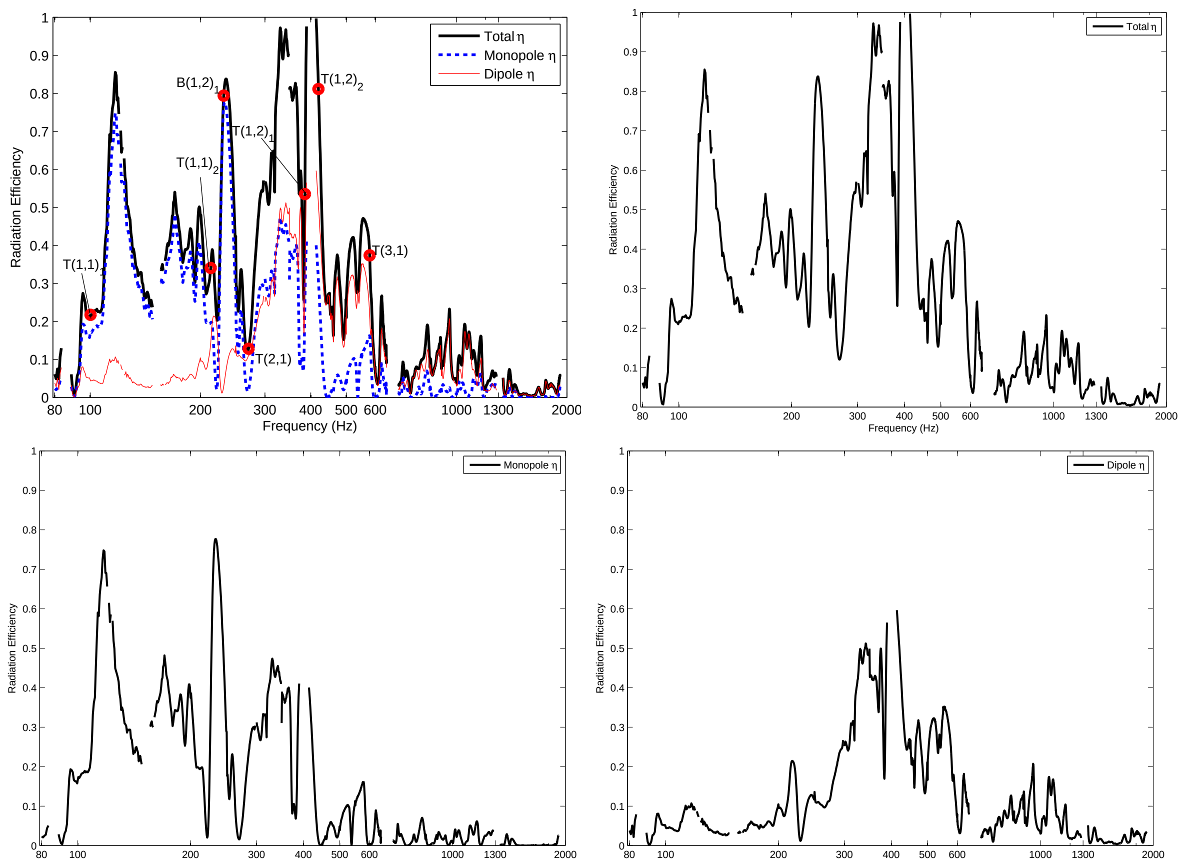

Figure A.7: η measured at position 1 on DLC.

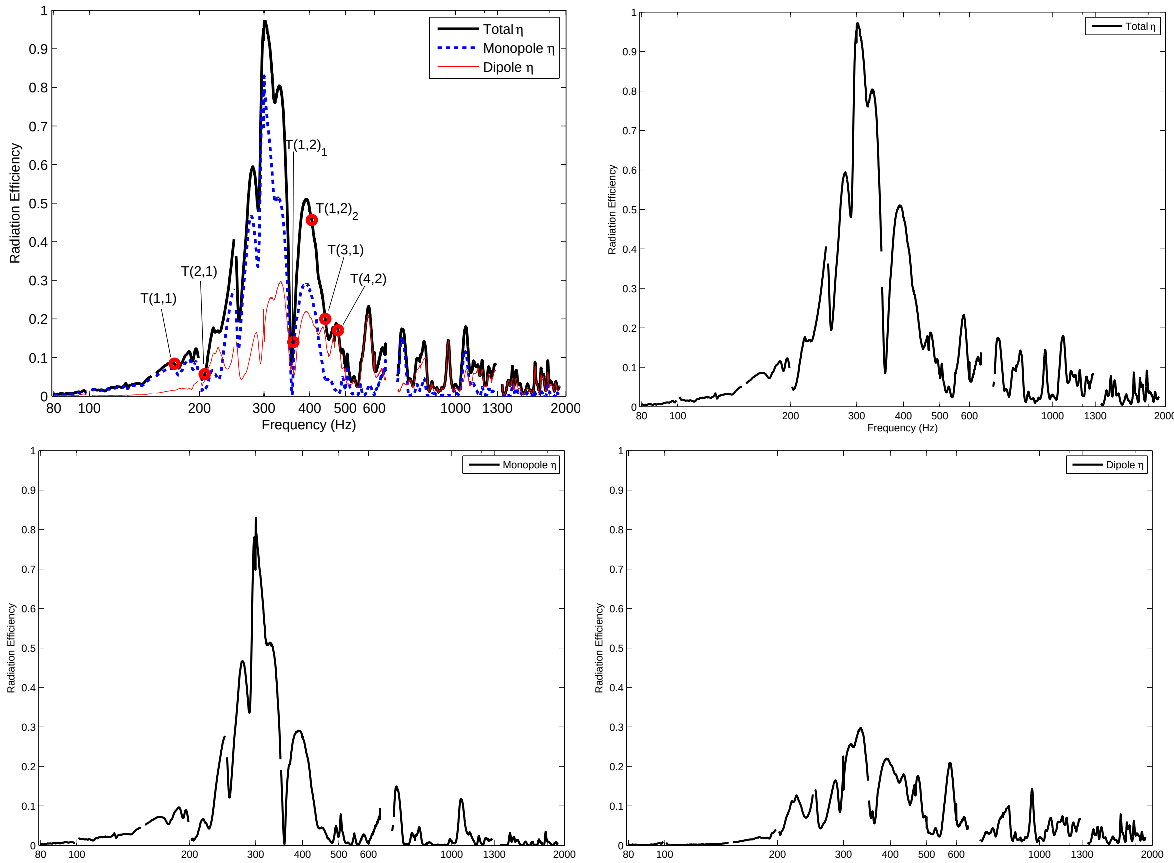

Figure A.8: η measured at position 1 on BR2 with its sound hole blocked.

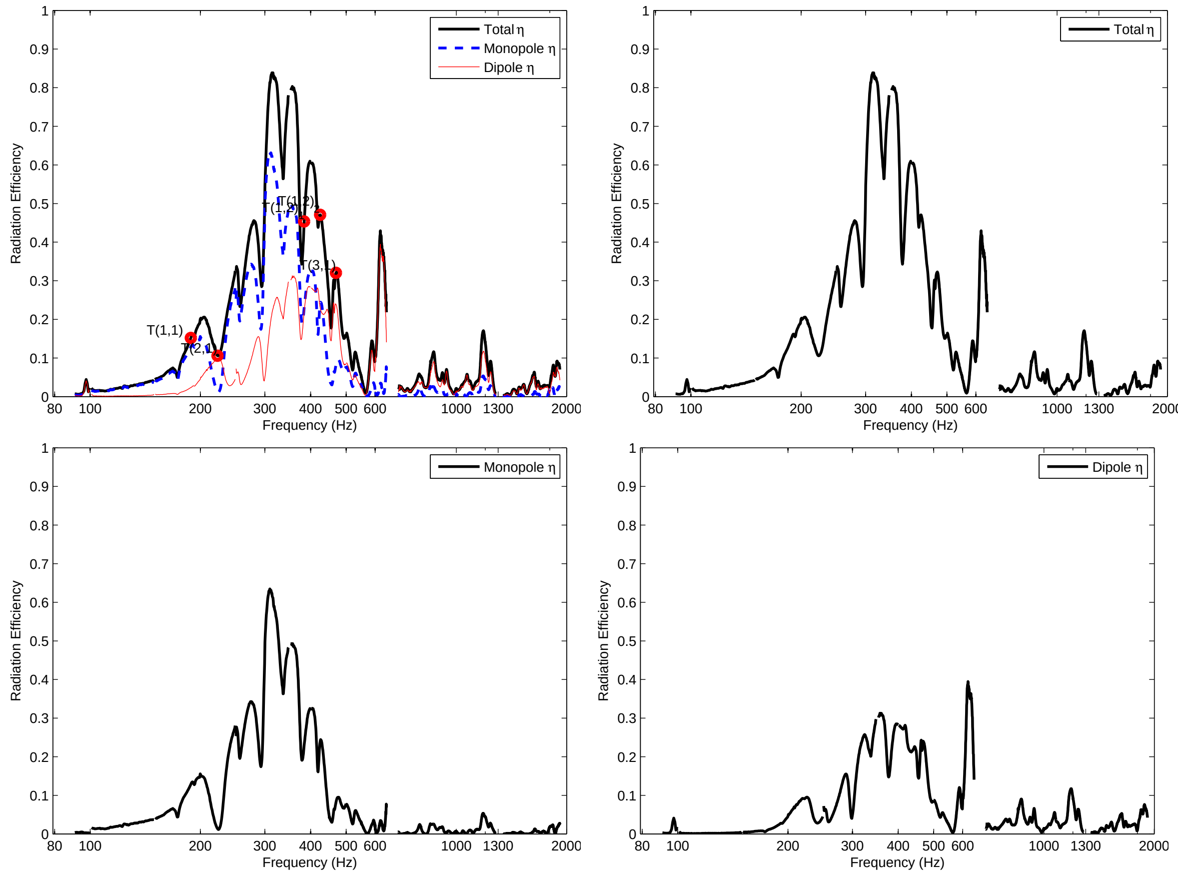

Figure A.9: η measured at position 1 on BR1 with its sound hole blocked.

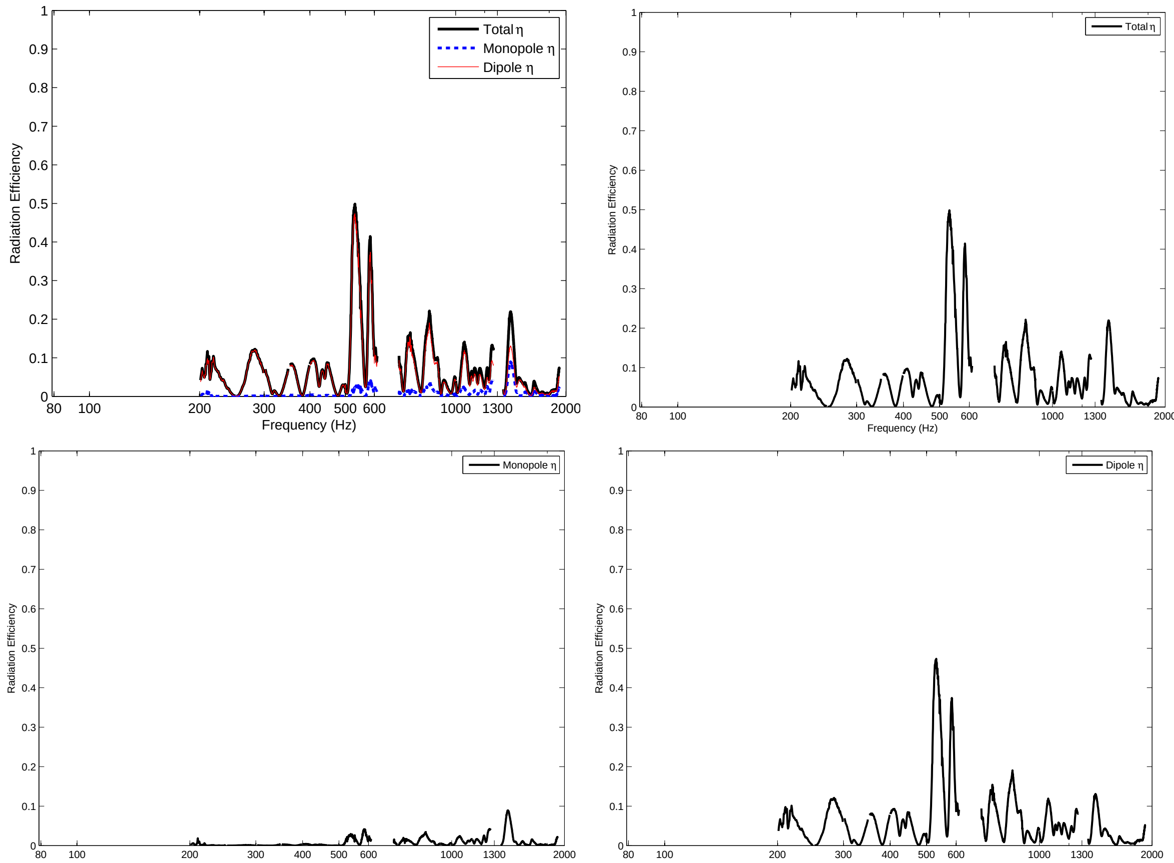

Figure A.10: η measured at position 1 on an isolated experimental top plate.

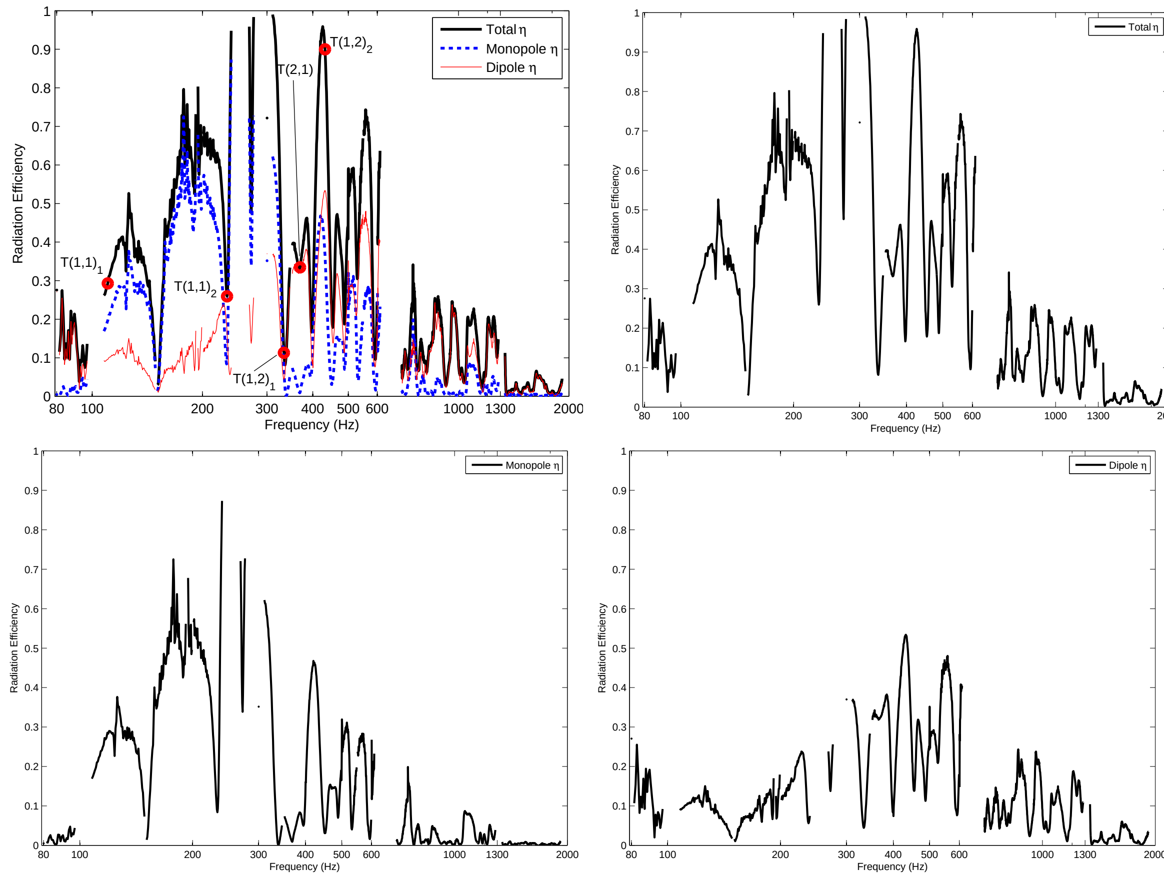

Figure A.11: η measured at position 1 on an experimental classical guitar with an 11.5 mm tall bridge bar.

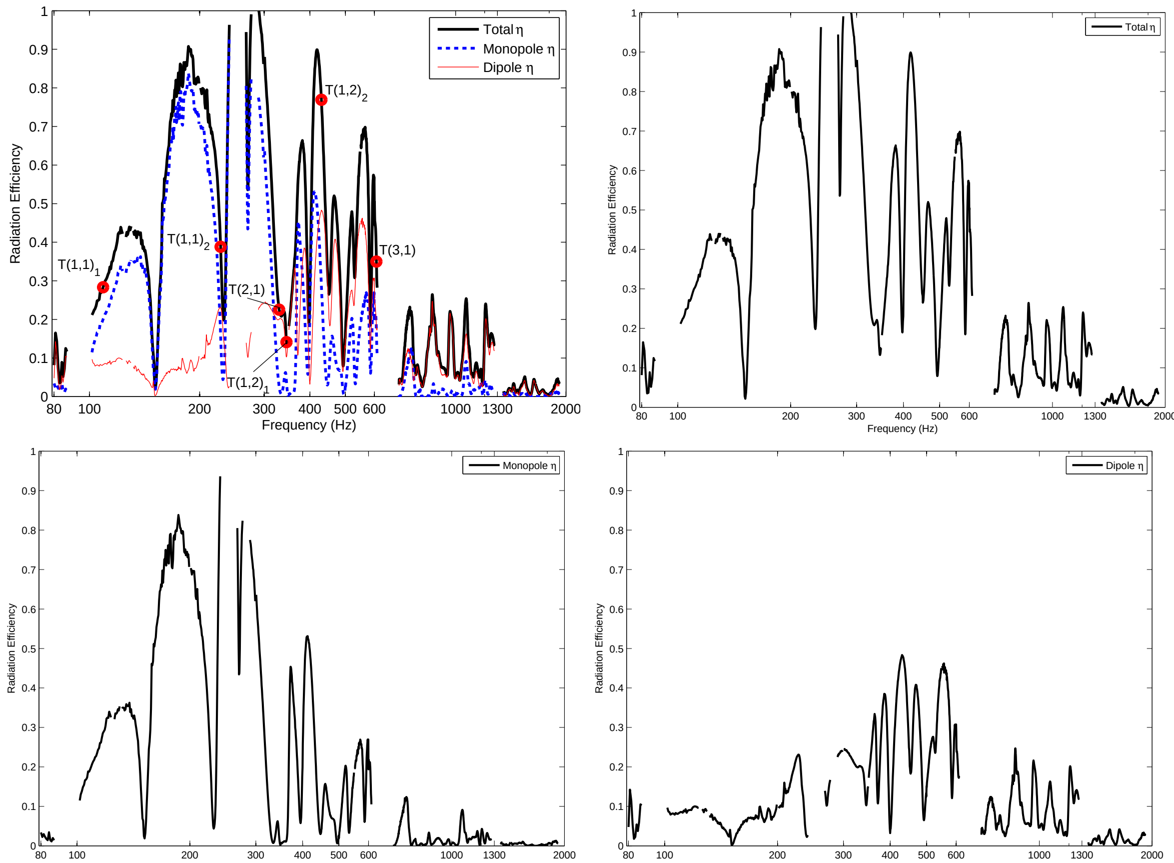

Figure A.12: η measured at position 1 on an experimental classical guitar with a 7 mm tall bridge bar.

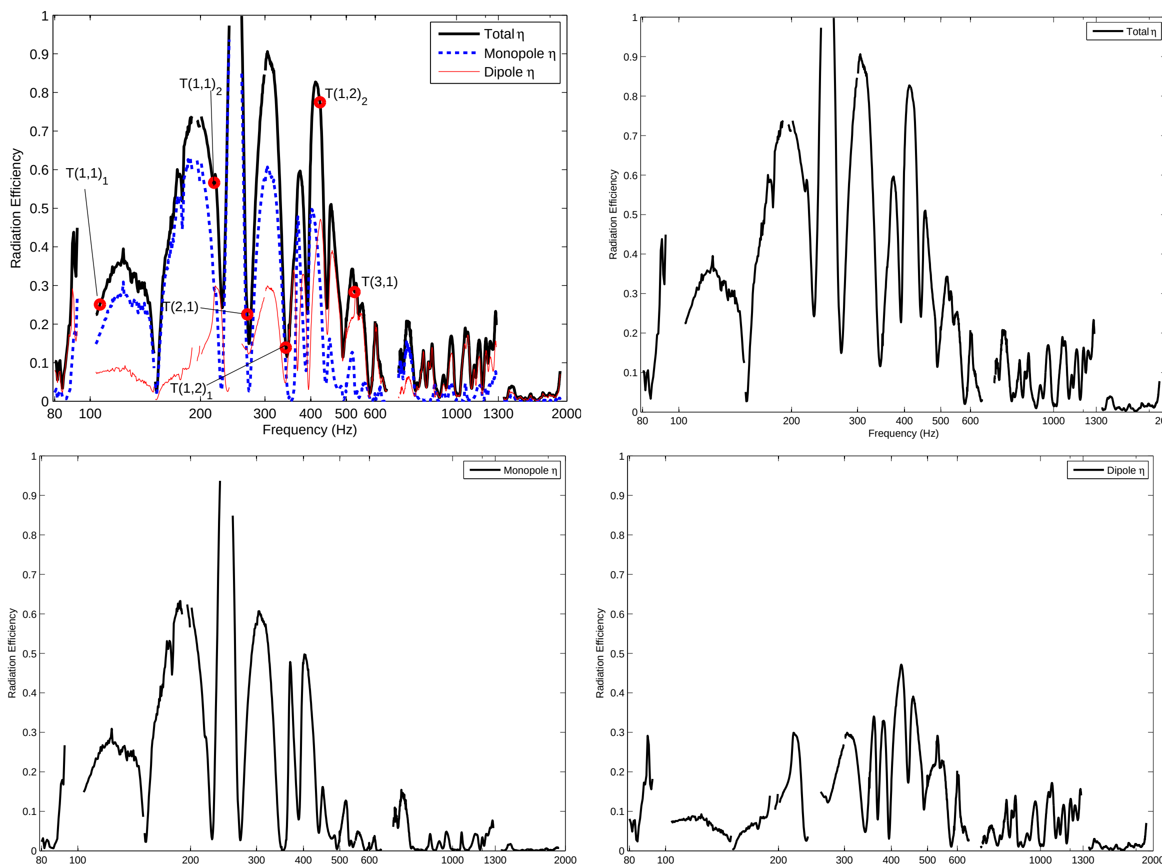

Figure A.13: η measured at position 1 on an experimental classical guitar with the bridge bar removed.

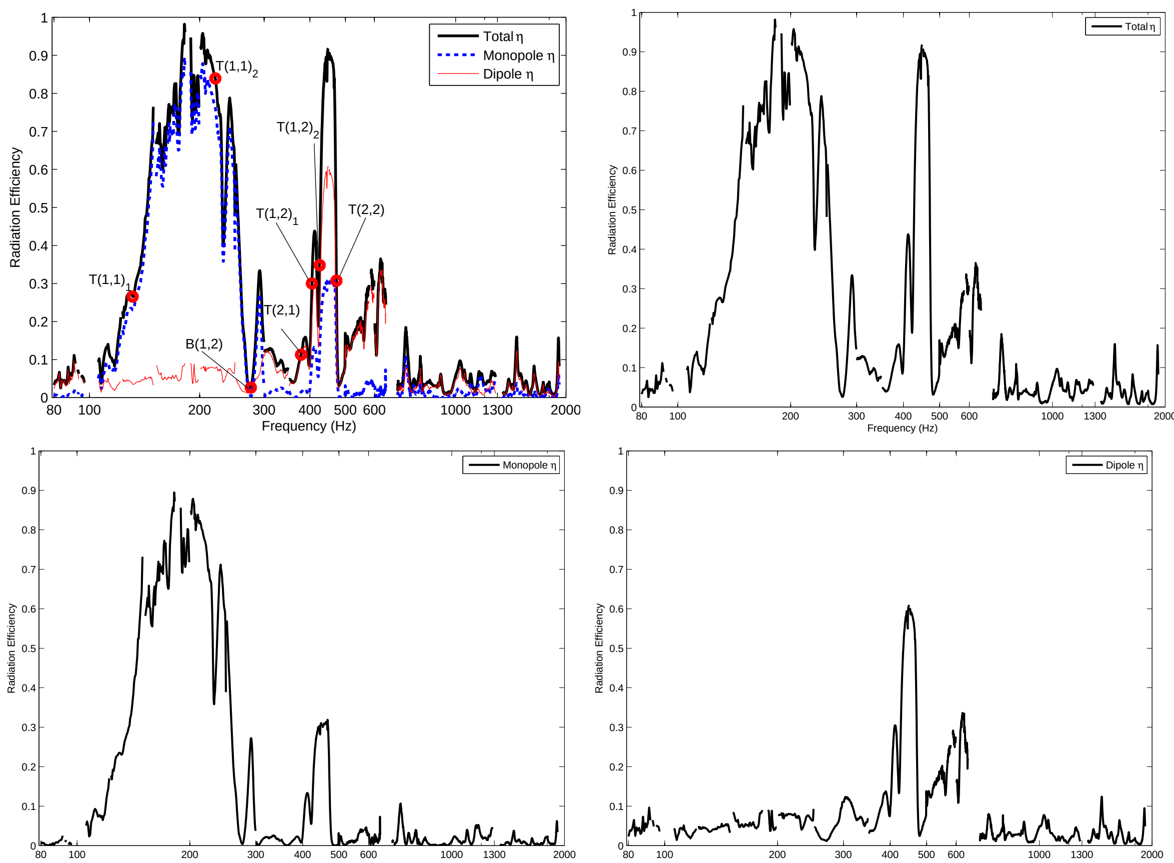

Figure A.14: η measured at position 1 on X10.

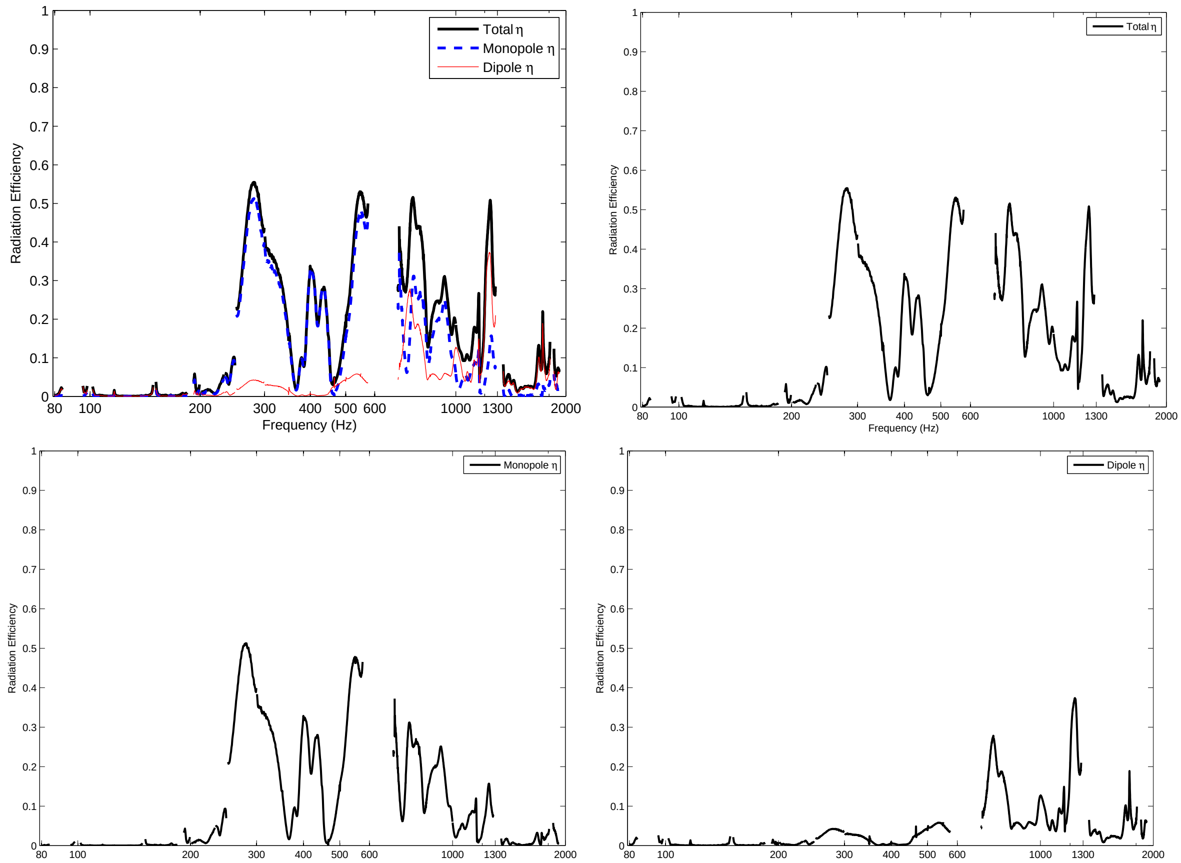

Figure A.15: η measured at the treble side of the bridge on the violin.

References

Bissinger, G. (**2001**). Modern vibration measurement techniques for bowed string instruments. *Experimental Techniques* **25**(4), 43 – 46.

Bissinger, G. (**2003**a). Relating normal mode properties of violins to overall quality: Part 1. signature modes. *Catgut Acoustical Society* **4 (8)**, 37 – 45.

Bissinger, G. (**2003**b). Relating normal mode properties of violins to overall quality: Part ii: Modal averages/trends. *Catgut Acoustical Society* **4(8)**(8), 46 – 52.

Bissinger, G. (**2004**). The role of radiation damping in violin sound. *Acoustics Research Letters Online* **5**(3), 82 – 87.

Bissinger, G. (**2008**). Structural acoustics of good and bad violins. *Journal of the Acoustical Society of America* **124**(3), 1764 – 1773.

Blanco, M. A., Flórez, M. and Bermejo, M. (**1997**). Evaluation of the rotation matrices in the basis of real spherical harmonics. *Journal of Molecular Structure: THEOCHEM* **419**, 19 – 27.

Boullosa, R. R. (**2001**). Admittance at the frets of a classical guitar. *Catgut Acoustical Society* **4**(4), 33 – 36.

Boullosa, R. R., Orduna-Bustamente, F. and Lopez, A. P. (**1999**). Tuning characteristics, radiation efficiency and subjective quality of a set of classical guitars. *Applied Acoustics* **56**, 183 – 197.

Boutillon, X. and Weinreich, G. (**1999**). Three-dimensional mechanical admittance: Theory and new measurement method applied to the violin bridge. *Journal of the Acoustical Society of America* **105**(6), 3524 – 3533.

Carne, T. and Stasiunas, E. (**2006**). Lessons learned in modal testing part 3: Transient excitation for modal testing, more than just hammer impacts. *Experimental Techniques* **30**(3), 69–79.

Carter, G. C., Knapp, C. H. and H.Nuttall, A. (1973). Estimation of the magnitude-squared coherence function via overlapped fast fourier transform processing. *IEEE transactions on audio and electroacoustics* **21**(4), 337 – 344.

Christensen, O. (1982). Quantitative models for low frequency guitar function. *Journal of Guitar Acoustics* **6**, 10–25.

Christensen, O. (1983). The response of played guitars at middle frequencies. *Acustica* **53**(1), 45 – 48.

Christensen, O. (1984). An oscillator model for analysis of guitar sound pressure response. *Acustica* **54**, 289–295.

Christensen, O. and Vistisen, B. B. (1980). Simple model for low-frequency guitar function. *Journal of the Acoustical Society of America* **68**(3), 758 – 766.

Cremer, L. (1984). *The Physics of the Violin.* Massachusetts Institute of Technology.

de Bree, H.-E. (2003). The microflown: An acoustic particle velocity sensor. *Acoustics Au* **31**, 91–94.

Elejabarrieta, M. J., Ezcurra, A. and Santamaria, C. (2000). Evolution of the vibrational behaviour of a guitar soundboard along successive construction phases by means of the modal analysis technique. *Journal of the Acoustical Society of America* **108**(1), 369 – 378.

Elejabarrieta, M. J., Ezcurra, A. and Santamaria, C. (2002a). Coupled modes of the resonance box of the guitar. *Journal of the Acoustical Society of America* **111**(5), 2283 – 2292.

Elejabarrieta, M. J., Santamaria, C. and Ezcurra, A. (2002b). Air cavity modes in the resonance box of the guitar: The effect of the sound hole. *Journal of Sound and Vibration* **252**(3), 584–590.

Ewins, D. J. (1984). *Modal Testing: Theory and Practise.* Engineering Dynamics Series. Research Studies Press.

Ezcurra, A. (1996). Influence of the material constants on the low frequency modes of a free guitar plate. *Journal of Sound and Vibration* **194**(4), 640 – 644.

Fahy, F. (1985). *Sound and Structural Vibration Radiation, Transmission and Response.* Academic Press.

Fahy, F. (**1989**). *Sound Intensity.* Elsevier Science Publishers Ltd.

Fleischer, H. and Zwicker, T. (**1998**). Mechanical vibrations of electric guitars. *Acta Acustica with Acustica* **84**, 758 – 765.

Fletcher, N. H. and Rossing, T. D. (**1991**). *The Physics of Musical Instruments.* Springer - Verlag.

Fritz, C., Cross, I., Moore, B. C. J. and Woodhouse, J. (**2007**). Perceptual thresholds for detecting modifications applied to the acoustical properties of a violin. *The Journal of the Acoustical Society of America* **122**(6), 3640–3650.

Garcia-Mayen, H. and Santillan, A. (**2011**). The effect of the coupling between the top plate and the fingerboard on the acoustic power radiated by a classical guitar (l). *The Journal of the Acoustical Society of America* **129**(3), 1153–1156.

Golińska, A. K. (**2011**). Coherence function in biomedical signal processing: a short review of applications in neurology, cardiology and gynecology. *Studies in Logic, Grammar and Rhetoric* **25**, 73 – 81.

Griffin, S., Luo, H. and Hanagud, S. (**1998**). Acoustic guitar function model including symmetric and asymmetric plate modes. *Acta Acustica united with Acustica* **84**(3), 563–569.

Haines, D. (**1981**). On musical instrument wood. *Journal of Guitar Acoustics* **2**, 35 – 52.

Hill, T. J. W., Richardson, B. E. and Richardson, S. J. (**2004**). Acoustical parameters for the characterisation of the classical guitar. *Acta Acustica with Acustica* **90**, 335 – 348.

Jacobsen, F. (**1997**). An overview of the sources of error in sound power determination using the intensity technique. *Applied Acoustics* **50**(2), 155 – 166.

Jacobsen, F. and de Bree, H.-E. (**2005**a). A comparison of two different sound intensity measurement principles. *Journal of the Acoustical Society of America* **118**(3), 1510 – 1517.

Jacobsen, F. and de Bree, H.-E. (**2005**b). *Measurement of sound intensity: p-u probes versus p-p probes.*

Jansson, E., Bork, I. and Meyer, J. (1986). Investigations into the acoustical properties of the violin. *Acustica* **62**(1), 1–15.

Jansson, E. V. (1971). A study of acoustical and hologram interferometric measurements of the top plate vibrations of a guitar. *Acustica* **25**, 95 – 100.

Kay, S. M. (1988). *Modern Spectral Estimation: Theory and Application*. Prentice-Hall.

Kinsler, L. E., Frey, A. R., Coppens, A. B. and Sanders, J. V. (1980). *Fundamentals of Acoustics*. John Wiley & Sons, 3rd edition.

Lai, J. and Burgess, M. (1990). Radiation efficiency of acoustic guitars. *Journal of the Acoustical Society of America* **88**(3), 1222–1227.

Lambourg, C. and Chaigne, A. (1993). Measurements and modeling of the admittance matrix at the bridge in guitars. In A. Friberg, J. Iwarsson, E. Jansson and J. Sundberg, editors, *Stockholm Music Acoustics Conference*, 448 – 453. Royal Swedish Academy of Music, Lambourg1983.

Lewney, M. (2000). The acoustics of the guitar. Ph.D. thesis, Cardiff School of Physics and Astronomy.

Lynn, P. A. (1973). *An Introduction to the Analysis and Processing of Signals*. The Macmillan Press.

Marshall, K. D. (1985). Modal analysis of a violin. *Journal of the Acoustical Society of America* **77**, 695 – 709.

McConnell, K. G. (1995). *Vibration Testing: Theory and Practice*. John Wiley & Sons.

Meyer, J. (1972). Directivity of the bowed stringed instruments and its effect on orchestral sound in concert halls. *Journal of the Acoustical Society of America* **51**(6 (pt 2)), 1994 – 2009.

Meyer, J. (1978). *Acoustics and the Performance of Music*. Verlag Das Musikinstrument Frankfurt.

Meyer, J. (1981). Relationships between the tonal quality and construction of guitars parts 1 and 2 (translated from german). *Das Musikinstrument* **30**, 1292 – 1303.

Moral, J. and Jansson, E. (**1982**). Eigenmodes, input admittance and the function of the violin. *Acustica* **50**(5), 329 – 337.

Morse, P. M. (**1948**). *Vibration and Sound*. International Series in Pure and Applied Physics. McGraw - Hill Book Company, 2nd edition.

Morse, P. M. and Ingard, K. U. (**1968**). *Theoretical Acoustics*. McGraw-Hill.

Ono, T. and Okuda, A. (**2007**). Acoustic characteristics of guitars with a top board of carbon fiber-reinforced composites. *Acoustical Science & Technology* **28**(6), 442 – 443.

PCB (). *White paper: Guide to Dynamic Force Sensors*. PCB Piezotronics.

PCB (**2007**a). *Model 087E80 Impact Hammer Installation and Operating Manual*. PCB.

PCB (**2007**b). *Model 352B10 ICP Accelerometer Installation and Operating Manual*.

Perry, I. and Richardson, B. E. (**2014**). Radiation efficiency and sound field measurements on stringed musical instruments. In *Proceedings of the International Symposium on Musical Acoustics*, 77 – 82.

Polytec (**2014**). Basic principles of vibrometry. http://www.polytec.com/us/solutions/vibration-measurement/basic-principles-of-vibrometry/. Accessed: 05/06/2014.

Richardson, B. E. (**1982**). A physical investigation into some factors affecting the musical performance of the guitar. Ph.D. thesis, University College, Cardiff.

Richardson, B. E., Hill, T. J. W. and Richardson, S. J. (**2002**). Input admittance and sound field measurements of ten classical guitars. In *Proceedings of the Institue of Acoustics Spring Conference 2002*, volume 24.

Richardson, B. E., Johnson, H., Joslin, A. D. and Perry, I. A. (**2012**). The three-mass model for the classical guitar revisited. In *Proceedings of the Acoustics 2012 Nantes Conference*, 2771 – 2776.

Richardson, S. J. (**2001**). Acoustical parameters for the classical guitar. Ph.D. thesis, Cardiff School of Physics and Astronomy.

Roberts, W. H. and Richardson, B. E. (**2013**). Perceptual thresholds for string-body coupling in guitars. In *Proceedings of the Institute of Acoustics*, volume 35.

Roberts, W. H. and Richardson, B. E. (**2014**). Perceptual thresholds for string-body coupling in plucked-string instruments. In *Proceedings of the International Symposium on Musical Acoustics*, 465–470.

Romanillos, J. L. (**1990**). *Antonio de Torres: Guitar maker - his life and work*. The Bold Strummer Ltd, 2nd edition.

Rossing, T., Popp, J. E. and Polstein, D. (**1985**). Acoustical response of guitars. In *SMAC 83: Proceedings of the Stockholm Music Acoustics Conference*.

Rossing, T. D., Moore, R. and Wheeler, P. (**2002**). *The Science of Sound 3rd ed*. Addison-Wesley, Reading, Massachusetts.

Schelleng, J. C. (**1963**). The violin as a circuit. *Journal of the Acoustical Society of America* **35**(3), 326 – 338.

Sloane, I. (**1976**). *Classic Guitar Construction*. Omnibus Press.

Suzuki, H. (**1986**). Vibration and sound radiation of a piano soundboard. *Journal of the Acoustical Society of America* **80**(6), 1573 – 1582.

Thompson, J. and Tree, D. (**1980**). Leakage error in fast fourier analysis. *Journal of Sound and Vibration* **71**(4), 531 – 544.

Torres, J. A. and Boullosa, R. R. (**2011**). Radiation efficiency of a guitar top plate linked with edge or corner modes and intercell cancellation. *Journal of the Acoustical Society of America* **130**(1), 546 – 556.

Waller, M. D. (**1961**). *Chladni figures - A study in symmetry*. G. Bell and Sons Ltd.

Wang, L. M. and Burroughs, C. B. (**2001**). Acoustic radiation from bowed violins. *Journal of the Acoustical Society of America* **110**(1), 543 – 555.

Wegst, U. G. (**2006**). Wood for sound. *American Journal of Botany* **93**(10), 1439–1448.

Weinreich, G. (**1985**). Sound hole sum rule and the dipole moment of the violin. *Journal of the Acoustical Society of America* **77**(2), 710 – 718.

Weinreich, G. and Arnold, E. B. (**1980**). Method for measuring acoustic radiation fields. *Journal of the Acoustical Society of America* **68**(2), 404 – 411.

Welch, P. D. (1967). The use of fast fourier transform for the estimation of power spectra: A method based on time averaging over short, modified periodograms. *IEEE Transactions on Audio Electroacoustics* **AU-15**, 70–73.

White, T. P. (1981). Impulse excitation of instrument resonances. *Journal of Guitar Acoustics* **4**, 68–78.

Williams, E. G. (1999). *Fourier Acoustics.* Academic Press.

Woodhouse, J. (2005). On the "bridge hill" of the violin. *Acta Acustica United with Acustica* **91**, 155 – 165.

Woodhouse, J., Manuel, E., Smith, L., Wheble, A. and Fritz, C. (2012). Perceptual thresholds for acoustical guitar models. *Acta Acustica united with Acustica* **98**(3), 475–486.

Wright, H. (1996). The acoustics and psychoacoustics of the guitar. Ph.D. thesis, University of Wales, Cardiff.

Yoshikawa, S. (2007). Acoustical classification of woods for string instruments. *Journal of the Acoustical Society of America* **122**(1), 568–573.